9-26-2011 12:00 AM

Structural Characterization of HIP2 Enzyme Interactions in Ubiquitination

Benjamin W. Cook, *University of Western Ontario*

Supervisor: Dr. Gary Shaw, *The University of Western Ontario*

A thesis submitted in partial fulfillment of the requirements for the Doctor of Philosophy degree in Biochemistry

STRUCTURAL CHARACTERIZATION OF HIP2 ENZYME INTERACTIONS IN UBIQUITINATION

(Spine title: HIP2 Enzyme Interactions in Ubiquitination)

(Thesis format: Integrated Article)

by

Benjamin Warren Cook

Graduate Program
in
Biochemistry

A thesis submitted in partial fulfillment
of the requirements for the degree of
Doctor of Philosophy

The School of Graduate and Postdoctoral Studies
The University of Western Ontario
London, Ontario, Canada

THE UNIVERSITY OF WESTERN ONTARIO
SCHOOL OF GRADUATE AND POSTDOCTORAL STUDIES

CERTIFICATE OF EXAMINATION

Supervisor	Examiners
Dr. Gary Shaw	Dr. James Omichinski
Supervisory Committee	Dr. Eric Ball
Dr. Eric Ball	Dr. Stanley Dunn
Dr. Brian Shilton	Dr. Miguel Valvano

The thesis by

Benjamin Warren Cook

entitled:

Structural Characterization of HIP2 Enzyme Interactions in Ubiquitination

is accepted in partial fulfillment of the
requirements for the degree of
Doctor of Philosophy

Date_____ _____
Chair of the Thesis Examination Board

Abstract

The ubiquitin proteolysis pathway utilizes three enzymes, an E1 activating enzyme, an E2 conjugating enzyme and an E3 ligating enzyme, to respectively activate, transfer and ligate ubiquitin (Ub) onto a substrate protein. The creation of a K48-linked poly-Ub chain on a substrate will target this protein to be degraded by the 26S proteosome. E2 conjugating enzymes are central proteins in this pathway and interact with the E1 and E3 enzymes to perform Ub transfer. The mechanism by which Ub molecules are interconnected remains poorly understood. The E2 enzymes HIP2 and Ubc1 have been shown to create poly-Ub chains in the absence of E3 enzymes and substrates. In this thesis, HIP2 and Ubc1 were investigated through physical and structural methods to clarify their mechanism of poly-Ub chain assembly.

The study of HIP2 and Ubc1 was aided by the formation and purification of stable HIP2-Ub and Ubc1-Ub disulphide linked complexes that closely resemble the HIP2~Ub and Ubc1~Ub thiolester intermediates. The physical techniques of sedimentation equilibrium and SAXS determined that HIP2 and Ubc1 as well as their disulphide complexes are predominantly monomeric. Activity assays were also performed on these enzymes indicating that the E2~Ub thiolester is the sole species required to create poly-Ub chains. Additionally, these assays determined that both free Ub and E2-Ub complexes could act as Ub acceptors for poly-ubiquitin chain extension. NMR experiments were also performed through the use of isotopically labelled HIP2, HIP2-Ub and HIP2-Ub_2 complexes. NMR chemical shift perturbation experiments identified significant intramolecular interactions between HIP2 and Ub in both HIP2-Ub and HIP2-

Ub_2 complexes. The intramolecular interaction within HIP2-Ub_2 utilizes a C-terminal Ub-associated (UBA) domain and this domain is not present in other human E2 enzymes. These intramolecular interactions indicate the HIP2-Ub and HIP2-Ub_2 complexes behave predominantly as Ub donors within poly-Ub chain formation. These results have allowed the formulation of mechanisms to describe HIP2 and Ubc1 function. The determination of these mechanisms is especially important for HIP2, as its function has been associated with the progression of both Huntington's and Alzheimer's disease.

Keywords: ubiquitin, HIP2, Ubc1, E2 conjugating enzyme, poly-ubiquitination, UBA domain, nuclear magnetic resonance, chemical shift perturbation, sedimentation equilibrium, small angle X-ray scattering, Huntington's disease, Alzheimer's disease

Co-authorship

Chapter 2

Amino acid substitutions in Ub and Ubc1 were incorporated by Kathryn R. Barber. The formation and purification of Ubc1, Ubc1-Ub^{Cys} and Ubc1-$Ub_{K48}{}^{Cys}$ complexes was performed by Kathryn R. Barber. Mass spectrometry results on these purified proteins was also performed by Kathryn R. Barber.

Chapter 4

SAXS data for HIP2-Ub_2 was collected by Dr. Brian H. Shilton at the Advanced Photon Source in Argonne, Illinois.

Dedication

For my parents, Robert and Pamela Cook

Acknowledgements

I would like to thank my supervisor Dr. Gary Shaw who has provided me with guidance and mentorship over the course of my graduate studentship. You have been especially beneficial to developing my scientific writing and organization.

I would also like to thank my advisory committee Dr. Brian Shilton and Dr. Eric Ball for helpful input and discussions, which has helped me progress with my research.

To Kathy, your help on this research project has been invaluable. Thank you for running a very well organized lab that encourages students to be efficient and careful with all equipment, especially size exclusion columns.

Thank you to all the members of the Shaw lab, both past and present. Thank you for the invaluable discussions on scientific principles and for providing laughter and friendship during hard (precipitation) times, especially back in ‘05.

Table of Contents

List of Tables

List of Figures

List of Abbreviations, Symbols and Nomenclature

*	Isotopically labelled protein in a protein complex
A_{600}	Absorbance at 600 nanometers wavelength
Å	Angstrom
Alexa	Fluorescent label (680nm) reactive with cysteine
ATP	Adenosine triphosphate
$CuCl_2$	Copper chloride
D_2O	Deuterium Oxide
Da	Daltons
DSS	2,2'-dimethyl-2-silapentane-5-sulfonate
DTT	Dithiothreitol
E1	Ubiquitin activating enzyme
E2	Ubiquitin conjugating enzyme
E2-Ub	E2 with disulphide bound ubiquitin (thiolester mimic)
E2~Ub	E2 with thiolester bound ubiquitin
E3	Ubiquitin ligating enzyme
E. coli	Escherichia coli
EDTA	Ethylenediaminetetraacetic acid
g	force of gravity (xg = multiplication of g)
GST	Glutathione S-transferase
HCl	Hydrochloric acid
HECT	Homologous to the E6-AP carboxyl terminus
HSQC	Heteronuclear Single Quantum Coherence
Hz	hertz
IPTG	Isopropyl β-D thiogalactopyranoside
I_o	Forward Scattering
K_d	Dissociation constant
kDa	Kilodalton
LB	Lysogeny broth

M	Molar
MgATP	Magnesium adenosine triphosphate
MHz	Megahertz
MW	Molecular weight
MWCO	Molecular weight cut off
NaCl	Sodium chloride
$NaHPO_4$	Sodium phosphate
NaN_3	Sodium azide
Ni^{2+}	Nickel
NMR	Nuclear magnetic resonance
PAGE	Polyacrylamide gel electrophoresis
PCR	Polymerase chain reaction
Poly-Ub	Poly-ubiquitin
ppm	Parts per million
R_g	Radius of gyration
RING	Really interesting new gene
RMSD	Root mean square deviation
rpm	Revolutions per minute
S. cerevisiae	Saccharomyces cerevisiae
SAXS	Small angle X-ray scattering
SDS	Sodium dodecyl sulfate
TCEP	Tris(2-carboxyethyl)phosphine
TEV	Tobacco etch virus
Tris	Tris(hydroxymethyl)aminomethane
TROSY	Transverse relaxation optimized spectroscopy
Ub	Ubiquitin
Ub_2	Diubiquitin
Ub_n	Poly-Ub chain
Ub^{K48R}	Ubiquitin with K48R
Ub^{Cys}	Ubiquitin with G76C and K48R

Ub_{K48}^{Cys}	Ubiquitin with G76C
Ub^{P}	Ubiquitin with G76C (aka Ub_{K48}^{Cys})
Ub^{D}	Ubiquitin with K48R (aka Ub^{K48R})
UBA	Ubiquitin-associated domain
UBB^{+1}	Ubiquitin variant carrying 19 residue C-terminal extension

Ala (A)	Alanine
Arg (R)	Arginine
Asn (N)	Asparagine
Asp (D)	Aspartic acid
Cys (C)	Cysteine
Gln (Q)	Glutamine
Glu (E)	Glutamic acid
Gly (G)	Glycine
His (H)	Histidine
Ile (I)	Isoleucine
Leu (L)	Leucine
Lys (K)	Lysine
Met (M)	Methionine
Phe (F)	Phenylalanine
Pro (P)	Proline
Ser (S)	Serine
Thr (T)	Threonine
Trp (W)	Tryptophan
Tyr (Y)	Tyrosine
Val (V)	Valine

Chapter 1

Introduction

1.1 The Ubiquitination Pathway

The genetic code of all organisms is held within DNA used to synthesize proteins that are responsible for carrying out virtually all cellular processes. These proteins exist in a dynamic state where both protein synthesis and protein degradation are regulated to maintain a state of homeostasis within the cell (*1, 2*). A major mechanism of protein degradation has been attributed to the ubiquitin proteolysis pathway, which has been found to be responsible for the degradation of short-lived, damaged, misfolded or denatured proteins within the cell (*3*). The ubiquitin proteolysis pathway was primarily discovered through the results of a single scientific study in 1978 that eventually lead to the awarding of the 2004 Nobel prize in chemistry to Hershko, Ciechanover and Rose (*4*). Further studies identified and characterized the primary enzymatic components and function of this pathway (*5-11*).

The ubiquitination pathway focuses on the small, heat stable, 76-residue protein named ubiquitin (Ub). Ubiquitin is highly conserved in eukaryotes as only four amino acids differ among yeast, plant and animal sequences (*12, 13*). The ubiquitination pathway consists of three key enzymes that activate and transfer Ub onto a lysine residue in a target protein (Fig 1.1). Ubiquitin first associates non-covalently with a ubiquitin-activating enzyme (E1) and the C-terminal glycine (G76) of Ub is adenylated through an ATP-dependant reaction. This adenylated Ub molecule then reacts with the E1 enzyme's

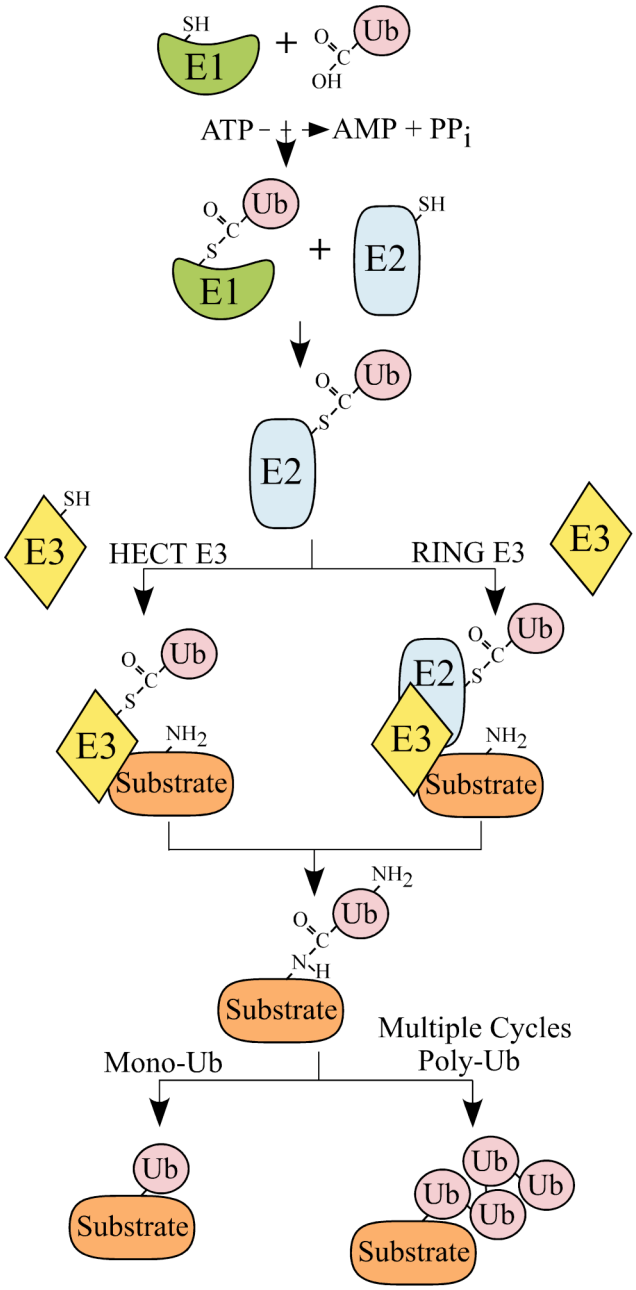

Figure 1.1 A schematic representation of the ubiquitination pathway. The ubiquitination pathway consists of three key enzymes, the E1 activating enzyme (green), the E2 conjugating enzyme (blue) and the E3 ligating enzyme (yellow) that activate and transfer Ub (pink) onto a lysine residue in a substrate (orange) protein. Chemical bonds are shown for the atoms representing the C-terminus of Ub (COOH), enzyme cysteine side chains (SH), and substrate or ubiquitin lysine side chains (NH_2). Thiolester bonds are formed on E1, E2 and E3 enzymes. Isopeptide bonds are created on Ub and substrate side chain lysines. Substrates undergo poly-ubiquitination through the interconnection of Ub lysine side chains with additional Ub molecules.

active site cysteine to covalently link Ub to the E1 enzyme through a reactive thiolester bond (Fig 1.1). The Ub is then transferred from the E1 active site cysteine to a ubiquitin-conjugating enzyme (E2) active site cysteine through a transthiolesterification reaction (Fig 1.1). A ubiquitin-ligating enzyme (E3) then binds simultaneously to a substrate protein and the E2 to transfer Ub to the ε-amino group of a lysine residue in a substrate. There are two major types of E3 enzymes, a RING (really interesting new gene) E3 aids in the transfer of Ub directly from the E2 enzyme onto the substrate, and a HECT (homologous to E6AP carboxyl terminus) E3 first forms a thiolester with Ub and then transfers Ub onto the substrate (Fig 1.1). The covalent linkage of Ub is converted from a reactive thiolester to a more stable isopeptide bond on the target substrate.

1.1.1 Poly-Ub chains

The ubiquitination pathway can result in the attachment of either a single Ub or multiple Ub molecules to a target protein (Fig 1.1). Multiple Ub molecules may be attached to substrates on several different lysine residues or by the creation of a poly-ubiquitin (poly-Ub) chain attached to a single lysine. Poly-Ub chains are formed by the connection of the C-terminus of one Ub to a lysine residue on another Ub creating an isopeptide bond resulting in a stable chain of interconnected Ub molecules. Ub contains seven lysine residues (K6, K11, K27, K29, K33, K48 and K63) and each lysine has been shown to participate in poly-Ub chain linkages, although K48, K63 and K11-linked poly-Ub chains are the most prominent (*14*). The type of poly-Ub chain linkage determines the biological function of the target substrate (*15, 16*). Proteins labelled with a single Ub have been identified to play roles in several cellular functions including protein sorting,

trafficking and processing, gene expression and silencing, and endocytosis (*15-17*). Proteins labelled with K63-linked poly-Ub chains have been linked to other non-proteolytic functions including DNA repair, kinase activation, protein trafficking, protein translation and endocytosis (*15, 16*). Proteins labeled with K11-linked poly-Ub chains have been linked to degradative and non-degradative roles within the cell (*18, 19*). Proteins labelled with K48-linked poly-Ub chains are the most prevalent form of ubiquitination. K48 poly-Ub chains composed of four or more Ub molecules are recognized by the 26S proteosome whereby the attached proteins are degraded and recycled by the cell (*20*). The poly-Ub chains are themselves are then dismantled back into single Ub molecules by deubiquitinases for the purpose of recycling Ub for further ubiquitination events (*21, 22*). The K48-linked poly-Ub degradation signal is the most common fate of ubiquitinated proteins within the cell. This ubiquitin proteolysis pathway will be the primary system studied in this work.

1.1.2 Substrate specificity

In humans, there are two known E1 enzymes, at least 35 E2 enzymes and over 1000 E3 ligases in the ubiquitination pathway (*23, 24*). Each E1 enzyme can interact with multiple E2 enzymes, and each E2 enzyme interacts with many different E3 enzymes. Substrate specificity within this pathway is partially determined by specific E2/E3 combinations but mostly by unique E3/substrate interactions (*25*). Substrate specificity is therefore driven by substrate-specific protein binding domains located in each E3 ligase. These various E2/E3 combinations allows for the specific regulation of

certain substrates during different cellular cycles and stresses to maintain cellular protein homeostasis.

1.1.3 Ubiquitin-like proteins

Following the discovery of the ubiquitin proteolysis pathway, many ubiquitin-like (Ubl) proteins have been identified. The Ubl proteins all contain a similar structure to that of Ub and function by an analogous enzyme cascade of E1, E2, and E3 enzymes that covalently attach Ubl proteins to lysine residues of specific substrate proteins (*26, 27*). Ubl conjugations do not primarily result in degradation of substrates, but rather act by regulating a wide variety of cellular functions (*27*). The Ub and Ubl pathways encompass a massive amount of regulatory control within the cell resulting in a large amount of research in this area in the recent decade. The two most well studied Ubl proteins are SUMO (small ubiquitin-like modifier) and NEDD8 (neural precursor cell-expressed developmentally downregulated-8). NEDD8 is the most similar Ubl to Ub sharing 60% sequence identity (*28*). NEDD8 is activated by the heterodimeric E1 Uba3-Ula1 and is conjugated by the E2 enzyme Ubc12 (*29*). SUMO is activated by the heterodimeric E1 Uba2-Aos1 and is conjugated by the E2 enzyme Ubc9 (*28*). Many other identified Ubl proteins include FAT10, ISG15, LC3, ATG12, UFM1, and URM1. These Ubl proteins are just beginning to be understood and have been linked to many highly divergent functions (*27*). Cross-talk between the Ub and Ubl pathways can be performed in many ways including multiple modifications of a single substrate such as tumor suppressor p53 that can be modified with Ub, NEDD8, SUMO and FAT10 (*28*). Cross-talk is also observed for the SUMO modification of the E2 enzyme HIP2 that

inhibits its function in the ubiquitination pathway (*30*). Due to the highly analogous enzyme cascades in the Ub and Ubl pathways, structural studies of NEDD8 and SUMO related enzymes have provided valuable insight into the function of Ub related enzymes. The structural knowledge acquired from Ubl pathways has greatly advanced the proposals for functional mechanisms utilized in the ubiquitin proteolysis pathway.

1.2 Diseases Related to Ubiquitination

Malfunction of the ubiquitination proteolysis pathway can result in many different diseases. The unwanted accumulation and aggregation of ubiquitinated proteins into inclusion bodies (large protein aggregates) is the hallmark of many neurodegenerative diseases. Ubiquitination has also been linked to several forms of cancer as well as muscle wasting disorders, and inflammatory diseases. Due to the wide variety of enzyme functions related to the ubiquitination pathway, the list of diseases known to be affected by ubiquitination is expected to rise significantly as more studies in this field are performed.

1.2.1 Neurodegenerative Diseases

The most prominent diseases linked to ubiquitination are neurodegenerative diseases including Alzheimer's disease, Parkinson's disease and polyglutamine disorders such as Huntington's disease and spinocerebellar ataxias (*31*). Alzheimer's disease is involved in progressive memory loss and is characterized by extracellular plaques that are composed of misfolded and aggregated amyloid β peptides (Aβ). Alzheimer's disease

has been linked to ubiquitination through the incorporation of the ubiquitin variant UBB^{+1} (*32*), reduced proteosomal activity (*33*), mutated ubiquitin hydrolyases (*34*), and the effect of specific E3 ubiquitin ligases (*35*). The UBB^{+1} Ub variant contains a C-terminal extension that does not allow thiolester formation and is therefore a non-functional Ub molecule. However, the UBB^{+1} is recognized as a substrate and is poly-ubiquitinated itself. This UBB^{+1} capped poly-Ub chain is resistant to disassembly by deubiquitinating enzymes and correspondingly inhibits the 26S proteosome (*36*). Autosomal recessive juvenile parkinsonism (ARJP) is an early-onset form of Parkinson's disease and has been shown to be caused by mutations in the protein parkin (*37*). The parkin protein was later identified to be a RING E3 ligase, and disease causing mutations result in the accumulation of parkin's substrate proteins (*38, 39*). Polyglutamine disorders including Huntington's disease and spinocerebellar ataxias are neurodegenerative diseases that are biochemically identified by intracellular inclusion bodies that contain ubiquitinated proteins (*31*). The polyglutamine region of the protein huntingtin is expanded in Huntington's disease and aggregates into these inclusion bodies. The biological function of wild type huntingtin remains poorly defined, however, huntingtin is associated with the ubiquitination pathway as mutant huntingtin is found to be ubiquitinated in vivo and has been shown to interact with the E2 enzyme HIP2 presumably responsible for this ubiquitination (*40*). Mutant huntingtin overexpression was also observed to inhibit proteosomal activity (*41*). All of these neurodegenerative diseases result in lower 26S proteosome levels and activity indicating that aberration in the proteolysis pathway is critical in all neurodegenerative diseases (*42-44*). Large protein aggregate formation in these diseases appears to be for the purpose of avoiding

the toxic effect of the accumulation of soluble ubiquitinated proteins and the aggregation is a way to handle these non-degradable proteins (*45*). The true nature of toxicity in these diseases is still poorly understood.

1.2.2 Cancers

Human Papillomaviruses (HPV's) exist in many different subtypes, some of which produce oncoproteins E6 and E7 that interact with tumor suppressor protein p53 and the retinoblastoma susceptibility protein Rb respectively (*31*). Interaction of the HPV oncoprotein E7 with Rb promotes the ubiquitination and degradation of Rb (*46*). Rb normally interacts inhibits growth promoting E2F transcription factors, and thus degradation of Rb promotes cell growth leading to cancer (*47*). The E6 protein binds to the E3 ligase E6AP and this complex then interacts with p53 promoting its ubiquitination and degradation (*48*). The p53 protein acts as a tumor suppressor by arresting cellular proliferation, inducing repair mechanisms and in extreme stress induces apoptosis. Regulation of p53 is normally achieved through ubiquitination by the E3 ligase Mdm2. The design of a chemical inhibitor (nutlin) for Mdm2 can result in extended p53 function by minimizing its degradation resulting in longer cell cycle arrest and increased apoptosis of tumor cells in various cancers (*49*).

During oxygen shortage (hypoxia) a transcription factor called hypoxia inducible factor (HIF-1α) promotes the synthesis of proteins important in red blood cell creation and angiogenesis. HIF-1α is normally an unstable protein with a half life in cells of less than 10 minutes and is ubiquitinated and degraded by the E3 ligase VCB-Cul2 complex (*31*). A component of the VCB-cul2 complex, pVHL, is a tumor suppressor that is

mutated in almost all renal cancers allowing HIF-1α to be constantly active promoting tumor formation (*50*).

1.3 The E1, E2 and E3 Enzyme Cascade

1.3.1 E1 activating enzyme

The initial enzyme utilized in ubiquitination is the E1 activating enzyme. The E1 activating enzymes are large proteins (~110-120 kDa) that initially bind Ub non-covalently and adenylate the C-terminus of Ub through ATP hydrolysis. The E1 activating enzyme uses a second domain that contains an active site cysteine to perform a nucleophilic reaction with the adenylated Ub moiety to create a reactive thiolester bond (*51*). After formation of an E1~Ub thiolester, the E1 activating enzyme binds to an E2 conjugating enzyme and through a transthiolesterification reaction transfers the Ub to a cysteine residue at the active site on the E2. There are two human E1 activation enzymes, Uba1 and Uba6, that activate Ub molecules and both of these enzymes interact with a different set of E2 conjugating enzymes allowing for increased specificity in the ubiquitination pathway (*23, 52*). The crystal structure of the yeast Uba1 E1 activating enzyme allows for further insights into how this enzyme functions (Fig 1.2A) (*51*). The yeast Uba1 shares 50% sequence identity to the human Uba1, indicating these enzymes are likely to function similarly (*51*). The E1 activating enzyme can be divided into several functional domains (Fig 1.2A). The core of E1 houses the adenylation domain (AD) that binds ATP and Ub and assists in the adenylation of the C-terminus of Ub. The N-terminal region of E1 contains the first and second catalytic cysteine half

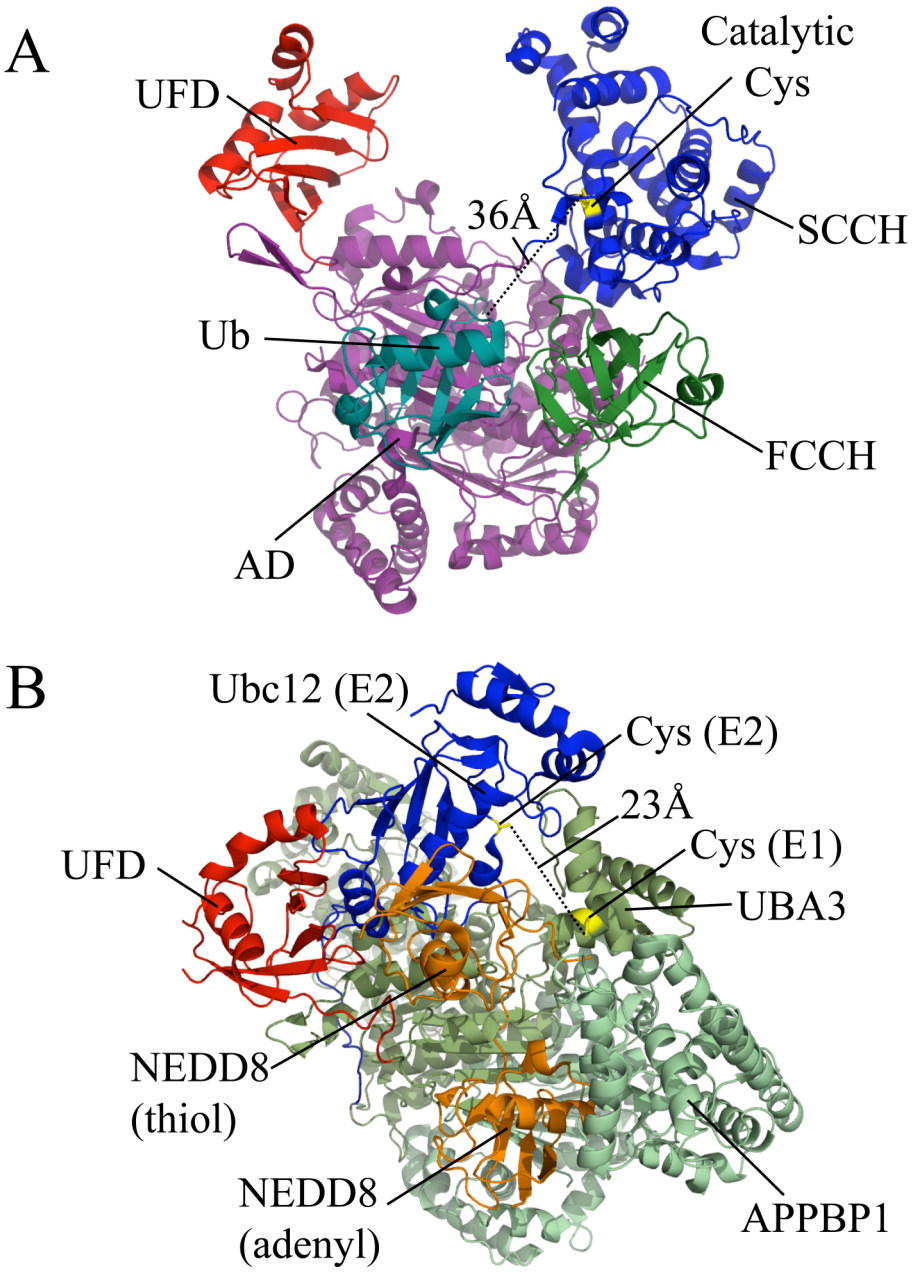

Figure 1.2 Structures of E1 activating enzymes. (**A**) The crystal structure for the *S. cerevisiae* Uba1 E1 activating enzyme (PDB: 3CMM). Different domains have been coloured differently to show the division of functional units within the enzyme where the adenylation domain (AD - purple) binds Ub (teal) non-covalently for adenylation, the first and second catalytic half domains (FCCH - green, SCCH - blue) contain the active cysteine used for creation of the E1~Ub thiolester, and the ubiquitin fold domain (UFD – red) is responsible for E2 binding. (**B**) The crystal structure of the human NEDD8 E1 heterodimer APPBP1-Uba3 (PDB: 2NVU) demonstrates how NEDD8 can be transferred onto the E2 enzyme. The E1 heterodimer APPBP1-Uba3 (2 shades of green) interacts with two NEDD8 (orange) molecules, one on the adenylation site and one through a thiolester linkage. The UFD (red) is rotated compared to (**A**) showing that UFD movement occurs upon Ubc12 (blue) E2 enzyme binding. The active site cysteine side chains (yellow) are the site of thiolester formation with Ub or Ubl proteins.

domains (FCCH and SCCH) responsible for housing the E1 active site cysteine for Ub thiolester bond formation. The C-terminal region of E1 contains the Ub fold domain (UFD) that binds to E2 conjugating enzymes to assist a transthiolesterification reaction to transfer Ub from an E1~Ub thiolester to an E2~Ub thiolester (*51*). The E1 enzyme can bind 2 Ub molecules at the same time, one on the active site cysteine and another on the adenylation domain. The method by which adenylated Ub is transferred onto the E1 active site cysteine is not obvious as there is a 36 Å separation between the cysteine side chain and the adenylated Ub C-terminus in this structure (Fig 1.2A). Experimental studies on the SUMO E1 activating enzyme have shown that adenylated SUMO is transferred to the catalytic cysteine domain (equivalent to FCCH/SCCH in Uba1) through allosteric changes and a rotation of this domain bringing the catalytic cysteine into close contact with the SUMO C-terminus (*53*). These allosteric changes are also expected to occur in the FCCH/SCCH domain of Uba1 to move adenylated Ub onto the catalytic site (*53*). Insights into the position of the E2 conjugating enzyme in relation to the E1 enzyme were elucidated through experimentation on the NEDD8 heterodimeric E1 activating enzyme APPBP1-Uba3 in complex with the NEDD8 E2 Ubc12 (Fig 1.2B) (*54*). In this E1/E2/NEDD8/NEDD8 quaternary structure, both thiolester linked and adenylated NEDD8 protein are represented and a rotation of the UFD domain is required to position the E2 enzyme's catalytic cysteine into close proximity (23 Å) with the E1 enzyme's catalytic cysteine. It is expected that a further rotation of the UFD domain will position the active sites of the E1 and E2 enzymes to within 5 Å allowing for a transthiolesterification transfer reaction to occur to form the E2~Ub thiolester (Fig 1.2B). The importance of a rotation in the UFD domain of Uba1 was shown through proline

mutations in the flexible linker that impaired thiolester transfer from E1 to E2 enzymes indicating the Ub E1 functions similarly to the NEDD8 E1 (*51*). The Uba1 enzyme also shows nanomolar affinity for E2 enzymes when it is dually loaded with Ub and has much weaker affinity for the E2 in the absence of ATP and Ub (*51*). These affinity changes on the E1 enzyme indicate that E2 enzymes bind to the E1 to accept Ub and then dissociate from the E1 once the E2~Ub thiolester has formed. This bind and release action likely allows the Ub E1 enzyme to efficiently charge a wide variety of Ub E2 conjugating enzymes.

1.3.2 E2 conjugating enzymes

The E2 conjugating enzyme is the central enzyme in the ubiquitination pathway. The E2 enzyme first interacts with the E1~Ub thiolester and Ub is transferred to the E2 enzyme to form the E2~Ub thiolester intermediate. The E2~Ub thiolester then interacts with an E3 ligase and transfers Ub to the E3 enzyme and then onto the substrate or directly onto a substrate. There are at least 35 E2 enzymes in the human proteome, 30 of which are known to directly activate Ub in the ubiquitination pathway (*24*). These E2 conjugating enzymes all contain an ~150 residue structurally conserved catalytic core domain (*55*). This catalytic core domain is found in all E2 enzymes and consists of 4 β-strands that make up an anti-parallel β-sheet, 4 α-helices, and a very short 3_{10} helix immediately following the active site cysteine (Fig 1.3A) (*55*). Many E2 enzymes also contain a highly conserved HPN motif about 7-8 residues upstream of the conserved catalytic cysteine at the active site (*56*). The conserved catalytic cysteine is utilized to form a thiolester with the C-terminus of Ub. The asparagine within the HPN motif has

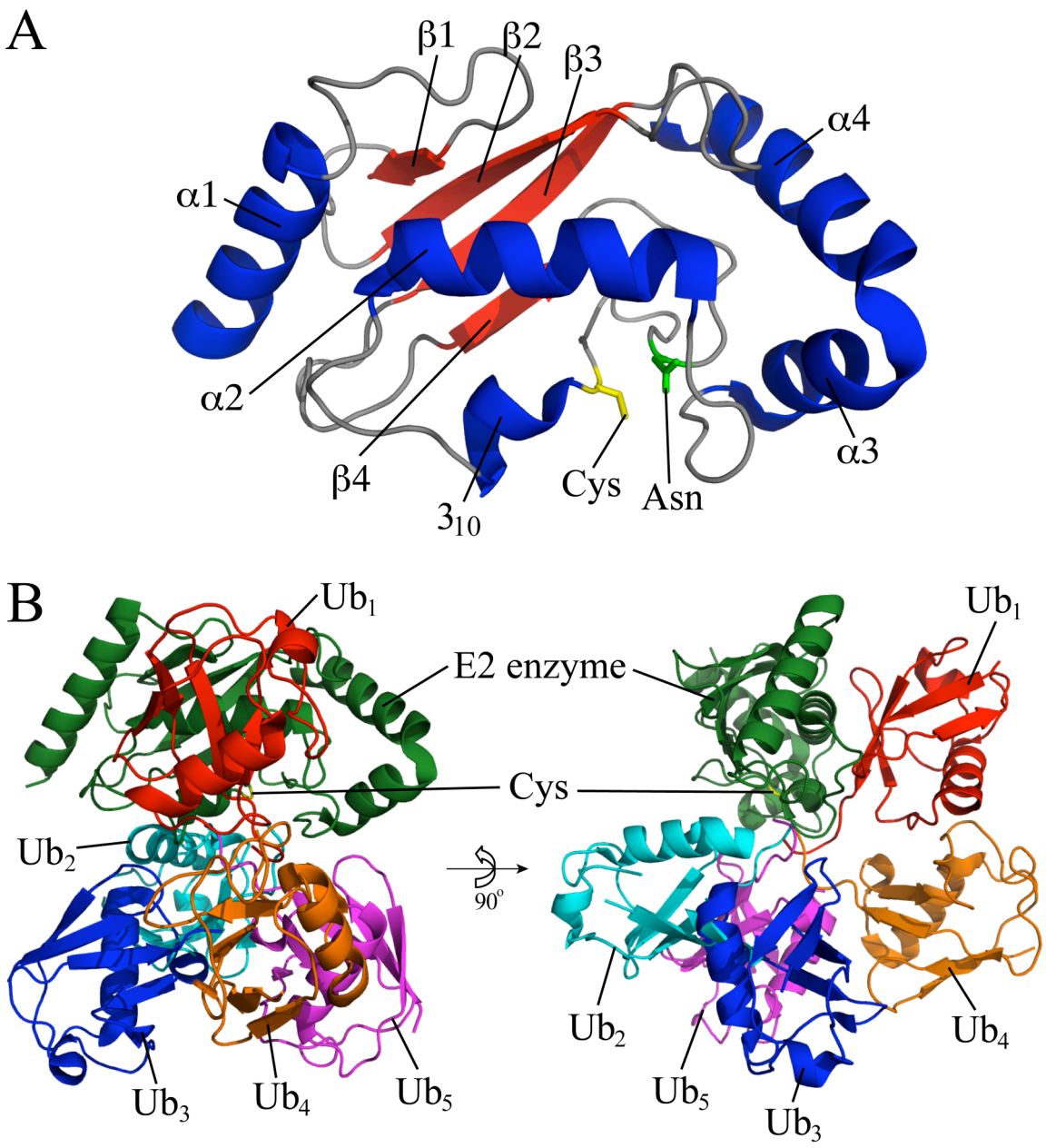

Figure 1.3 General structure of E2 conjugating enzymes and E2~Ub thiolesters. (**A**) The crystal structure for human UbcH5a (PDB: 2C4P) illustrates the general structure of all E2 enzymes. The structurally conserved catalytic core domain of E2 enzymes consists of 4 β-strands that make up an anti-parallel β-sheet, 4 α-helices, a very short 3_{10} helix, and the active site is centered around the conserved active site cysteine (yellow) and oxyanion hole stabilizing asparagine (green). (**B**) The structural alignment and overlay of five E2~Ub thiolesters demonstrates the variation of reported Ub positions in relation to the catalytic core domain. For clarity only the UbcH5b (green) catalytic core is shown while the Ub is positioned and coloured differently for each E2~Ub thiolester: Ubc1~Ub (PDB: 1FXT - red), UbcH5b~Ub (PDB: 3A33 - cyan), Ubc13~Ub (PDB: 2GMI - blue), UbcH5b~Ub (PDB: 3JVZ - orange), and UbcH8~Ub (PDB: 2KJH - magenta) are labelled Ub_1, Ub_2, Ub_3, Ub_4 and Ub_5 respectively.

been proposed to stabilize an oxyanion intermediate of the E2~Ub thiolester to aid in the preceding nucleophilic attack of a lysine side chain on a substrate (*56-58*). The function of the histidine in the HPN motif remains unknown, although it could be used to aid the catalytic activity of the asparagine or be involved in protein stability (*56, 59*).

Although the structures of these E2 enzymes are highly conserved, there are very few highly conserved residues within these proteins providing a large diversity between E2 enzyme surface residues (*59*). The electrostatic properties of E2 enzymes have also been shown to vary widely based on significantly different surface charges (*60, 61*). These variations in residues and electrostatics may facilitate specific interactions for each individual E2 enzyme. An added variation of E2 enzymes includes additional N-terminal and C-terminal protein extensions to the catalytic core domain, and these can be sub-categorized into 4 classes. Class I E2 enzymes contain only the catalytic core (Fig 1.3A) (*62*). Class II, III and IV E2 enzymes contain a C-terminal extension, a N-terminal extension, and both C-terminal and N-terminal extensions respectively (*62*). These extensions form unstructured and structured protein domains of various sizes and provide additional protein interaction surfaces to modulate the specific functions of individual E2 enzymes.

The E2 enzyme must interact with both the E1 and E3 enzymes to carry out Ub transfer. The E2 enzyme utilizes its N-terminal α1 helix and loop between β1 and β2 to contact the E1 enzymes UFD domain (*63*). The E2 enzyme also utilizes its N-terminal α1 helix, loop between β3 and β4, and loop between the 3_{10} helix and α2 to contact E3 enzymes (*64*). These interaction regions on the E2 enzyme for E1 and E3 involve overlapping surfaces. E2 enzymes have been shown to bind either the E1 or E3, but not

both simultaneously, indicating that the E1-E2-E3 ubiquitination pathway is a stepwise cascade reaction as opposed to a large protein complex (*65*). This fact also indicates that the E2 enzyme is in a constant state of association and dissociation with its E1 and E3 interacting partners (*65*).

1.3.3 The E2~Ub thiolester and stable intermediate

The E2~Ub reactive intermediate represents an active 'charged' conjugating enzyme. Most structural knowledge of E2 enzymes has been accumulated on free E2 enzymes as the E2~Ub thiolester is highly reactive and unstable, making its purification and characterization difficult. Experimental study of the E2~Ub reactive intermediate is vital towards advancing knowledge in this pathway as it is predicted that most E2 enzymes are usually found in the active E2~Ub state *in vivo* and therefore the E2~Ub thiolesters are more likely to be recognized by interacting proteins than E2 enzymes alone (*66*). Two different types of stable E2-Ub thiolester mimic complexes have been produced to study the E2~Ub thiolester intermediate. The first E2-Ub complex can be formed by an E2 active site cysteine to serine mutation that results in a longer lived ester bond (*67*). The second E2-Ub complex can be formed by a Ub C-terminal glycine to cysteine mutation that can be used to form a stable disulphide bond with the active site cysteine of the E2 enzyme (*68*). There are currently 5 structures of E2-Ub intermediate complexes including Ubc1~Ub (*69*), UbcH8-Ub (*70*), Ubc13-Ub (*67*), and two UbcH5b-Ub structures (*71, 72*). The alignment and overlay of these 5 structures illustrates the varying reported positions of Ub in these different E2~Ub structures (Fig 1.3B). The covalent attachment of Ub to the E2 enzyme does not result in any significant

conformational changes in either protein, which indicates that the mere placement of Ub onto the E2 enzyme is responsible for alterations in protein interactions (*55*). The structure of the Ubc1~Ub thiolester (truncated Ubc1) was produced through NMR studies where the unstable short lived Ubc1~Ub thiolester was produced in situ and the observed interactions between Ubc1 and Ub allowed the structure of this thiolester to be modelled (Fig 1.3B – Ub_1/red) (*69*). The UbcH8-Ub disulphide complex was also solved using NMR and the Ub position on the E2 enzyme was found to be much different to that of Ubc1~Ub (Fig 1.3B – Ub_5/magenta) (*70*). Additionally, crystal structures of Ubc13-Ub and two UbcH5b-Ub ester complexes also place Ub in several different positions. These crystal structures make some contact with neighbouring molecules within the crystal lattice allowing for the possibility that the Ub position may be affected by these contacts (Fig 1.3B – Ub_2/cyan, Ub_3/blue, Ub_4/orange) (*67, 71, 72*). Taken together these structures all adopt significantly different positions for Ub in their E2~Ub thiolesters (Fig 1.3B). The various positions for Ub on different E2 enzymes can affect access to the reactive thiolester and expose or block different surfaces of the E2~Ub, which may affect reactivity in regards to interactions with E3 enzymes and substrates, although this has not yet been well investigated (*70, 73*). The variation in Ub positioning between these structures also supports recent experimental evidence that the E2-Ub intermediate may be highly dynamic and mobile (*74*). This would indicate that the observed Ub positions in these E2-Ub structures may be 'snap shots' or predominant species of a mobile Ub molecule (Fig 1.3B). Further studies on E2-Ub intermediate complexes are required to fully understand the dynamics and effects of Ub placement within E2~Ub thiolesters.

The E2~Ub thiolester also affects protein affinities to drive the E1-E2-E3 enzyme cascade. This is observed as unconjugated E2 enzymes strongly bind E1 enzymes and upon formation of the E2~Ub thiolester, these enzymes preferably dissociate (*51*). Recent studies have shown that certain E2~Ub species have increased affinity for E3 enzymes over the free E2 enzyme (*72, 75*) (Dr Spratt personal communication). The E2~Ub would then enhance interaction with E3 enzymes and after transfer the E2 enzyme may preferably dissociate to recharge on the E1 enzyme. A fixed or mobile position of Ub in the E2~Ub thiolester may or may not affect these interactions. More experimentation on affinity of E2~Ub versus free E2 enzymes is required to clarify association and dissociation within the E1-E2-E3 enzyme cascade.

1.3.4 E3 ligating enzymes

The E3 ligases are the final enzyme in the ubiquitination pathway responsible for the selective binding of substrates and E2 enzymes to assist transfer of the thiolester linked Ub onto a substrate. The thiolester linked Ub is converted to a stable isopeptide bond when the C-terminus of Ub is linked to the ε-amino group of a lysine residue in a substrate. There are more than 1000 E3 ligases and substrate specificity is accomplished by each E3 ligase having a different set of substrates allowing for differential regulation of various proteins within the cell (*24*). E3 ligases can be distinguished by their enzymatic function and fall into two major categories, the HECT (homologous to E6AP carboxyl terminus) E3 ligases and RING (really interesting new gene) E3 ligases. More than 95% of all known human E3 enzymes are RING E3 ligases (*76*). HECT E3 ligases contain a conserved active site cysteine used for the transfer of Ub from the E2~Ub

thiolester to make an E3~Ub thiolester prior to reaction with an E3 bound substrate lysine residue. The RING E3 ligase does not contain an active site cysteine, but rather works as a scaffold in substrate ubiquitination by placing the E2~Ub thiolester in close proximity to a substrate to aid Ub transfer.

Structural knowledge of E2 enzyme interactions with E3 ligases is aided by the crystal structure of the E2 enzyme UbcH7 interacting with the E6AP (human papillomavirus E6 associated protein) E3 ligase HECT domain (Fig 1.4A) (*77*). The E6AP HECT domain contains an N-terminal region (N-lobe) that binds the E2 enzyme, and a C-terminal region (C-lobe) that contains the conserved cysteine residue responsible for thiolester formation (Fig 1.4A). This UbcH7/E6AP structure indicates that a 41 Å distance exists between the E2 and HECT E3 active site cysteine residues (Fig 1.4A). Additional structures of other HECT E3 ligases have shown that the C-lobe can adopt alternative positions due to a flexible linker that can result in the reduction in this spatial gap between cysteine residues (*78*). This was confirmed with the structure of UbcH5b~Ub with the Nedd4L HECT E3, which illustrates a significantly moved C-lobe placing the E3 catalytic cysteine within 8 Å of the thiolester bound Ub C-terminus (Fig 1.4B) (*72*). This structure shows that movement of the C-lobe of the HECT domain is required for Ub transfer from the E2 to the E3. Contacts between the E2 attached Ub moiety and the C-lobe stabilize the movement of the C-lobe to aid in Ub transfer (*72*).

Structural knowledge of E2 enzyme interactions with RING E3 ligases is revealed by the crystal structure of c-Cbl (casitas B-lineage lymphoma) RING E3 ligase in complex with the E2 enzyme UbcH7 and a substrate peptide (Fig 1.4C) (*64*). The c-Cbl RING E3 associates with the E2 enzyme UbcH7 through its zinc-stabilized RING domain

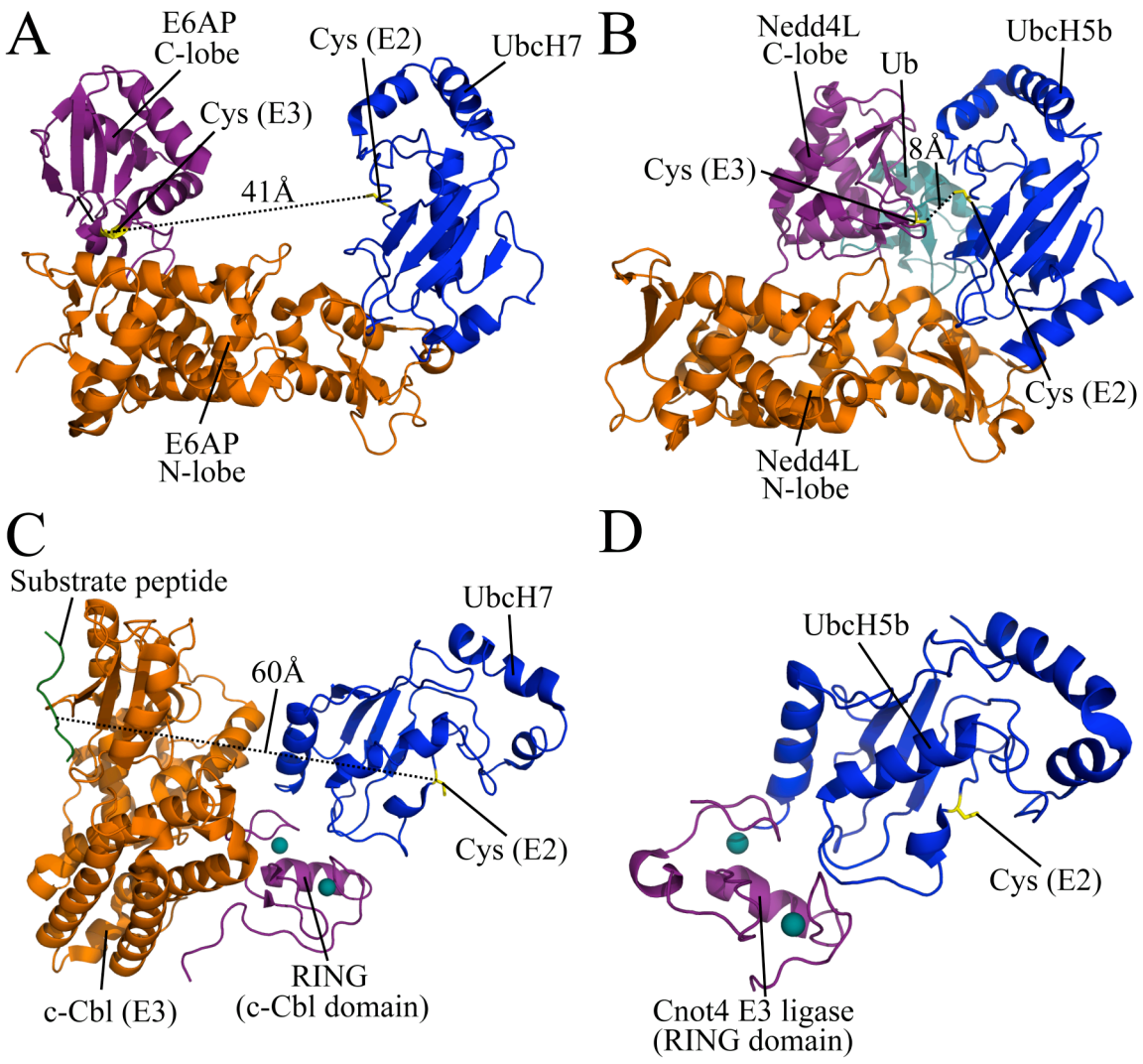

Figure 1.4 Structures of a several E2/E3 enzyme complexes. (**A**) The crystal structure of UbcH7-E6AP (PDB: 1C4Z) and (**B**) UbcH5b~Ub-Nedd4L (PDB: 3JVZ) illustrate the binding of an E2 (UbcH7 - blue) and E2~Ub (UbcH5b~Ub – blue ~ teal) thiolester to the HECT E3 ligases E6AP and Nedd4L respectively. The HECT domain is divided into 2 lobes, the N-lobe (orange) and C-lobe (purple). Movement of the C-lobe details the allosteric changes required to position the E2 and E3 active site cysteine residues (yellow) into close proximity. (**C**) The crystal structure of ZAP-70/c-Cbl/UbcH7 (PDB: 1FBV) illustrates the interaction between the RING domain (purple) of the E3 c-Cbl (orange) interacting with the E2 UbcH7 (blue). There is a large distance between the E2 active site (yellow) and the substrate peptide ZAP-70. (**D**) The crystal structure of UbcH5b (blue) and Cnot4 RING domain (purple) illustrates the common interface between RING domains and the N-terminal region of the E2 enzyme (PDB: 1UR6). The RING domains are structurally stabilized by two Zn^{2+} ions (teal spheres).

(Fig 1.4C). RING domains contain a highly conserved C_3HC_4 motif that coordinates two zinc ions to stabilize its structure (*79*). RING E3 ligases utilize the RING domain to bind the E2 enzyme's N-terminal α1 helix as well as several loops near the N-terminus (Fig 1.4C). The UbcH7/c-Cbl complex is one of very few solved E2/RING E3 structures. Other solved E2/E3 RING structures include UbcH5b/Cnot4 RING E3 (Fig 1.4D), Ubc13/TRAF6 RING E3, and UBE2D1/IDOL RING E3, which show very similar protein interaction surfaces are utilized in all reported E2/RING E3 structures (*80-82*). E3 ligases incorporate many other protein binding domains for the purpose of binding substrates and recruiting other proteins required for larger functional E3 complexes (*79*). The UbcH7/c-Cbl complex also includes a peptide from the ZAP-70 protein kinase, a known ubiquitinated substrate of this E2/E3 complex (Fig 1.4C) (*64*). The distance from the E2 enzyme active site's bound Ub thiolester to the ZAP-70 substrate is 60 Å. A similar large spatial gap has been observed between an E2~Ub thiolester and substrate in the large E3 RING ligase containing SCF complexes (*83*). The mechanism utilized by these enzymes for bridging this spatial gap is still under investigation, although it is likely that some allosteric change in the E3 enzyme or protein interactors is required to allow substrate ubiquitination. There are currently no structural details that show how Ub is transferred from the E2~Ub thiolester directly to a substrate.

1.4 Formation of Poly-Ub Chains

Structural knowledge acquired from E1, E2 and E3 enzymes in various complexes has illustrated the general mechanisms utilized to activate and transfer Ub onto the E2 and E3 enzymes. Additional structures of E2~Ub/RING-E3/substrate or HECT-

E3~Ub/substrate are required to clarify how the thiolester linked Ub is directly transferred to an ε-amino group on a substrate lysine residue. It is expected that conformational changes in E3 enzymes are required to transfer Ub onto substrates. The general mechanism of Ub activation and transfer onto substrates has been developed from these various E1, E2 and E3 structures, however, the mechanism by which these enzymes interconnect Ub molecules into poly-Ub chains remains very poorly understood.

1.4.1 Proposed Poly-Ub chain formation mechanisms

Several mechanisms have been proposed to explain how the ubiquitination pathway enzymes position Ub molecules for the creation of various Ub-Ub linkages found in poly-Ub chains (*84, 85*). The simplest proposed mechanism for poly-Ub chain formation is the sequential addition model. In this model, the substrate lysine reacts with the first Ub and subsequent Ub additions are attached to the lysine residues on Ub itself, thus creating a chain sequentially (Fig 1.5A). The logical complication with this mechanism is that the site of attachment of each new ubiquitin molecule becomes more remote as the chain extends, presumably making the required nucleophilic attack from each Ub lysine's ε-amino group less probable. Alternative methods for poly-Ub chain formation are supported by experimentation on many E2 and E3 enzymes that show poly-Ub chains can be produced prior to interaction with substrates. These results suggest poly-Ub chains may not be constructed on the substrate but rather preassembled

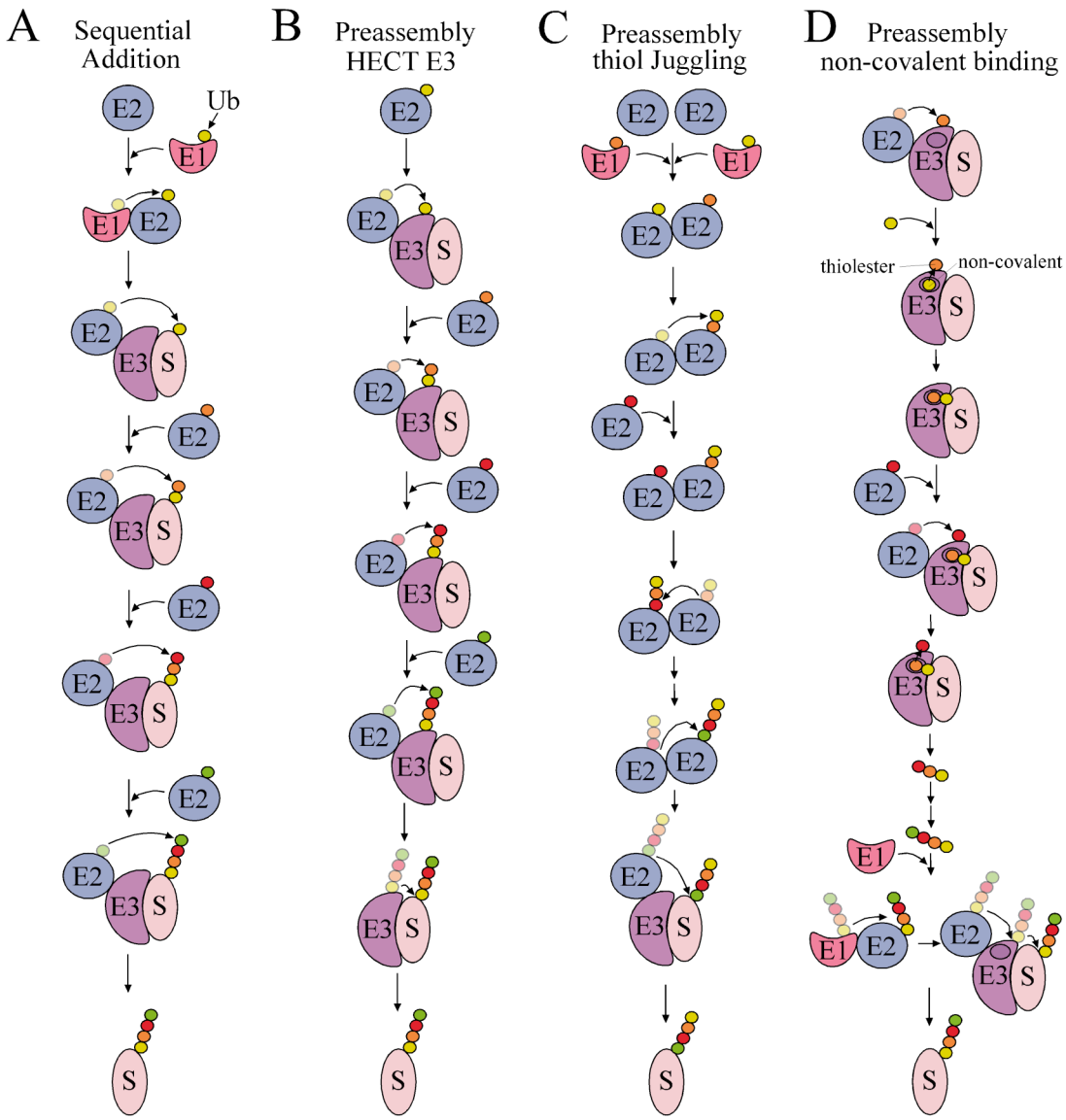

Figure 1.5 Schematic representation of several proposed mechanisms for the formation of poly-Ub chains. Ub molecules (yellow, orange, red and green) are depicted by small coloured circles. (**A**) The sequential addition model involves Ub added one at a time to first the substrate and then lysine side chains of Ub itself. (**B**) Preassembly of chains on the HECT E3 enzyme is performed like the sequential addition model only the chain is built on the E3 enzyme and then transferred onto the substrate. (**C**) A thiolester attached juggling model suggests an E2/E2 dimer allows for chains to be built on the E2 enzyme. In this model, both Ub molecules are thiolester bound and proper Ub positioning would allow one Ub to act as an acceptor and the other to act as a donor. In this manner chains extend on the proximal side of the growing chain. A similar juggling model can be performed using an E2/E3 HECT pairing. (**D**) Preassembly of chains may also require non-covalent binding of an acceptor Ub to be positioned so its lysine side chain can react with a thiolester bound Ub donor. In this model, a HECT E3 is depicted to have both the active site thiolester and non-covalent binding site for Ub. This model could also be replaced with any combination of E2 monomer, E2/E2, or E2/E3 complex where a non-covalently connected Ub acceptor can be positioned for reaction with an E2 or E3 thiolester bound Ub donor.

prior to attachment to substrate. One mechanism to preassemble poly-Ub chains would be similar to the sequential addition model except that poly-Ub chains would be built on a HECT E3 ligase and then transferred in a single step onto the substrate (Fig 1.5B). This mechanism would require an E2~Ub/E3~Ub interaction that would position the two thiolester bound Ub molecules in an orientation such that a lysine side chain of the E3~Ub could react with the E2~Ub reactive thiolester to yield E3~Ub_2. In this process the chain extends via multiple charging of the E2 enzyme. Another mechanism to preassemble poly-Ub chains would require an E2-E2 dimer to positions two Ub molecules such that one E2~Ub lysine can react with the thiolester of a second E2~Ub (Fig 1.5C). In this process the chain extends via multiple charging of the E2 enzymes, and a back and forth juggling of the thiolester attached proximally extending poly-Ub chain. Alternative mechanisms of poly-Ub chain preassembly may also utilize non-covalent Ub interacting surfaces on either the E2 or E3 enzyme (Fig 1.5D). These mechanisms would be driven by the positioning of a non-covalently bound Ub within reactive distance to a thiolester bound Ub on either the E2 or E3 enzymes. The model depicted in Figure 1.5D could also be replaced with any combination of E2 monomer, E2/E2 complex, or E2/E3 complex where a non-covalently connected Ub acceptor can be positioned for reaction with an E2 or E3 thiolester bound Ub donor. These preassembled poly-Ub chain mechanisms all require the placement of two Ub molecules in close proximity to allow one Ub's lysine ε-amino side chain to react with the C-terminus of a thiolester bound Ub to create a stable isopeptide bond. More detailed experimentation is required to clarify how poly-Ub chains can be created in the ubiquitination pathway.

1.4.2 K63 poly-Ub chain formation

The only well defined structural model showing poly-Ub chain formation involves the Ubc13/Mms2 complex responsible for the production of K63-linked poly-Ub chains (*73*). Ubc13 is an 'active' E2 conjugating enzyme that contains an active site cysteine utilized to form a Ubc13~Ub thiolester. Mms2 is a ubiquitin conjugating enzyme variant that is an 'inactive' E2 paralogue that shares significant sequence similarity with E2 enzymes but does not contain an active site cysteine. The Mms2 protein does not form a thiolester bond with Ub, but rather forms a non-covalent bond with free Ub in solution (*86*). Ubc13 interacts with Mms2 and the crystal structure of the Ubc13/Mms2 can be combined with the NMR modelled non-covalent Mms2/Ub structure and the Ubc1~Ub thiolester structure to place both Ub molecules on this E2 heterodimer such that the K63 side chain of the Mms2 bound Ub comes into close proximity of the C-terminus of the Ubc13~Ub thiolester (Fig 1.6) (*67, 69, 73, 87, 88*). This model constructed from three PDB files contains a 12 Å reaction distance between one Ub's K63 lysine and the thiolester Ub C-terminus, but another NMR modeled version of this same structure indicates the reactive distance to be ~3 Å (*73*). This model directly shows how one Ub can be reacted with a second Ub to create a K63-linked diubiquitin (Ub_2) molecule in the absence of an E3 enzyme or substrate. Cycles of this reaction presumably explain how longer K63-linked poly-Ub chains are created by the Ubc13/Mms2 E2 heterodimer (*67*). The method utilized to build these chains is a mixture of the mechanisms depicted in Figure 1.5C and 1.5D, where an E2 dimer is used to position the non-covalently bound Ub to react with the thiolester bound Ub for poly-

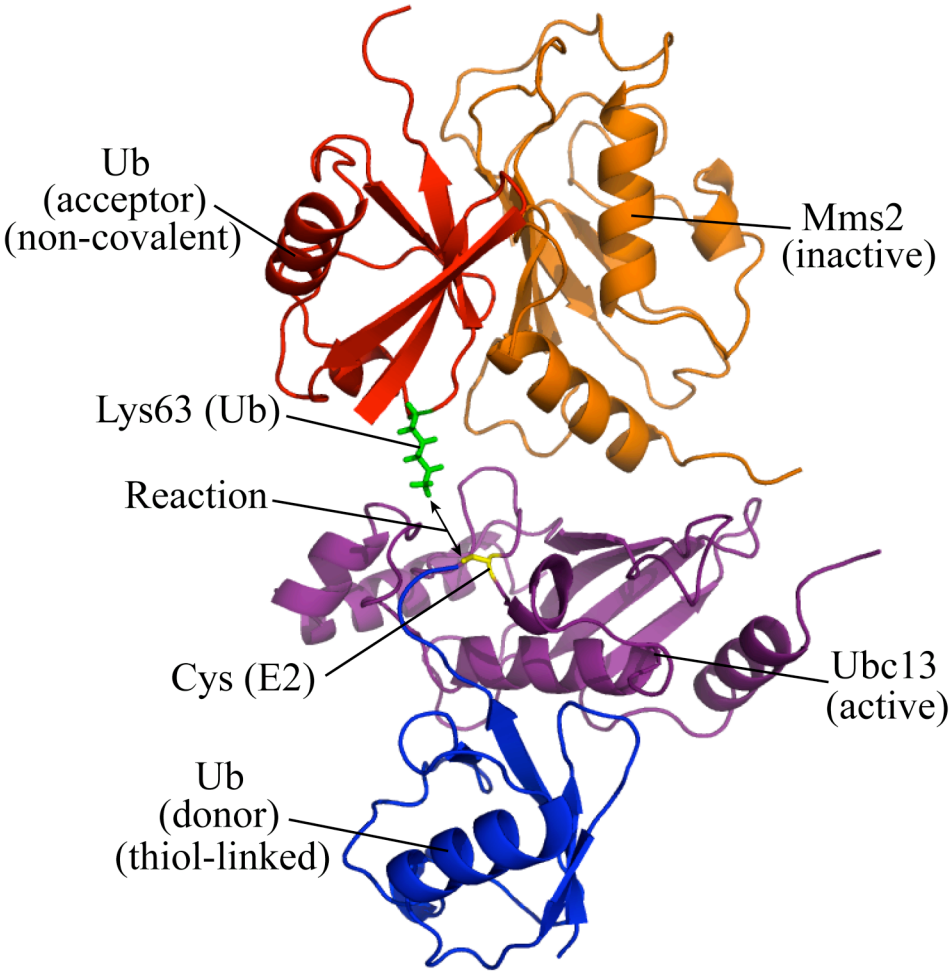

Figure 1.6 The human E2 heterodimer Ubc13/Mms2 structurally illustrates the mechanism for K63-linked poly-Ub chain formation. This four protein complex is composed of the Ubc13 (purple) and Mms2 (orange) which were crystallized in complex (PDB: 1J7D), aligned with the thiolester connected Ub (blue) positioned from Ubc1~Ub (PDB: 1FXT) and the non-covalent interaction of Ub (red) on Mms2 (PDB: 1ZGU). The side chain Lys63 (green) of Ub (red) acts as an acceptor for reaction with a thiolester bound Ub (blue) donor connected at the Ubc13 active site (yellow). This model contains a roughly 12 Å reaction distance.

Ub chain attachment. In this way the growing chain would be free in solution as opposed to attached at the active site thiolester. A highly detailed Ub-Ub positioning for attachment has not yet been presented for any other poly-ubiquitination pathways.

1.4.3 Cdc34 experiments indicate Cdc34~Ub may directly dimerize for activity

Initial studies using chemical cross-linking reagents indicated possible dimerization of the E2 enzymes Ubc1, Ubc4 and Cdc34 (Ubc3) (*89-91*). Further investigation of Cdc34 determined that this E2 produces both free K48-linked poly-Ub chains and Cdc34 attached K48-linked chains in the presence of Ub, ATP, E1, Cdc34, and its E3 RING protein complex (*92*). Fusion proteins that force Cdc34 to dimerize were found to increase poly-Ub chain formation activity in the absence of the normally required E3, suggesting that dimerization activates Cdc34 activity (*92*). Further studies on Cdc34 showed that two differentially tagged E2 enzymes can coimmunoprecipitate *in vivo* (yeast cells) (*93*). Coimmunoprecipitations could still be performed on Cdc34 proteins absent E3 enzyme binding, and the active site cysteine was required for coimmunoprecipitation, indicating that dimerization of Cdc34 appears to be dependant on the presence of an activated thiolester (*93*). Previous sedimentation equilibrium studies on free Cdc34 indicate the enzyme is monomeric, although the Cdc34~Ub thiolester was not investigated (*92*). Combining these results indicates either the E3 enzyme or Cdc34~Ub thiolester may assist dimerization to drive the mechanism depicted in Figure 1.5C. Regardless of the exact mechanism used, the fact that poly-Ub chains can be formed without substrate further supports the possibility that poly-Ub chains may be preassembled prior to substrate attachment.

1.4.4 K48-linked Poly-Ub chains can be built on Ube2g2 enzymes

Another example of poly-Ub chain formation activity prior to substrate addition comes from the E2 enzyme Ube2g2 (Ubc7). Activity assays performed on Ube2g2 with its RING E3 ligase gp78 resulted in K48-linked poly-Ub chain formation (*94*). In this study, reactions of ATP, E1 and Ube2g2 with either wild type Ub or Flag tagged Ub with a K48R substitution (Ub^{K48R}-Flag) were used to create two different Ube2g2 thiolesters, Ube2g2~Ub and Ube2g2~Ub^{K48R}-Flag. The Ube2g2~Ub thiolester contains the reactive K48 residue on Ub that can act as a Ub acceptor, while the Ube2g2~Ub^{K48R}-Flag thiolester contains the unreactive K48R substitution and therefore can only act as a Ub donor. The addition of the RING E3 ligase gp78 causes the reaction of these two intermediates to yield a diubiquitin attached thiolester Ube2g2~Ub-Ub^{K48R}-Flag. These results indicate a direct reaction between two Ube2g2 (E2) enzymes can occur causing the attachment of one Ub to a second Ub while both are covalently linked to the E2. This reaction required the gp78 RING E3 enzyme that has been shown to oligomerize (*95*). Therefore, the requirement for E3 may be to allow oligomerization of Ube2g2 enzymes in order to position Ub molecules in proximity for poly-ubiquitination activity. Further supporting the biological significance of this *in vitro* activity is the fact that poly-Ub chains linked to Ube2g2 can also be transferred onto a substrate, HERPc, indicating that preassembled chains can be transferred from the E2 enzyme onto a substrate (*94*). This evidence suggests a dimeric mechanism for Ube2g2 in which chains are preassembled prior to their attachment to substrates by thiol juggling as depicted in Figure 1.5C.

1.4.5 HECT E3 enzymes in poly-Ub chain extension

A study of two HECT E3 ligases has shown poly-Ub chain activity in the absence of substrates (*85*). In these studies the HECT E6AP E3 ligase was found to synthesize poly-Ub chains using an E2/E3 heterodimer by reacting two covalently bound Ub molecules, one connected to the UbcH5a (E2~Ub) and one connected to the E6AP (E3~Ub), to yield E6AP~Ub_2 (*85*). These results indicate that poly-Ub chains could form on the E3 enzyme and the growing chain's distal Ub would continually act as the Ub acceptor during chain extension (Fig 1.5B). This model of Ub chain extension is presumably assisted by movement in the C-lobe of E6AP to allow positioning of a growing chain attached to the E3 ligase (Fig 1.4A/B) (*85*).

An alternative mechanism for poly-Ub chain activity was observed for the HECT E3 ligase KIAA10 and UbcH5a. In this mechanism KIAA10 was observed to bind Ub non-covalently and this Ub acts as the acceptor by reacting with the KIAA10 thiolester bound Ub donor to build unanchored poly-Ub chains (*85*). The non-covalent Ub binding on KIAA10 must position the acceptor Ub lysine into reactive distance with the KIAA10~Ub donor as is depicted in Figure 1.5D. Chain extension would occur on the distal end of the growing chain where a K48 lysine is still available to be positioned by the non-covalent binding site (Fig 1.5D).

1.4.6 Alternative poly-Ub chain mechanisms

Non-covalent Ub binding has been observed on the UbcH5c E2 enzyme on the backside of the enzyme far removed from the active site cysteine (*96, 97*). The positioning of the non-covalently bound Ub is too far to interact with the active site

linked UbcH5c~Ub thiolester. This result indicates UbcH5c can bind 2 Ub molecules simultaneously, but does not position them for direct interaction in poly-Ub chain activity. The non-covalent binding of Ub on UbcH5c is however required for its observed poly-Ub chain formation activity in the presence of several different E3 enzymes (*97*). This non-covalent binding also causes oligomerization of UbcH5c~Ub thiolesters as the E2 bound Ub can associate with the non-covalent binding surface of a neighbouring UbcH5c (*97*). The mechanism of poly-Ub chain formation in this enzyme remains poorly understood but oligomerization may be a key requirement for function. The Ubl proteins SUMO2 and SUMO3 have also been shown to interact non-covalently with an equivalent region of the E2 enzyme Ubc9. The non-covalent binding in Ubc9 is also required for SUMO chain formation, likely through a similar mechanism to UbcH5c (*98*).

The process of dimerization is not solely limited to E2 enzymes, as many E3 ligases have been shown to dimerize including Brca1/Bard1 involved in breast cancer and Ring1b/Bmi involved in histone mono-ubiquitination (*99, 100*). This E3 dimerization was shown to be very important as mutations in the dimerization domain of Brca1 promotes cancer formation (*99*).

1.5 HIP2 and Ubc1 E2 conjugating enzymes

The mechanisms of poly-Ub chain formation become complicated as interactions involve E2/E3, E3/E3, or more complex dimeric combinations of these enzymes to position Ub molecules for reactivity. The simpler function of the E2 heterodimer Ubc13/Mms2 that does not require an E3 enzyme or substrate has provided very sound

structural information towards the assembly of K63-linked poly-Ub chains. Similar structural information is lacking for K48-linked poly-Ub chains. Two well studied enzymes that also have K48-linked poly-Ub chain formation activity in the absence of both E3 ligases and substrates are the yeast E2 enzyme Ubc1, and its human homolog HIP2. Since these E2 enzymes do not require E3 ligases, they should utilize a simpler mechanism for poly-Ub chain assembly in comparison to other K48 poly-ubiquitination pathways. How these two E2 enzymes function still remains poorly understood.

1.5.1 Ubc1

The E2 conjugating enzyme Ubc1 from yeast *Saccharomyces cerevisiae* was first identified in 1990 (*101*). The primary function for Ubc1 in yeast was found to be the selective degradation of short lived and abnormal proteins during early stages of growth after spore germination (*101*). Ubc1 also appears to functionally overlap with the other E2 enzymes Ubc4 and Ubc5 as single mutants of Ubc1 or Ubc4 have a slow growth phenotype, while double mutants fail to sporulate (*101*). This result shows that Ubc4, Ubc5, and Ubc1 have overlapping function. Ubc4 and Ubc5 are class I E2 enzymes containing only the traditional ~150 residue catalytic core domain while Ubc1 is a longer 215 residue class II E2 conjugating enzyme that possesses an additional C-terminal extension. The first experimental work on purified Ubc1 showed that K48-linked poly-Ub chains were formed on the Ubc1 enzyme itself in the presence of only E1, MgATP, Ubc1 and Ub (*102*). These poly-Ub chains were linked to the Ubc1 K93 residue indicating that Ubc1 performs an auto-ubiquitination of itself reminiscent of substrate ubiquitination. Auto-ubiquitination assays were also performed on a Ubc1 truncation

(Ubc1Δ) that had the C-terminal domain removed. Comparison of activity in Ubc1 and Ubc1Δ demonstrated that wild type Ubc1 could form poly-Ub chains up to four Ub molecules in length, while Ubc1Δ resulted in much longer poly-Ub chains up to 12 Ub molecules in length (*102*). This result indicates that the 65 residue C-terminal domain may control the length of poly-Ub chains produced. Further investigation indicated Ubc1 may dimerize as it was shown to chemically crosslink and elute earlier than expected by size exclusion column chromatography (*89*). The poly-Ub chain formation activity of Ubc1 may therefore require a dimeric mechanism to function.

The structure of full length Ubc1 was solved using NMR spectroscopy and is composed of the traditional catalytic core domain of 4 α-helices, 4 β-strands, and the very short 3_{10} helix immediately following the active site cysteine C88 residue (Fig 1.7A). The Ubc1 enzyme also contains a C-terminal Ub-associated (UBA) domain that is composed of a small 3 helix bundle (α5-α7) (Fig 1.7A) (*103*). UBA domains are found in several other proteins and have been shown to bind Ub non-covalently (*104*), in some cases bind poly-Ub chains preferentially (*105*), and also been implicated as a dimerization domain (*106*). The Ubc1 UBA domain was shown to interact non-covalently with free Ub (*103*). The full length Ubc1 NMR structure shows that the catalytic core domain and the UBA domain are connected by a flexible linker (*103*). This flexible linker allows a wide range of movement of the UBA domain in relation to the catalytic core. Therefore, the structure of full length Ubc1 is elongated, which may explain prior results in gel filtration experiments where Ubc1 eluted earlier than expected (*89*). The Ubc1 structure also shows that the proximity of K93 in the 3_{10} helix is very

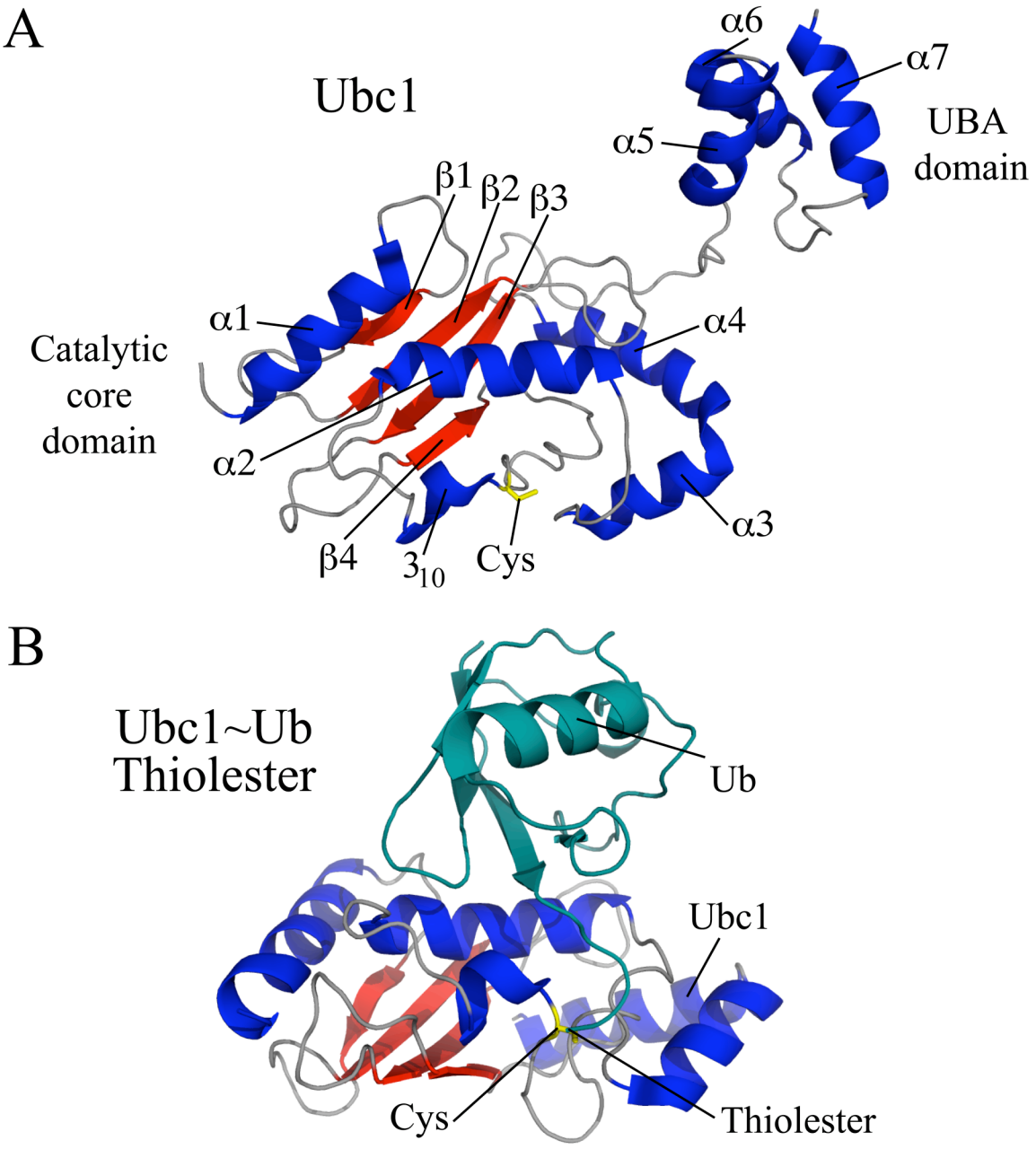

Figure 1.7 Structure of the E2 conjugating enzyme Ubc1 and Ubc1Δ~Ub thiolester. (**A**) The full length Ubc1 was solved using NMR spectroscopy (PDB: 1TTE) showing the classic catalytic core domain of 4 α-helices, a short 3_{10} helix, and 4 β-strands that form an anti-parallel β-sheet that wraps around the central α2 helix. Ubc1 also contains a C-terminal ubiquitin associated (UBA) domain composed of a 3-helix bundle of α5-α7. The catalytic core domain is connected to the UBA domain through an unstructured flexible linker. (**B**) Ubc1Δ (no UBA domain) was modelled with a thiolester bound Ub (teal) to position this Ub on the surface of Ubc1Δ (PDB: 1FXT). In this structure the hydrophobic side of Ub (located on the β-sheet) faces and interacts with the α2 helix in Ubc1. In this way the Ubc1~Ub thiolester bound Ub is held closely to the Ubc1 enzyme. Ubc1 secondary structural elements include α-helices (blue), β-strands (red), unstructured loops (grey) and the active site cysteine (yellow).

close to the C88 active site indicating that auto-ubiquitination may occur as a result of an intramolecular transfer of Ub directly from the active site to the K93 residue.

The structure of the Ubc1Δ~Ub thiolester was modelled using NMR spectroscopy by creating the thiolester in situ (Fig 1.7B) (*69*). In this structure the hydrophobic surface of Ub (located on the β-sheet) faces and interacts with the α2 helix in Ubc1Δ. This results in Ub being tightly bound to the Ubc1 catalytic core domain. Further experimentation on Ubc1 was greatly aided by the creation of a stable thiolester mimic formed with a disulphide bond between a substituted Ub (Ub^{G76C}) and the C88 of the active site (*68*). This Ubc1-Ub disulphide complex was shown to accurately mimic the Ubc1~Ub thiolester complex through NMR experiments (*68*). Experimentation on this Ubc1-Ub complex indicates that the UBA domain does not interact non-covalently with the thiolester bound Ub, but can interact with free Ub (*68*). The ability of the UBA domain to bind Ub in the Ubc1-Ub complex shows that Ubc1 has the ability to bind two Ub molecules simultaneously. The binding of two Ub molecules may support a monomeric mechanism of Ubc1 as the UBA domain could theoretically position the non-covalently bound Ub in proximity to a thiolester bound Ub. The Ubc1 protein was also shown to be monomeric by sedimentation equilibrium (*107*), although the formation of Ubc1~Ub thiolester may facilitate dimerization as was observed in Cdc34 (*93*).

Very recent work on Ubc1Δ has suggested a novel function of the E1 enzyme that would be required for poly-Ub chain formation on the auto-ubiquitinated Ubc1Δ (*108*). This implies that an E1/E2 complex is required to position 2 Ub molecules together for poly-Ub attachment rather than an E2/E2 complex. This could imply the E1 enzyme directly extends chains on E2 enzymes, or may assist E2 dimerization. Additional recent

Ubc1 experimentation has shown that Ubc1 and Ubc4 E2 conjugating enzymes can poly-ubiquitinate Cyclin B involved in cell cycle progression with a large RING E3 complex called APC (anaphase-promoting complex) (*109*). In this study Ubc4 and Ubc1 appear to have different functions as Ubc4 is more active in initial Ub attachment to substrates and Ubc1 is more active at extending chains on substrates that already have a single attached Ub (*109*). This study also tested Ubc1Δ (UBA removal) and observed products with shorter chain length (*109*). This result contrasts with the Ubc1Δ auto-ubiquitination experiments where longer poly-Ub chains were produced (*102*). These results may support a sequential addition model using combinations of E2 enzymes. Even with these few activity results, the mechanism for poly-Ub chain formation of Ubc1 remains very poorly understood.

1.5.2 E2 conjugating enzyme HIP2 (E2-25K)

The E2 conjugating enzyme E2-25K was shown to interact with the protein huntingtin and is suspected to poly-ubiquitinate huntingtin for degradation resulting in E2-25K being renamed HIP2 (huntingtin interacting protein 2) (*40, 110*). HIP2 is a 200 residue E2 conjugating enzyme that is highly conserved as human HIP2 has 100% sequence identity with bovine HIP2, and 66% sequence similarity with its yeast homolog Ubc1 (*40, 111*). The active site of HIP2 contains even greater conservation having 90% identity with Ubc1 within 20 residues around the active site (*111*). HIP2 has been shown to be widely expressed in many tissues but is highly expressed in brain tissue (*40*). The HIP2 structure was solved as a dimer by X-ray crystallography and is classified as a class II E2 indicating it possesses the traditional catalytic core domain and a C-terminal UBA

domain (Fig 1.8A) (PDB: 1YLA - unpublished). HIP2 was not observed to crosslink (*112*), and its dimerization capacity is not well investigated. Therefore the relevance of this dimeric crystal structure remains unknown. The monomer of this structure is depicted in Figure 1.8B. The HIP2 structure is again composed of the classic 4 α-helices, 4 β-strands, a 3_{10} helix, and a C-terminal UBA domain (Fig 1.8B). Compared to the similar Ubc1, HIP2 has a shorter linker connecting the catalytic core to the UBA domain, and it is unknown if this linker is also flexible (Fig 1.7A versus Fig 1.8B). The C92 catalytic active site is used to create a thiolester with Ub, and the UBA domain has recently been shown to bind free Ub non-covalently, giving HIP2 the ability to bind 2 Ub molecules simultaneously, just like Ubc1 (*113, 114*). These structural similarities to Ubc1 indicate that HIP2 should function by a similar mechanism to Ubc1.

Very recently the crystal structure of HIP2 with non-covalently bound Ub was solved showing the nature of Ub binding to the HIP2 UBA domain (Fig 1.8C) (*113*). UBA domains are characterized by a conserved hydrophobic MGF patch between α1 and α2 in the 3 helix bundle used for protein interactions (*115*). It is this MGF region of the HIP2 UBA domain that was seen to bind free Ub (*113*). Ubc1 also utilizes its similar QGF residues in UBA/Ub binding (*103*). This general UBA/Ub binding surface has been observed for several other UBA domains and is shown in more detail on an example UBA domain (Ede1) in Figure 1.8D (*104*). The major binding interface between these two proteins is composed of the MGF and α3 of the UBA domain and the C-terminal end and hydrophobic residues in the β-sheet portion of Ub. The HIP2 UBA domain has also been shown to bind poly-Ub chains (Ub_4) with higher strength than single Ub

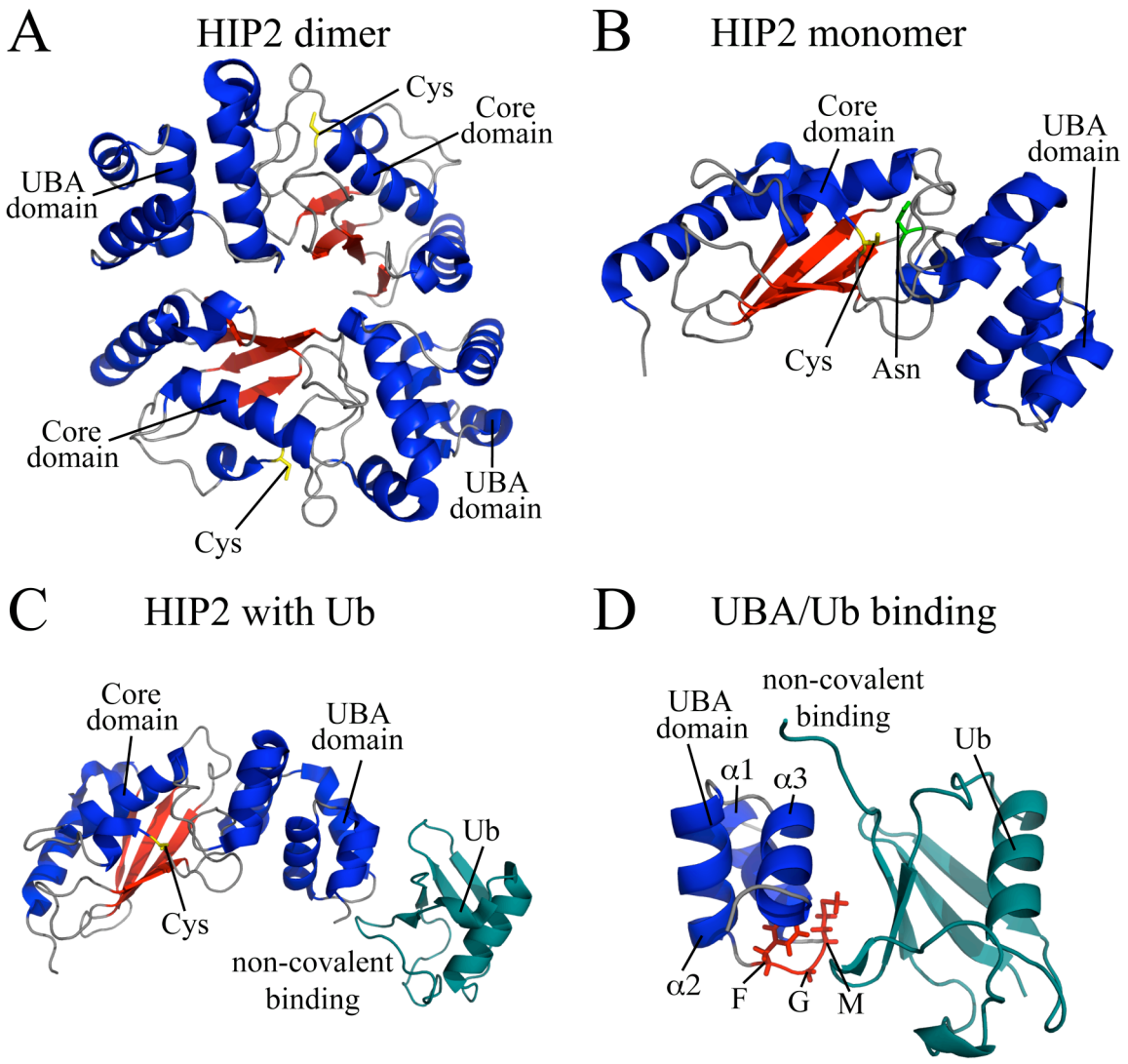

Figure 1.8 Structure insight into the human HIP2 E2 conjugating enzyme. (**A**) The full length HIP2 enzyme was solved using X-ray crystallography (PDB: 1YLA) as a dimer where the β-sheet side of HIP2 opposite the active sites contact each other. (**B**) Half of the structure shown in (**A**) leaves a monomeric HIP2 showing the classic catalytic core domain and a C-terminal UBA domain. The unstructured linker between the catalytic core and UBA domain is shorter than that observed for Ubc1. (**C**) A recent structure of HIP2 has shown the non-covalent binding of Ub with the UBA domain (PDB: 3K9P). In this structure the hydrophobic face of Ub interacts with a highly conserved MGF sequence in the UBA domain of HIP2. (**D**) Many other UBA domains show a similar interaction with Ub. An example from the protein Ede1 depicts a similar UBA/Ub non-covalent interaction (PDB: 2G3Q). Most UBA domains contain this MGF motif and use a large portion of the third α-helix in this 3-helix bundle to contact the hydrophobic face of Ub. HIP2 secondary structural elements include α-helices (blue), β-strands (red), unstructured loops (grey) and the active site cysteine (yellow) and oxyanion stabilizing asparagine (green) while Ub (teal) is coloured uniformly.

molecules (*105*). NMR experiments on a similar UBA domain (UBA2 from hHR23A) have shown a K48-linked Ub_2 used both Ub hydrophobic surfaces to contact the UBA domain (*116*). These results are consistent with stronger binding to poly-Ub chains indicating that HIP2 may bind poly-Ub chains in a similar manner.

HIP2 activity was initially found to create unanchored K48-linked poly-Ub chains with only E1, MgATP, and Ub (*117*). The function of HIP2 is similar to Ubc1 only the K48-linked poly-Ub chains are free in solution as opposed to connected to the K93 residue in Ubc1. HIP2 was also found to be able to use non-thiolester linked Ub molecules as Ub acceptors indicating Ub acceptors may be thiolester linked or bound non-covalently (*117*). Diubiquitin (Ub_2) was also found to be a better Ub acceptor than Ub alone indicating the kinetics of poly-Ub chain formation become more favourable as the chain grows (*117*). Since the HIP2 UBA domain has also been shown to bind poly-Ub chains (Ub_4) with higher strength than single Ub molecules, the UBA domain may account for the use of longer poly-Ub chains as more efficient Ub acceptors (*105*). These results imply that the UBA domain is required for chain extension. Further experimental studies on HIP2 were performed with a truncated HIP2Δ155 (UBA removed at residue 155) or HIP2Δ159 and these truncations still retained poly-Ub chain activity although they were not as efficient (*30, 114*). These results indicate that UBA aids in activity but may not be essential. Very recent experiments have shown the UBA domain is required for full activity of HIP2 (*114*), and its yeast homolog Ubc1 (*109*). The presence of even partial activity with UBA removal indicates HIP2 dimerization may be required to place two Ub molecules in close proximity. The purpose of the UBA domain therefore remains

poorly understood but its known affinity for Ub and poly-Ub chains allows for many possible interactions with E2, E3 or substrate linked Ub or poly-Ub molecules.

The purpose of HIP2 building unanchored poly-Ub chains remains unknown, although the E1 enzyme can form thiolesters with both Ub and Ub_2 and transfer these thiolesters onto HIP2 with similar kinetics (*117*). This indicates that preassembled Ub_2 can be utilized to form HIP2~Ub_2 that could act as a Ub donor in further chain extension or substrate labelling (*117*). This is supported by the discovery that unanchored poly-Ub chains are found *in vivo* and can be loaded onto substrates using Ubc4 with similar kinetics to a single Ub (*118*). These results show HIP2 may function by preassembling poly-Ub chains prior to substrate attachment.

Very little is known about HIP2's cognate E3 enzymes or substrates. The biological activity of HIP2 remains widely unknown. Only a small number of RING E3 enzymes were implicated to interact with HIP2 through yeast two-hybrid studies (*119*). HIP2 ubiquitinates the substrate p105 a precursor for p50, involved in NF-kB signaling, through an unknown E3 ligase (*120*). Very recent work has identified HIP2 to bind the RING E3 NARF (Nemo-like Kinase (NLK)-associated Ring finger) to ubiquitinate transcription factors TCF/LEF, and their corresponding degradation suppresses Wnt-β-catenin signaling involved in embryonic development and tumorigenesis (*121*). HIP2 has also been linked to Cyclin B1 degradation and DIABLO degradation but no E3 ligase has been identified (*122, 123*). HIP2 may also be involved in the degradation of Rb (retinoblastoma tumor suppressor protein) involved with HPV oncoprotein E7 resulting in the promotion of cancer (*124*). The lack of many identified E3 ligases for HIP2 has limited the study of HIP2 activity on specific substrates.

The most interesting HIP2 function is in both Alzheimer's and Huntingtin's disease. Alzheimer's disease has been characterized by extracellular plaques that are composed of misfolded and aggregated amyloid β peptides (Aβ). HIP2 was shown to be upregulated in neurons exposed to Aβ peptides (*125*). Alzheimer's disease has been linked to ubiquitination through the incorporation of the ubiquitin variant UBB^{+1} (*32*) and reduced proteosomal activity (*33*). The UBB^{+1} variant contains a C-terminal extension that when added to the end of a K48-linked poly-Ub chain is resistant to deubiquitinating enzymes and correspondingly inhibits the 26S proteosome (*36*). HIP2 may largely affect these functions by incorporating UBB^{+1} into poly-Ub chains as HIP2 has recently been found to bind both Ub and UBB^{+1} by the UBA with equivalent affinity (*113*). HIP2 is expressed in many tissue types (*126*) and is highly expressed in the brain (*40*), the site of polyglutamine and Alzheimer's diseases. Huntington's disease is characterized by the expansion of the polyglutamine portion of the protein huntingtin that results in their aggregation into inclusion bodies. HIP2 interacts with the huntingtin protein and presumably is responsible for its ubiquitination (*40*). HIP2 was also found to exist in Huntington's disease inclusions also containing huntingtin, Ub and UBB^{+1} (*127*). Additionally, HIP2 is suspected to play a role in aggregate formation and cell death (*127, 128*). HIP2 involvement in both Huntington's and Alzheimer's disease may be related by a similar mechanism of pathogenesis.

1.6 Scope of Thesis

The ubiquitination pathway is an important regulatory pathway within the cell and its disruption has been linked to many neurodegenerative diseases and cancer. A

significant amount of work over the last two decades has expanded the understanding of the E1-E2-E3 enzyme cascade used to poly-ubiquitinate substrates for degradation. However, the mechanism by which most these enzymes build poly-Ub chains on their substrates remains poorly understood. An improved understanding of the mechanisms of poly-Ub chain assembly will aid in determining how these pathways are disrupted in many diseases.

HIP2 and Ubc1 do not require E3 enzymes and substrates to create poly-Ub chain linkages. HIP2 and Ubc1 employ a simple functional mechanism that only requires the addition of Ub, ATP and the E1 enzyme. Investigating these enzyme structures and protein interactions is crucial to fully comprehending their function in the ubiquitination pathway.

The work in this thesis is based on the following hypotheses:

- The E2 conjugating enzymes HIP2 and Ubc1 dimerize upon formation of E2~Ub thiolesters. (investigated in Chapter 2)
- The E1 enzyme does not directly extend a poly-Ub chain on the HIP2~Ub and Ubc1~Ub thiolesters. (investigated in Chapter 2)
- Unique intramolecular interactions exist for HIP2~Ub and HIP2~Ub_2 thiolesters that will provide a rationale for poly-Ub assembly. (investigated in Chapter 3 and 4)

These hypotheses were studied through the creation of disulphide complexes to mimic Ubc1~Ub, HIP2~Ub and HIP2~Ub_2 thiolesters. Investigation of these complexes was

performed using sedimentation equilibrium, small angle X-ray scattering (SAXS), and activity assays using unlabelled and fluorescently labelled proteins. NMR spectroscopy chemical shift mapping was utilized to determine protein interactions within HIP2-Ub and HIP2-Ub_2 through isotopic labelling (^{15}N and ^{13}C) of individual proteins within these complexes. These investigations have led to the clarification of possible mechanisms that HIP2 and Ubc1 utilize to assemble poly-Ub chains.

Bibliography

1. Ciechanover, A. (2009) Tracing the history of the ubiquitin proteolytic system: the pioneering article, *Biochem Biophys Res Commun 387*, 1-10.

2. Varshavsky, A. (2006) The early history of the ubiquitin field, *Protein Sci 15*, 647-654.

3. Hershko, A., and Ciechanover, A. (1998) The ubiquitin system, *Annu Rev Biochem 67*, 425-479.

4. Ciechanover, A., Hod, Y., and Hershko, A. (1978) A heat-stable polypeptide component of an ATP-dependent proteolytic system from reticulocytes., *Biochem. Biophys. Res. Commun. 81*, 1100-1105.

5. Hershko, A., Ciechanover, A., Heller, H., Haas, A. L., and Rose, I. A. (1980) Proposed role of ATP in protein breakdown: Conjugation of proteins with multiple chains of the polypeptide of ATP-dependent proteolysis, *Proc. Natl. Acad. Sci. USA 77*, 1783-1786.

6. Hershko, A., Heller, H., Elias, S., and Ciechanover, A. (1983) Components of ubiquitin-protein ligase system, *J. Biol. Chem. 258*, 8206-8214.

7. Ciechanover, A., Finley, D., and Varshavsky, A. (1984) Ubiquitin dependence of selective protein degradation demonstrated in the mammalian cell cycle mutant ts85, *Cell 37*, 57-66.

8. Finley, D., Ciechanover, A., and Varshavsky, A. (1984) Thermolability of ubiquitin-activating enzyme from the mammalian cell cycle mutant ts85, *Cell 37*, 43-55.

9. Finley, D., Ozkaynak, E., and Varshavsky, A. (1987) The yeast polyubiquitin gene is essential for resistance to high temperatures, starvation, and other stresses, *Cell 48*, 1035-1046.

10. Bachmir, A., and Varshavsky, A. (1989) The Degradation Signal in a Short-Lived Protein, *Cell 56*, 1019-1032.

11. Johnson, E. S., Bartel, B., Seufert, W., and Varshavsky, A. (1992) Ubiquitin as a degradation signal, *EMBO J 11*, 497-505.

12. Catic, A., and Ploegh, H. L. (2005) Ubiquitin--conserved protein or selfish gene?, *Trends Biochem Sci 30*, 600-604.

13. Glickman, M. H., and Ciechanover, A. (2002) The ubiquitin-proteasome proteolytic pathway: destruction for the sake of construction, *Physiol Rev 82*, 373-428.

14. Peng, J., Schwartz, D., Elias, J. E., Thoreen, C. C., Cheng, D., Marsischky, G., Roelofs, J., Finley, D., and Gygi, S. P. (2003) A proteomics approach to understanding protein ubiquitination, *Nat Biotechnol 21*, 921-926.

15. Pickart, C. M., and Fushman, D. (2004) Polyubiquitin chains: polymeric protein signals, *Curr Opin Chem Biol 8*, 610-616.

16. Kuhlbrodt, K., Mouysset, J., and Hoppe, T. (2005) Orchestra for assembly and fate of polyubiquitin chains, *Essays Biochem 41*, 1-14.

17. Hicke, L. (2001) Protein regulation by monoubiquitin, *Nat Rev Mol Cell Biol 2*, 195-201.

18. Bremm, A., Freund, S. M., and Komander, D. (2010) Lys11-linked ubiquitin chains adopt compact conformations and are preferentially hydrolyzed by the deubiquitinase Cezanne, *Nat Struct Mol Biol 17*, 939-947.

19. Bremm, A., and Komander, D. (2011) Emerging roles for Lys11-linked polyubiquitin in cellular regulation, *Trends Biochem Sci 36*, 355-363.

20. Ciechanover, A., Orian, A., and Schwartz, A. L. (2000) Ubiquitin-mediated proteolysis: biological regulation via destruction, *Bioessays 22*, 442-451.

21. Reyes-Turcu, F. E., Ventii, K. H., and Wilkinson, K. D. (2009) Regulation and cellular roles of ubiquitin-specific deubiquitinating enzymes, *Annu Rev Biochem 78*, 363-397.

22. Komander, D. (2010) Mechanism, specificity and structure of the deubiquitinases, *Subcell Biochem 54*, 69-87.

23. Groettrup, M., Pelzer, C., Schmidtke, G., and Hofmann, K. (2008) Activating the ubiquitin family: UBA6 challenges the field, *Trends Biochem Sci 33*, 230-237.

24. van Wijk, S. J., and Timmers, H. T. (2010) The family of ubiquitin-conjugating enzymes (E2s): deciding between life and death of proteins, *FASEB J 24*, 981-993.

25. Kumar, S., Kao, W. H., and Howley, P. M. (1997) Physical interaction between specific E2 and Hect E3 enzymes determines functional cooperativity, *J Biol Chem 272*, 13548-13554.

26. Welchman, R. L., Gordon, C., and Mayer, R. J. (2005) Ubiquitin and ubiquitin-like proteins as multifunctional signals, *Nat Rev Mol Cell Biol 6*, 599-609.

27. Bedford, L., Lowe, J., Dick, L. R., Mayer, R. J., and Brownell, J. E. (2011) Ubiquitin-like protein conjugation and the ubiquitin-proteasome system as drug targets, *Nat Rev Drug Discov 10*, 29-46.

28. Herrmann, J., Lerman, L. O., and Lerman, A. (2007) Ubiquitin and ubiquitin-like proteins in protein regulation, *Circ Res 100*, 1276-1291.

29. Hochstrasser, M. (2009) Origin and function of ubiquitin-like proteins, *Nature 458*, 422-429.

30. Pichler, A., Knipscheer, P., Oberhofer, E., van Dijk, W. J., Korner, R., Olsen, J. V., Jentsch, S., Melchior, F., and Sixma, T. K. (2005) SUMO modification of the ubiquitin-conjugating enzyme E2-25K, *Nat Struct Mol Biol 12*, 264-269.

31. Schwartz, A. L., and Ciechanover, A. (2009) Targeting proteins for destruction by the ubiquitin system: implications for human pathobiology, *Annu Rev Pharmacol Toxicol 49*, 73-96.

32. van Leeuwen, F. W., de Kleijn, D. P., van den Hurk, H. H., Neubauer, A., Sonnemans, M. A., Sluijs, J. A., Koycu, S., Ramdjielal, R. D., Salehi, A., Martens, G. J., Grosveld, F. G., Peter, J., Burbach, H., and Hol, E. M. (1998) Frameshift mutants of beta amyloid precursor protein and ubiquitin-B in Alzheimer's and Down patients, *Science 279*, 242-247.

33. Gregori, L., Fuchs, C., Figueiredo-Pereira, M. E., Van Nostrand, W. E., and Goldgaber, D. (1995) Amyloid beta-protein inhibits ubiquitin-dependent protein degradation in vitro, *J Biol Chem 270*, 19702-19708.

34. Gong, B., Cao, Z., Zheng, P., Vitolo, O. V., Liu, S., Staniszewski, A., Moolman, D., Zhang, H., Shelanski, M., and Arancio, O. (2006) Ubiquitin hydrolase Uch-L1 rescues beta-amyloid-induced decreases in synaptic function and contextual memory, *Cell 126*, 775-788.

35. Niikura, T., Hashimoto, Y., Tajima, H., Ishizaka, M., Yamagishi, Y., Kawasumi, M., Nawa, M., Terashita, K., Aiso, S., and Nishimoto, I. (2003) A tripartite motif protein TRIM11 binds and destabilizes Humanin, a neuroprotective peptide against Alzheimer's disease-relevant insults, *Eur J Neurosci 17*, 1150-1158.

36. Lam, Y. A., Pickart, C. M., Alban, A., Landon, M., Jamieson, C., Ramage, R., Mayer, R. J., and Layfield, R. (2000) Inhibition of the ubiquitin-proteasome system in Alzheimer's disease, *Proc Natl Acad Sci U S A 97*, 9902-9906.

37. Kitada, T., Asakawa, S., Hattori, N., Matsumine, H., Yamamura, Y., Minoshima, S., Yokochi, M., Mizuno, Y., and Shimizu, N. (1998) Mutations in the *parkin* gene cause autosomal recessive juvenile parkinsonism, *Nature 392*, 605-608.

38. Hatano, T., Kubo, S., Sato, S., and Hattori, N. (2009) Pathogenesis of familial Parkinson's disease: new insights based on monogenic forms of Parkinson's disease, *J Neurochem 111*, 1075-1093.

39. Imai, Y., Soda, M., Inoue, H., Hattori, N., Mizuno, Y., and Takahashi, R. (2001) An unfolded putative transmembrane polypeptide, which can lead to endoplasmic reticulum stress, is a substrate of parkin, *Cell 105*, 891-902.

40. Kalchman, M. A., Graham, R. K., Xia, G., Koide, H. B., Hodgson, J. G., Graham, K. C., Goldberg, Y. P., Gietz, R. D., Pickart, C. M., and Hayden, M. R. (1996) Huntingtin is ubiquitinated and interacts with a specific ubiquitin-conjugating enzyme, *J Biol Chem 271*, 19385-19394.

41. Bence, N. F., Sampat, R. M., and Kopito, R. R. (2001) Impairment of the ubiquitin-proteasome system by protein aggregation, *Science 292*, 1552-1555.

42. McNaught, K. S., Belizaire, R., Isacson, O., Jenner, P., and Olanow, C. W. (2003) Altered proteasomal function in sporadic Parkinson's disease, *Exp Neurol 179*, 38-46.

43. Seo, H., Sonntag, K. C., and Isacson, O. (2004) Generalized brain and skin proteasome inhibition in Huntington's disease, *Ann Neurol 56*, 319-328.

44. Keller, J. N., Hanni, K. B., and Markesbery, W. R. (2000) Impaired proteasome function in Alzheimer's disease, *J Neurochem 75*, 436-439.

45. Treusch, S., Cyr, D. M., and Lindquist, S. (2009) Amyloid deposits: protection against toxic protein species?, *Cell Cycle 8*, 1668-1674.

46. Dyson, N., Howley, P. M., Munger, K., and Harlow, E. (1989) The human papilloma virus-16 E7 oncoprotein is able to bind to the retinoblastoma gene product, *Science 243*, 934-937.

47. Dyson, N. (1998) The regulation of E2F by pRB-family proteins, *Genes Dev 12*, 2245-2262.

48. Crook, T., Tidy, J. A., and Vousden, K. H. (1991) Degradation of p53 can be targeted by HPV E6 sequences distinct from those required for p53 binding and trans-activation, *Cell 67*, 547-556.

49. Vassilev, L. T., Vu, B. T., Graves, B., Carvajal, D., Podlaski, F., Filipovic, Z., Kong, N., Kammlott, U., Lukacs, C., Klein, C., Fotouhi, N., and Liu, E. A. (2004) In vivo activation of the p53 pathway by small-molecule antagonists of MDM2, *Science 303*, 844-848.

50. Hoeller, D., and Dikic, I. (2009) Targeting the ubiquitin system in cancer therapy, *Nature 458*, 438-444.

51. Lee, I., and Schindelin, H. (2008) Structural insights into E1-catalyzed ubiquitin activation and transfer to conjugating enzymes, *Cell 134*, 268-278.

52. Jin, J., Li, X., Gygi, S. P., and Harper, J. W. (2007) Dual E1 activation systems for ubiquitin differentially regulate E2 enzyme charging, *Nature 447*, 1135-1138.

53. Olsen, S. K., Capili, A. D., Lu, X., Tan, D. S., and Lima, C. D. (2010) Active site remodelling accompanies thioester bond formation in the SUMO E1, *Nature 463*, 906-912.

54. Huang, D. T., Hunt, H. W., Zhuang, M., Ohi, M. D., Holton, J. M., and Schulman, B. A. (2007) Basis for a ubiquitin-like protein thioester switch toggling E1-E2 affinity, *Nature 445*, 394-398.

55. Wenzel, D. M., Stoll, K. E., and Klevit, R. E. (2010) E2s: structurally economical and functionally replete, *Biochem J 433*, 31-42.

56. Wu, P. Y., Hanlon, M., Eddins, M., Tsui, C., Rogers, R. S., Jensen, J. P., Matunis, M. J., Weissman, A. M., Wolberger, C., and Pickart, C. M. (2003) A conserved catalytic residue in the ubiquitin-conjugating enzyme family, *EMBO J 22*, 5241-5250.

57. Reverter, D., and Lima, C. D. (2005) Insights into E3 ligase activity revealed by a SUMO-RanGAP1-Ubc9-Nup358 complex, *Nature 435*, 687-692.

58. Yunus, A. A., and Lima, C. D. (2006) Lysine activation and functional analysis of E2-mediated conjugation in the SUMO pathway, *Nat Struct Mol Biol 13*, 491-499.

59. Burroughs, A. M., Jaffee, M., Iyer, L. M., and Aravind, L. (2008) Anatomy of the E2 ligase fold: implications for enzymology and evolution of ubiquitin/Ub-like protein conjugation, *J Struct Biol 162*, 205-218.

60. Winn, P. J., Religa, T. L., Battey, J. N., Banerjee, A., and Wade, R. C. (2004) Determinants of functionality in the ubiquitin conjugating enzyme family, *Structure 12*, 1563-1574.

61. Winn, P. J., Zahran, M., Battey, J. N., Zhou, Y., Wade, R. C., and Banerjee, A. (2007) Structural and electrostatic properties of ubiquitination and related pathways, *Front Biosci 12*, 3419-3430.

62. Jentsch, S. (1992) The ubiquitin-conjugation system, *Annu Rev Genet 26*, 179-207.

63. Huang, D. T., Paydar, A., Zhuang, M., Waddell, M. B., Holton, J. M., and Schulman, B. A. (2005) Structural basis for recruitment of Ubc12 by an E2 binding domain in NEDD8's E1, *Mol Cell 17*, 341-350.

64. Zheng, N., Wang, P., Jeffrey, P. D., and Pavletich, N. P. (2000) Structure of a c-Cbl-UbcH7 complex: RING domain function in ubiquitin-protein ligases, *Cell 102*, 533-539.

65. Eletr, Z. M., Huang, D. T., Duda, D. M., Schulman, B. A., and Kuhlman, B. (2005) E2 conjugating enzymes must disengage from their E1 enzymes before E3-dependent ubiquitin and ubiquitin-like transfer, *Nat Struct Mol Biol 12*, 933-934.

66. Siepmann, T. J., Bohnsack, R. N., Tokgoz, Z., Baboshina, O. V., and Haas, A. L. (2003) Protein interactions within the N-end rule ubiquitin ligation pathway, *J Biol Chem 278*, 9448-9457.

67. Eddins, M. J., Carlile, C. M., Gomez, K. M., Pickart, C. M., and Wolberger, C. (2006) Mms2-Ubc13 covalently bound to ubiquitin reveals the structural basis of linkage-specific polyubiquitin chain formation, *Nat Struct Mol Biol 13*, 915-920.

68. Merkley, N., Barber, K. R., and Shaw, G. S. (2005) Ubiquitin manipulation by an E2 conjugating enzyme using a novel covalent intermediate, *J Biol Chem 280*, 31732-31738.

69. Hamilton, K. S., Ellison, M. J., Barber, K. R., Williams, R. S., Huzil, J. T., McKenna, S., Ptak, C., Glover, M., and Shaw, G. S. (2001) Structure of a conjugating enzyme-ubiquitin thiolester intermediate reveals a novel role for the ubiquitin tail, *Structure 9*, 897-904.

70. Serniwka, S. A., and Shaw, G. S. (2009) The structure of the UbcH8-ubiquitin complex shows a unique ubiquitin interaction site, *Biochemistry 48*, 12169-12179.

71. Sakata, E., Satoh, T., Yamamoto, S., Yamaguchi, Y., Yagi-Utsumi, M., Kurimoto, E., Tanaka, K., Wakatsuki, S., and Kato, K. (2010) Crystal structure of UbcH5b~ubiquitin intermediate: insight into the formation of the self-assembled E2~Ub conjugates, *Structure 18*, 138-147.

72. Kamadurai, H. B., Souphron, J., Scott, D. C., Duda, D. M., Miller, D. J., Stringer, D., Piper, R. C., and Schulman, B. A. (2009) Insights into ubiquitin transfer cascades from a structure of a UbcH5B approximately ubiquitin-HECT(NEDD4L) complex, *Mol Cell 36*, 1095-1102.

73. McKenna, S., Moraes, T., Pastushok, L., Ptak, C., Xiao, W., Spyracopoulos, L., and Ellison, M. J. (2003) An NMR-based model of the ubiquitin-bound human ubiquitin conjugation complex Mms2.Ubc13. The structural basis for lysine 63 chain catalysis, *J Biol Chem 278*, 13151-13158.

74. Pruneda, J. N., Stoll, K. E., Bolton, L. J., Brzovic, P. S., and Klevit, R. E. (2011) Ubiquitin in motion: structural studies of the ubiquitin-conjugating enzyme approximately ubiquitin conjugate, *Biochemistry 50*, 1624-1633.

75. Levin, I., Eakin, C., Blanc, M. P., Klevit, R. E., Miller, S. I., and Brzovic, P. S. (2010) Identification of an unconventional E3 binding surface on the UbcH5 ~ Ub conjugate recognized by a pathogenic bacterial E3 ligase, *Proc Natl Acad Sci U S A 107*, 2848-2853.

76. Li, W., Bengtson, M. H., Ulbrich, A., Matsuda, A., Reddy, V. A., Orth, A., Chanda, S. K., Batalov, S., and Joazeiro, C. A. (2008) Genome-wide and functional annotation of human E3 ubiquitin ligases identifies MULAN, a mitochondrial E3 that regulates the organelle's dynamics and signaling, *PLoS One 3*, e1487.

77. Huang, L., Kinnucan, E., Wang, G., Beaudenon, S., Howley, P. M., Huibregtse, J. M., and Pavletich, N. P. (1999) Structure of an E6AP-UbcH7 complex: insights into ubiquitination by the E2-E3 enzyme cascade, *Science 286*, 1321-1326.

78. Verdecia, M. A., Joazeiro, C. A., Wells, N. J., Ferrer, J. L., Bowman, M. E., Hunter, T., and Noel, J. P. (2003) Conformational flexibility underlies ubiquitin ligation mediated by the WWP1 HECT domain E3 ligase, *Mol Cell 11*, 249-259.

79. Deshaies, R. J., and Joazeiro, C. A. (2009) RING domain E3 ubiquitin ligases, *Annu Rev Biochem 78*, 399-434.

80. Dominguez, C., Bonvin, A. M., Winkler, G. S., van Schaik, F. M., Timmers, H. T., and Boelens, R. (2004) Structural model of the UbcH5B/CNOT4 complex revealed by combining NMR, mutagenesis, and docking approaches, *Structure (Camb) 12*, 633-644.

81. Yin, Q., Lin, S. C., Lamothe, B., Lu, M., Lo, Y. C., Hura, G., Zheng, L., Rich, R. L., Campos, A. D., Myszka, D. G., Lenardo, M. J., Darnay, B. G., and Wu, H. (2009) E2 interaction and dimerization in the crystal structure of TRAF6, *Nat Struct Mol Biol 16*, 658-666.

82. Zhang, L., Fairall, L., Goult, B. T., Calkin, A. C., Hong, C., Millard, C. J., Tontonoz, P., and Schwabe, J. W. (2011) The IDOL-UBE2D complex mediates sterol-dependent degradation of the LDL receptor, *Genes Dev 25*, 1262-1274.

83. Petroski, M. D., and Deshaies, R. J. (2005) Function and regulation of cullin-RING ubiquitin ligases, *Nat Rev Mol Cell Biol 6*, 9-20.

84. Hochstrasser, M. (2006) Lingering mysteries of ubiquitin-chain assembly, *Cell 124*, 27-34.

85. Wang, M., and Pickart, C. M. (2005) Different HECT domain ubiquitin ligases employ distinct mechanisms of polyubiquitin chain synthesis, *EMBO J 24*, 4324-4333.

86. McKenna, S., Spyracopoulos, L., Moraes, T., Pastushok, L., Ptak, C., Xiao, W., and Ellison, M. J. (2001) Noncovalent interaction between ubiquitin and the human DNA repair protein Mms2 is required for Ubc13-mediated polyubiquitination, *J Biol Chem 276*, 40120-40126.

87. Lewis, M. J., Saltibus, L. F., Hau, D. D., Xiao, W., and Spyracopoulos, L. (2006) Structural basis for non-covalent interaction between ubiquitin and the ubiquitin conjugating enzyme variant human MMS2, *J Biomol NMR 34*, 89-100.

88. Moraes, T. F., Edwards, R. A., McKenna, S., Pastushok, L., Xiao, W., Glover, J. N., and Ellison, M. J. (2001) Crystal structure of the human ubiquitin conjugating enzyme complex, hMms2-hUbc13, *Nat Struct Biol 8*, 669-673.

89. Leggett, D. S., and Candido, P. M. (1997) Biochemical characterization of Caenorhabditis elegans UBC-1: self-association and auto-ubiquitination of a RAD6-like ubiquitin-conjugating enzyme in vitro, *Biochem J 327 (Pt 2)*, 357-361.

90. Gwozd, C. S., Arnason, T. G., Cook, W. J., Chau, V., and Ellison, M. J. (1995) The yeast UBC4 ubiquitin conjugating enzyme monoubiquitinates itself in vivo: evidence for an E2-E2 homointeraction, *Biochemistry 34*, 6296-6302.

91. Ptak, C., Prendergast, J. A., Hodgins, R., Kay, C. M., Chau, V., and Ellison, M. J. (1994) Functional and physical characterization of the cell cycle ubiquitin-conjugating enzyme CDC34 (UBC3). Identification of a functional determinant within the tail that facilitates CDC34 self-association, *J Biol Chem 269*, 26539-26545.

92. Gazdoiu, S., Yamoah, K., Wu, K., Escalante, C. R., Tappin, I., Bermudez, V., Aggarwal, A. K., Hurwitz, J., and Pan, Z. Q. (2005) Proximity-induced activation of human Cdc34 through heterologous dimerization, *Proc Natl Acad Sci U S A 102*, 15053-15058.

93. Varelas, X., Ptak, C., and Ellison, M. J. (2003) Cdc34 self-association is facilitated by ubiquitin thiolester formation and is required for its catalytic activity, *Mol Cell Biol 23*, 5388-5400.

94. Li, W., Tu, D., Brunger, A. T., and Ye, Y. (2007) A ubiquitin ligase transfers preformed polyubiquitin chains from a conjugating enzyme to a substrate, *Nature 446*, 333-337.

95. Li, W., Tu, D., Li, L., Wollert, T., Ghirlando, R., Brunger, A. T., and Ye, Y. (2009) Mechanistic insights into active site-associated polyubiquitination by the ubiquitin-conjugating enzyme Ube2g2, *Proc Natl Acad Sci U S A 106*, 3722-3727.

96. Brzovic, P. S., and Klevit, R. E. (2006) Ubiquitin transfer from the E2 perspective: why is UbcH5 so promiscuous?, *Cell Cycle 5*, 2867-2873.

97. Brzovic, P. S., Lissounov, A., Christensen, D. E., Hoyt, D. W., and Klevit, R. E. (2006) A UbcH5/ubiquitin noncovalent complex is required for processive BRCA1-directed ubiquitination, *Mol Cell 21*, 873-880.

98. Knipscheer, P., van Dijk, W. J., Olsen, J. V., Mann, M., and Sixma, T. K. (2007) Noncovalent interaction between Ubc9 and SUMO promotes SUMO chain formation, *EMBO J 26*, 2797-2807.

99. Brzovic, P. S., Rajagopal, P., Hoyt, D. W., King, M. C., and Klevit, R. E. (2001) Structure of a BRCA1-BARD1 heterodimeric RING-RING complex, *Nat Struct Biol 8*, 833-837.

100. Buchwald, G., van der Stoop, P., Weichenrieder, O., Perrakis, A., van Lohuizen, M., and Sixma, T. K. (2006) Structure and E3-ligase activity of the Ring-Ring complex of polycomb proteins Bmi1 and Ring1b, *EMBO J 25*, 2465-2474.

101. Seufert, W., McGrath, J. P., and Jentsch, S. (1990) UBC1 encodes a novel member of an essential subfamily of yeast ubiquitin-conjugating enzymes involved in protein degradation, *EMBO J 9*, 4535-4541.

102. Hodgins, R., Gwozd, C., Arnason, T., Cummings, M., and Ellison, M. J. (1996) The tail of a ubiquitin-conjugating enzyme redirects multi-ubiquitin chain synthesis from the lysine 48-linked configuration to a novel nonlysine-linked form, *J Biol Chem 271*, 28766-28771.

103. Merkley, N., and Shaw, G. S. (2004) Solution structure of the flexible class II ubiquitin-conjugating enzyme Ubc1 provides insights for polyubiquitin chain assembly, *J Biol Chem 279*, 47139-47147.

104. Zhang, D., Raasi, S., and Fushman, D. (2008) Affinity makes the difference: nonselective interaction of the UBA domain of Ubiquilin-1 with monomeric ubiquitin and polyubiquitin chains, *J Mol Biol 377*, 162-180.

105. Raasi, S., Varadan, R., Fushman, D., and Pickart, C. M. (2005) Diverse polyubiquitin interaction properties of ubiquitin-associated domains, *Nat Struct Mol Biol 12*, 708-714.

106. Peschard, P., Kozlov, G., Lin, T., Mirza, I. A., Berghuis, A. M., Lipkowitz, S., Park, M., and Gehring, K. (2007) Structural basis for ubiquitin-mediated dimerization and activation of the ubiquitin protein ligase Cbl-b, *Mol Cell 27*, 474-485.

107. Merkley, N., and Shaw, G. S. (2003) Interaction of the tail with the catalytic region of a class II E2 conjugating enzyme, *J Biomol NMR 26*, 147-155.

108. Huzil, J. T., Pannu, R., Ptak, C., Garen, G., and Ellison, M. J. (2007) Direct catalysis of lysine 48-linked polyubiquitin chains by the ubiquitin-activating enzyme, *J Biol Chem 282*, 37454-37460.

109. Rodrigo-Brenni, M. C., and Morgan, D. O. (2007) Sequential E2s drive polyubiquitin chain assembly on APC targets, *Cell 130*, 127-139.

110. Tanno, Y., Mori, T., Yokoya, S., Kanazawa, K., Honma, Y., Nikaido, T., Takeda, J., Tojo, M., Yamamoto, T., and Wanaka, A. (1999) Localization of huntingtin-interacting protein-2 (Hip-2) mRNA in the developing mouse brain, *J Chem Neuroanat 17*, 99-107.

111. Chen, Z. J., Niles, E. G., and Pickart, C. M. (1991) Isolation of a cDNA encoding a mammalian multiubiquitinating enzyme (E225K) and overexpression of the functional enzyme in Escherichia coli, *J Biol Chem 266*, 15698-15704.

112. Haldeman, M. T., Xia, G., Kasperek, E. M., and Pickart, C. M. (1997) Structure and function of ubiquitin conjugating enzyme E2-25K: the tail is a core-dependent activity element, *Biochemistry 36*, 10526-10537.

113. Ko, S., Kang, G. B., Song, S. M., Lee, J. G., Shin, D. Y., Yun, J. H., Sheng, Y., Cheong, C., Jeon, Y. H., Jung, Y. K., Arrowsmith, C. H., Avvakumov, G. V., Dhe-Paganon, S., Yoo, Y. J., Eom, S. H., and Lee, W. (2010) Structural basis of E2-25K/UBB+1 interaction leading to proteasome inhibition and neurotoxicity, *J Biol Chem 285*, 36070-36080.

114. Wilson, R. C., Edmondson, S. P., Flatt, J. W., Helms, K., and Twigg, P. D. (2011) The E2-25K ubiquitin-associated (UBA) domain aids in polyubiquitin chain synthesis and linkage specificity, *Biochem Biophys Res Commun 405*, 662-666.

115. Mueller, T. D., and Feigon, J. (2002) Solution structures of UBA domains reveal a conserved hydrophobic surface for protein-protein interactions, *J Mol Biol 319*, 1243-1255.

116. Varadan, R., Assfalg, M., Raasi, S., Pickart, C., and Fushman, D. (2005) Structural determinants for selective recognition of a Lys48-linked polyubiquitin chain by a UBA domain, *Mol Cell 18*, 687-698.

117. Chen, Z., and Pickart, C. M. (1990) A 25-kilodalton ubiquitin carrier protein (E2) catalyzes multi-ubiquitin chain synthesis via lysine 48 of ubiquitin, *J Biol Chem 265*, 21835-21842.

118. van Nocker, S., and Vierstra, R. D. (1993) Multiubiquitin chains linked through lysine 48 are abundant in vivo and are competent intermediates in the ubiquitin proteolytic pathway, *J Biol Chem 268*, 24766-24773.

119. Lee, S. J., Choi, J. Y., Sung, Y. M., Park, H., Rhim, H., and Kang, S. (2001) E3 ligase activity of RING finger proteins that interact with Hip-2, a human ubiquitin-conjugating enzyme, *FEBS Lett 503*, 61-64.

120. Coux, O., and Goldberg, A. L. (1998) Enzymes catalyzing ubiquitination and proteolytic processing of the p105 precursor of nuclear factor kappaB1, *J Biol Chem 273*, 8820-8828.

121. Yamada, M., Ohnishi, J., Ohkawara, B., Iemura, S., Satoh, K., Hyodo-Miura, J., Kawachi, K., Natsume, T., and Shibuya, H. (2006) NARF, an nemo-like kinase (NLK)-associated ring finger protein regulates the ubiquitylation and degradation of T cell factor/lymphoid enhancer factor (TCF/LEF), *J Biol Chem 281*, 20749-20760.

122. Bae, Y., Choi, D., Rhim, H., and Kang, S. (2010) Hip2 interacts with cyclin B1 and promotes its degradation through the ubiquitin proteasome pathway, *FEBS Lett 584*, 4505-4510.

123. Bae, Y., Kho, C. W., Lee, S. Y., Rhim, H., and Kang, S. (2010) Hip2 interacts with and destabilizes Smac/DIABLO, *Biochem Biophys Res Commun 397*, 718-723.

124. Oh, K. J., Kalinina, A., and Bagchi, S. (2010) Destabilization of Rb by human papillomavirus E7 is cell cycle dependent: E2-25K is involved in the proteolysis, *Virology 396*, 118-124.

125. Song, S., Kim, S. Y., Hong, Y. M., Jo, D. G., Lee, J. Y., Shim, S. M., Chung, C. W., Seo, S. J., Yoo, Y. J., Koh, J. Y., Lee, M. C., Yates, A. J., Ichijo, H., and Jung, Y. K. (2003) Essential role of E2-25K/Hip-2 in mediating amyloid-beta neurotoxicity, *Mol Cell 12*, 553-563.

126. Kikuchi, J., Furukawa, Y., Kubo, N., Tokura, A., Hayashi, N., Nakamura, M., Matsuda, M., and Sakurabayashi, I. (2000) Induction of ubiquitin-conjugating enzyme by aggregated low density lipoprotein in human macrophages and its implications for atherosclerosis, *Arterioscler Thromb Vasc Biol 20*, 128-134.

127. de Pril, R., Fischer, D. F., Roos, R. A., and van Leeuwen, F. W. (2007) Ubiquitin-conjugating enzyme E2-25K increases aggregate formation and cell death in polyglutamine diseases, *Mol Cell Neurosci 34*, 10-19.

128. Howard, R. A., Sharma, P., Hajjar, C., Caldwell, K. A., Caldwell, G. A., du Breuil, R., Moore, R., and Boyd, L. (2007) Ubiquitin conjugating enzymes participate in polyglutamine protein aggregation, *BMC Cell Biol 8*, 32.

Chapter 2

Determination of the Dimerization Capacity and Enzymatic Component Requirements for Poly-ubiquitin Chain Assembly in the E2 Conjugating Enzymes HIP2 and Ubc1

2.1 Introduction

The ubiquitin proteolysis pathway utilizes three enzymes, E1, E2 and E3 to respectively activate, transfer and ligate ubiquitin (Ub) onto a target protein (Fig 2.1A). These enzymes work together to build K48-linked poly-Ub chains that are formed on substrate proteins, targeting them to be degraded by the 26S proteosome. The mechanism of Ub-Ub covalent attachment in poly-Ub chain formation remains poorly understood.

There are various competing hypotheses describing the formation of poly-Ub chains, and it is possible that different E2 enzymes use different mechanisms to link Ub molecules (*1*). The sequential addition model, suggests one ubiquitin at a time is added to a substrate eventually forming a poly-Ub chain. Other models involve the preassembly of poly-Ub chains that are then transferred as a block onto a substrate. There is growing evidence that preassembly of poly-Ub chains may require the dimerization of E2 enzymes to position two Ub molecules to be connected together prior to attachment to substrate (*2-9*).

The E2 conjugating enzymes Ubc1 and HIP2 have poly-ubiquitination chain activity in the absence of E3 enzymes and substrates, and thus these E2 enzymes may

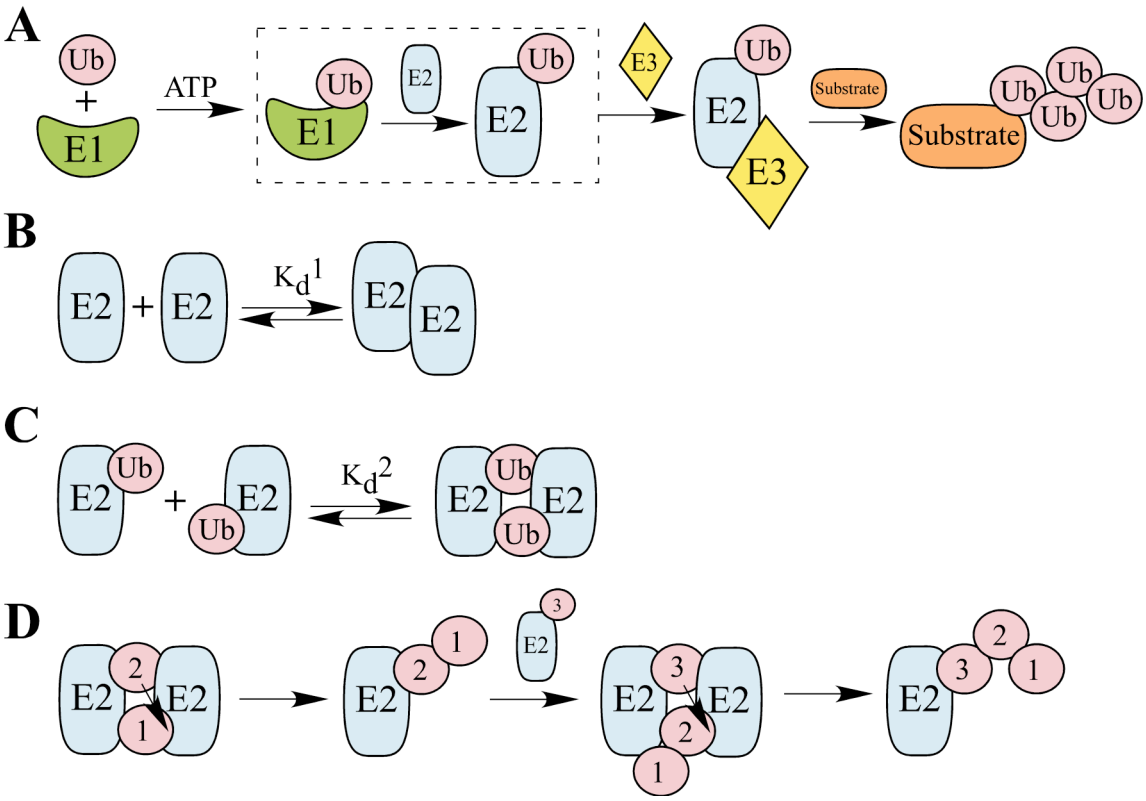

Figure 2.1 A schematic representation of the ubiquitin proteolysis pathway and a method by which poly-Ub chains may be constructed. (**A**) Ubiquitin is attached to a ubiquitin activating enzyme (E1) through an ATP dependant process that creates a highly reactive thiolester linkage. The Ub is then transferred to a ubiquitin conjugating enzyme (E2), and through the use of a ubiquitin ligating enzyme (E3) reacts with a lysine residue on a substrate. Proteins destined for degradation are labelled with a poly-Ub chain of four or more Ub molecules targeting the substrate to the 26S proteosome. (**B**) A model of E2 dimerization driven by interaction between the E2 enzymes whereby K_d^1 defines the dissociation constant of this interaction. (**C**) A model of E2~Ub thiolester dimerization driven by interactions between Ub and the E2 enzymes whereby K_d^2 defines the dissociation constant of this interaction. (**D**) A possible mechanism showing how poly-Ub chain formation can be performed using an E2 dimer to position Ub molecules (numbered 1-3) for attachment. Each arrow between Ub molecules represents the K48 side chain nucleophilic attack to the reactive thiolester of a second Ub. For simplicity these models do not depict the UBA domain of Ubc1 and HIP2, nor attempt to show the exact interaction surfaces used in dimerization.

function through dimerization (*10, 11*). If these E2 enzymes do indeed dimerize, they may do so directly (Fig 2.1B) or dimerize through the creation of the E2~Ub thiolester by providing the additional interaction surface of Ub to the E2 enzyme (Fig 2.1C). Determination of the strength of these possible dimeric interactions will aid in determining the mechanism by which Ubc1 and HIP2 function. One possible mechanism for the creation of a poly-Ub chain through an E2 dimer involves the placing of the K48 side chain of one Ub in close proximity to the reactive thiolester of a second Ub to allow a Ub-Ub connection. In this process the chain extends via multiple charging of the E2 enzymes with the building chain transferring onto newly charged E2 enzymes (Fig 2.1D). The determination of K_d^1 and K_d^2 in Figure 2.1B and C will indicate the plausibility of these models for Ubc1 and Hip2 function.

2.2 Materials and Methods

2.2.1 Cloning

Wild-type HIP2 cDNA in a pET28a vector was a generous gift from the Structural Genomics Consortium (Toronto). A C170S substitution in HIP2 was introduced using the Quikchange Site-Directed Mutagenesis (Stratagene, La Jolla, CA) protocol. The design of forward and reverse complement primers also included base changes for L169 to convert it from a rare to common *E. coli.* codon.

Ubiquitin (Ub) and Ubc1 from *S. cerevisiae* were expressed from a pET3a vector as described previously (*11*). Incorporation of substitutions into Ub and Ubc1 were accomplished by traditional PCR methods or the Quikchange protocol. Kathryn R.

Barber incorporated all substitutions in Ub and Ubc1. These substitutions include a G76C substitution (Ub^{G76C}) and/or a K48R substitution (Ub^{K48R}) in yeast Ub, and a K93R substitution in Ubc1 ($Ubc1^{K93R}$) to inhibit auto-ubiquitination. Human Ub with an N-terminal cysteine tag (GPCLGS) in the pGEX-6P1 GST fusion vector was a kind gift from Dr. Leo Spyrocopoulos (University of Alberta) and was modified to generate a K48R version by the Quikchange protocol. All substitutions were confirmed to be correct by DNA sequencing performed at the London Regional Genomics Centre.

2.2.2 Protein expression and purification of HIP2, Ubc1 and substituted ubiquitins

Various substituted ubiquitins and $Ubc1^{K93R}$ (hence forward just Ubc1) from *S. cerevisiae* were over expressed in BL21(DE3)pLysS *E. coli* strain and purified using a Q anion exchange column, followed by a Sephadex G75 (GE Healthcare) size exclusion column as previously described (*11*). Electrospray ionization mass spectrometry confirmed the integrity of Ubc1 (MW_{obs} 24162.4 ± 0.8Da, MW_{calc} 24162.2). Kathryn R. Barber purified Ubc1. Protein concentrations of Ubc1 were determined through Bradford (BioRad) reactions performed in triplicate. Protein concentrations of Ub were determined by weight of lyophilized proteins.

Hexahistidine (His^6) tagged $HIP2^{C170S}$ (hence forward just HIP2) was overexpressed in the BL21(DE3)star *E. coli* strain. The bacteria were grown at 37 °C overnight in LB media (10 mL) containing the antibiotic kanamycin (30 μg / mL). The culture was then diluted 1:100 into 1 L of LB containing the same antibiotics and grown at 37 °C to an A_{600} between 0.60-0.75. Protein expression was induced for 16-20 hours with 0.7 mM IPTG at 15 °C. Harvested cells were re-suspended in 20 mM Tris-HCl, 200

mM NaCl, 1 mM TCEP, 5 mM imidazole at pH 8.0 with the addition of a COMPLETE mini EDTA-free protease inhibitor cocktail tablet (Roche Diagnostics). Cells were lysed with a French pressure cell and cellular debris was removed by centrifugation at 95500 xg. All following purification procedures were performed at 4 °C to minimize protein degradation. The clarified extract containing His^6-HIP2 was applied to Ni-NTA Agarose (Qiagen) and washed with 20 mM Tris-HCl, 200 mM NaCl, 1 mM TCEP, 10 mM imidazole at pH 8.0 to elute non specifically bound material. His^6-HIP2 was eluted with 20 mM Tris-HCl, 200 mM NaCl, 1mM TCEP, 200 mM imidazole pH 8.0. The protein was concentrated and loaded on to a Superdex 75 10/300 GL column (GE Healthcare) in 20 mM Tris-HCl, 200 mM NaCl, 1mM TCEP, 10 mM imidazole pH 8.0. Thrombin (2 μg / mL) was utilized to cleave the His^6 tag at room temperature for two hours and a subsequent Ni-NTA Agarose column was utilized to remove the tag and any uncut protein from HIP2. A final Superdex 75 10/300 GL column run in 20 mM Tris-HCl, 200 mM NaCl, 1 mM TCEP pH 8.0 was used to remove residual thrombin from the purified HIP2 protein. Purification steps were monitored using SDS-PAGE. SDS-PAGE was performed using 16.5% tris-tricine gels in a mini-gel system (BioRad) and was stained with Coomassie dye. HIP2 concentrations were determined through Bradford (BioRad) reactions performed in triplicate. Purified HIP2 was confirmed using electrospray ionization mass spectrometry (MW_{obs} 22534.8 ± 0.3Da, MW_{calc} 22534.7).

2.2.3 Protein expression and purification of N^{Cys}-Ub and N^{Cys}-Ub^{K48R}

Human Ub proteins were modified to contain a cysteine residue in a peptide extension (GPCLGS) at the N-terminus of both wild type Ub (N^{Cys}-Ub) and Ub^{K48R}

(N^{Cys}-Ub^{K48R}). GST fusion proteins of N^{Cys}-Ub and N^{Cys}-Ub^{K48R} were over expressed in the BL21(DE3)pLysS *E. coli* strain. Cell cultures were grown overnight in LB media (10 mL) containing the antibiotic carbenicillin (50 μg / mL). The culture was then diluted 1:100 in LB media containing the same antibiotic and grown at 37 °C to an A_{600} of 0.60. Protein expression was induced with 0.5 mM IPTG for 4 hours at 37 °C. Harvested cells were re-suspended in binding buffer consisting of 25 mM Tris-HCl, 100 mM NaCl, 3 mM DTT at pH 7.5 with the addition of a COMPLETE mini EDTA-free protease inhibitor cocktail tablet (Roche Diagnostics). Cells were lysed with a French pressure cell and cellular debris was removed by centrifugation at 95500 xg. The lysate was purified using a GST affinity column (GE Biosciences), washed with the same binding buffer and eluted with 25 mM Tris-HCl, 100 mM NaCl, 3 mM DTT, and 20 mM glutathione. The GST affinity tag was cut using TEV (Shaw lab; 50 μg / mL) and removal of the GST tag, any uncut protein and the TEV protease was achieved by size exclusion chromatography on a Sephadex G-75 column (GE Healthcare) with 25 mM Tris-HCl, 100 mM NaCl, 0.5 mM EDTA pH 7.4. Purification steps were monitored using SDS-PAGE. SDS-PAGE was performed using 16.5% tris-tricine gels in a mini-gel system (BioRad) and was stained with Coomassie dye. N^{Cys}-Ub and N^{Cys}-Ub^{K48R} concentrations were determined through SDS-PAGE comparison to Ub substitutions. Purified N^{Cys}-Ub and N^{Cys}-Ub^{K48R} were confirmed using electrospray ionization mass spectrometry (N^{Cys}-Ub^{K48R}: MW_{obs} 9107.61 ± 0.42 MW_{calc} 9107.4; N^{Cys}-Ub: MW_{obs} 9079.08 ± 0.94 MW_{calc} 9079.44).

N^{Cys}-Ub and N^{Cys}-Ub^{K48R} were then reacted with Alexa-Fluor 680 C2-Maleimide (Invitrogen) to fluorescently label the Ub and Ub^{K48R}. The cysteine in N^{Cys}-Ub and N^{Cys}-

Ub^{K48R} reacts with the C2-maleimide to yield Alexa-Ub and Alexa-Ub^{K48R}. These reactions were performed by a 10:1 (v/v) mixing of 100 μM N^{Cys}-Ub in 100 mM NaCl, 0.5 mM EDTA, 25 mM Tris-HCl pH 7.4 and 5 mM Alexa-Flour in 100% isopropanol respectively. This reaction was stopped with the addition of 5 mM DTT, and then purified using a PD-10 desalting column (GE Healthcare) and extensive dialysis with 25 mM Tris-HCl, 100 mM NaCl pH 7.3 was used to remove unreacted Alexa dye. Ub molecules were confirmed to be labelled with Alexa via electrospray ionization mass spectrometry (Alexa-Ub^{K48R} MW_{obs} 10089.21 ± 0.31 agrees with expected values for N^{Cys}-Ub^{K48R} (9107.46 Da) and Alexa dye (~982 Da)); Alexa-Ub MW_{obs} 10061.89 ± 0.40 agrees with expected values for N^{Cys}-Ub (9079.44 Da) and Alexa dye (~982 Da)).

2.2.4 E2-Ub disulphide complex formation

Two different versions of disulphide complexes were created for both HIP2 and Ubc1. $Ub^{K48R-G76C}$ (shortened to Ub^{Cys}) was used for all protein interaction studies while Ub^{G76C} ($Ub_{K48}{}^{Cys}$) was used for activity assays on disulphide chain extension. Since the choice of Ub^{Cys} or $Ub_{K48}{}^{Cys}$ is immaterial to purification, only Ub^{Cys} shall be described for simplicity. Solutions of Ub^{Cys}, Ubc1 or HIP2 (0.1 mM) were fully reduced with 2 mM TCEP. Ubc1 or HIP2 was combined with an excess of Ub^{Cys} and dialyzed at 4 °C against several changes of 100 mM Na_2HPO_4/NaH_2PO_4, 100 mM NaCl, 10 μM $CuCl_2$ at pH 7.5. The progress of the disulphide complex formation was monitored by non-reducing SDS-PAGE and was considered complete when Ubc1 or HIP2 was exhausted, usually requiring 72-96 hours. The completed E2-Ub^{Cys} reaction also contains the disulphide by-products Ub^{Cys}-Ub^{Cys} and E2-E2 dimers. The protein solution was concentrated and the

by-products removed by size exclusion chromatography on a Sephadex G-75 column with 25 mM Tris-HCl, 1 mM EDTA, and 150 mM NaCl (Ubc1-Ub^{Cys}) or 400 mM NaCl (HIP2-Ub^{Cys}), at pH 7.5. Purification steps were monitored using SDS-PAGE. SDS-PAGE was performed using 16.5% tris-tricine gels in a mini-gel system (BioRad) and was stained with Coomassie dye. Ubc1-Ub^{Cys} and HIP2-Ub^{Cys} concentrations were determined through Bradford (BioRad) reactions performed in triplicate. HIP2-Ub^{Cys} concentrations for SAXS studies were determined with amino acid analysis (Advanced Protein Technology Center). Fractions containing pure Ubc1-Ub^{Cys} or HIP2-Ub^{Cys} were pooled and their purity and identity confirmed by mass spectrometry (Ubc1-Ub^{Cys} MW_{calc} 32791.1, MW_{obs} 32,794.59 ± 4.0Da; HIP2-Ub^{Cys} MW_{obs} 31163.2 ± 1.0Da, MW_{calc} 31163.5).

2.2.5 Analytical ultracentrifugation

Sedimentation equilibrium experiments were performed on a Beckman Optima XL-A analytical ultracentrifuge capable of UV/VIS wavelength scanning. An An-60 Ti analytical rotor was used with six-channel equilibrium double sector Epon-charcoal center pieces, which contain three protein/buffer pairs. Quartz windows were used on the ends of the 12 mm thick center pieces to allow absorbance values to be collected at either 250 or 280 nm in 0.002 cm radial steps and averaged over 10 readings. Experiments were performed at 5 °C and at rotor speeds of 15000, 18000, 22000 and 26000 rpm. A delay of 20 hours (Ubc1, HIP2) or 16 hours (Ubc1-Ub^{Cys}, HIP2-Ub^{Cys}) was used to reach the initial state of equilibrium, and further increases in speed were allowed 8 hours to reach equilibrium before readings were measured. At each speed two scans were

performed two hours apart. These scans were superimposed to confirm that a state of equilibrium had been properly achieved. Protein sample cells were loaded with 100 μL protein and reference sample cells were loaded with 110 μL buffer. All protein samples were dialyzed into their respective buffers (Ubc1 and Ubc1-Ub^{Cys}: 25 mM Tris-HCl, 1 mM EDTA, 150 mM NaCl at pH 7.5 (plus 2 mM TCEP for Ubc1); and HIP2: 20 mM Tris-HCl, 200 mM NaCl, 1 mM TCEP at pH 8.0; and HIP2-Ub^{Cys}: 25 mM Tris-HCl, 400 mM NaCl, 1 mM EDTA at pH 7.5) and diluted with this dialysis buffer to the desired concentrations. The experiments were performed on Ubc1 and HIP2 with concentrations of 14.7 μM and 9.6 μM respectively. Three different concentrations were analyzed for both HIP2-Ub^{Cys} (7.2, 14.4 and 24 μM) and Ubc1-Ub^{Cys} (10.8, 21.5 and 43 μM). The solvent densities were calculated from published tables of buffer components (*12*) (*13*). Partial specific volumes of all proteins were calculated using their amino acid compositions (*14*). Data was analyzed using Prism 4 (Graphpad) with two different models using a global analysis for multiple data sets on an Apple iMac G4 computer. One analysis involved the single ideal species model defined by equation 1,

$$C_r = C_o \exp[(\omega^2/2RT)M_{obs}(1-\upsilon\rho)(r^2-r_o^2)]+I_o \qquad (1)$$

where C_r is the protein concentration at radius r, C_o is the concentration at the reference radius r_o, ω is the angular velocity of the rotor, R is the ideal gas constant, T is the temperature in Kelvin, M_{obs} is the protein molecular weight, υ is the partial specific volume of the protein, ρ is the density of the solvent, and I_o is the baseline offset. A self-associating model defined by equation 2 was also used to fit data for a monomer-dimer equilibrium,

$$C_r=\{C_o\exp[(\omega^2/2RT)M_p(1-\upsilon\rho)(r^2-r_o^2)]\}+\{C_o^2K_a\exp[(\omega^2/2RT)2M_p(1-\upsilon\rho)(r^2-r_o^2)]\}+I_o \quad (2)$$

$$K_d = 1/K_a = [\text{monomer}]^2 / [\text{dimer}] \quad (3)$$

where M_p is the mass of the monomer, K_a and K_d are the equilibrium association and dissociation constants (in absorbance units, AU) defined by equation 3, and all other terms are identical to equation 1. K_d values were converted from absorbance units to molarity using the extinction coefficients calculated for each protein from low speed scans.

2.2.6 Small angle X-ray scattering

Small angle X-ray scattering (SAXS) data was collected on three separate occasions at BioCAT Beamline ID-18 of the Advanced Photon Source (Argonne, Illinois) using X-rays with a wavelength of 1.03 Å. The beam centre was determined from silver behenate powder diffraction, and the sample to detector distance varied from 1892 mm to 2810 mm. Data were recorded on a Brandeis II or Mar165 CCD detector.

The sample chamber consisted of a 1.5 mm diameter quartz capillary mounted in a brass holder maintained at 10 °C and connected to a syringe pump. Three to ten exposures (approximately 2 s each) were recorded for each sample and its matched buffer. During the recording the sample (80 µL volume) was kept moving through the capillary to limit radiation-induced aggregation. The two dimensional images were radially integrated using either Fit2D (*15*) or Igor Pro (Wavemetrics, Lake Oswego, Oregon), and the individual frames were averaged after removal of outliers. Scattering from buffer alone was subtracted from the protein-containing samples to yield scattering from the hydrated protein. Additional data processing was carried out in Microsoft Excel

and/or the Igor Pro macros developed at BioCAT. The momentum transfer (Q) is defined as $4\pi\sin\theta/\lambda$, where 2θ is the scattering angle.

The buffer conditions used for SAXS data collection are identical to sedimentation equilibrium studies, except HIP2-Ub^{Cys} that had a pH change to 8.0. A second data set for HIP2-Ub^{Cys} SAXS data was collected in 100 mM phosphate, 400 mM NaCl, 3 mM EDTA at pH 7.4. The change in buffer conditions had little affect on HIP2-Ub^{Cys} protein scattering.

CRYSOL (*16*) was used to calculate theoretical scattering from atomic coordinates and adjust hydration parameters to compare to experimental data. The quality of the match of theoretical scattering to experimental scattering is measured with a goodness of fit value (χ^2) that is defined as:

$$\chi^2 = 1/N\ (N\Sigma i=1)\ [\ (I_e(s_i) - cI_c(s_i))/\sigma(s_i)\ ]^2 \qquad (4)$$

where N is the number of data points, s is the magnitude of the scattering vector, c is a scale factor, I_e is the experimental intensity, I_c is the calculated intensity, and σ is the experimental error (*16*).

All figures for SAXS CRYSOL curves were produced using the default input parameters for CRYSOL curve fitting (*16*). The PDB files used in CRYSOL analysis figures were 1TTE (for Ubc1), 1UBQ (for ubiquitin), 1YLA (for HIP2), 1FXT (for the Ub position in the 'compact' thiolester), and 2GMI (for the Ub position in the 'elongated' thiolester).

2.2.7 E2 poly-ubiquitination activity assays

Ubiquitination reactions were performed with purified E2 enzymes, disulphide complexes and unlabelled Ub proteins. Several reactions were performed which contained different combinations of E2 enzymes and Ub proteins. All reactions contain a subset of the following final protein concentrations: 150 nM E1 enzyme, 4.1 μM HIP2 conjugating enzyme, 2.0 μM HIP2-Ub_{K48}^{Cys} thiolester mimic, 4.1 μM Ubc1 conjugating enzyme, 2.0 μM Ubc1-Ub_{K48}^{Cys} thiolester mimic, 11.0 μM Ub, and 10.8 μM Ub^{K48R}. All reactions also had final concentrations of 10 mM Mg-ATP and 50 mM Hepes pH 8.0. Reaction protein species were visualized using 16.5% tris-tricine gels in a mini-gel system (BioRad) stained with Coomassie dye. Reactions were carried out for 5 min, 30 min and 1 hour with the HIP2 conjugating enzyme, and 5 min, 2 hours, and 5 hours with the Ubc1 conjugating enzyme since Ubc1 seems to have a lower poly-ubiquitination activity. Each reaction was stopped with excess EDTA buffer and then combined with non-reducing SDS running buffer and heated for 5 min at 95 °C.

2.2.8 HIP2 and Ubc1 activity assays with Alexa labeled Ub

Alexa dye labelled ubiquitination reactions were performed with purified E2 enzymes, disulphide complexes and Alexa fluorescent dye labelled N^{Cys}-Ub or N^{Cys}-Ub^{K48R}. Several reactions were performed with different combinations of E2 enzymes and Ub proteins. All HIP2 enzyme reactions had a subset of the following final protein concentrations: 225 nM E1 enzyme, 12 μM HIP2 conjugating enzyme, 15.2 μM HIP2-Ub_{K48}^{Cys} thiolester mimic, 3.9 μM Alexa-Ub^{K48R}, and 3.9 μM Alexa-Ub. All Ubc1 reactions had a subset of the following final protein concentrations: 214 nM E1 enzyme,

12.3 μM Ubc1 conjugating enzyme, 10.5 μM Ubc1-Ub_{K48}^{Cys} thiolester mimic, 5.5 μM Alexa-Ub^{K48R}, and 5.5 μM Alexa-Ub. Both of the above reactions use final concentrations of 10 mM Mg-ATP and 50 mM Hepes pH 8.0. Reactions were carried out in a manner similar to previous activity assays except the Ubc1 reaction was performed for 4 hours, and the HIP2 reaction was performed for 1 hour. Reactions were visualized using 16.5% tris-tricine gels in a mini-gel system (BioRad) stained with Coomassie dye or visualized by fluorescence using an Odyssey imaging system (LI-COR).

Additional activity assays were performed utilizing purified E2 thiolesters to remove E1 from poly-ubiquitination reactions. The Alexa-Ub^{K48R} thiolester was formed with either Ubc1 or HIP2 in a 30 min reaction with final concentrations of 18.3 μM Alexa-Ub^{K48R}, 12.3 μM Ubc1, 214 nM E1 for the Ubc1 thiolester and 16.4 μM Alexa-Ub^{K48R}, 32.8 μM HIP2, 214 nM E1 for the HIP2 thiolester. This thiolester reaction mixture was then immediately loaded onto a Sephadex G75 10/300 size exclusion column to purify the thiolester from unconjugated Alexa-Ub^{K48R} and E1 enzyme. Thiolesters were then concentrated with a 3K Nanosep concentrator (Pall). Purified thiolesters were then reacted with different mixtures of purified proteins. All Ubc1 thiolester reactions contained a subset of the following final protein concentrations: 500 nM reactive Alexa dye, 90 μM Ub, 90 μM Ub^{K48R}, 9.2 μM Ubc1-Ub_{K48}^{Cys}. All HIP2 thiolester reactions contained a subset of the following final protein concentrations: 500 nM reactive Alexa dye, 54 μM Ub, 54 μM Ub^{K48R}, 6 μM HIP2-Ub_{K48}^{Cys}. HIP2 thiolester reactions proceed for 1 hour at 37 °C, while Ubc1 thiolester reactions proceeded for 5 hours at 37 °C. All of the above reactions used final concentrations of 10 mM Mg-ATP solution, and 50 mM Hepes at pH 8.0.

2.3 Results

2.3.1 Expression and purification of HIP2

A C170S substitution was introduced into the E2 enzyme HIP2 to ensure that the active site C92 was the only cysteine residue available for the future creation of a disulphide thiolester mimic. Previous studies have shown this C170S substitution does not affect enzyme activity (*17*). $HIP2^{C170S}$ (hence forward just HIP2) was overexpressed with an N-terminal hexahistidine (His^6) tag and was soluble in BL21(DE3)star *E. coli* cells when induced with IPTG (Fig 2.2A). Purification of His^6-HIP2 from *E. coli* cells was performed by cell lysis with a French Press, followed by centrifugation to remove cellular debris. The remaining lysate was then subjected to Ni^{2+}-affinity chromatography that selectively binds to the N-terminal His^6 fusion tag (Fig 2.2B – lane 5). The fusion tag was removed by the cleavage enzyme thrombin leaving an N-terminal GS extension on the normally 200 amino acid long HIP2 protein. A second Ni^{2+}-affinity chromatography purification step was performed on thrombin treated protein leaving only the purified HIP2 in the flow through fraction (Fig 2.2B - lane 7). Size exclusion purification was then performed on the pure protein to remove any minor trace proteases and residual thrombin. Using electrospray ionization mass spectrometry, a single major peak was observed (MW_{obs} 22534.8 ± 0.3Da) at the expected molecular weight (MW_{calc} 22534.7) confirming that the purified HIP2 protein was intact (Fig 2.2C).

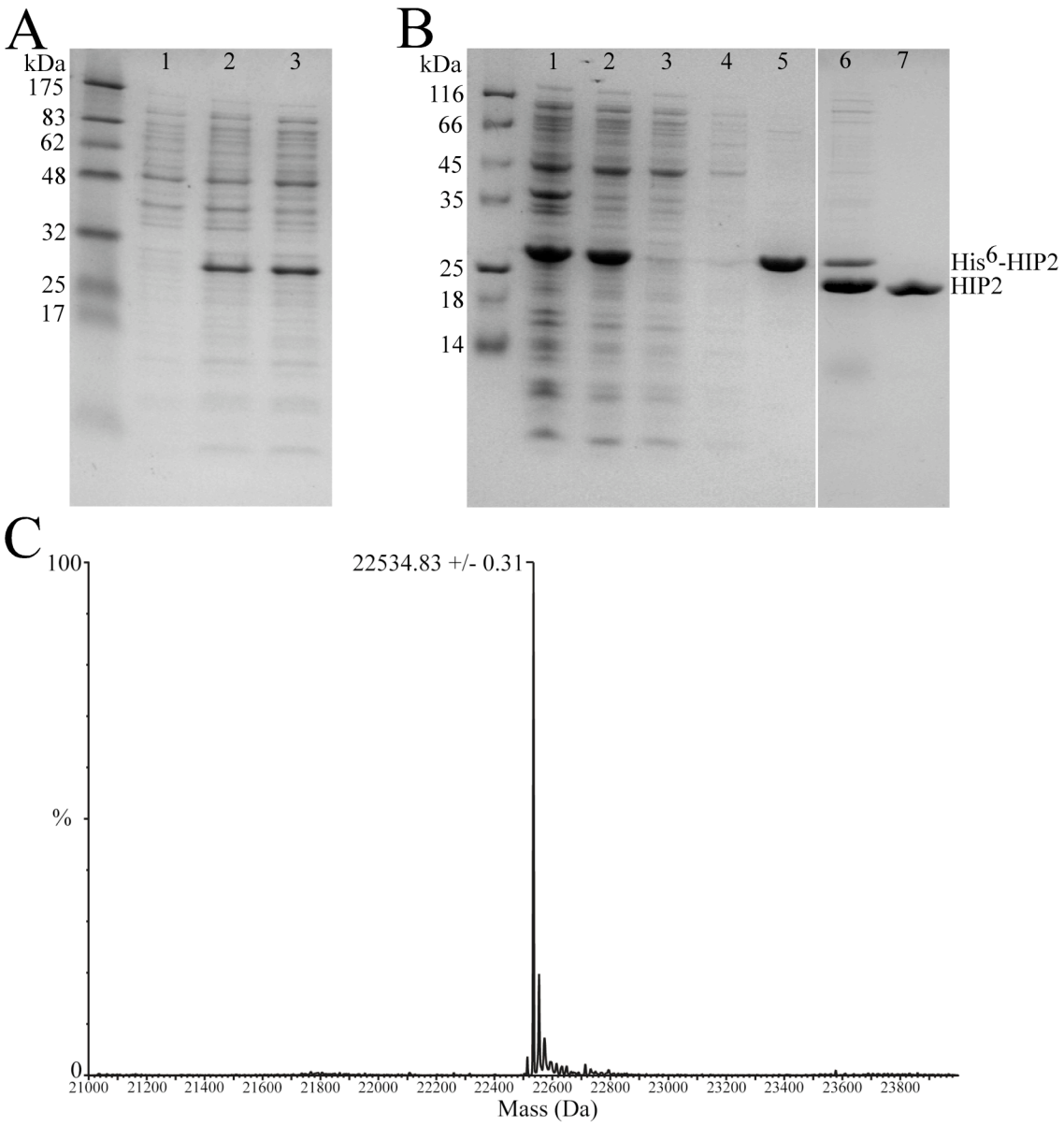

Figure 2.2 Expression and purification of the E2 conjugating enzyme HIP2. The E2 conjugating enzyme HIP2 was first expressed with a His^6 tag. (**A**) Protein expression testing of His^6-HIP2 was performed using 2 mL LB cultures, and analyzed using SDS-PAGE samples on cell cultures. The Coomassie stained gel shows first uninduced sample (lane 1) followed by IPTG induced cells showing the expression of His^6-HIP2 (lane 2), and finally the soluble fraction of protein was isolated by lysozyme cell lysis and centrifugation to remove insoluble protein (lane 3). (**B**) Purification of His^6-HIP2 depicted by Coomassie stained SDS-PAGE gels following procedures listed in Section 2.2.2. The HIP2 purification gel is loaded from left to right with induced cells (lane 1), lysate following centrifugation (lane 2), Ni^{2+}-affinity column flow through (lane 3), wash (lane 4) and elution (lane 5), HIP2 following thrombin cleavage (lane 6) and flow through from the second Ni^{2+} affinity column (lane 7). Molecular weight standards are listed in kDa to the left of each gel. (**C**) Electrospray ionization mass spectrometry analysis of purified HIP2 indicates the correct mass.

2.3.2 Expression and purification of substituted ubiquitins

Specific Ub substitutions are essential for the creation of E2-Ub thiolester mimics and for use in wild type and blocked poly-Ub chain activity assays with HIP2 and Ubc1. The Ub molecule carrying a G76C substitution was required for C-terminal disulphide formation used to make E2 enzyme thiolester mimics while a K48R substitution on Ub was utilized to block K48-linked poly-Ub chain extension. Wild type Ub and UbK48R (Ub^{K48R}) were purified for use in poly-Ub chain activity assays as functional and blocked Ub species respectively. $Ub^{K48R\text{-}G76C}$ (shortened to Ub^{Cys}) and Ub^{G76C} ($Ub_{K48}{}^{Cys}$) were used to create blocked and extendable thiolester mimics respectively. All of these Ub substitutions were purified as previously described (*11, 18*).

2.3.3 Formation and purification of HIP2-Ub disulphide thiolester mimics

Ubc1 and HIP2 conjugating enzymes function by allowing a highly reactive thiolester to be formed between their active site cysteine side chain and the C-terminal carboxylic acid of G76 in ubiquitin. This thiolester intermediate is susceptible to hydrolysis at basic pH and thus only lasts a few hours in solution (*19*). The instability of the thiolester limits in depth structural studies on these species. Through the use of a Ub G76C substitution a much more stable thiolester mimic can be created by the formation of a disulphide bond between the newly added C-terminal cysteine side chain on Ub and the active site cysteine on the E2 enzyme. This disulphide bond will persist for months allowing direct study of the E2 intermediate. Previous NMR studies on this disulphide show that the E2-Ub interactions are nearly identical compared to the activated thiolester, and thus the E2-Ub disulphide model accurately mimics the E2~Ub thiolester

intermediate (*18*). NMR chemical shift index analysis of this disulphide bond has also shown that the secondary structures of the E2 enzyme and Ub undergo no major changes upon bond formation (*18, 20*).

HIP2 disulphide complexes were created for both Ub^{Cys} that is blocked from K48 poly-Ub chain formation and $Ub_{K48}{}^{Cys}$ that has an available K48 residue for poly-Ub chain formation. Ub^{Cys} was used for all protein interaction studies while $Ub_{K48}{}^{Cys}$ was used for activity assays on disulphide chain extension. Ub^{Cys} and $Ub_{K48}{}^{Cys}$ are purified identically so only purification of Ub^{Cys} shall be described for simplicity. In order to create the disulphide intermediate, both HIP2 and Ub^{Cys} are chemically reduced and then dialyzed into an oxidization buffer over the course of 72-96 hrs promoting the formation of disulphide bonds (Fig 2.3A). The resulting HIP2-Ub^{Cys} disulphide was contaminated with the disulphide by-products of HIP2-HIP2 and Ub^{Cys}-Ub^{Cys} dimers as well as unreacted HIP2. These unwanted by-products were removed by size exclusion chromatography yielding pure HIP2-Ub^{Cys} disulphide (Fig 2.3B). Using electrospray ionization mass spectrometry, a single major peak was observed (MW_{obs} 31163.2 ± 1.0Da) at the expected molecular weight (MW_{calc} 31163.5) confirming that the purified HIP2-Ub^{Cys} thiolester mimic was the correct mass (Fig 2.3C).

2.3.4 Expression and Purification of Ubc1 and the Ubc1-Ub disulphide

The E2 enzyme Ubc1 is the yeast homolog of HIP2 and was purified as previously described (*11, 18*). The Ubc1-Ub^{Cys} and Ubc1-$Ub_{K48}{}^{Cys}$ disulphides were created and purified in an identical manner to the HIP2-Ub^{Cys} and HIP2-$Ub_{K48}{}^{Cys}$ disulphides. An example SDS-PAGE gel shows a single band demonstrating the extent of purification

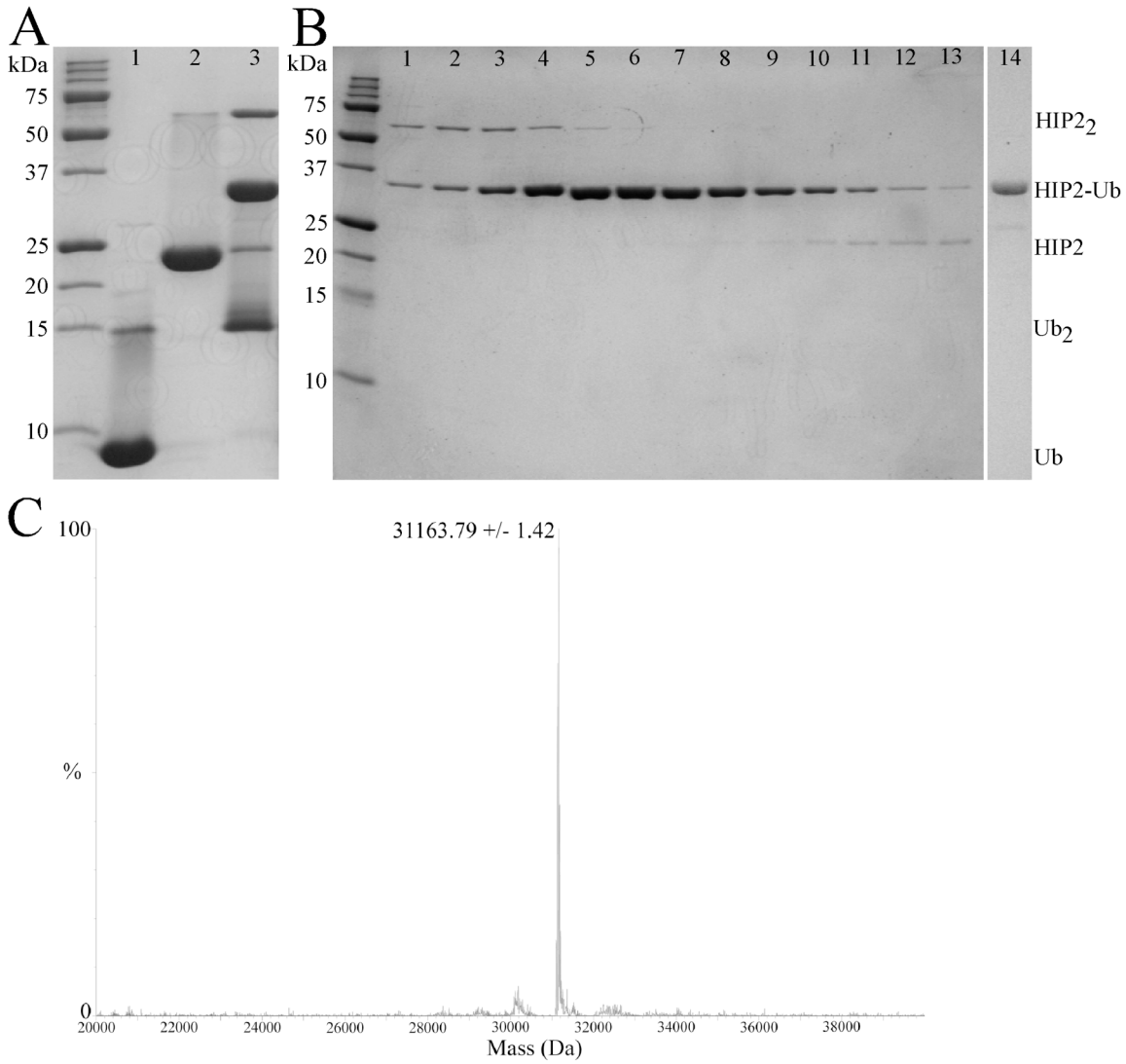

Figure 2.3 Creation and purification of the HIP2-Ub^{Cys} disulphide. (**A**) Purified and TCEP reduced Ub^{Cys} (lane 1) is mixed with purified and TCEP reduced HIP2 (lane 2) and dialyzed into an oxidation buffer containing 10 μM $CuCl_2$ driving disulphide bond creation to produce HIP2-HIP2, HIP2-Ub^{Cys} and Ub^{Cys}-Ub^{Cys} (lane 3). (**B**) Protein purification of HIP2-Ub^{Cys} from other disulphide byproducts using size exclusion chromatography (Sephadex G-75) depicted by Coomassie stained SDS-PAGE. A sample set of size exclusion elution fractions are shown whereby the larger HIP2-HIP2 byproduct elutes first (lane 1-5), followed by overlap of the HIP2-Ub^{Cys} disulphide (lane 1-13), and finally unreacted HIP2 elutes last (lane 10-13). Pure HIP2-Ub^{Cys} fractions (lane 7-8) are combined with other runs to give the final purified HIP2-Ub^{Cys} disulphide preparation (lane 14). Molecular weight standards are listed in kDa to the left of each gel. (**C**) Electrospray ionization mass spectrometry analysis of purified HIP2-Ub^{Cys} indicating the protein is the correct mass.

of Ubc1 and Ubc1-Ub^{Cys} (Fig 2.4A). Using electrospray ionization mass spectrometry, a single major peak was observed for both Ubc1 and Ubc1-Ub^{Cys} confirming the correct mass of the proteins (Ubc1: MW_{obs} 24162.4 ± 0.8Da, MW_{calc} 24162.2; Ubc1-Ub^{Cys} MW_{calc} 32791.1, MW_{obs} 32794.59 ± 4.0Da).

2.3.5 Expression and purification of N-terminal cysteine tagged ubiquitin

The sensitivity of activity assays was improved through the use of Alexa-Fluor 680 C2-maleimide fluorescent dye to label Ub proteins. The fluorescent Alexa dye was covalently bound to Ub molecules containing a cysteine residue in an N-terminal peptide extension (GPCLGS) on Ub (N^{Cys}-Ub) and Ub^{K48R} (N^{Cys}-Ub^{K48R}). The GST fusion proteins GST-N^{Cys}-Ub and GST-N^{Cys}-Ub^{K48R} were overexpressed and soluble in *E. coli* BL21(DE3)pLysS cells when induced with IPTG. Purification of these GST fusion proteins from *E. coli* cells was performed by cell lysis with a French Press, followed by centrifugation to remove cellular debris. The remaining lysate was subjected to GST-affinity chromatography that selectively binds to the N-terminal GST-fusion tag leaving mostly purified protein (Fig 2.4B - lane 4). The GST fusion tag was cut off by the cleavage enzyme TEV (50 μg / mL) and removal of the GST-fusion tag, any uncut protein, and the TEV enzyme was accomplished with size exclusion chromatography leaving purified N^{Cys}-Ub or N^{Cys}-Ub^{K48R} (Fig 2.4B - lane 6). Using electrospray ionization mass spectrometry, a single major peak was observed at the expected molecular weights confirming that the purified N^{Cys}-Ub and N^{Cys}-Ub^{K48R} proteins were the correct mass (N^{Cys}-Ub^{K48R}: MW_{obs} 9107.61 ± 0.42, MW_{calc} 9107.4; N^{Cys}-Ub: MW_{obs} 9079.08 ± 0.94, MW_{calc} 9079.44). These N-terminally cysteine tagged ubiquitins are then

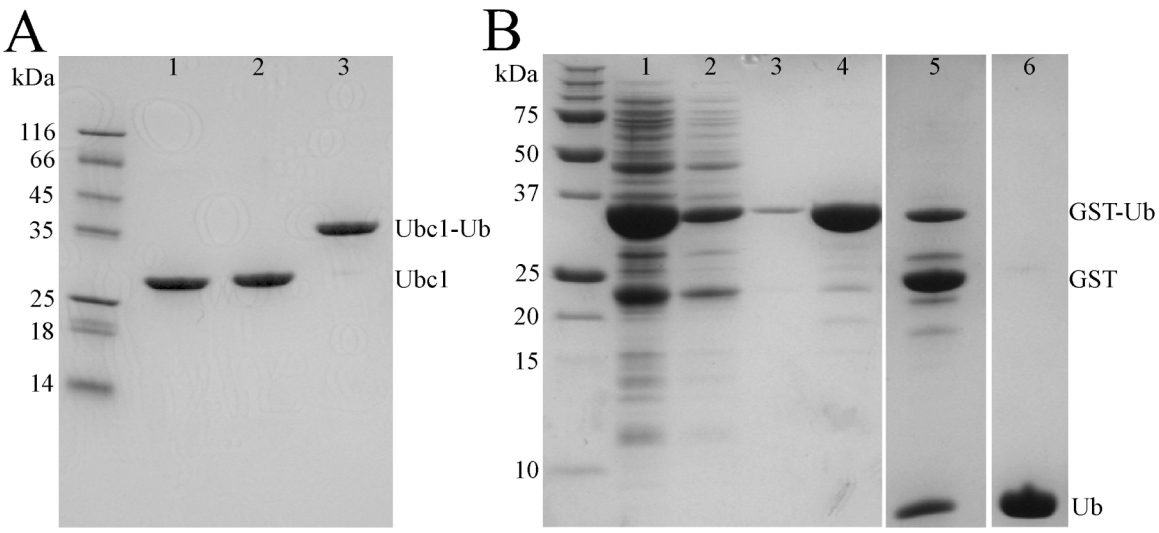

Figure 2.4 Purity check of Ubc1 and Ubc1-Ub^{Cys}, and purification of N^{Cys}-Ub. (**A**) SDS-PAGE gels run on purified samples of Ubc1 (lane 1 and with DTT lane 2) and Ubc1-Ub^{Cys} (lane 3) show proteins to be relatively pure for further studies. (**B**) Protein purification GST-N^{Cys}-Ub depicted by Coomassie stained SDS-PAGE shows centrifuged cell lysate of overexpressed GST-N^{Cys}-Ub (lane 1) followed by GST affinity chromatography flow through (lane 2), wash (lane 3), and elution with 20mM Glutathione (lane 4). The GST is then removed by addition of the cleavage enzyme TEV (lane 5) and finally a size exclusion column (Sephadex G-75) is used to purify N^{Cys}-Ub (lane 6) from uncut protein and freed GST fusion tag. Molecular weight standards are listed in kDa to the left of each gel, and protein species are listed to the right of each gel.

reacted with Alexa-Fluor 680 C2-maleimide to yield Alexa-N^{Cys}-Ub (Alexa-Ub) and Alexa-N^{Cys}-Ub^{K48R} (Alexa-Ub^{K48R}). Purification of Alexa-Ub and Alexa-Ub^{K48R} was performed using desalting columns and extensive dialysis to remove unreacted Alexa dye. The identity of Alexa-Ub and Alexa-Ub^{K48R} were confirmed by electrospray ionization mass spectrometry (Alexa-Ub^{K48R} MW_{obs} 10089.21 ± 0.31 agrees with expected values for N^{Cys}-Ub^{K48R} (9107.46 Da) and Alexa dye (~982 Da)); Alexa-Ub MW_{obs} 10061.89 ± 0.40 agrees with expected values for N^{Cys}-Ub (9079.44 Da) and Alexa dye (~982 Da)).

2.3.6 HIP2 and Ubc1 can build poly-Ub chains on their E2-$Ub_{K48}{}^{Cys}$ disulphides

The best example of an E2~Ub thiolester interacting with another E2~Ub thiolester involves the Ube2g2 (Ubc7) E2 enzyme. In this example, poly-Ub chains form on the E2 active site presumably assisted by dimerization (*2, 3*). A similar approach was used to test the dimerization capacity of Ubc1 and HIP2 by testing the possible reaction of an E2~Ub thiolester with an E2-Ub disulphide. This reaction was accomplished using two specific Ub substitutions, $Ub_{K48}{}^{Cys}$ and Ub^{K48R} (Fig 2.5A/2.6A). $Ub_{K48}{}^{Cys}$ containing a reactive K48 residue was used as the ubiquitin acceptor, while Ub^{K48R}, which is blocked from K48 chain extension, was used as the ubiquitin donor. A reaction containing ATP, Ub^{K48R}, E1, and either E2 enzyme was used to create the E2~Ub^{K48R} thiolester that is unable to build poly-Ub chains on its own. The E2~Ub^{K48R} thiolester can however, act as a ubiquitin donor. The E2-$Ub_{K48}{}^{Cys}$ disulphide was formed to incorporate an available K48 residue on the attached Ub, and therefore act as the acceptor in poly-Ub chain

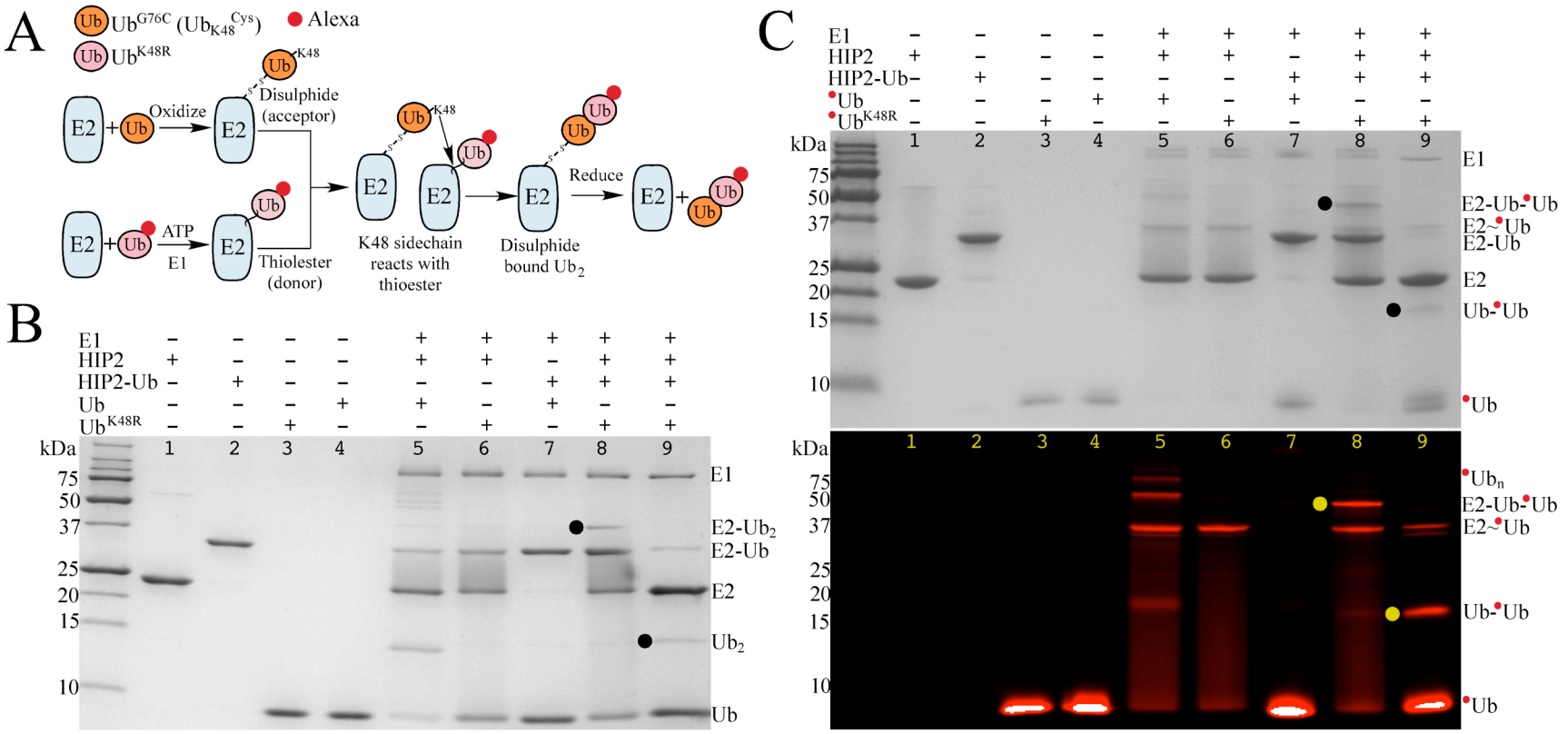

Figure 2.5 HIP2 activity gels showing Ub transfer from the HIP2~Ub^{K48R} thiolester onto the HIP2-$Ub_{K48}{}^{Cys}$ disulphide. (**A**) Reaction of the HIP2-$Ub_{K48}{}^{Cys}$ disulphide and the HIP2~Ub^{K48R} thiolester to produce HIP2-$Ub_{K48}{}^{Cys}$-Ub^{K48R} (HIP2-Ub_2). The use of Ub^{K48R} or Alexa-Ub^{K48R} result in similar products. (**B**) HIP2 enzyme reactions contain a subset of the following: 150 nM E1, 4.1 µM HIP2, 2.0 µM HIP2-$Ub_{K48}{}^{Cys}$ disulphide, 11.0 µM Ub (wild type), 10.8 µM Ub^{K48R}, 10 mM Mg-ATP solution, in 50 mM Hepes pH 8.0. (**C**) Reactions from (**B**) repeated with Alexa-Ub and Alexa-Ub^{K48R} and visualized with Coomassie (top gel) or 700 nm fluorescence (bottom gel). Each reaction contains a subset of the following: 225 nM E1, 12 µM HIP2, 15.2 µM HIP2-$Ub_{K48}{}^{Cys}$ disulphide, 3.85 µM Alexa-Ub, 3.85 µM Alexa-Ub^{K48R}, 10 mM Mg-ATP solution, in 50 mM Hepes pH 8.0. Reaction components are listed above each gel with a (+) or (-). Reactions were performed for 1 hr at 37 °C, and reducing agent is only added to lane 9 (10 mM DTT and 10 mM TCEP) to break the disulphide. Ub-Ub attachments are indicated by the filled black/yellow circles. Molecular weight standards and protein species are listed to the left and right of each gel respectively.

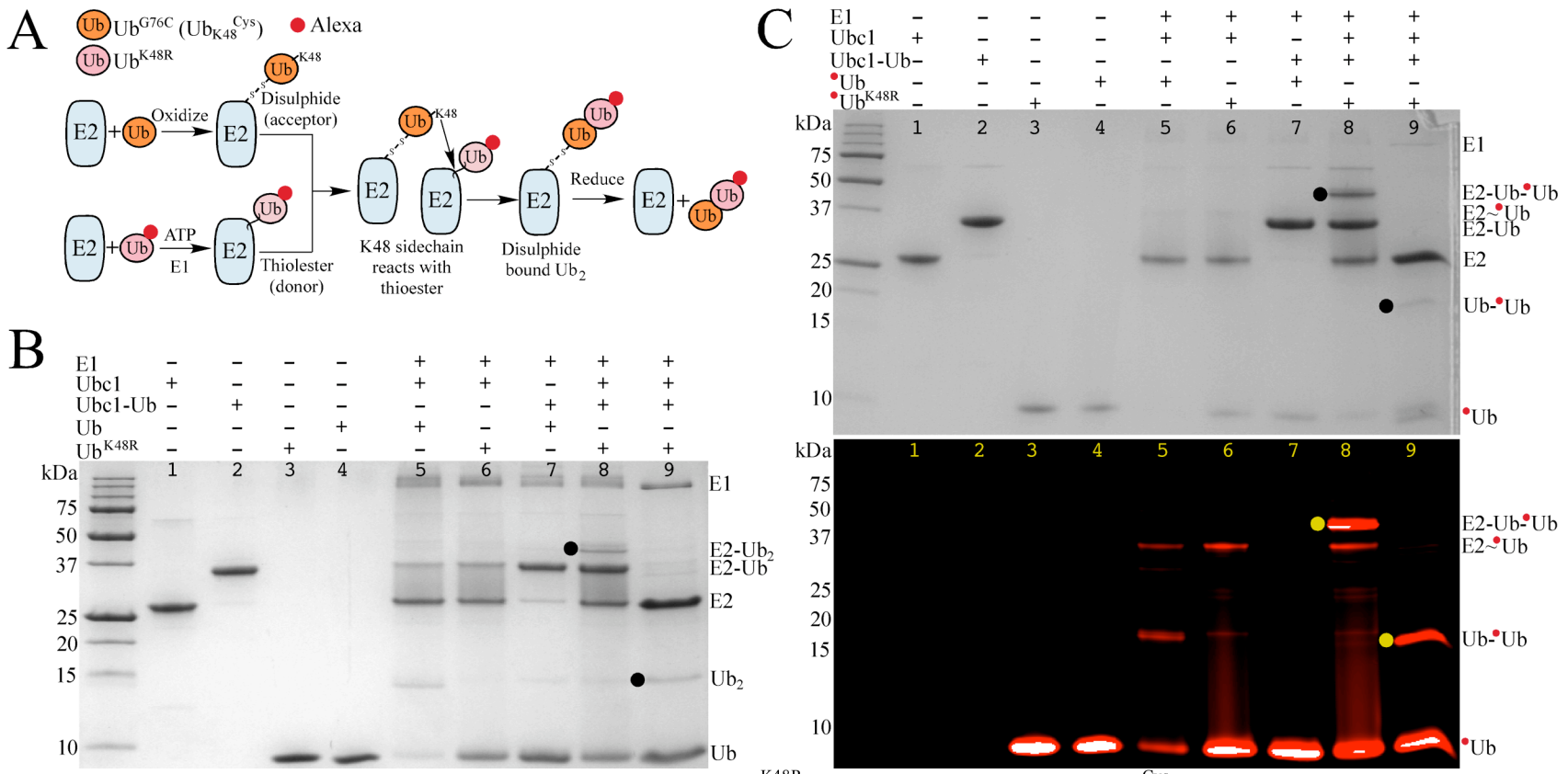

Figure 2.6 Ubc1 activity gels showing Ub transfer from the Ubc1~Ub^{K48R} thiolester onto the Ubc1-$Ub_{K48}{}^{Cys}$ disulphide. (**A**) Reaction of Ubc1-$Ub_{K48}{}^{Cys}$ disulphide and the Ubc1~Ub^{K48R} thiolester to produce Ubc1-$Ub_{K48}{}^{Cys}$-Ub^{K48R} (Ubc1-Ub_2). The use of Ub^{K48R} or Alexa-Ub^{K48R} result in similar products. (**B**) Ubc1 enzyme reactions containing a subset of the following purified proteins: 150 nM E1, 4.1 µM Ubc1, 2.0 µM Ubc1-$Ub_{K48}{}^{Cys}$ disulphide, 11.0 µM Ub (wild type), 10.8 µM Ub^{K48R}, 10 mM Mg-ATP, in 50 mM Hepes pH 8.0. (**C**) Reactions from (**B**) repeated with Alexa-Ub and Alexa-Ub^{K48R} and visualized with Coomassie (top gel) or 700 nm fluorescence (bottom gel). Reactions contain a subset of: 214 nM E1, 12.3 µM Ubc1, 10.5 µM Ubc1-$Ub_{K48}{}^{Cys}$ disulphide, 5.5 µM Alexa-Ub, 5.5 µM Alexa-Ub^{K48R}, 10 mM Mg-ATP, in 50 mM Hepes pH 8.0. Reaction components are listed above each gel with a (+) or (-). Reactions were performed for (**B**) 5 hrs and (**C**) 4 hrs at 37 °C, and reducing agent is only added to lane 9 (10 mM DTT and 10 mM TCEP) to break the disulphide. Ub-Ub attachments are indicated by the filled black/yellow circles. Molecular weight standards and protein species are listed to the left and right of each gel respectively.

extension. Therefore, a mixture of E2~Ub^{K48R} and E2-$Ub_{K48}{}^{Cys}$ will only be able to form one possible poly-Ub chain resulting from the transfer of Ub^{K48R} to E2-$Ub_{K48}{}^{Cys}$ to form E2-$Ub_{K48}{}^{Cys}$-Ub^{K48R}. This reaction is predicated on the proposal that the E2~Ub^{K48R} thiolester and E2-$Ub_{K48}{}^{Cys}$ thiolester mimic can indeed interact to allow a Ub-Ub connection to occur representing the basis for poly-Ub chain formation (Fig 2.5A/2.6A).

Several reactions were carried out with identical controls using purified HIP2 and HIP2-$Ub_{K48}{}^{Cys}$ (Fig 2.5B) as well as Ubc1 and Ubc1-$Ub_{K48}{}^{Cys}$ (Fig 2.6B). HIP2 and Ubc1 contain minute traces of the oxidized disulphide E2-E2 dimer, but these trace high MW bands will have no bearing on any observed products as their active sites are joined together and are therefore unreactive (Fig 2.5B/2.6B – lane 1). A standard ubiquitination reaction with the presence of E1, ATP, Ub, and either E2 yields a clearly visible HIP2~Ub or Ubc1~Ub thiolester as well as formation of free Ub_2 species thus showing the enzymes Ubc1 and HIP2 are active (Fig 2.5B/2.6B – lane 5). In the case of HIP2, higher molecular weight poly-Ub unanchored chains are visible since HIP2 has a high activity for unanchored chain formation (*10*). Ub^{K48R} was used with E1, E2 and ATP to form the E2~Ub^{K48R} thiolester, and the lack of Ub_2 formation proves HIP2 and Ubc1 poly-Ub activity is K48 specific (Fig 2.5B/2.6B – lane 6). When either E2-$Ub_{K48}{}^{Cys}$ disulphide was mixed with E1, Ub and ATP, no reaction was seen to occur for both HIP2 and Ubc1 (Fig 2.5B/2.6B – lane 7). This indicates that a reactive active site on these E2 enzymes is essential for their poly-Ub activity, and that the E1~Ub thiolester cannot directly react with either the HIP2-$Ub_{K48}{}^{Cys}$ or Ubc1-$Ub_{K48}{}^{Cys}$ disulphide. In the next reaction the E2-$Ub_{K48}{}^{Cys}$ disulphide is combined with all of the components used to form the E2~Ub^{K48R} thiolester, and a larger molecular weight band forms that corresponds to a

E2-Ub_2 for both HIP2 and Ubc1 (Fig 2.5B/2.6B – lane 8). The apparent E2-Ub_2 was produced only with addition of the E2-Ub_{K48}^{Cys} disulphide as the same components used previously did not produce this species with either HIP2 or Ubc1 (Fig 2.5B/2.6B – lane 6 vs lane 8). This reaction therefore represents the nucleophilic attack of the K48 residue in the E2-Ub_{K48}^{Cys} disulphide to the E2~Ub^{K48R} thiolester to allow formation of E2-Ub_{K48}^{Cys}-Ub^{K48R} (E2-Ub_2). This reaction product accumulates for both HIP2 and Ubc1 as the distal Ub is now blocked from further reactions by the K48R substitution (solid black dot on Fig 2.5B/2.6B – lane 8). Addition of reducing agent leads to reduction of the disulphide separating the HIP2 or Ubc1 E2 enzyme and Ub_2 proving the product is E2-Ub_2 (solid black dot in Fig 2.5B/2.6B – lane 9).

These activity assays were repeated using Alexa fluorophore (680 nm) tagged forms of Ub (Alexa-Ub) and Ub^{K48R} (Alexa-Ub^{K48R}) and the use of the untagged E2-Ub_{K48}^{Cys} complex for both HIP2 and Ubc1. In this way, the donor Ub protein is provided by E2~Alexa-Ub and E2~Alexa-Ub^{K48R} thiolesters that can be independently tracked by fluorescence imaging. Reactions using Alexa labelled proteins can be visualized through standard Coomassie dye staining (Fig 2.5C/2.6C – top gel) or the Alexa label can be directly observed through fluorescence (Fig 2.5C/2.6C – bottom gel). These reactions distinctly show the formation of E2-Ub_{K48}^{Cys}-Alexa-Ub^{K48R} (E2-Ub_2-Alexa) and reduction of this disulphide separates E2 and Ub_{K48}^{Cys}-Alexa-Ub^{K48R} (Ub_2-Alexa). The reaction of the E2~Alexa-Ub^{K48R} thiolester with the E2-Ub_{K48}^{Cys} disulphide shows that these two molecules can indeed interact to place the K48 sidechain of the disulphide in reactive distance to the thiolester bond to create a Ub-Ub connection (Fig 2.5C/2.6C – lane 8, 9).

These activity assays show that the thiolester mimic and active thiolester can associate and react to form an E2 attached Ub_2 molecule. These results may be consistent with a dimerization mechanism for the observed poly-Ub chain formation activity of HIP2 and Ubc1. Further studies to investigate direct dimerization of the Ubc1 and HIP2 enzymes and their HIP2-Ub and Ubc1-Ub thiolester mimics were performed.

2.3.7 HIP2, Ubc1, HIP2-Ub^{Cys} and Ubc1-Ub^{Cys} show minimal tendency to dimerize at low concentrations

Sedimentation equilibrium was utilized to assess the propensity of the E2 enzymes Ubc1 and HIP2 to dimerize. This technique is ideal for acquiring accurate molecular weights in solution since it is not dependant on protein standards. Molecular weights determined by sedimentation equilibrium are also not affected by protein shape, which is important as Ubc1 and HIP2 are expected to be elongated proteins (*21*). Sedimentation equilibrium experiments were performed at four different rotor speeds on 14.7 μM Ubc1 and 9.6 μM HIP2. Global fits using all rotor speeds were first performed for an ideal monomeric species model. The global fit for the HIP2 enzyme to an ideal monomeric species yielded a mass of 23441 ± 136 Da that was within 4% of the expected monomeric mass of 22534.7 Da (Table 2.1). A representative solution curve of the global fit to an ideal monomeric species is shown for HIP2 at 22000 rpm (Fig 2.7A). Similar results were acquired upon analysis of the Ubc1 enzyme whereby the experimental weight yielded a mass of 24464 ± 107 Da that agrees within 1.3% of the expected monomeric mass of 24162.2 Da (Table 2.1). A representative solution curve of the global fit to an ideal monomeric species is shown for Ubc1 at 26000 rpm (Fig 2.7C).

Table 2.1 Observed molecular weight of E2 enzymes and their thiolester mimics by sedimentation equilibrium

Protein[a]	Concentration (μM)	MW_{Calc} (Da)	MW_{Obs}[b] (Da)	K_d[c] (μM)
Ubc1	14.7	24162.2	24464 ± 107	1920 ± 658
Ubc1-Ub^{Cys}	43.0	32791.1	31347 ± 222	N/A
Ubc1-Ub^{Cys}	21.5	32791.1	32536 ± 212	N/A
Ubc1-Ub^{Cys}	14.3	32791.1	35238 ± 265	376 ± 55
HIP2	9.6	22534.7	23441 ± 136	455 ± 74
HIP2-Ub^{Cys}	24.0	31163.5	34619 ± 175	266 ± 16
HIP2-Ub^{Cys}	14.4	31163.5	34220 ± 169	214 ± 14
HIP2-Ub^{Cys}	7.2	31163.5	34461 ± 219	105 ± 9

[a] Hip2 and Ubc1 were analyzed at 280 nm, while Ubc1-Ub^{Cys} and HIP2-Ub^{Cys} were analyzed at 250nm to allow for higher protein concentrations.
[b] Molecular weight determined using global fits of 15k, 18k, 22k and 26k rpm to a single species model
[c] K_d values for self-association determined using global fits of 15k, 18k, 22k and 26k rpm to a self association model with molecular weights fixed to the expected monomeric weight

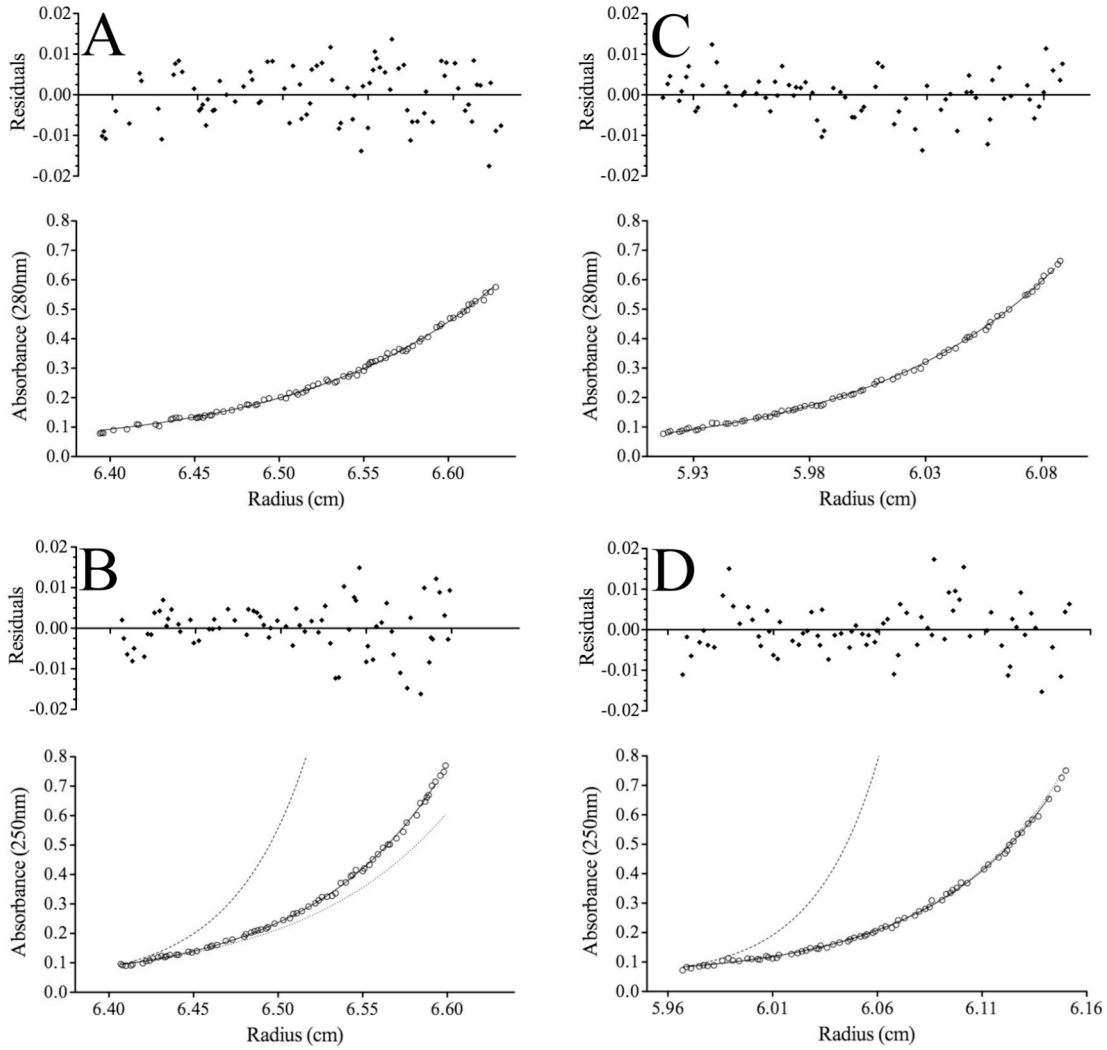

Figure 2.7 Sedimentation equilibrium analysis indicates both HIP2 and Ubc1, and their HIP2-Ub^{Cys} and Ubc1-Ub^{Cys} disulphides do not significantly dimerize. Sedimentation equilibrium was performed on each sample at four different rotor speeds (15k, 18k, 22k, and 26k rpm) at 5 °C to determine their solution based molecular weight. Experimental data was globally fit from triplicate measurements at each rotor speed to a single species model. A representative data set (open circles) is graphed with the globally fit line (solid line) for (**A**) 9.6 µM Hip2 at 22k rpm, (**B**) 24 µM HIP2-Ub^{Cys} at 22k rpm, (**C**) 14.7 µM Ubc1 at 26k rpm, and (**D**) 21.5 µM Ubc1-Ub^{Cys} at 26k rpm. Residuals of the data points to the fit line (filled diamonds) are shown above each curve fit. The expected curve for the monomer (dotted line) and dimer (dashed line) species for HIP2-Ub^{Cys} and Ubc1-Ub^{Cys} are also plotted using fixed molecular weights and the same baseline offset as was used in that window for the global fits.

Experimental data points compared to the globally fit curves for both proteins showed a random spread of the residual errors, indicating that the single species model was appropriate (Fig 2.7A,C). The observed molecular weights for Ubc1 and HIP2 are within the accuracy of this technique, which is around 5% (Biomolecular Interactions and Conformations Facility – UWO – personal communication).

Assuming that the 1.3% and 4% increase in molecular weights observed for Ubc1 and HIP2 respectively, were the result of dimerization, this data was fit to a self-association model. The global fit for HIP2 to a self-associating model yielded a dimerization K_d of 455 ± 74 μM (Table 2.1). The global fit for Ubc1 to a self-associating model yielded a dimerization K_d of 1920 ± 658 μM (Table 2.1). The quality of the fits and spread of residuals in the self-associating model fits are of equal quality to those observed with a single species model, and therefore the simplified equation for the single species solution is preferred to the self-associating solution. Since the experimental protein concentrations of Ubc1 and HIP2 are significantly lower than the determined K_d values, and since calculated molecular weights are within the accuracy range for a monomeric species, these K_d values are for illustrative purposes and any minute self-association cannot be accurately determined without the use of higher protein concentrations. Overall these K_d values are extremely weak and molecular weights are very close to the expected monomeric species showing these enzymes have minimal tendency to dimerize at low concentrations.

Sedimentation equilibrium experiments on HIP2-Ub^{Cys} and Ubc1-Ub^{Cys} disulphides were performed in a similar manner to the isolated E2 enzymes. Three different concentrations of the protein complexes were used to determine any possible

concentration dependence that might arise due to oligomerization. Global fits were performed for an ideal monomeric species model using all rotor speeds for each protein concentration. Experiments on HIP2-Ub^{Cys} at concentrations of 7.2, 14.4 and 24 μM yielded masses of 34461 ± 219, 34220 ± 169 and 34619 ± 175 Da respectively (Table 2.1). These masses are 10.6% (7.2 μM), 9.8% (14.4 μM) and 11.1% (24 μM) larger than the expected monomeric mass of 31163.5 Da. These results are beyond the expected error rate of 5%. This overestimation of molecular weight could be consistent with weak dimerization of HIP2-Ub^{Cys}, however, molecular weight would then be expected to increase as concentration was elevated from 7.2 μM to 24 μM, and no such increase was observed (Table 2.1). A representative solution curve of the global fit to an ideal monomeric species is shown for 24μM HIP2-Ub^{Cys} at 22000 rpm (Fig 2.7B). A random spread of residual errors from the data showed that the single species equation used to analyze the data was acceptable even though molecular weight was larger than expected (Fig 2.7B).

By fitting the data to a self-association model, the dimerization capacity of HIP2-Ub^{Cys} can be measured, although use of this model did not improve the quality of fits or residuals. The global fit for all speeds of HIP2-Ub^{Cys} to a self-associating model yielded K_d values of 105 ± 9, 214 ± 14, and 266 ± 16 μM for concentrations of 7.2, 14.4, and 24.0 μM HIP2-Ub^{Cys} respectively (Table 2.1). These dimerization K_d values for HIP2-Ub^{Cys} vary widely from 7.2 to 24.0 μM and since the concentrations are much less than the observed dissociation constants, these K_d values are not reliable. These results illustrate that the dimerization K_d of HIP2 is at best in the order of 100's of μM. Although the observed molecular weights for HIP2-Ub^{Cys} are slightly higher than

expected, they are relatively consistent while protein concentration is increased indicating it is highly likely that the true K_d for HIP2-Ub^{Cys} dimerization is significantly higher than the range of 105-266 μM.

Similar experiments were performed on the Ubc1-Ub^{Cys} disulphide with four rotor speeds and three different concentrations of 14.3, 21.5 and 43 μM. Global fits were performed for all speeds at each protein concentration and the data was fit to a single species model. Experiments on Ubc1-Ub^{Cys} at concentrations of 14.3, 21.5 and 43.0 μM yielded masses of 35238 ± 265, 32536 ± 212 and 31347 ± 222 Da respectively (Table 2.1). These masses are 4.4% (43.0 μM), and 1.8% (21.5 μM) lower than the expected monomeric mass, and 7.5% (14.3 μM) larger than the expected monomeric mass of 31163.5 Da respectively. Only one of these measurements is beyond the expected error rate of 5%. If molecular weights were affected by dimerization of Ubc1-Ub^{Cys}, then these values would be expected to increase as concentration was elevated from 14.3 μM to 43.0 μM, but the opposite was observed (Table 2.1). A representative solution curve of the global fit to an ideal monomeric species is shown for 21.5 μM Ubc1-Ub^{Cys} at 26000 rpm (Fig 2.7D). A random spread of residual errors from the data showed that the single species equation used to analyze the data was appropriate (Fig 2.7D).

By fitting the data to a self-association model, the dimerization capacity of Ubc1-Ub^{Cys} was measured, although use of this model did not improve the quality of fits or residuals. The global fit for all speeds of Ubc1-Ub^{Cys} to a self associating model yielded K_d values that are negative (non-existent) for 21.5 and 43.0 μM experiments, and 376 ± 55 μM for 14.3 μM Ubc1-Ub^{Cys} (Table 2.1). Since the molecular weights apparently reduced upon concentration increase, the K_d value for Ubc1-Ub^{Cys} is not accurate. These

results indicate Ubc1-Ub^{Cys} does not appear to dimerize to any degree at the concentrations tested, and thus higher concentrations need to be analyzed to determine if there is any significant dimerization of this protein.

The sedimentation equilibrium results provide strong evidence that the propensity for HIP2, Ubc1, and their disulphide thiolester mimics to dimerize at the concentrations tested is extremely low, as this technique has shown the observed molecular weights closely agree with the expected molecular weights.

2.3.8 HIP2, Ubc1, HIP2-Ub^{Cys} and Ubc1-Ub^{Cys} show minimal tendency to dimerize at high concentrations

In order to provide greater detail about the degree of association, size, and shape of the E2 enzymes and their disulphide complexes, small angle X-ray scattering (SAXS) experiments were performed. SAXS is a method that is used to investigate low-resolution structural details of proteins at high concentrations in solution. The increased concentration range for the study of HIP2 and Ubc1 should be complementary to the sedimentation equilibrium analysis. SAXS experiments can be used to determine the radius of gyration (R_g) for a protein, which is the root mean square of the distances of all electrons from their common center of mass, and the forward scattering (I_o), which is proportional to the molecular weight (MW) of the protein. The R_g and MW values are acquired using the low angle region of the scattering curves that when plotted using Guinier plots are linear near the axis. Guinier plots were produced for HIP2, HIP2-Ub^{Cys}, Ubc1 and Ubc1-Ub^{Cys} for five protein concentrations ranging from 36-284 μM, 44-218 μM, 29-235 μM, and 24-197 μM respectively. These Guinier plots display excellent

linear relationships indicating these proteins behave in a monodisperse fashion in solution (Fig 2.8). Large protein aggregates would cause a significant upwards inflection in the Guinier plots near the y-axis and since these effects are not observed, the proteins tested were considered well behaved.

The R_g and apparent MW values were calculated for each protein in a dilution series to determine the variation of these values in regards to protein concentration. If self-association of any of these proteins occurs as protein concentration increases, than significant increases in R_g and apparent MW values will also be observed. The R_g for HIP2 increases from 20.9 to 22.4 Å as protein concentration is increased from 36 to 284 μM (Fig 2.9A – open triangles). The R_g for Ubc1 was found to be slowly increasing from 23.1 to 24.3 Å over a protein concentration range of 29-235 μM (Fig 2.9B – open circles). The increase in R_g values for HIP2 and Ubc1 are very small, indicating a relatively stable protein shape in solution for both HIP2 and Ubc1 over a relatively large increase in protein concentrations. These results provide minimal support for a significant self-association of HIP2 and Ubc1. Comparison of R_g values to high-resolution structures will be reported later in this chapter (Section 2.3.9 and 2.3.10). SAXS data was also used to calculate the apparent MW of HIP2 and Ubc1 using a known concentration of a cytochrome C standard. The apparent MW of HIP2 was observed to increase from 24.3 to 27.8 kDa (Fig 2.9C – open triangles), which was 8% to 23.5% higher than the expected MW of 22.5 kDa. The apparent MW of Ubc1 ranges from 27.8 to 30.5 kDa over the concentration range of 29-235 μM (Fig 2.9D – open circles). These MW values are 14.9% to 26% higher than the expected monomeric weight of 24.2 kDa for Ubc1. SAXS can determine MWs within an accuracy of 10% (*22*), but small errors in

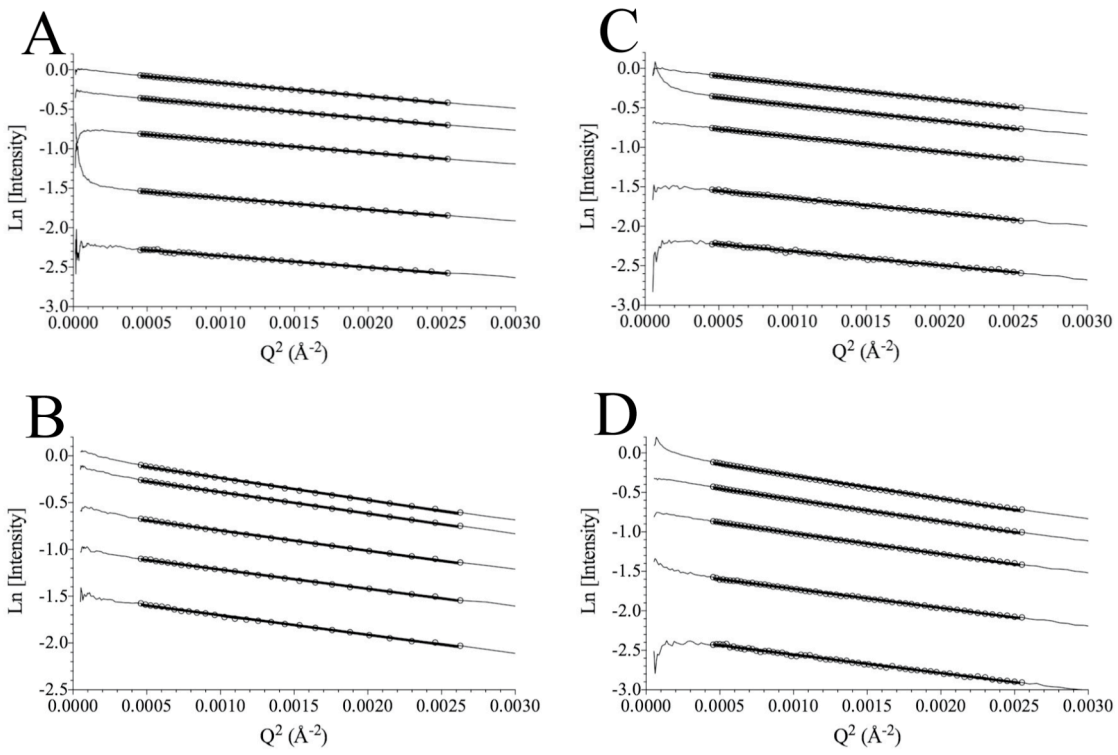

Figure 2.8 SAXS data displayed using Guinier plots for HIP2, HIP2-Ub^{Cys}, Ubc1 and Ubc1-Ub^{Cys} at various concentrations. Data is presented for five concentrations of each protein whereby the top curve (solid line) is the most concentrated sample followed by successive dilutions for lower curves (solid lines) whereby all data is normalized to the top concentration. Data was collected for (**A**) HIP2 at 284, 213, 142, 71.0 and 35.5 µM (**B**) HIP2-Ub^{Cys} at 218, 175, 131, 87.3 and 43.6 µM (**C**) Ubc1 at 235, 176, 118, 58.8, and 29.4 µM (**D**) Ubc1-Ub^{Cys} at 197, 148, 98.7, 49.3 and 24.6 µM. Similar angular ranges are used to calculate the linear region (open circles) for each data set allowing for a good comparison between experiments. Each data set was fit over the linear region (thick straight line) to determine the forward scattering (I_o) and radius of gyration (R_g) at each concentration.

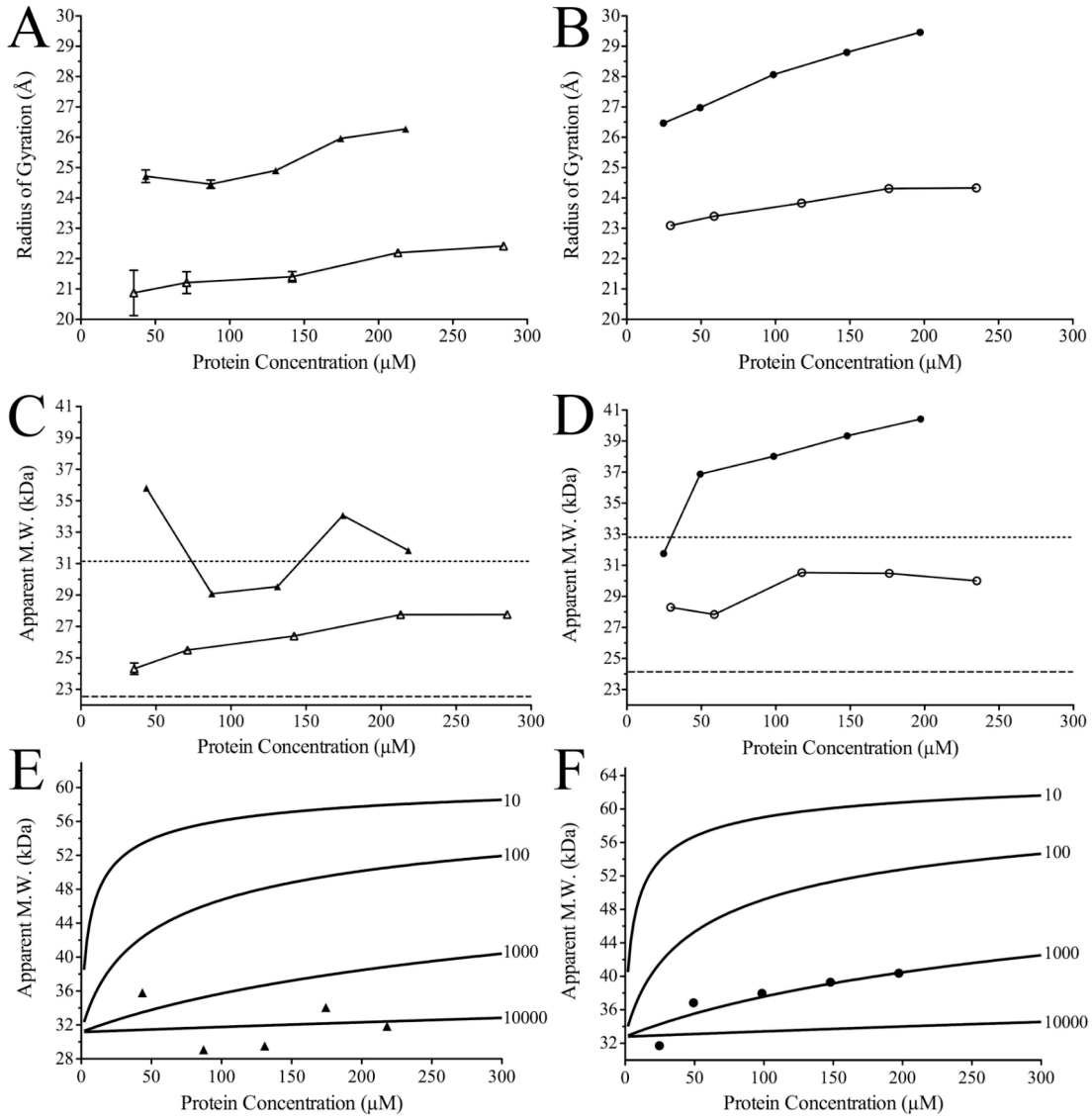

Figure 2.9 Radius of gyration and apparent MW data displayed for HIP2, HIP2-Ub^{Cys}, Ubc1 and Ubc1-Ub^{Cys} at various concentrations. (**A**) and (**C**) show data points for the proteins HIP2 (open triangles) and HIP2-Ub^{Cys} (filled triangles) at five different concentrations of 284, 213, 142, 71.0 and 35.5 μM HIP2 and 218, 175, 131, 87.3 and 43.6 μM HIP2-Ub^{Cys}. (**B**) and (**D**) show data points for the proteins Ubc1 (open circles) and Ubc1-Ub^{Cys} (filled circles) at five different concentrations of 235, 176, 118, 58.8, and 29.4 μM Ubc1 and 197, 148, 98.7, 49.3 and 24.6 μM Ubc1-Ub^{Cys}. The expected molecular weight for HIP2 and Ubc1 (dashed line) as well as HIP2-Ub^{Cys} and Ubc1-Ub^{Cys} (dotted line) are displayed on the apparent MW graphs. There are various expected radius of gyration values depending on positioning of the UBA tail domain and the position of attached Ub in relation to the catalytic core for these E2 enzymes and thus no one value is displayed for an expected radius of gyration for each protein. (**E**) and (**F**) show the theoretical binding curves for dimerization of HIP2-Ub^{Cys} and Ubc1-Ub^{Cys} respectively whereby the K_d is listed to the right of the line in μM.

protein concentrations of either sample or standards will affect the accuracy of the apparent MWs reported. Since this experiment was performed with a series of dilutions, the trend of MW change over the change in protein concentration is more accurate than the absolute value of any single MW measurement. The apparent MWs undergo minimal change (11.1% for Ubc1 and 15.5% for HIP2) as concentration is increased significantly, thus indicating HIP2 and Ubc1 are undergoing minimal dimerization as detailed by this technique up to concentrations of 284 and 235 μM respectively. If these apparent MW trends are plotted against a series of theoretical curves defined by a K_d of 10, 100, 1000 and 10000 μM, the trend in MW change is consistent with a K_d of at least 1000 μM. The trends in apparent molecular weight and R_g appear relatively stable across the large concentration range tested, it is therefore very likely that these E2 enzymes do not dimerize in solution with a K_d lower than 1000 μM (1 mM).

The R_g and apparent MW values were also calculated for HIP2-Ub^{Cys} and Ubc1-Ub^{Cys} to determine if these proteins had an increased capacity for dimerization. The R_g for HIP2-Ub^{Cys} increases from 24.7 to 26.3 Å as protein concentration is increased from 44 to 218 μM (Fig 2.9A – filled triangles). The R_g for Ubc1-Ub^{Cys} slowly increases from 26.5 to 29.5 Å over a protein concentration range of 25-197 μM (Fig 2.9B – filled circles). The change in R_g values for HIP2-Ub^{Cys} (1.6 Å) and Ubc1-Ub^{Cys} (3 Å) is larger than was observed for HIP2 (1.5 Å) and Ubc1 (1.2 Å) alone over similar concentration increases. Although the increase in R_g values is more prominent for the disulphide complexes, the increase is still small thus providing only weak support for increased self-association of these proteins. SAXS data was also used to calculate the apparent MW of HIP2-Ub^{Cys} and Ubc1-Ub^{Cys}. The apparent MW of HIP2-Ub^{Cys} was observed to vary

between 29.1 to 35.8 kDa as concentration was varied between 44 and 218 μM (Fig 2.9C – filled triangles). These MWs ranged from 6.6% smaller to 14.9% larger than the expected MW of 31.2 kDa, but there was no overall trend in the MW changes as concentration was increased. The apparent MW of Ubc1-Ub^{Cys} increased from 31.8 to 40.4 kDa over the concentration range of 25-197 μM (Fig 2.9D – filled circles). The highest MW value for Ubc1-Ub^{Cys} was 23% higher than the expected monomeric weight of 32.8 kDa. The apparent MW of Ubc1-Ub^{Cys} also increased as protein concentrations were increased, which could indicate minimal dimerization. There are not enough data points from these results to accurately produce a curve to determine the K_d of dimerization for either HIP2-Ub^{Cys} or Ubc1-Ub^{Cys}. A series of theoretical curves defined by a K_d of 10, 100, 1000 and 10000 μM, however, can be used on a comparative basis to find an appropriate range for K_d values that are consistent with the experimental data points for HIP2-Ub^{Cys} and Ubc1-Ub^{Cys} (Fig 2.9E, F). The trend in MW change for both HIP2-Ub^{Cys} and Ubc1-Ub^{Cys} is consistent with a K_d of dimerization of at least 1000 μM.

The overall trends of increasing values for R_g and apparent MW for both HIP2 and Ubc1 is consistent with an extremely weak dimerization of these enzymes. The addition of Ub in HIP2-Ub^{Cys} and Ubc1-Ub^{Cys} appears to increase the dimerization capacity of these enzymes. The dimerization capacity of HIP2, HIP2-Ub^{Cys}, Ubc1, and Ubc1-Ub^{Cys} however, is on the whole very weak, as the dimerization K_d values were found to be >1000 μM. Since the concentrations tested in SAXS are far below 1000 μM, the reported K_d values are not accurate, but still indicate that HIP2, Ubc1, HIP2-Ub^{Cys}, and Ubc1-Ub^{Cys} proteins are predominantly monomeric in solution during these experiments.

2.3.9 HIP2 and Ubc1 SAXS data comparison to high-resolution structures

SAXS is a method that is used to investigate low-resolution structural details of proteins at high concentrations in solution. The overall shape of proteins can be determined through analysis of the radius of gyration (R_g) for a protein acquired from the low angle regions of SAXS. Analysis of the full scattering curves in SAXS were performed using the program CRYSOL (*16*) that allows experimental scattering curves to be compared to the theoretical scattering curves calculated from high-resolution structural PDB coordinates. In this way NMR and X-ray crystallographic structures of HIP2, HIP2-Ub^{Cys}, Ubc1, and Ubc1-Ub^{Cys} can be directly tested against the experimental data. If the proteins are predominantly monomeric, the experimental data should allow a quality fit to the experimental data.

Ubc1 is an elongated, two-domain protein possessing a 15-residue flexible linker that separates the catalytic core and UBA domains, thus allowing a variety of spatial arrangements between the UBA and the catalytic core (*21*). In order to sample unique UBA domain positions with respect to the core domain, 13 of the 21 lowest energy Ubc1 NMR structures (PDB: 1TTE) (*21*) that vary the UBA domain position were analyzed. These Ubc1 structures were analyzed by CRYSOL (*16*) to give theoretical scattering curves that could be fit to the experimental data. The most important region in these scattering curve fits are at low scattering angles (low q values), which are most closely related to the overall averaged shape of the molecule. The quality of the fits of these various Ubc1 structures to the experimental data was assessed by the goodness of fit value (χ^2) defined by Equation 4 (Section 2.2.6). The representative data set (118 μM

Ubc1) was best fit to a Ubc1 structure that oriented the UBA domain directly opposite the N-terminus and close to helix 4 of the catalytic core (Fig 2.10A). Structures where the UBA domain was moved away from this position yet retained a similar Rg (Fig 2.10B) or the UBA domain was extended further away from the catalytic core (Fig 2.10C) result in poorer fits. Similar results were obtained on all other concentrations of Ubc1 fit to these various structures. For all Ubc1 structures analyzed, the best fits were consistently acquired from models where the UBA domain is not fully extended away from, nor tightly associated with the catalytic core. This general UBA domain positioning is best fit by Figure 2.10A, and thus this structure likely represents the average UBA position for Ubc1 in solution. The CRYSOL calculated R_g for the best fit Ubc1 structure is 24.95 Å. SAXS Guinier plot analysis of Ubc1 reveals the experimental R_g to be 23.1 Å to 24.3 Å over a protein concentration range of 29-235 μM (Table 2.2). These experimental R_g values are at most 7.4% lower than the expected value of 24.95 Å showing good agreement to the best fit Ubc1 structure (Fig 2.10A). The best fit structure of Ubc1 is therefore supported by both high quality fits to the full scattering curves and close agreement to experimental R_g values. The fact that this monomeric model can be well fit to the data also supports the notion that Ubc1 is predominantly monomeric at the concentrations examined, providing further support for very weak (>1000 μM) K_d values.

Unlike Ubc1, wild type HIP2 was initially solved as a dimer (PDB: 1YLA) by X-ray crystallography. Recently, two more X-ray crystallography structures of wild type HIP2 were solved as monomers (PDB: 2BEP, 3K9P) (*23, 24*). These structures were backbone residue aligned to the catalytic core (1-155) of 1YLA giving RMSD measurements of 0.53 Å and 1.09 Å respectively. These results indicate these structures

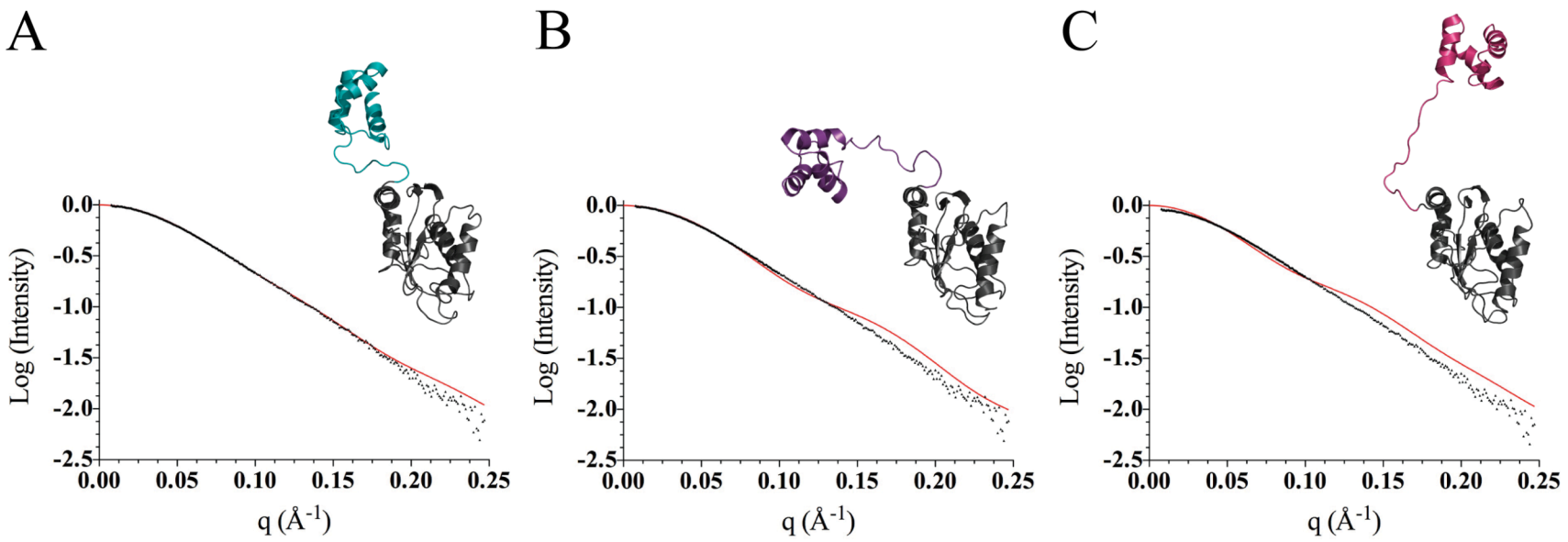

Figure 2.10 CRYSOL analysis allows SAXS data to be compared to high-resolution structures of Ubc1. SAXS data is presented for Ubc1 (118 μM), where the momentum transfer (q) is plotted versus the normalized log of scattering intensity (measured in arbitrary units). Experimental data points are shown in black (filled triangles) and the theoretical scattering of the PDB structure is shown in red (solid line). The structure used for theoretical scattering is located directly above the scattering curve. Three representative structures were selected, (**A**) Ubc1 NMR structure 18 (cyan) (χ^2 of 2.20, R_g of 24.95 Å), (**B**) Ubc1 NMR structure 17 (purple) (χ^2 of 8.10, R_g of 24.59 Å), (**C**) Ubc1 NMR structure 4 (pink) (χ^2 of 16.86, R_g of 27.60 Å), whereby the major variation is the location of the UBA domain (coloured) in comparison to the core domain (grey). Panel (**A**) represents the best fit of all structures tested, with all other quality fits similar to this UBA orientation. χ^2 defines the quality of the fits whereby a lower score indicates a better fit.

Table 2.2 Radius of gyration and molecular weight for E2 enzymes and their thiolester mimics derived from Small Angle X-ray Scattering Guinier Plots

Protein	Conc. (μM)	R_g (Å)	MW_{Obs}[a] (kDa)	MW_{Exp} (kDa)
Ubc1	29.4	23.1	28.3	24.2
	58.8	23.4	27.8	24.2
	118	23.8	30.5	24.2
	176	24.3	30.5	24.2
	235	24.3	30.0	24.2
Ubc1-Ub^{Cys}	24.6	26.5	31.8	32.8
	49.3	27.0	36.9	32.8
	98.7	28.1	38.0	32.8
	148	28.8	39.3	32.8
	197	29.5	40.4	32.8
HIP2	35.5	20.8 ± 0.8	24.3 ± 0.4	22.5
	71.0	21.2 ± 0.4	25.5 ± 0.2	22.5
	142	21.4 ± 0.2	26.4 ± 0.1	22.5
	213	22.2 ± 0.1	27.8 ± 0.1	22.5
	284	22.4 ± 0.1	27.8 ± 0.1	22.5
HIP2-Ub^{Cys}	43.6	24.7 ± 0.2	35.8 ± 0.2	31.2
	87.3	24.5 ± 0.1	29.1 ± 0.1	31.2
	131	24.9 ± 0.1	29.5 ± 0.1	31.2
	175	26.0 ± 0.1	34.1 ± 0.1	31.2
	218	26.3 ± 0.1	31.8 ± 0.1	31.2

[a] Molecular Weight determined by comparison to cytochrome c samples of similar concentration

[b] Error analysis only available for data analyzed by Igor Pro (HIP2 and HIP2-Ub^{Cys}). Error analysis based on I_0 errors.

are redundant and therefore only the 1YLA was utilized as the high-resolution HIP2 structure to fit to experimental data. A representative SAXS data set (142 μM HIP2) was found to poorly fit the dimeric model (Fig 2.11A), while a much better fit was acquired for the monomeric model (Fig 2.11B, half of the dimer coordinates). Similar results were obtained on all other concentrations of HIP2 consistently showing much better fits to the monomeric model. Guinier plot analysis of HIP2 SAXS data reveals the experimental R_g to be 20.8 Å to 22.4 Å over a protein concentration range of 29-235 μM (Table 2.2). These experimental values are 6.1% to 14.3% larger than the expected R_g of 19.6 Å calculated from the monomer crystal structure of HIP2 (Fig 2.11B). On the assumption the UBA domain of HIP2 is connected by a flexible linker, the position of the UBA domain was moved to a similar location seen in the well fit Ubc1 structure. The resulting 'relaxed' UBA position for HIP2, which places the UBA domain further away from the catalytic core, had an R_g of 21.8 Å that agreed more closely with the Guinier determined R_g values of 20.8-22.4 Å. This 'relaxed' HIP2 structure provided a better fit than the crystal monomer at all concentrations, and is illustrated by the representative data set in Figure 2.11C. These results support the idea that the HIP2 crystal structure may have the UBA domain positioned too closely to the catalytic core and may be a crystal artifact. It is therefore likely that HIP2, like Ubc1, contains a flexible linker region allowing the UBA domain to act as a tethered yet independent element in relation to the catalytic core domain, thus explaining a more extended structure in solution than was observed in crystal structures. This 'relaxed' HIP2 structure therefore likely represents the average position of the UBA domain in solution during SAXS experiments. The fact

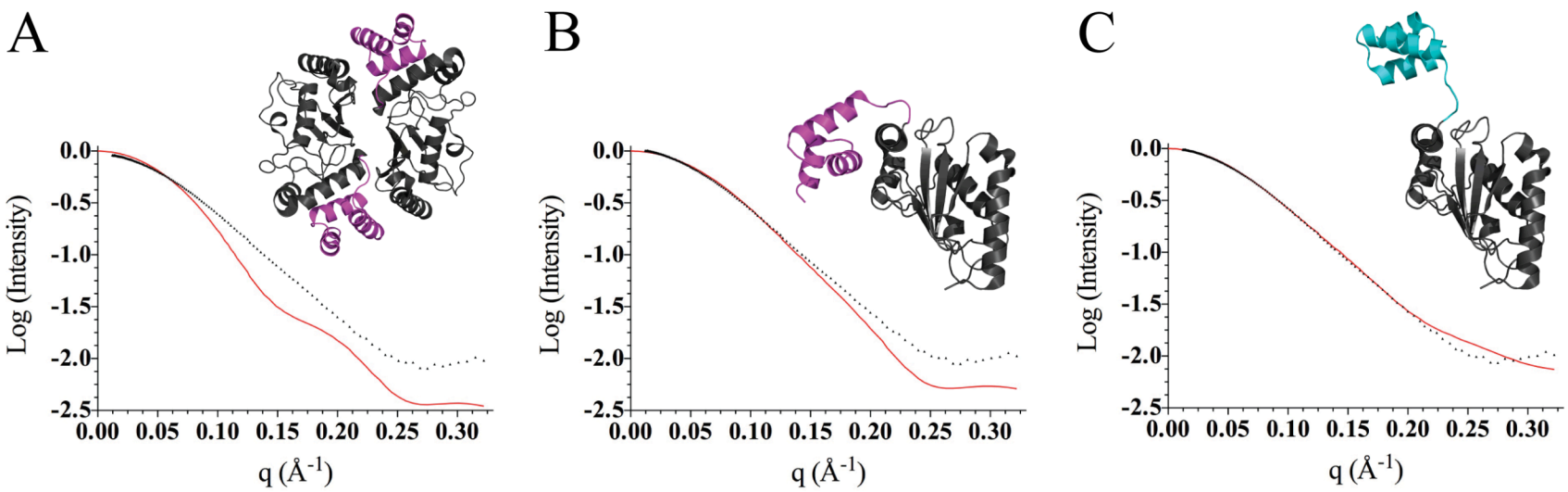

Figure 2.11 CRYSOL analysis allows SAXS data to be compared to high-resolution structures of HIP2. SAXS data is presented for HIP2 (142 μM), where the momentum transfer (q) is plotted versus the normalized log of scattering intensity (measured in arbitrary units). Experimental data points are shown in black (filled triangles) and the theoretical scattering of the PDB structure is shown in red (solid line). The structure used for theoretical scattering is located directly above the scattering curve. (**A**) shows data fit to the dimeric crystal structure of HIP2 for 1YLA (χ^2 of 11.10, R_g of 23.48 Å) and (**B**) shows data fit to the resulting monomeric structure of HIP2 (χ^2 of 2.18, R_g of 19.55 Å). The core domain is coloured grey, and the UBA domain is coloured magenta. (**C**) shows data fit to the same monomeric HIP2 with the UBA domain (cyan) slightly moved in the direction similar to the Ubc1 monomer UBA orientation (χ^2 of 0.62, R_g of 21.79 Å). χ^2 defines the quality of the fits whereby a lower score indicates a better fit.

that a monomeric model of HIP2 can be well fit to the data supports the notion that these proteins are predominantly monomeric at the concentrations examined, providing further support for very weak (>1000 μM) K_d values.

2.3.10 HIP2-Ub^{Cys} and Ubc1-Ub^{Cys} SAXS data comparison to high-resolution structures

SAXS analysis performed on Ubc1-Ub^{Cys} and HIP2-Ub^{Cys} can be used to determine the general position of Ub within the thiolester mimic. To perform this analysis high-resolution structures of Ubc1-Ub^{Cys} and HIP2-Ub^{Cys} need to be created to compose theoretical scattering curves to compare to experimental data. Previous NMR studies show that the UBA domain in Ubc1 does not interact with the thiolester bound Ub (*18*). As a result the average UBA position found to match SAXS data from Ubc1 alone (Fig 2.10A) should be unperturbed and thus was used as a starting point to position the Ub molecule onto Ubc1 in Ubc1-Ub^{Cys}. An NMR based model for the short lived Ubc1~Ub thiolester has been previously determined with a Ubc1 truncation (Ubc1Δ) and Ub (PDB: 1FXT) (*19*). This Ubc1Δ~Ub model was aligned with the full length Ubc1 protein structure modelled from SAXS data (Fig 2.10A) to generate a model for Ubc1-Ub^{Cys}. The theoretical scattering curves for this model fit the experimental scattering curves poorly at all concentrations, and is illustrated by the representative data set (99 μM) in Figure 2.12A. These results indicate that this model does not accurately depict the average shape of the Ubc1-Ub^{Cys} complex in solution (Fig 2.12A). To determine if poor fits to this model were due to the presence of dimeric Ubc1-Ub^{Cys}, several theoretical models were produced to sample possible dimeric structures. No quality fits

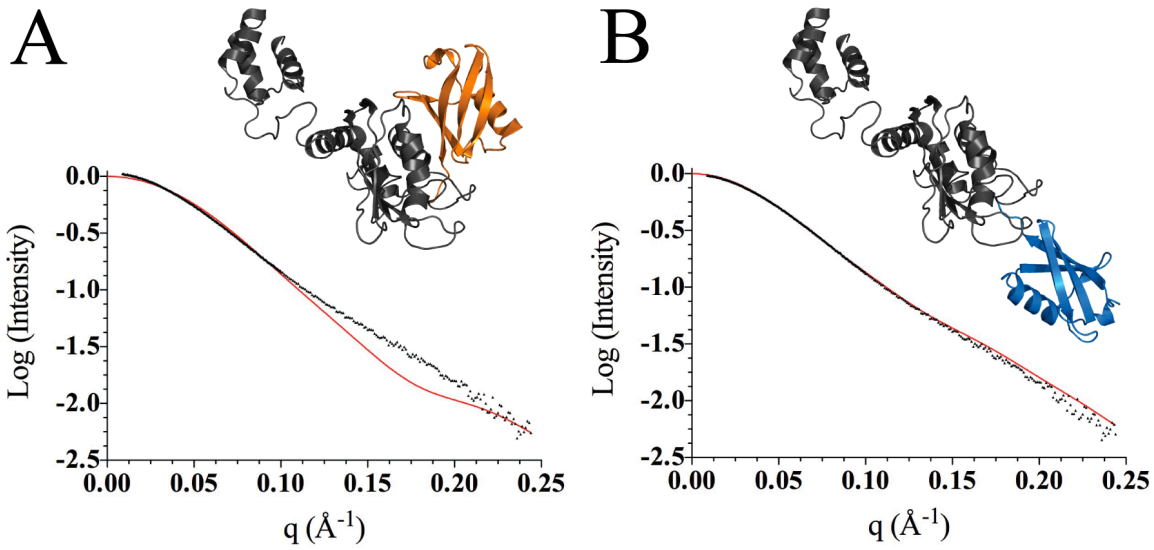

Figure 2.12 CRYSOL analysis allows SAXS data to be compared to high-resolution structures of Ubc1-Ub^{Cys}. SAXS data is presented for Ubc1-Ub^{Cys} (99 µM), where the momentum transfer (q) is plotted versus the normalized log of scattering intensity (measured in arbitrary units). Experimental data points are shown in black (filled triangles) and the theoretical scattering of the PDB structure is shown in red (solid line). The structure used for theoretical scattering is located directly above the scattering curve. (**A**) SAXS data fit to the 'compact model' for Ubc1-Ub^{Cys} (χ^2 of 13.39, R_g of 25.18 Å). The 'compact model' was produced with the full length Ubc1 structure (Fig 2.10A) with the covalently attached Ub modelled by alignment to the truncated Ubc1~Ub (1FXT) structure. (**B**) SAXS data fit to the 'elongated model' for Ubc1-Ub^{Cys} (χ^2 of 3.41, R_g of 29.78 Å). The 'elongated model' was produced with the full length Ubc1 structure (Fig 2.10A) and the covalently attached Ub modelled by alignment to the Ubc13 portion of the hMms2/Ubc13~Ub (2GMI) structure. χ^2 defines the quality of the fits whereby a lower score indicates a better fit.

could be produced for Ubc1-Ub^{Cys} from any dimeric structure or mixture of the monomeric and dimeric species.

The expected structure of Ubc1-Ub^{Cys} does not represent the average position of the disulphide bound Ub, and thus alternative models were investigated. There are presently four other E2~Ub conjugate structures that place the Ub in various positions: Ubc13-Ub (PDB: 2GMI (*7*)), UbcH8-Ub (PDB: 2KJH (*20*)), and two structures for UbcH5b-Ub (PDB: 3A33 (*25*), and PDB: 3JW0 (*26*)). Alternative models for Ubc1-Ub^{Cys} were created from these four structures. All of these new models position the Ub molecule in varying positions further from the catalytic core. These structures are more elongated and thus the model built in Figure 2.12A (PDB: 1FXT/1TTE) is termed the 'compact' model. The theoretical scattering curves for these new 'elongated' models were compared to a representative data set (99 μM) with the best fit belonging to the most extended Ubc1-Ub^{Cys} structure based on the Ubc13-Ub complex (PDB: 2GMI) (Fig 2.12B). The other new models fit more poorly than the 'elongated' model (Fig 2.12B), but better than the 'compact' model (Fig 2.12A) and these fits are consistent across all concentrations examined. Guinier plot analysis of the Ubc1-Ub^{Cys} reveals the experimental R_g to be 26.5 Å to 29.5 Å over a protein concentration range of 25-197 μM (Table 2.2). The R_g value of the poorly fit 'compact' model for Ubc1-Ub^{Cys} is 25.18 Å and the R_g value of the well fit 'elongated' model for Ubc1-Ub^{Cys} is 29.78 Å. The increasing experimental R_g values vary between the expected R_g values for both the 'elongated' and 'compact' models of Ubc1-Ub^{Cys} structure indicating that some dimerization or aggregation may be occurring. In either case, the experimental R_g values are closer to the expected R_g for the 'elongated' Ubc1-Ub^{Cys} structure indicating Guinier

plots also support this model. These results indicate that the 'elongated' model best represents the average shape of Ubc1-Ub^{Cys} in solution (Fig 2.12B). Since the Ubc1-Ub^{Cys} SAXS data can be fit to a monomeric structure, this further supports a very weak (>1000 μM) K_d value describing dimerization of this protein complex.

In a similar analysis to Ubc1-Ub^{Cys}, two models of HIP2-Ub^{Cys} were constructed to analyze SAXS data. These HIP2-Ub^{Cys} models were built by alignment to the 'compact' and 'elongated' models created for Ubc1-Ub^{Cys} whereby the Ubc1 is replaced with the HIP2 'relaxed' UBA structure from Figure 2.11C. As was seen for the Ubc1-Ub^{Cys}, the theoretical scattering curves for the 'elongated' model of HIP2-Ub^{Cys} fit the experimental scattering curves very well at all concentrations, and is illustrated by the representative data set (96 μM) in Figure 2.13A. The theoretical scattering curves for the 'compact' model of HIP2-Ub^{Cys} fit the experimental scattering curves poorly at all concentrations tested, and is illustrated by the representative data set (96 μM) in Figure 2.13B. Alternative models built from the other E2~Ub structures provided fitting score values in between the 'compact' and 'elongated' models. Again, no reasonable fits could be produced for HIP2-Ub^{Cys} SAXS data with any dimeric structure or mixture of monomeric and dimeric species. Guinier plot analysis of HIP2-Ub^{Cys} SAXS data reveals the R_g to vary between 24.7 Å to 26.3 Å over a protein concentration range of 44-218 μM (Table 2.2). The expected R_g for the 'elongated' model is 26.85 Å, while the 'compact' model has an R_g of 22.33 Å. The experimental R_g values are closer to the expected R_g for the 'elongated' HIP2-Ub^{Cys} structure indicating Guinier plots also support this model. Based on these results, it can be concluded that the 'elongated' model (Fig 2.13A) for HIP2-Ub^{Cys} best represents the average shape of HIP2-Ub^{Cys} in solution. The fact that

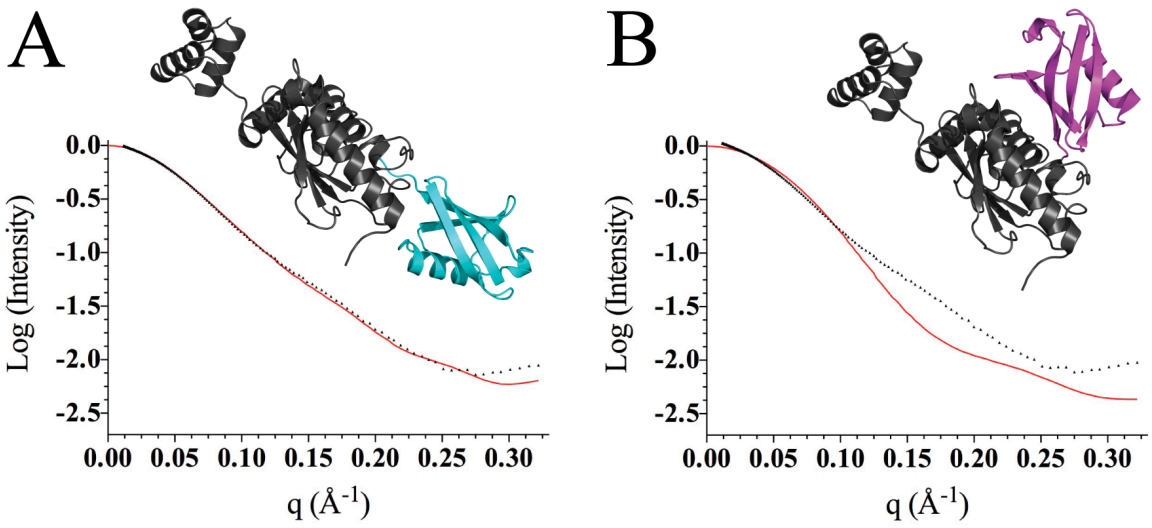

Figure 2.13 CRYSOL analysis allows SAXS data to be compared to high-resolution structures of HIP2-Ub^{Cys}. SAXS data is presented for HIP2-Ub^{Cys} (96 µM), where the momentum transfer (q) is plotted versus the normalized log of scattering intensity (measured in arbitrary units). Experimental data points are shown in black (filled triangles) and the theoretical scattering of the PDB structure is shown in red (solid line). The structure used for theoretical scattering is located directly above the scattering curve. (**A**) SAXS data fit to the 'elongated model' for HIP2-Ub^{Cys} (χ^2 of 0.97, R_g of 26.85 Å). The 'elongated model' was produced with the 'relaxed' HIP2 structure (Fig 2.11C) with the covalently attached Ub modelled by alignment to the truncated Ubc1~Ub (1FXT) structure. (**B**) SAXS data fit to the 'compact model' for HIP2-Ub^{Cys} (χ^2 of 6.44, R_g of 22.33 Å). The 'compact model' was produced with the 'relaxed' HIP2 structure (Fig 2.11C) and the covalently attached Ub modelled by alignment to the Ubc13 portion of the hMms2/Ubc13~Ub (2GMI) structure. χ^2 defines the quality of the fits whereby a lower score indicates a better fit.

HIP2-Ub^{Cys} SAXS data can provide a good fit to a monomeric structure further supports very weak (>1000 μM) K_d values describing dimerization of this protein.

2.3.11 Activity assays on HIP2 and Ubc1 show that E2~Ub^{K48R} is the primary reactive molecule and directly interacts with E2-$Ub_{K48}{}^{Cys}$ or free Ub

Initial activity reactions (Section 2.3.6) provided evidence that the E2-Ub disulphide and the E2~Ub active thiolester for both HIP2 and Ubc1 might associate to form an E2-Ub_2 molecule. These results implied a possible E2 dimerization mechanism driving poly-Ub chain formation. Analytical ultracentrifugation and SAXS results, however, indicate Ubc1 and HIP2 alone as well as Ubc1-Ub^{Cys} and HIP2-Ub^{Cys} have very little tendency (K_d >1000 μM) to self-associate. In order to clarify the mechanism for formation of the E2-Ub_2 product, experiments were expanded to include the purification of the E2~Ub thiolester to determine the direct contribution of the E2 enzyme to reactivity.

Activity assays were performed with the use of Alexa fluorophore (680 nm) tagged Ub such that the reactivity of the E2~Alexa-Ub thiolester can be tracked directly through fluorescence imaging. The use of Ub^{K48R} ensures that the E2~Ub^{K48R} thiolester can only act as a Ub donor in future reactions, as K48 poly-Ub chain elongation is blocked. This blocked thiolester was made by mixing E1, E2, ATP and Alexa tagged Ub^{K48R} (Alexa-Ub^{K48R}) that react to give the E2~Alexa-Ub^{K48R} thiolester. This reaction was then subjected to size exclusion chromatography to remove the E1 enzyme, the MgATP solution, and the unreacted Alexa-Ub^{K48R}. These purified E2~Alexa-Ub^{K48R} thiolesters were produced for HIP2 (Fig 2.14) and Ubc1 (Fig 2.15). Reactions were then

performed by mixing these E2~Alexa-Ub^{K48R} thiolester Ub donors with varying purified proteins that may contain Ub acceptors. HIP2 and Ubc1 reactions were performed nearly identically and for simplicity only the HIP2 experiments will be explained in detail.

Reactive free Alexa dye was utilized to visualize any unconjugated E1 or E2 enzymes, and the lack of a fluorescent band confirmed the removal of E1 enzyme from the HIP2~Alexa-Ub^{K48R} thiolester (Fig 2.14B – lane 1,2). The purified thiolester was shown to be intact (Fig 2.14B – lane 3) and its reactivity is confirmed through reduction by DTT that can break the thiolester (Fig 2.14B – lane 4). The HIP2~Alexa-Ub^{K48R} thiolester was then tested for reactivity with three different possible Ub acceptors: unlabelled Ub^{K48R} (Fig 2.14B – lane 5), unlabelled wild type Ub (Fig 2.14B – lane 6 and 7), and the HIP2-$Ub_{K48}{}^{Cys}$ disulphide complex (Fig 2.14B – lane 8, 9).

The HIP2~Alexa-Ub^{K48R} thiolester reacted with the HIP2-$Ub_{K48}{}^{Cys}$ disulphide as was seen in previous assays (Section 2.3.6) only in this instance E1 is absent. The presence of E1 is therefore not required for this reaction to proceed showing that the HIP2~Alexa-Ub^{K48R} thiolester is directly interacting with HIP2-$Ub_{K48}{}^{Cys}$ to yield HIP2-$Ub_{K48}{}^{Cys}$-Alexa-Ub^{K48R} (marked with (1) and a solid dot, Fig 2.14B – lane 8). Addition of reducing agent shows the appearance of the Ub_2 ($Ub_{K48}{}^{Cys}$-Alexa-Ub^{K48R}) band (Fig 2.14B – lane 9). This proves that reaction scheme (1) shown in Figure 2.14A is in fact occurring and that E1 was not causing the reaction or indirectly assisting the reaction. The purified HIP2~Alexa-Ub^{K48R} thiolester was also reacted with two forms of free Ub, the substituted Ub^{K48R}, and wild type Ub. The HIP2~Alexa-Ub^{K48R} thiolester reacted with wild type Ub to yield free Ub_2, while the Ub^{K48R} mutant does not react to

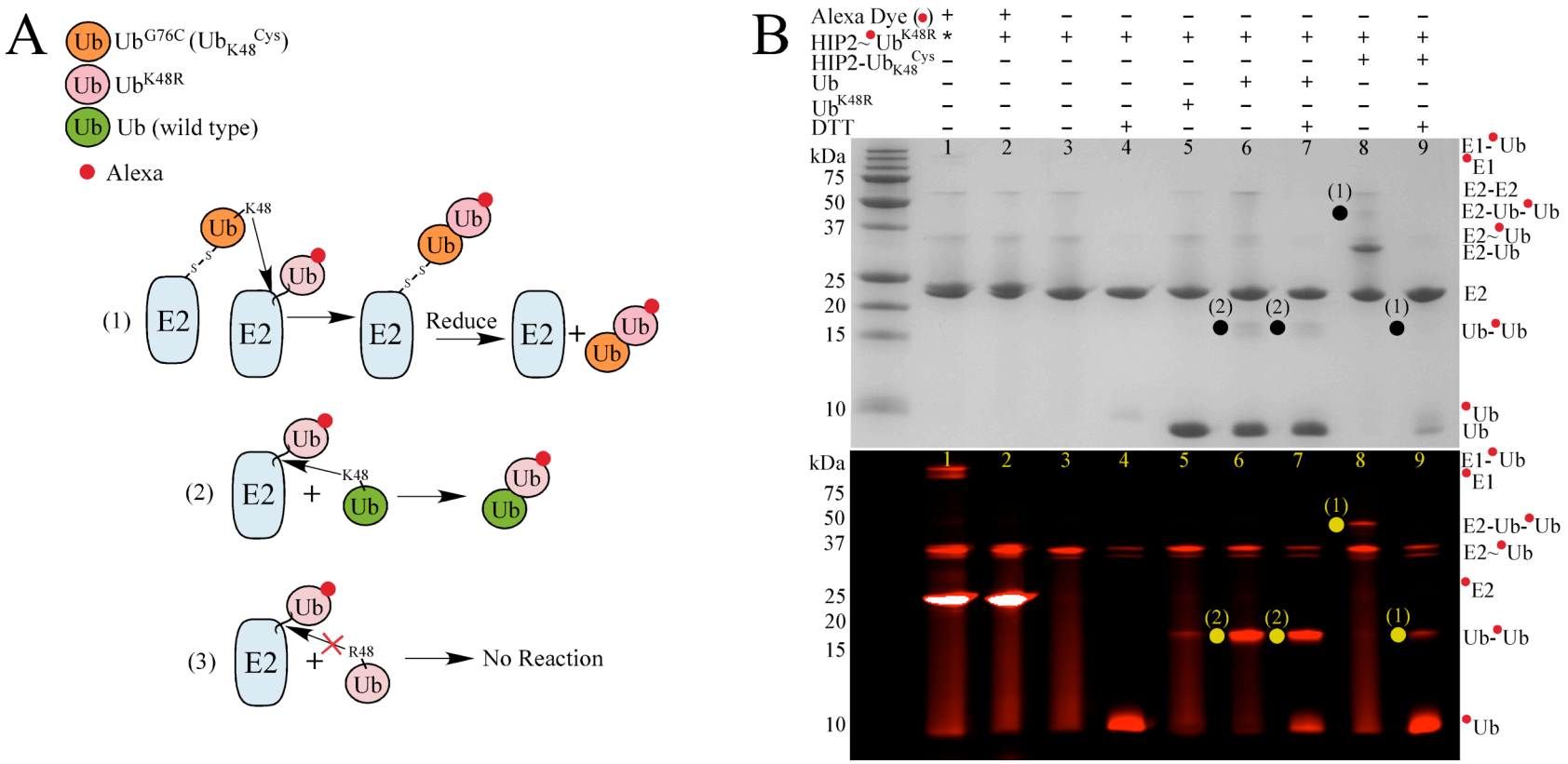

Figure 2.14 Purified HIP2~Alexa-Ub^{K48R} thiolester reacts with both HIP2-Ub$_{K48}{}^{Cys}$ disulphide and free Ub. (**A**) Mechanisms detailing HIP2~Alexa-Ub^{K48R} thiolester reaction with (1) HIP2-Ub$_{K48}{}^{Cys}$ disulphide, (2) wild type Ub, and (3) Ub^{K48R}. (**B**) Coomassie stained image (top gel) and fluorescent image at 700 nm (bottom gel) of HIP2~Alexa-Ub^{K48R} thiolester reactions. Thiolester formation was performed for 30 min at 37 °C with 214 nM E1, 32.8 µM HIP2, 16.4 µM Alexa-Ub^{K48R}, 10mM Mg-ATP solution, in 50mM Hepes pH 8.0. Purified thiolester was reacted with either 6 µM HIP2-Ub$_{K48}{}^{Cys}$, 54 µM wild type Ub, or 54 µM Ub^{K48R} for 1 hr at 37 °C. Reaction components are listed above each gel with a (+) or (-). All components for thiolester formation are signified in lane 1 with (*) while 'purified' HIP2~Alexa-Ub^{K48R} thiolester for all other lanes contains no E1 or ATP. Unconjugated E1 and E2 are visualized with 500 nM reactive Alexa dye, and 10mM DTT is used for reducing disulphides. Reaction products for scheme (1) (HIP2-Ub$_{K48}{}^{Cys}$-Alexa-Ub^{K48R}) and (2) (Ub-Alexa-Ub^{K48R}) are labeled with filled black/yellow circles. Molecular weight standards are listed to the left and protein species to the right of each gel.

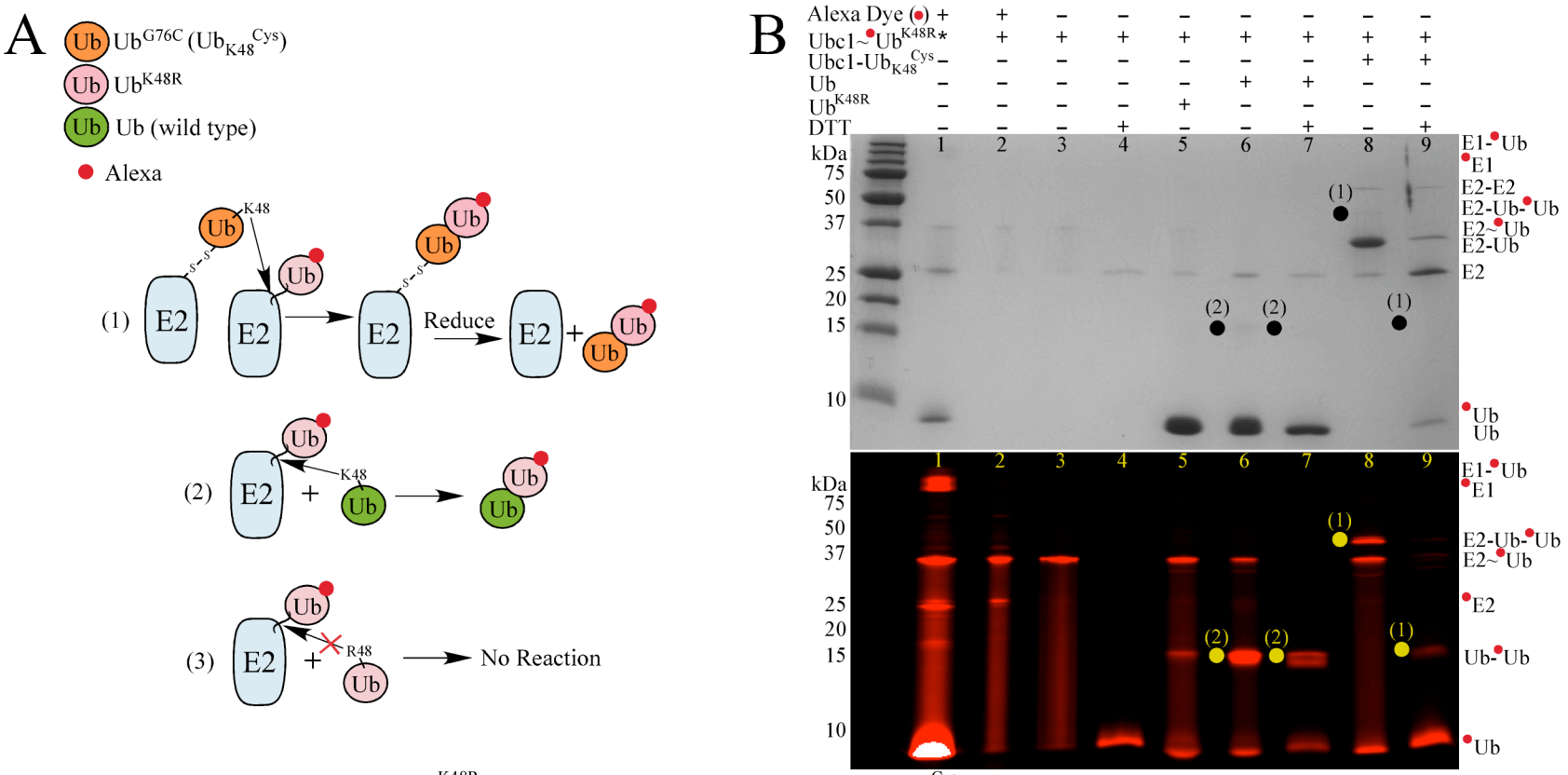

Figure 2.15 Purified Ubc1~Alexa-Ub^{K48R} thiolester reacts with both Ubc1-Ub$_{K48}{}^{Cys}$ disulphide and free Ub. (**A**) Mechanisms detailing Ubc1~Alexa-Ub^{K48R} thiolester reaction with (1) Ubc1-Ub$_{K48}{}^{Cys}$ disulphide, (2) wild type Ub, and (3) Ub^{K48R}. (**B**) Coomassie stained image (top gel) and fluorescent image at 700 nm (bottom gel) of Ubc1~Alexa-Ub^{K48R} thiolester reactions. Thiolester formation was performed for 30 min at 37 °C with 214 nM E1, 12.3 µM Ubc1, 18.3 µM Alexa-Ub^{K48R}, 10mM Mg-ATP solution, in 50mM Hepes pH 8.0. Purified thiolester was reacted with either 9.2 µM Ubc1-Ub$_{K48}{}^{Cys}$, 90 µM wild type Ub, or 90 µM Ub^{K48R} for 5 hrs at 37 °C. Reaction components are listed above each gel with a (+) or (-). All components for thiolester formation are signified in lane 1 with (*) while 'purified' Ubc1~Alexa-Ub^{K48R} thiolester for all other lanes contains no E1 or ATP. Unconjugated E1 and E2 are visualized with 500 nM reactive Alexa dye, and 10mM DTT is used for reducing disulphides. Reaction products for scheme (1) (Ubc1-Ub$_{K48}{}^{Cys}$-Alexa-Ub^{K48R}) and (2) (Ub-Alexa-Ub^{K48R}) are labeled with filled black/yellow circles. Molecular weight standards are listed to the left and protein species to the right of each gel.

any significant extent (Fig 2.14B – lane 5, 6). This Ub_2 was also stable to reducing agent (Fig 2.14B – lane 7). Due to the absence of ATP and E1, the reactive Ub molecules must remain free and cannot form a thiolester with the E2 enzyme. This indicates that the free forms of Ub are conclusively the reactive Ub acceptors for the HIP2 thiolester bound Alexa-Ub^{K48R} donors. These results illustrate that the HIP2~Alexa-Ub^{K48R} thiolester can directly react with any free Ub with an available K48 residue to cause chain extension (Fig 2.14A, reaction scheme (2) and (3)). This assay also shows that reaction scheme (1) and reaction scheme (2) can both occur, and therefore both free Ub and HIP2-$Ub_{K48}{}^{Cys}$ can act as ubiquitin acceptors when reacted with the HIP2~Alexa-Ub^{K48R} thiolester ubiquitin donor. Since the HIP2~Alexa-Ub^{K48R} thiolester can interact with either free wild type Ub or the HIP2-$Ub_{K48}{}^{Cys}$ disulphide, it is possible that the HIP2-$Ub_{K48}{}^{Cys}$ disulphide is simply acting as a reactant because it is being treated as a free Ub molecule albeit attached to another protein. This reaction would then not be driven by dimerization of E2 enzymes but simply by HIP2 and Ubc1's affinity and reactivity towards any Ub molecule, either free or attached to another protein. This would make reaction scheme (1) mechanistically the same as reaction scheme (2), whereby both simply rely on an available and at least temporarily exposed K48 residue in Ub (Fig 2.14A). The nearly identical reaction procedure produces very similar results for the reaction of the Ubc1~Alexa-Ub^{K48R} thiolester with both free Ub and Ubc1-$Ub_{K48}{}^{Cys}$ indicating these enzymes are functionally very similar (Fig 2.15).

2.4 Discussion

2.4.1 Previous evidence for E2 dimerization

Recently there have been numerous experiments performed to shed light on the mechanism of poly-Ub chain formation and transfer in regards to the E1, E2, and E3 enzymes in various ubiquitination pathways. The observation that Ub-Ub linkages can be formed in many of these systems prior to interaction with substrates provides evidence that poly-Ub chains may be assembled prior to attachment to substrates. One hypothesis for how these Ub-Ub linkages are created involves E2 dimerization. Solid structural evidence for E2 dimerization has been found for Ubc13/Mms2, while reactive experimental evidence for E2 dimerization has been found for Ube2g2, Cdc34, and Ubc1 (*2-9, 27*). In this chapter, HIP2 and Ubc1 enzymes were investigated for dimerization. These enzymes are highly active in poly-Ub chain formation in the absence of E3 enzymes and substrates, indicating a simple E2-E2 mechanism could exist for these enzymes (*10, 11*). Previous studies on Cdc34 also indicated that the presence of the Cdc34~Ub thiolester may be required for dimerization. Therefore, thiolester mimics (disulphide complexes) of Ubc1 and HIP2 were also created and studied. In addition to understanding HIP2 and Ubc1 function, insights into the mechanisms utilized by these enzymes may shed light on more complicated ubiquitination systems involving E3 enzymes and substrates.

Many early experiments on E2 enzymes including Ubc1 and HIP2 used size exclusion elution profiles and chemical crosslinking to test for possible dimerization. Both Ubc1 and HIP2 had early size exclusion elution profiles that implied significant dimerization (*17, 27*). The high-resolution structures of these proteins have since been

solved, and their elongated shapes were likely the cause for early elution profiles. Crosslinking experiments were also performed on both of these proteins where Ubc1 was observed to chemically crosslink (*27*), and HIP2 did not (*17*). These results likely do not properly predict dimerization since the Ubc1 and HIP2 structures illustrate the presence of unstructured flexible linkers that can explain their reactivity to lysine reactive cross-linking agents. Ubc1 contains a rather long unstructured tether between its two domains (*21*) with an exposed and highly mobile K157 residue that may be responsible for the observed crosslinking activity. This is supported by another study where the removal of this flexible tether, including the UBA domain, greatly reduced crosslinking (*27*). HIP2 contains a shorter tether that lacks an exposed lysine residue, which may explain why this protein does not crosslink. These observations support that these crosslinking studies measure specific lysine reactivity as opposed to actual E2 dimerization. The previous studies on the dimerization of HIP2 and Ubc1 are clearly debatable and therefore more specific experimentation is required.

2.4.2 In depth studies into dimerization of HIP2 and Ubc1

The possible dimerization of HIP2 and Ubc1 as well as HIP2-Ub^{Cys} and Ubc1-Ub^{Cys} was thoroughly investigated. Sedimentation equilibrium was used as a technique to investigate dimerization since it reports molecular weights to high accuracy, it is not sensitive to protein shape, and it offers the ability to quantify any type of oligomerization. The molecular weights (MW) for HIP2 and Ubc1 were found to be within 4% of the expected value. These results are in good agreement with an expected error rate of 5%. HIP2-Ub^{Cys} and Ubc1-Ub^{Cys} were within 11.1% of the expected values. These MW

measurements were larger than expected and if these small increases are interpreted as self-association, we can calculate K_d values around 500 and 2000 of μM for HIP2 and Ubc1 respectively, and K_d values around 200-300 of μM for HIP2-Ub^{Cys} and Ubc1-Ub^{Cys}. These reported K_d values for self-association are much too high to be considered reliable since the concentrations used in sedimentation equilibrium are in the range of 10-20 μM. To further characterize any possible self-association of these enzymes, SAXS was performed at higher protein concentrations in the range of around 25-250 μM. The MW measurements from SAXS were acquired with a dilution series, so any change in MW as concentrations are increased are more reliable. It is important to note the exact MW values determined by SAXS can be distorted by inaccurate concentrations of proteins or standards in addition to the 10% accuracy of MWs reported by this technique (*22*). There are not enough data points to accurately fit an entire K_d curve, however, approximate K_d limitations can be determined by comparing the experimental data to theoretical K_d curves. The K_d for dimerization of HIP2 and Ubc1 as well as HIP2-Ub^{Cys} and Ubc1-Ub^{Cys} were determined to be >1000 μM, and these K_d's may in fact be much weaker. Since HIP2-Ub^{Cys} and Ubc1-Ub^{Cys} appear to increase in MW and R_g more so than HIP2 or Ubc1 alone, it is likely that these disulphide species increase the very weak dimerization capacity of these enzymes. Although the K_d for dimerization is affected by disulphide formation with Ub, these proteins are still predominantly monomeric in solution even at concentrations up to ~200 μM. The cellular concentration of Ub is roughly 10 μM (*28, 29*) and the cellular concentrations of E2 enzymes are likely in the low μM (<10 μM) to nM range. Comparison of these cellular concentrations to the E2

and E2-Ub K_d for dimerization of >1000 μM (1 mM) indicates these proteins are almost exclusively monomeric at cellular concentrations.

2.4.3 Dimerization scaffold proteins are not used for Ubc1 or HIP2

Previous experiments on the E2 enzyme Ube2g2 have indicated poly-Ub chain formation occurs between two different Ube2g2 enzymes and this activity required the E3 enzyme gp78 (*2*). Subsequent studies on this enzyme deduced that these E2 interactions were aided by the dimerization of the E3 enzyme, indicating the E3 enzyme may be a scaffold for E2 dimerization in the Ube2g2 pathway (*3*). The Ubc1 and HIP2 enzymes have poly-Ub chain activity without an E3 enzyme indicating that they do not require an E3 scaffold like Ube2g2. The only protein left in our reactions that could act as a dimerization scaffold is the E1 enzyme. There is currently no evidence that an E1 enzyme can bind two E2 enzymes, however, HIP2 and Ubc1 retain the ability to form Ub-Ub linkages upon removal of the E1 enzyme, which suggests that the E1 enzyme does not act as a scaffold for E2 dimerization. These results indicate that there are no additional proteins present in the activity assays performed in this work that increase the K_d of dimerization of Ubc1 or HIP2.

2.4.4 The E1 enzyme is not directly used to create Ub-Ub linkages

It has been previously reported that the E1 enzyme may be directly responsible for the formation of a poly-Ub chain on the E2 enzyme Ubc1 (*30*). This proposed function of E1 is novel and was performed with K93 auto-ubiquitination on a truncated

version of Ubc1, which lacks the UBA domain (*30*). The Ubc1 enzyme utilized in this chapter has a K93R substitution to avoid auto-ubiquitination, and retains the UBA domain to ensure proper enzymatic function. Activity assays on the full length HIP2 and Ubc1 do not support an E1 catalyzed poly-Ub chain formation mechanism since the addition of E1 enzyme, ATP, and wild type Ub could not react with the HIP2-Ub_{K48}^{Cys} or Ubc1-Ub_{K48}^{Cys} disulphides. These results demonstrate that the K48 residue on disulphide bound Ub does not act as a Ub acceptor with the E1~Ub thiolester.

The requirement for the E1 enzyme was further investigated by forming E2~Ub thiolesters followed by a purification procedure to remove the E1 enzyme. This process created 'purified' E2~Ub thiolesters to determine if they can react alone with Ub acceptors. The 'purified' E2~Ub thiolesters reacted with both E2-Ub_{K48}^{Cys} disulphides and free wild type Ub to create Ub_2 in the absence of the E1 enzyme. Therefore, the E1 is only required for E2 thiolester charging, and not required for the extension of poly-Ub chains.

2.4.5 A proposed monomeric mechanism for Ubc1 and HIP2 activity

Poly-ubiquitination activity assays with HIP2 and Ubc1 were performed without E3 enzymes or substrates, indicating only E1 and E2 enzymes are involved in poly-Ub chain formation. Activity assays demonstrated that the E1 was only required for E2 charging, proving that poly-Ub activity is driven solely by HIP2 and Ubc1. Initial work on E2 enzymes in several pathways suggested that these enzymes function using a dimeric mechanism. The HIP2 and Ubc1 enzymes were determined to have a weak K_d of dimerization of >1000 μM (Fig 2.16A). Weak dimerization could occur through

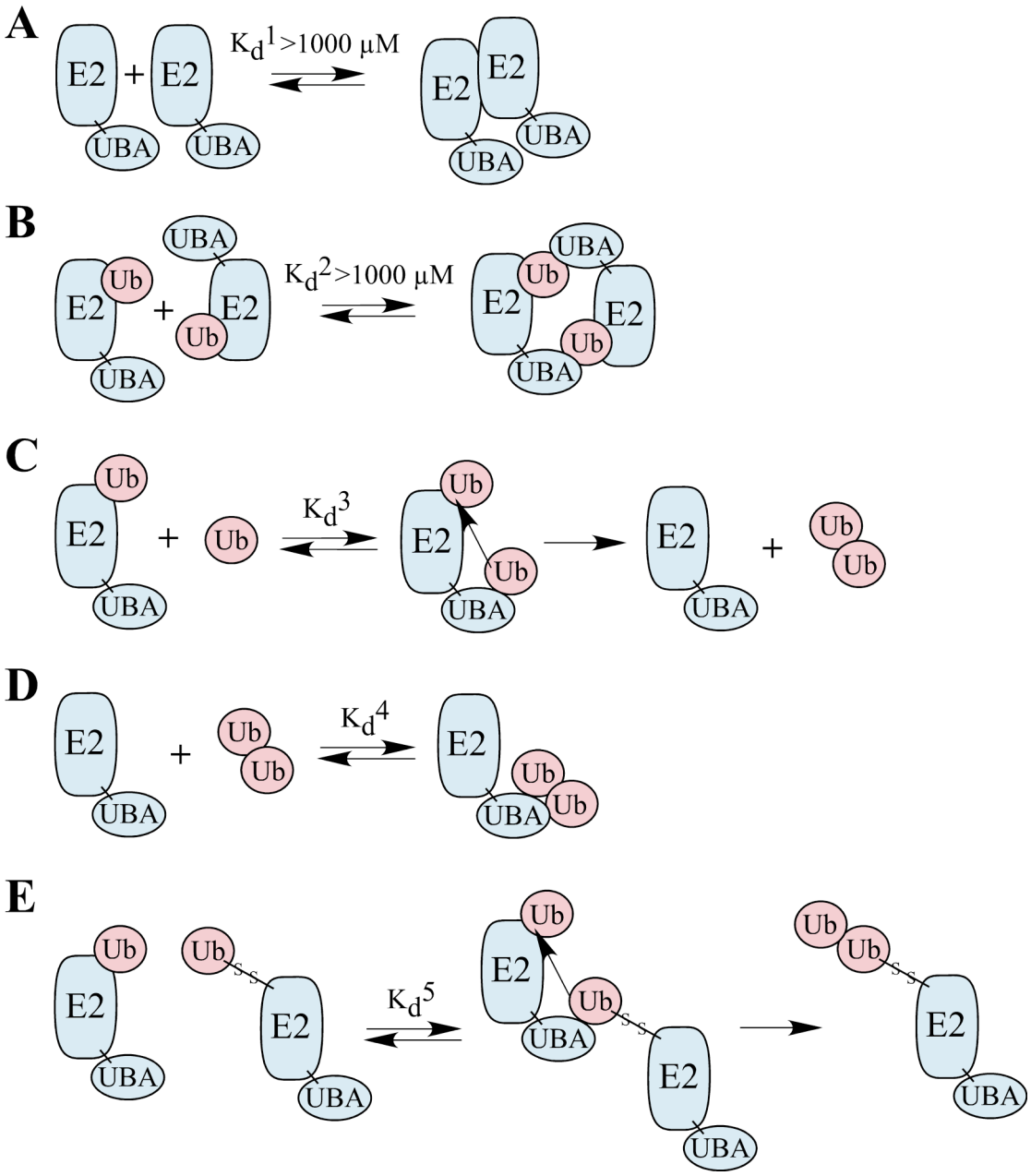

Figure 2.16 A schematic representation of the strength of protein interactions and possible mechanisms involved in poly-Ub chain formation activity observed for the E2 enzymes Ubc1 and HIP2. The strength of protein interactions are reported as dissociation constants (K_d values). (**A**) The self-association of E2 enzymes presumably through core-core interactions. (**B**) The self-association of E2~Ub enzymes presumably driven by UBA domain interactions with attached ubiquitin. (**C**) The association of Ub with the UBA domain resulting in reaction with the E2~Ub thiolester causing the formation of Ub_2. (**D**) The association of Ub_2 with the E2 UBA domain. (**E**) The association of the disulphide attached Ub with the UBA domain of another E2~Ub thiolester reacting to yield E2-Ub_2. All reactions shown with arrows account for the nucleophilic attack of a K48 side chain to a thiolester attached Ub, resulting in a Ub-Ub K48-linked poly-Ub. Each arrow between Ub molecules represents the K48 side chain nucleophilic attack to the reactive thiolester of a second Ub.

catalytic core interactions between E2 enzymes (*7*) or through UBA-UBA domain interactions (*31*). Another method for E2 dimerization would be through the formation of an E2~Ub thiolester. The HIP2 and Ubc1 C-terminal UBA domains have been observed to bind Ub non-covalently (*21, 23, 32, 33*). These UBA/Ub binding interactions could drive dimerization whereby the UBA domain of each E2 could interact with the Ub attached to the neighbouring E2 enzyme (Fig 2.16B). By examining HIP2-Ub^{Cys} and Ubc1-Ub^{Cys} disulphides designed to mimic the active thiolester the dimerization capacity was determined to also have a weak K_d of >1000 μM. The models depicted in Figure 2.16A and 2.16B have weak K_d values indicating that these E2 enzymes alone and in their thiolester mimic form are predominantly monomeric at typical cellular protein concentrations in the range of low μM to nM. Although the K_d of >1000 μM indicates <1% of these enzymes are dimeric during the activity assays performed, this weak dimeric mechanism may still explain the reaction of purified E2~Ub^{K48R} thiolester with the E2-$Ub_{K48}{}^{Cys}$ disulphide for both HIP2 and Ubc1. The low amount of dimerization may be the reason these reactions occur slowly, on the order of hours.

Both purified HIP2~Ub^{K48R} and Ubc1~Ub^{K48R} thiolesters can react with unconjugated wild type Ub. Previous studies have also implied the use of free Ub in HIP2 unanchored poly-Ub chain formation through the use of C-terminal Ub truncations that could not form thiolesters (*10, 17*). The use of free Ub as an acceptor indicates that the activity of the HIP2 and Ubc1 enzymes may be driven by UBA affinity towards free Ub. This activity can be rationalized with a monomeric mechanism. HIP2 and Ubc1 have the ability to interact with at least two Ub molecules at once, one through a thiolester linkage and a second Ub non-covalently through the UBA domain (*21, 33*).

The UBA/Ub binding may simply increase the local concentration of Ub or the UBA could provide the E2 enzyme with an ability to place 2 Ub molecules in close proximity to assist in the formation of a Ub-Ub linkage (Fig 2.16C). The monomeric mechanism depicted in Figure 2.16C would be driven by UBA affinity for an acceptor Ub that would be positioned so its K48 residue can perform a nucleophilic attack on the thiolester bound donor Ub. The K_d^3 value in Figure 2.16C represents the UBA domain's affinity for Ub and has been previously measured to be 400 μM for HIP2 (*33*) and 228 ± 69 μM for Ubc1 (*21*). Upon comparison to the dissociation constants for dimerization (K_d^1 and K_d^2 >1000 μM), the affinity of E2 to Ub is stronger than the monomer-dimer equilibrium for both these enzymes (Fig 2.16A, B, C). This K_d comparison means the E2 enzymes have higher affinity for free Ub than another E2 enzyme. Therefore, if the monomeric mechanism can occur, it would be more probable than the dimeric mechanism.

A previous study on several isolated UBA domains has shown a higher affinity for poly-Ub chains than single Ub molecules (*33*). In this study, the HIP2 UBA domain's affinity for Ub_4 was measured to have a K_d of 155 μM showing that the UBA domain binds poly-Ub chains more strongly than a single Ub with a K_d of 400 μM (*33*). It is likely the UBA domain in Ubc1 behaves in a similar manner. Figure 2.16D depicts the affinity of E2 for Ub_2 that likely has a K_d^4 that lies somewhere between the 155 and 400 μM for HIP2 and less than 228 ± 69 μM for Ubc1 (*21, 33*). The fact that the value for K_d^4 is less than that for K_d^3 indicates that the association seen in Figure 2.16D is stronger than that for Figure 2.16C. This affinity difference may explain why HIP2 has previously been shown to kinetically favor Ub_2 as a Ub acceptor over a single Ub (*10*). These results indicate that poly-Ub chains should be extended faster than a single Ub.

A monomeric mechanism for HIP2 and Ubc1 function does not initially seem to explain the reaction of E2~Ub^{K48R} thiolesters with E2-$Ub_{K48}{}^{Cys}$ disulphides. However, if the mechanism depicted in Figure 2.16C is redrawn with a disulphide in place of Ub (Fig 2.16E) the reaction that proceeds would be very similar. The common feature of both reactants is simply a reactive K48 residue available in the Ub acceptor. In this manner, both the E2-$Ub_{K48}{}^{Cys}$ disulphide and free wild type Ub may react with E2~Ub^{K48R} by the same mechanism. The $K_d{}^5$ is likely >1000 μM as the affinity for E2~Ub^{K48R} thiolester and E2-$Ub_{K48}{}^{Cys}$ disulphide should be identical to the K_d measured for the self-association of E2-Ub^{Cys} disulphide. The $K_d{}^5$ comparison to $K_d{}^3$ indicates that the E2-$Ub_{K48}{}^{Cys}$ disulphide is a less efficient Ub acceptor than free wild type Ub, presumably due to a partially or transiently blocked Ub surface. SAXS results show the E2-$Ub_{K48}{}^{Cys}$ disulphides have an exposed disulphide bound Ub that could be recognized by the UBA domain. The idea of a partially exposed thiolester bound Ub is also supported by previous experimentation on E2~Ub conjugates suggesting that the Ub is highly mobile on the surface of the E2 (*34*). Therefore, the reaction of E2~Ub^{K48R} thiolesters and E2-$Ub_{K48}{}^{Cys}$ disulphides may occur only due to lack of a preferred free Ub acceptor in these reactions. Comparison of the K_d's in the mechanisms in Figure 2.16 indicates free Ub and poly-Ub chains are the preferred acceptors for the E2~Ub^{K48R} thiolesters.

2.4.6 UBA domain and Ub positioning in HIP2 and Ubc1 structures

SAXS experiments yield low-resolution structural data for HIP2 and Ubc1 and their disulphide complexes that can be used to determine the average shape of these proteins in solution. These low-resolution shapes are sufficient to distinguish between

greatly varying positions for the UBA domain and disulphide bound Ub, however the fine details describing the exact orientation of the UBA domain or Ub in relation to the catalytic core domain cannot be determined. SAXS analysis in comparison to high-resolution structures allowed for the determination of the average position of the UBA domain in relation to the catalytic core for both HIP2 and Ubc1. These results indicated that both HIP2 and Ubc1 contain few interactions between their catalytic core and UBA domains. This result indicates that the UBA domain is likely mobile in relation to the core domain.

The position of Ub in HIP-Ub^{Cys} and Ubc1-Ub^{Cys} adheres more closely to the 'elongated' models (Fig 2.12B, 2.13A) than the 'compact' models (Fig 2.12A, 2.13B). Although the 'elongated' models are based on a rigid high-resolution structure, the high quality fits to SAXS data indicates that these structures accurately represent the average position of both the mobile UBA domain, and bound Ub in the E2-Ub^{Cys} disulphides. Alternative structures with varied positions for the UBA domain and Ub as well as dimeric structures yielded poor fits to the SAXS data.

SAXS data for both HIP2-Ub^{Cys} and Ubc1-Ub^{Cys} disulphides can be fit to models where the hydrophobic surface of Ub is highly exposed to solution. However, previous NMR experiments on the Ubc1Δ~Ub thiolester (no UBA) show that there are significant contacts between the hydrophobic face of Ub and the Ubc1 enzyme (*19*). Similar contacts were also observed in NMR studies with HIP2-Ub^{Cys} (Chapter 4). These results indicate that the hydrophobic face of Ub is at least partially blocked from solution in Ubc1-Ub^{Cys} and HIP2-Ub^{Cys}. These results are consistent with previous experiments on E2~Ub structures that indicated the thiolester attached Ub on E2 enzymes may be highly

mobile (*34*). SAXS experiments provide the general position of Ub in the E2-Ub^{Cys} 'elongated' models, but the orientation of the hydrophobic face of Ub may in fact point towards the core domain accounting for the partially blocked Ub surface in this extended structure. Since E2-$Ub_{K48}{}^{Cys}$ disulphides can be reacted with the E2~Ub^{K48R} thiolesters, the K48 residue of Ub must be occasionally exposed to allow a reaction. This means that regardless of the exact position of the disulphide bound Ub, there is likely a dynamic equilibrium between a partially blocked and a more fully exposed disulphide bound Ub.

2.4.7 Purpose of the UBA domain

The poly-Ub chain formation activity of Ubc1 and HIP2 seems to be driven by reactivity towards attached or free Ub (Fig 2.16C, D, E). This reactivity towards Ub is likely due to the UBA domains of Ubc1 and HIP2 that have been shown to bind Ub through NMR titration experiments (*21*, *23, 32*). Complicating the theory that UBA/Ub binding drives Ubc1 and HIP2 activity, is the fact that both HIP2 (*32, 35*) and Ubc1 (*11, 30, 36*) retain some poly-Ub chain activity upon UBA domain removal. The removal of the UBA domains from both HIP2 and Ubc1 reduced the full processivity of these enzymes causing shorter poly-Ub chains to form (*32, 36*). These results indicate that the UBA domain aids in reaction efficiency, but is not essential for poly-Ub chain formation. In previous studies a chimeric protein created with the catalytic core of the E2 enzyme Ubc4 with addition of the HIP2 UBA domain, was not active in poly-Ub chain formation (*17*). This result suggests the addition of HIP2's UBA domain on any E2 enzyme is not solely responsible for poly-Ub chain formation and that the HIP2 catalytic core domains contain unique residues directly responsible for proper Ub placement to allow formation

of poly-Ub chains. This may imply that their catalytic cores have some affinity for Ub themselves. However, Ub has not been observed to bind at the catalytic core of either Ubc1 or HIP2 in previous NMR titration experiments (*21, 23*). The crystal structure of HIP2 with non-covalently bound Ub also did not show any contacts between the catalytic core and Ub (*23*). The fact that these enzymes still retain some activity upon UBA domain removal is perplexing, although it is possible that the UBA domain aids in reaction efficiency by increasing the local concentration of reactant (Ub or Ub chains), but is not completely required for specific orientation of an acceptor Ub for reaction with the reactive thiolester. The UBA domain may also increase the rate of reaction through efficient physical placement of two Ub molecules in close proximity. There is currently no clear mechanism defining how HIP2 and Ubc1 accomplish K48-linkage specificity in these poly-Ub chain formation reactions.

2.4.8 Purpose of chain building by Ubc1 and HIP2

HIP2 and Ubc1 are homologs from human and yeast respectively, and appear to function in a similar manner as both have been shown to build K48-linked poly-Ub chains. Activity assays have demonstrated that E2-Ub^{K48R} thiolesters can react with either E2-$Ub_{K48}{}^{Cys}$ disulphides to form E2-Ub_2 or free Ub to form unanchored Ub_2. Comparison of K_d values favours free poly-Ub chains and free Ub as the acceptor for HIP2~Ub and Ubc1~Ub thiolesters. Removal of the E1 enzyme in activity assays indicates that the E2~Ub^{K48R} thiolester is the sole reactive enzyme in poly-Ub chain extension and is directly responsible for reaction with free Ub. These free Ub acceptors

must then be non-covalently interacting with the E2 enzyme presumably through the UBA domain and possibly additional contacts on the E2 catalytic core.

The resulting reaction from these E2 enzymes is the formation of unanchored poly-Ub chains, with HIP2 producing much longer chains (*10, 11*). The purpose of unanchored poly-Ub chains remains unknown, but free unconjugated poly-Ub chains are found *in vivo* (*38*). Previous experimentation has found that Ub_2 and Ub_4 chains can be just as easily activated on E1 and transferred to E2 as mono Ub (*10, 38*). Therefore, free Ub chains can be utilized to form thiolester intermediates and then act as Ub donors. The creation of these poly-Ub chains without substrate, and the fact that these chains can be loaded onto E2 enzymes to act as poly-Ub chain donors, supports the mechanism of preassembling chains prior to attachment to substrate.

It is also possible that HIP2 and Ubc1 are involved in a sequential addition model by extending chains on ubiquitinated substrates by a method similar to that seen in unanchored chain assembly. This mechanism is supported by recent work on Ubc4 and Ubc1 that found both enzymes can ubiquitinate APC (large RING E3 complex) substrates. These enzymes appear to have different functions as Ubc4 is more active in initial Ub attachment to substrates and Ubc1 is more active at extending chains on substrates that already have a single attached Ub (*36*). The *in vitro* poly-Ub chain activity in the absence of E3 enzymes and substrates may then be a non-physiological by-product reaction due to lack of a preferred mono or poly ubiquitinated substrate. Therefore, the poly-Ub chain activity of these enzymes *in vivo* may prefer ubiquitinated substrate, but in the absence of this substrate, free Ub or auto-ubiquitinated proteins may act as substitute reactants.

The activity assays performed show direct interaction of E2 thiolesters with both free Ub and E2-Ub thiolester mimics. E2 dimerization is likely not a driving factor for these reactions. These results point towards Ubc1 and HIP2 functioning primarily in a monomeric manner in solution with the components tested. The creation of poly-Ub chains may be an artifactual activity due to limited reactants in the sequential addition model, or could be the first steps of poly-Ub chain formation in a preassembly model.

Bibliography

1. Hochstrasser, M. (2006) Lingering mysteries of ubiquitin-chain assembly, *Cell 124*, 27-34.

2. Li, W., Tu, D., Brunger, A. T., and Ye, Y. (2007) A ubiquitin ligase transfers preformed polyubiquitin chains from a conjugating enzyme to a substrate, *Nature 446*, 333-337.

3. Li, W., Tu, D., Li, L., Wollert, T., Ghirlando, R., Brunger, A. T., and Ye, Y. (2009) Mechanistic insights into active site-associated polyubiquitination by the ubiquitin-conjugating enzyme Ube2g2, *Proc Natl Acad Sci U S A 106*, 3722-3727.

4. Varelas, X., Ptak, C., and Ellison, M. J. (2003) Cdc34 self-association is facilitated by ubiquitin thiolester formation and is required for its catalytic activity, *Mol Cell Biol 23*, 5388-5400.

5. Gazdoiu, S., Yamoah, K., Wu, K., Escalante, C. R., Tappin, I., Bermudez, V., Aggarwal, A. K., Hurwitz, J., and Pan, Z. Q. (2005) Proximity-induced activation of human Cdc34 through heterologous dimerization, *Proc Natl Acad Sci U S A 102*, 15053-15058.

6. McKenna, S., Moraes, T., Pastushok, L., Ptak, C., Xiao, W., Spyracopoulos, L., and Ellison, M. J. (2003) An NMR-based model of the ubiquitin-bound human ubiquitin conjugation complex Mms2.Ubc13. The structural basis for lysine 63 chain catalysis, *J Biol Chem 278*, 13151-13158.

7. Eddins, M. J., Carlile, C. M., Gomez, K. M., Pickart, C. M., and Wolberger, C. (2006) Mms2-Ubc13 covalently bound to ubiquitin reveals the structural basis of linkage-specific polyubiquitin chain formation, *Nat Struct Mol Biol 13*, 915-920.

8. VanDemark, A. P., Hofmann, R. M., Tsui, C., Pickart, C. M., and Wolberger, C. (2001) Molecular insights into polyubiquitin chain assembly: crystal structure of the Mms2/Ubc13 heterodimer, *Cell 105*, 711-720.

9. Moraes, T. F., Edwards, R. A., McKenna, S., Pastushok, L., Xiao, W., Glover, J. N., and Ellison, M. J. (2001) Crystal structure of the human ubiquitin conjugating enzyme complex, hMms2-hUbc13, *Nat Struct Biol 8*, 669-673.

10. Chen, Z., and Pickart, C. M. (1990) A 25-kilodalton ubiquitin carrier protein (E2) catalyzes multi-ubiquitin chain synthesis via lysine 48 of ubiquitin, *J Biol Chem 265*, 21835-21842.

11. Hodgins, R., Gwozd, C., Arnason, T., Cummings, M., and Ellison, M. J. (1996) The tail of a ubiquitin-conjugating enzyme redirects multi-ubiquitin chain

synthesis from the lysine 48-linked configuration to a novel nonlysine-linked form, *J Biol Chem 271*, 28766-28771.

12. Wolf, A. V. (1966) *Aqueous Solutions and Body Fluids*, Hoeber.

13. Sohnel, O., and Novotny, P. (1985) *Densities of Aqueous Solutions of some Inorganic Substances*, Elsevier, Amsterdam.

14. Cohn, E. J., and Edsall, J. T., (Eds.) (1943) *Proteins, Amino Acids and Peptides as Ions and Dipolar Ions*, New York.

15. Hammersley, A. P. http://www.esrf.eu/computing/scientific/FIT2D/.

16. Svergun, D., Barberato, C., and Koch, M. H. J. (1995) CRYSOL - A program to evaluate x-ray solution scattering of biological macromolecules from atomic coordinates, *Journal of Applied Crystallography 28*, 768-773.

17. Haldeman, M. T., Xia, G., Kasperek, E. M., and Pickart, C. M. (1997) Structure and function of ubiquitin conjugating enzyme E2-25K: the tail is a core-dependent activity element, *Biochemistry 36*, 10526-10537.

18. Merkley, N., Barber, K. R., and Shaw, G. S. (2005) Ubiquitin manipulation by an E2 conjugating enzyme using a novel covalent intermediate, *J Biol Chem 280*, 31732-31738.

19. Hamilton, K. S., Ellison, M. J., Barber, K. R., Williams, R. S., Huzil, J. T., McKenna, S., Ptak, C., Glover, M., and Shaw, G. S. (2001) Structure of a conjugating enzyme-ubiquitin thiolester intermediate reveals a novel role for the ubiquitin tail, *Structure 9*, 897-904.

20. Serniwka, S. A., and Shaw, G. S. (2009) The structure of the UbcH8-ubiquitin complex shows a unique ubiquitin interaction site, *Biochemistry 48*, 12169-12179.

21. Merkley, N., and Shaw, G. S. (2004) Solution structure of the flexible class II ubiquitin-conjugating enzyme Ubc1 provides insights for polyubiquitin chain assembly, *J Biol Chem 279*, 47139-47147.

22. Svergun, D. I., and Mylonas, E. (2007) Accuracy of molecular mass determination of proteins in solution by small-angle X-ray scattering, *Journal of Applied Crystallography 40*, S245-S249.

23. Ko, S., Kang, G. B., Song, S. M., Lee, J. G., Shin, D. Y., Yun, J. H., Sheng, Y., Cheong, C., Jeon, Y. H., Jung, Y. K., Arrowsmith, C. H., Avvakumov, G. V., Dhe-Paganon, S., Yoo, Y. J., Eom, S. H., and Lee, W. (2010) Structural basis of E2-25K/UBB+1 interaction leading to proteasome inhibition and neurotoxicity, *J Biol Chem 285*, 36070-36080.

24. Wilson, R. C., Hughes, R. C., Flatt, J. W., Meehan, E. J., Ng, J. D., and Twigg, P. D. (2009) Structure of full-length ubiquitin-conjugating enzyme E2-25K (huntingtin-interacting protein 2), *Acta Crystallogr Sect F Struct Biol Cryst Commun 65*, 440-444.

25. Sakata, E., Satoh, T., Yamamoto, S., Yamaguchi, Y., Yagi-Utsumi, M., Kurimoto, E., Tanaka, K., Wakatsuki, S., and Kato, K. (2010) Crystal structure of UbcH5b~ubiquitin intermediate: insight into the formation of the self-assembled E2~Ub conjugates, *Structure 18*, 138-147.

26. Kamadurai, H. B., Souphron, J., Scott, D. C., Duda, D. M., Miller, D. J., Stringer, D., Piper, R. C., and Schulman, B. A. (2009) Insights into ubiquitin transfer cascades from a structure of a UbcH5B approximately ubiquitin-HECT(NEDD4L) complex, *Mol Cell 36*, 1095-1102.

27. Leggett, D. S., and Candido, P. M. (1997) Biochemical characterization of Caenorhabditis elegans UBC-1: self-association and auto-ubiquitination of a RAD6-like ubiquitin-conjugating enzyme in vitro, *Biochem J 327 (Pt 2)*, 357-361.

28. Mastrandrea, L. D., You, J., Niles, E. G., and Pickart, C. M. (1999) E2/E3-mediated assembly of lysine 29-linked polyubiquitin chains, *J Biol Chem 274*, 27299-27306.

29. Rodrigo-Brenni, M. C., Foster, S. A., and Morgan, D. O. (2010) Catalysis of lysine 48-specific ubiquitin chain assembly by residues in E2 and ubiquitin, *Mol Cell 39*, 548-559.

30. Huzil, J. T., Pannu, R., Ptak, C., Garen, G., and Ellison, M. J. (2007) Direct catalysis of lysine 48-linked polyubiquitin chains by the ubiquitin-activating enzyme, *J Biol Chem 282*, 37454-37460.

31. Kozlov, G., Peschard, P., Zimmerman, B., Lin, T., Moldoveanu, T., Mansur-Azzam, N., Gehring, K., and Park, M. (2007) Structural basis for UBA-mediated dimerization of c-Cbl ubiquitin ligase, *J Biol Chem 282*, 27547-27555.

32. Wilson, R. C., Edmondson, S. P., Flatt, J. W., Helms, K., and Twigg, P. D. (2011) The E2-25K ubiquitin-associated (UBA) domain aids in polyubiquitin chain synthesis and linkage specificity, *Biochem Biophys Res Commun 405*, 662-666.

33. Raasi, S., Varadan, R., Fushman, D., and Pickart, C. M. (2005) Diverse polyubiquitin interaction properties of ubiquitin-associated domains, *Nat Struct Mol Biol 12*, 708-714.

34. Pruneda, J. N., Stoll, K. E., Bolton, L. J., Brzovic, P. S., and Klevit, R. E. (2011) Ubiquitin in motion: structural studies of the ubiquitin-conjugating enzyme approximately ubiquitin conjugate, *Biochemistry 50*, 1624-1633.

35. Pichler, A., Knipscheer, P., Oberhofer, E., van Dijk, W. J., Korner, R., Olsen, J. V., Jentsch, S., Melchior, F., and Sixma, T. K. (2005) SUMO modification of the ubiquitin-conjugating enzyme E2-25K, *Nat Struct Mol Biol 12*, 264-269.

36. Rodrigo-Brenni, M. C., and Morgan, D. O. (2007) Sequential E2s drive polyubiquitin chain assembly on APC targets, *Cell 130*, 127-139.

37. Deffenbaugh, A. E., Scaglione, K. M., Zhang, L., Moore, J. M., Buranda, T., Sklar, L. A., and Skowyra, D. (2003) Release of ubiquitin-charged Cdc34-S - Ub from the RING domain is essential for ubiquitination of the SCF(Cdc4)-bound substrate Sic1, *Cell 114*, 611-622.

38. van Nocker, S., and Vierstra, R. D. (1993) Multiubiquitin chains linked through lysine 48 are abundant in vivo and are competent intermediates in the ubiquitin proteolytic pathway, *J Biol Chem 268*, 24766-24773.

Chapter 3

^{1}H, ^{15}N, and ^{13}C Backbone Resonance Assignments of the E2 Conjugating Enzyme HIP2

3.1 Introduction

HIP2 is a Class II E2 conjugating enzyme containing the conserved catalytic core and a C-terminal UBA domain. Importantly, it is the only human E2 enzyme known to possess this domain. HIP2 also appears to be one of the most active E2 enzymes in poly-Ub chain assembly (*1*), and yet very few E3 enzymes have been documented to function with HIP2. These results may indicate that HIP2 has a rather novel function in comparison to other E2 enzymes. Most importantly HIP2 has been shown to interact with several disease related substrates including the huntingtin protein found to be poly-ubiquitinated in Huntington's disease and UBB^{+1}, a frame shift mutant of Ub that HIP2 can effectively incorporate into poly-Ub chains known to be a factor in Alzheimer's disease.

The structure of HIP2 has been determined through X-ray crystallography (PDB: 1YLA and 3E46) (unpublished) (*2*). A limited number of physical studies on the HIP2 enzyme prompted the need for NMR experimentation that can be utilized to determine protein interactions with residue specific information. In order to perform mechanistic and structural studies of HIP2, the assignment of ^{1}H, ^{15}N and ^{13}C backbone resonances are required. These to be determined resonance assignments will be used in future experiments (Chapter 4) to determine interaction surfaces between HIP2 and attached Ub

or Ub_2 to develop a more thorough understanding of the purpose and function of the HIP2 conjugating enzyme.

3.2 Materials and Methods

3.2.1 Cloning

The hexahistidine (His^6)-tagged $HIP2^{C170S}$ (HIP2) cDNA was inserted in the pET28a vector (Chapter 2). This vector was then mutated to swap the thrombin cleavage site for a TEV (tobacco etch virus) cleavage site. The 18 DNA bases encoding the TEV cleavage sequence was substituted for 12 DNA bases encoding the thrombin cleavage sequence in the pET28a vector using the Quikchange Site-Directed Mutagenesis protocol (Stratagene, La Jolla, CA). Forward and reverse complement primers were subjected to polymerase chain reaction (PCR) against the pET28a template, followed by digestion of the methylated template by DpnI for 1 hour at 37 °C. The PCR product was then transformed into the JM-109 *E. coli* strain and the correct substitutions were confirmed by DNA sequencing. This plasmid was also transformed into the BL21 CodonPlus(DE3)RIL *E. coli* cell line for protein expression.

3.2.2 Protein expression and purification

For the production of uniformly ^{15}N, ^{13}C-labelled His^6-HIP2, BL21 CodonPlus(DE3)RIL cells were grown at 37 °C in M9 minimal media (10 mL) with unlabelled ingredients to ensure growth, then diluted 1:100 into 1L of M9 minimal media containing 1.0 g / L $^{15}NH_4Cl$ and 2 g / L ^{13}C-glucose as well as kanamycin (30 µg / mL)

and chloramphenicol (34 μg / mL). The culture was grown to an A_{600} between 0.60-0.75 and protein expression was induced with 0.7 mM IPTG. The temperature was reduced to 15 °C and cells were allowed to grow for 16-20 hrs. Harvested cells were re-suspended in 25 mM Tris-HCl, 200 mM NaCl, 1 mM TCEP, 5 mM imidazole at pH 7.5 with the addition of a COMPLETE mini EDTA-free protease inhibitor cocktail tablet (Roche Diagnostics). All the following purification procedures were performed at 4 °C to minimize protein degradation. Cells were lysed with a French Press and cellular debris was removed via centrifugation at 95500 xg. The clarified extract containing His^6-HIP2 was applied to Ni-NTA Agarose (Qiagen) and washed with 25 mM Tris-HCl, 200 mM NaCl, 1mM TCEP, 10 mM imidazole at pH 7.5 to elute non specifically bound material. His^6-HIP2 was eluted with 25 mM Tris-HCl, 200 mM NaCl, 1mM TCEP, 200 mM imidazole pH 7.5. TEV (Shaw lab) (50 μg / mL) was added to cleave the His^6-tag at room temperature for 1.5 hours and then overnight at 4 °C while dialyzing into the same buffer containing 10 mM imidazole. A subsequent Ni-NTA Agarose column was utilized with the same buffer to remove the His^6 fusion tag, any uncut protein and hexahistidine tagged TEV. Immediately following the final Ni-NTA Agarose column, 1 mM EDTA is added to the buffer. EDTA was essential for avoiding subsequent protein degradation by trace proteases. Another tablet of COMPLETE mini EDTA-free protease inhibitor tablet (Roche) was also added to avoid protein degradation. A final Superdex 75 10/300 GL column (GE Biosciences) was used to remove trace impurities and perform buffer exchange into 25 mM Tris-HCl, 200 mM NaCl, 5 mM DTT, 1 mM EDTA pH 7.5. Earlier purifications of HIP2 used for optimization of NMR samples to avoid degradation and oxidization, used final buffers with 1 mM TCEP, and no EDTA. Purification of ^{15}N,

^{13}C-labelled HIP2 was monitored using SDS-PAGE using 16.5% tris-tricine gels in a mini-gel system (BioRad) and was stained with Coomassie dye. HIP2 concentrations were determined through Bradford (BioRad) reactions performed in triplicate. HIP2 molecular weight was confirmed using electrospray ionization mass spectrometry (MW_{obs} 23779.0 ± 1.4Da, MW_{calc} 23812.8).

3.2.3 NMR sample preparation

Purified ^{15}N, ^{13}C-labelled HIP2 used for initial NMR optimization experiments was dialyzed into 25 mM Tris-HCl, 200 mM NaCl, 1 mM TCEP pH 7.5. HIP2 buffer conditions were optimized to be 25 mM Tris-HCl, 200 mM NaCl, 5 mM DTT, 1 mM EDTA pH 7.5 was used for NMR backbone assignments. The relatively high DTT component was substituted for TCEP used during purification as DTT was found to be a more stable reducing agent over the long experimental times required for NMR experiments. ^{15}N, ^{13}C-labelled HIP2 was concentrated using a 10000 MWCO Amicon spin concentrator (Millipore). NMR samples (575 μM) were prepared from this concentrated HIP2 solution by adding 10% D_2O (v/v), 1% 10 mM DSS (v/v), 0.05% NaN_3 (v/v), and 0.8% Complete MINI EDTA-free protease inhibitor tablet (Roche) solubilized with 1 mL H_2O (v/v). The final HIP2 concentration in NMR samples was 320 μM for degradation observations, 750 μM for initial optimization tests, and 575 μM for samples used in triple resonance experiments for backbone assignments.

3.2.4 NMR spectroscopy

All NMR spectra were acquired using a Varian INOVA 600 MHz spectrometer (University of Western Ontario) equipped with a pulse field gradient triple resonance cold probe. It was determined that triple resonance experiments were of much higher quality at 30 °C then at 25 °C, and thus NMR resonance assignments of ^{15}N, ^{13}C-labelled HIP2 were performed at 30 °C.

For all NMR experiments, the carrier frequencies for ^{1}H, ^{15}N, $^{13}C\alpha$, $^{13}C\beta$ and $^{13}C'$ were set to 4.73, 117.01, 57.39, 45.91 and 173.90 ppm respectively. ^{1}H-^{15}N HSQC (*3*) spectra were collected with 1024 complex data points and a spectral width of 8000 Hz in the ^{1}H (F2) dimension and 128 increments with a spectral width of 1900 Hz in the ^{15}N (F1) dimension. Sequential assignment of the polypeptide backbone resonances of HIP2 were completed utilizing the following triple resonance experiments: HNCA (*4*), HN(CO)CA (*5*), HNCACB (*6*), HBCBCA(CO)NH (*7*), HC(CO)NH (*8*), HNCO (*9*). For all these experiments, the ^{1}H (F3) dimension was collected with 1024 complex data points with a spectral width of 8000 Hz, and the ^{15}N (F2) dimension was collect with 32 increments and a spectral width of 1900 Hz. The ^{13}C (F1) dimension for the HNCA and HN(CO)CA experiments used 32 increments and a spectral width of 4524 Hz. The ^{13}C (F1) dimension for the HNCACB and HBCBCA(CO)NH experiments used 56 and 52 increments respectively with spectral widths of 9000 Hz. The ^{13}C (F1) dimension for the HNCO experiment used 24 increments with a spectral width of 3300 Hz, and the ^{13}C (F1) dimension for the HC(CO)NH experiment used 40 increments with a spectral width of 10000 Hz.

All data was processed using NMRPipe and NMRDraw (*10*). Linear prediction was used in the F2 dimension to double the number of points, and zero-filling was performed in the F1 and F3 dimensions to 512 and 1024 points respectively. A π/3 phase shifted $sine^2$ bell was applied to the F2 and F3 dimensions, and a π/2 phase shifted $sine^2$ bell was applied to the F1 dimension prior to Fourier transformation of data. All spectra were analyzed with NMRView (*11*)**.**

3.2.5 Determination of HIP2 secondary structure

The secondary structure of HIP2 was predicted using Chemical Shift Indexing (CSI) (*12, 13*) by comparing the assigned $^{13}C\alpha$, $^{13}C\beta$ and $^{13}C'$ chemical shift values of HIP2 to chemical shift values expected for these atoms if they adopt a random coil. The CSI program assigns an index value of -1, +1 or 0 indicating that a particular atom has a chemical shift similar to an α-helical, β-strand or random coil region respectively. Three or more consecutive residues possessing a value of +1 will result in assignment of a β-strand secondary structure, while four or more densely packed -1 values will result in assignment of an α-helical secondary structure. A consensus secondary structure is produced from the analysis of all analyzed atoms. The secondary structure from the CSI calculation was compared to the previously solved X-ray crystal structure of HIP2 (PDB: 1YLA) (unpublished).

3.3 Results

3.3.1 Mutagenesis

The pET28a vector contained the His^6-HIP2 fusion protein with a thrombin cleavage site for fusion tag removal (Chapter 2). The TEV (tobacco etch virus) cleavage sequence was substituted for the thrombin cleavage sequence in the pET28a-LIC vector using the Quikchange Site-Directed Mutagenesis protocol (Stratagene, La Jolla, CA). Insertion of the new cleavage site was confirmed by DNA sequencing (London Regional Genomics Centre - UWO).

3.3.2 Expression and purification of ^{15}N, ^{13}C-labelled HIP2 for NMR studies

The production of uniformly ^{15}N, ^{13}C-labelled HIP2 was performed by growth in M9 minimal media containing $^{15}NH_4Cl$ and ^{13}C-glucose with IPTG used for protein induction. The key changes to the previously described purification protocol (Chapter 2) include the buffer pH being lowered from 8.0 to 7.5, and the use of TEV enzyme to remove the His^6 tag from HIP2 after the first Ni^{2+}-affinity purification step. Since the TEV enzyme was also a hexahistidine tagged fusion protein (His^6-TEV), a second Ni^{2+}-affinity column was used to remove the cleaved His^6 tag, any remaining uncut His^6-HIP2 protein and all the His^6-TEV enzyme leaving only purified HIP2 in the flow through (Fig 3.1 B – lane 6). Once the final Ni^{2+}-affinity column was performed, it was essential to add EDTA to the protein solution as well as another Roche tablet of protease inhibitors to prevent protein degradation by trace proteases (details in Section 3.3.3). The ^{15}N, ^{13}C-labelled HIP2 was then subjected to an additional size exclusion column to remove any

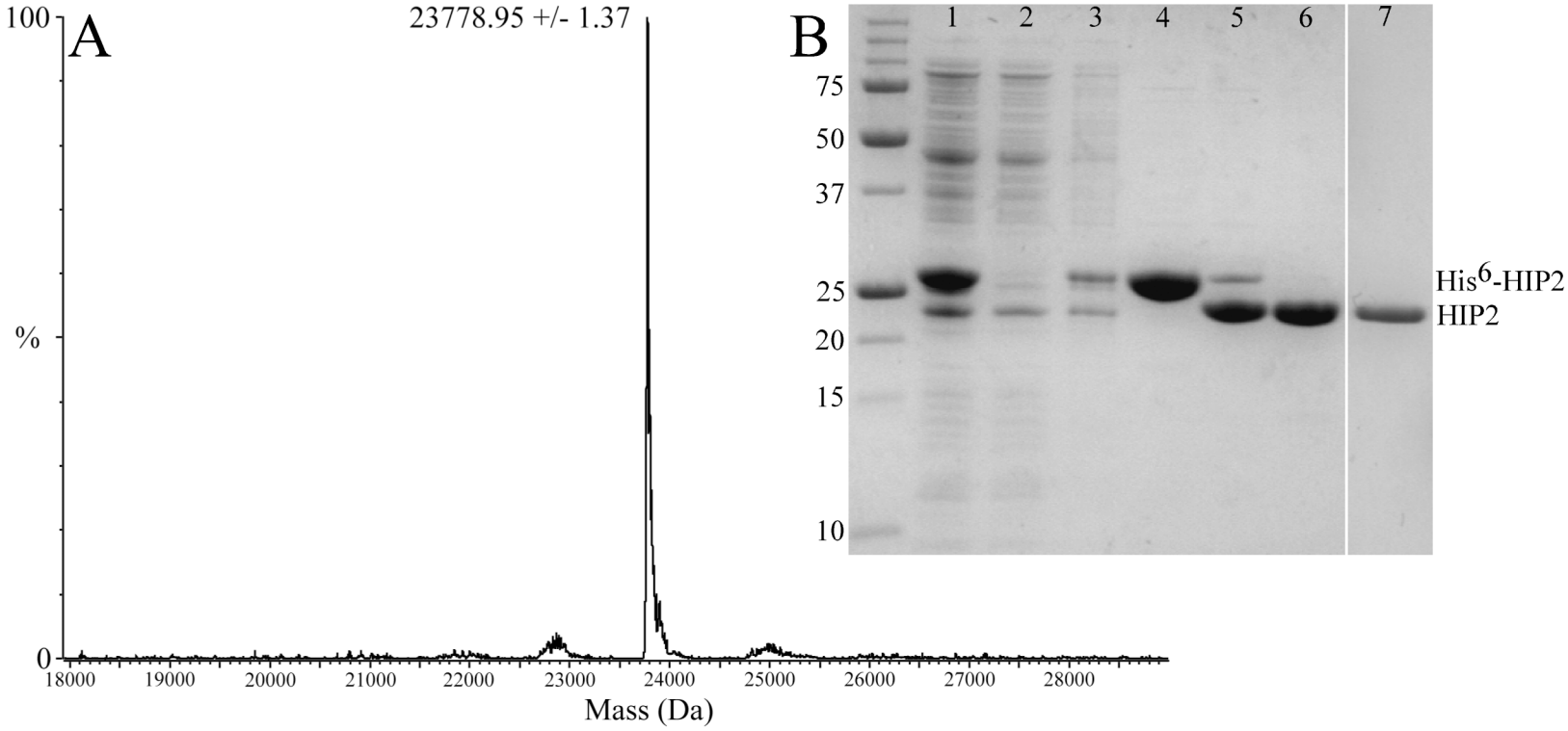

Figure 3.1 Expression and purification of ^{15}N, ^{13}C-labelled HIP2. (**B**) The E2 conjugating enzyme HIP2 was isotopically labelled with ^{15}N and ^{13}C by protein expression in M9 media containing $^{15}NH_4Cl$ and ^{13}C-glucose. The purification of HIP2 was monitored by Coomassie stained SDS-PAGE gels following procedures listed in Section 3.2.2. The protein purification gel is loaded from left to right containing initial expression of His^6-HIP2 centrifuged lysate (lane 1), Ni^{2+} affinity column flow through (lane 2), wash (lane 3) and elution (lane 4), TEV-cleaved protein (lane 5) and second Ni^{2+} affinity column flow (lane 6), and a size exclusion purification is performed representing purified HIP2 (lane 7). (**A**) Electrospray ionization mass spectrometry analysis of purified ^{15}N, ^{13}C-labelled HIP2 indicates the protein is the correct mass.

trace proteases (Fig 3.1B – lane 7). Using electrospray ionization mass spectrometry, a single major peak was observed at a molecular weight of 23779.0 ± 1.4 Da which accounts for 97.3% of the expected molecular weight of full isotopic incorporation of 23812.8 Da (Fig 3.1 A).

3.3.3 NMR sample preparation and optimization

In order to obtain high quality NMR spectra, HIP2 must be exposed to high temperatures (>25 °C). Initial NMR experiments on purified ^{15}N, ^{13}C-labelled HIP2 resulted in severe protein degradation within days due to prolonged exposure to these high temperatures. The original purpose of TEV substitution of the thrombin cleavage site was to minimize HIP2 degradation by using a highly pure and removable cleavage enzyme. Even though TEV enzyme was used, NMR samples would degrade in roughly 72 hours causing obvious changes in the NMR spectra (Fig 3.2). This degradation was confirmed with SDS-PAGE analysis (Fig 3.2 – insets). The NMR spectral changes are caused by a drastic decrease in signal from intact HIP2 as the protein degrades (Fig 3.2 – upper boxed region), as well as the appearance of many new signals in the spectrum (Fig 3.2 – lower boxed region) from the creation of small polypeptides. Protease inhibitor tablets (Roche) and NaN_3 were added to all future NMR samples to reduce degradation and inhibit possible contaminant growth, respectively. These measures alone resulted in minimal increases in HIP2 sample stability. The addition of EDTA immediately following Ni^{2+}-affinity chromatography was essential to increase protein stability of HIP2 NMR samples from days to weeks. This indicates that trace amounts of metalloproteases

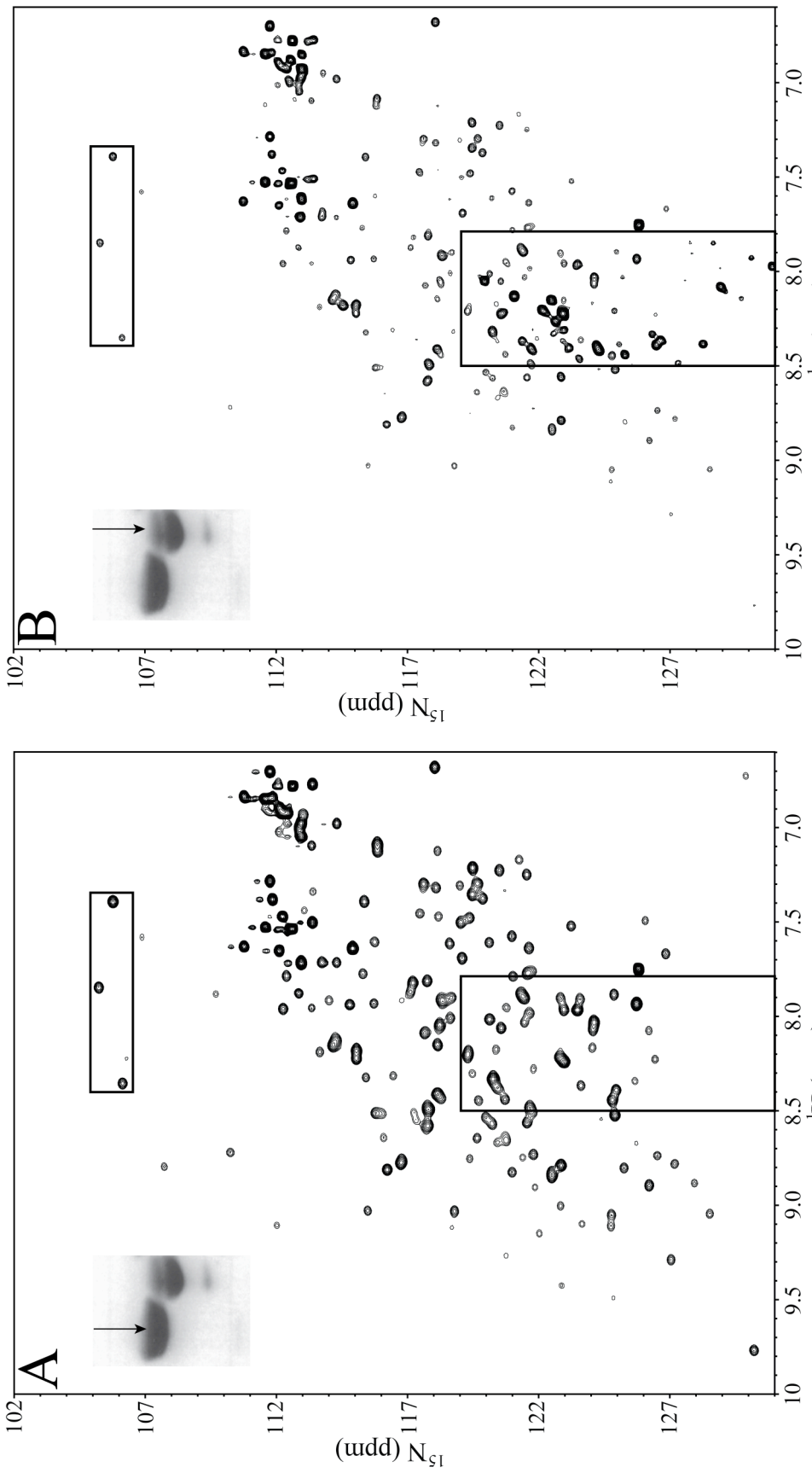

Figure 3.2 Illustration of degradation effects on the ^{1}H-^{15}N HSQC spectrum of HIP2. Backbone amide signals are shown for ^{1}H-^{15}N HSQC spectra of (**A**) HIP2 and (**B**) HIP2 after 72 hour exposure at 25 °C. The inset gel shows a protein sample from each HSQC spectrum identified with an arrow. Boxed signals are to aid in visual comparison of spectral regions. These spectra were collected using an ^{15}N, ^{13}C-labelled HIP2 sample (320 µM) in 10% D_2O, 200 mM NaCl, 1 mM TCEP, 25 mM Tris-HCl pH 7.5 at 25 °C (No EDTA).

were the likely cause of HIP2 degradation. Therefore, the addition of EDTA to all NMR buffers was required to obtain high quality NMR spectra.

NMR samples of the ^{15}N, ^{13}C-labelled HIP2 were then optimized for experimental temperatures. NMR experiments were performed at 25 °C and 30 °C. Analysis of the resulting ^{1}H-^{15}N HSQC spectra showed that data collected at 30 °C showed higher signal intensity due to narrower linewidths (Fig 3.3 – boxed signals) and improved signal resolution was obtained (Fig 3.3 – circled signals). At this experimental temperature, there was sufficient signal intensity for unambiguous resonance assignments of the triple resonance experiments.

In addition to stability problems, depletion of reducing agent affected spectral appearance of certain signals over time, presumably through oxidation. To alleviate this problem, TCEP was replaced with the longer-lived reducing agent DTT to keep the sample sufficiently reduced for several weeks. The final NMR samples used for ^{1}H-^{15}N HSQC and triple resonance experiments were prepared with all the optimized conditions described.

3.3.4 Sequential backbone assignments of HIP2

A series of standard multidimensional NMR experiments were used to determine the sequential backbone resonance assignment of HIP2. Sequential assignment of residues in any protein is made possible through a series of paired experiments that compare the current residue (i) and the previous residue (i-1). The first pair of NMR experiments used for backbone assignments were the HNCA and HN(CO)CA (*4, 5*).

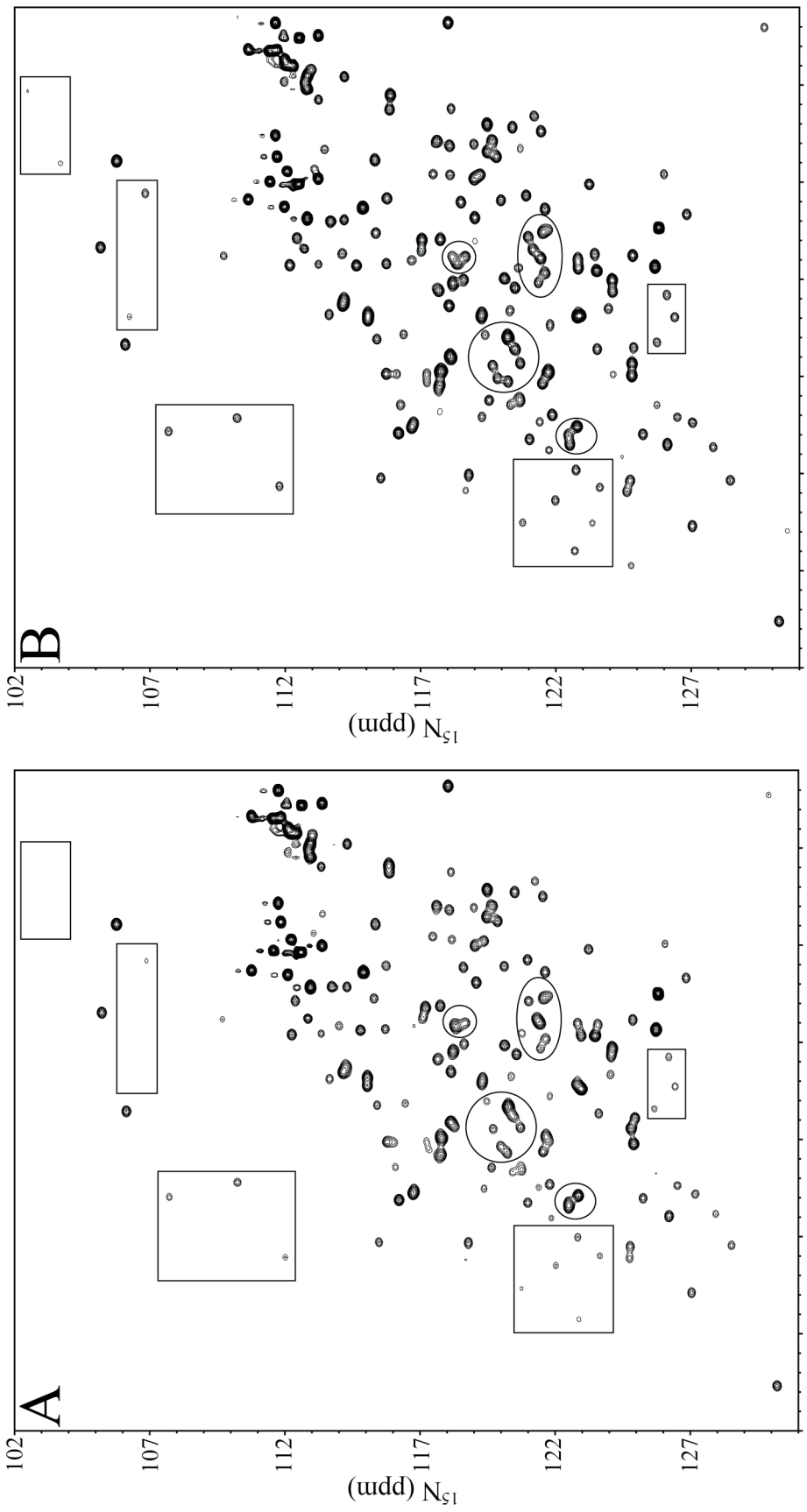

Figure 3.3 ^{1}H-^{15}N HSQC spectrum of HIP2 at varying temperatures. Backbone amide signals are shown for ^{1}H-^{15}N HSQC spectra of HIP2 at (**A**) 25 °C and (**B**) 30 °C. Boxed and circled signals are added to aid in visual comparison of spectral regions, showing increased signal intensity and resolution respectively at 30 °C. The spectra were collected on a ^{15}N, ^{13}C-labelled HIP2 sample (750 µM), in 10% D_2O, 200 mM NaCl, 1 mM TCEP, 1 mM EDTA, 25 mM Tris-HCl pH 7.5.

These two experiments correlate the backbone amide proton and nitrogen chemical shifts to the Cα resonances, with HNCA showing the current (i) residue and the preceding (i-1) residue, whereas the HN(CO)CA shows only the preceding (i-1) residue. These experiments alone can provide backbone residue linkage, but a moderately high level of Cα resonance overlap necessitates the use of a second set of paired experiments, the HNCACB and HBCBCA(CO)NH (*6, 7*). The HNCACB and HBCBCA(CO)NH experiments allow for the determination of both Cα and Cβ resonances. The HNCACB experiment correlates the backbone amide proton and nitrogen chemical shifts to the Cα and Cβ resonances, while the Cα(i-1), Cβ(i-1) correlations can often be observed at a lower intensity. The HBCBCA(CO)NH experiment correlates the amide and nitrogen chemical shifts to the Cα(i-1), Cβ(i-1) resonances. When analyzed together, these experiments can be used to connect the Cα and Cβ resonances for the i and i-1 residues. These results when combined with the HNCA and HN(CO)CA experiments usually leads to unambiguous strings of connected backbone residues. By comparing the chemical shifts of these atoms to the BMRB (Biological Magnetic Resonance Data Bank) standard chemical shift tables, the amino acid identity can be determined to complete the assignment of the HIP2 protein sequence. Figure 3.4 shows the sequential assignment of HIP2 residues A115, L116, L117, A118, and A119 depicted in a strip plot of the HNCACB and HBCBCA(CO)NH experiments. When Cα and Cβ resonances do not provide enough variance to unambiguously assign a residue, the HC(CO)NH (*8*) experiment provides resonances for any Cγ, Cδ, and Cε atoms present in the i-1 residue. By combining information from all of these triple resonance experiments, and through

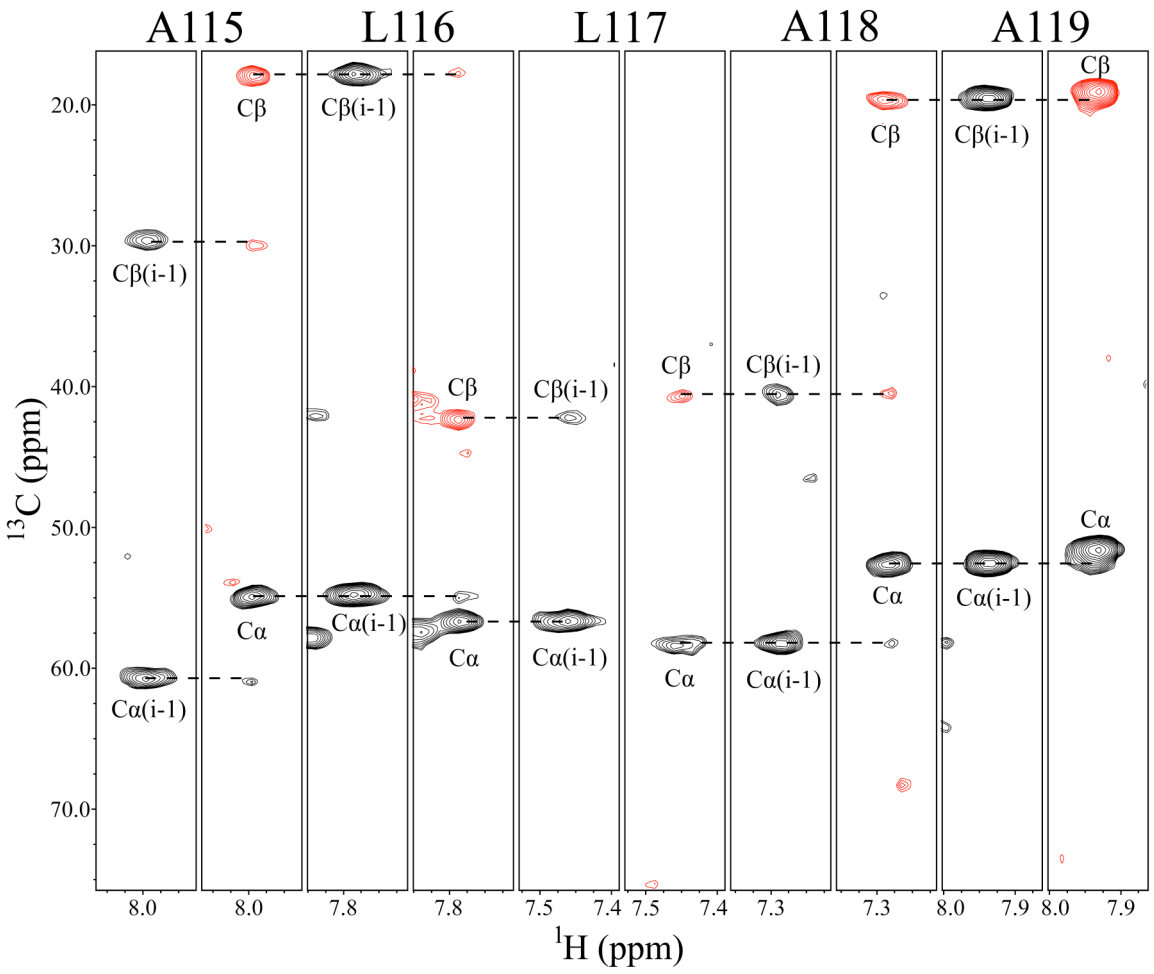

Figure 3.4 Sequential backbone assignment of HIP2. The strip plot shows alternating panels of the HBCBCA(CO)NH spectrum (left) and HNCACB spectrum (right) for each residue of A115 through A119. Each strip depicts a ^{15}N plane of the triple resonance experiment, leaving a 2D representation of the remaining ^{1}H and ^{13}C correlations. For each residue the Cα (black) and Cβ (red) are shown in the HNCACB spectrum and the corresponding Cα and Cβ for the previous residue (i-1) are shown in the HBCBCA(CO)NH (both black). Connections between i and i-1 residues are indicated with a dashed line. The spectra were collected using a ^{15}N, ^{13}C-labelled HIP2 sample (575 µM) in 10% D_2O, 200 mM NaCl, 5 mM DTT, 1 mM EDTA, 25 mM Tris-HCl pH 7.5 at 30 °C.

the use of distinct chemical shifts for glycine, serine, threonine, and alanine residues, almost every residue in HIP2 can be sequentially assigned in an unambiguous manner. Finally an HNCO (*9*) experiment is performed to assign the backbone carbonyl carbons for each residue.

3.3.5 Assignment of the ^{1}H-^{15}N HSQC spectrum of HIP2

In a ^{1}H-^{15}N HSQC spectrum of HIP2, each amino acid residue is depicted by a single signal based on the amide correlation of the ^{1}H and ^{15}N atoms, and is the primary type of spectra used to illustrate NMR resonance assignments. The ^{1}H-^{15}N HSQC spectrum for HIP2 was assigned by comparison to the assigned triple resonance values for ^{1}H and ^{15}N on Cα and Cβ signals. The ^{1}H-^{15}N HSQC spectra for HIP2 assignment of 175 out of 187 (94%) non-proline ^{1}H and ^{15}N amide resonances (Fig 3.5). Many of the remaining unassigned 12 residues are located in the N-terminus (M1, N3), the loop between α1 and β1 (E20, T22), the loop between β1 and β2 (D33, E34, F36), and within the proposed flexible linker between the catalytic core and UBA domain (V157, S159, E161). These residues are likely in highly flexible and solvent exposed regions, resulting in their ^{1}H and ^{15}N amide resonances to be unobservable due to fast amide exchange with water. Table 3.1 shows all the chemical shift assignments acquired from a combination of the HSQC experiment and all triple resonance experiments. These assignments include the amide H and N, Cα and C' protein backbone atoms, as well as many Cβ, Cγ, Cδ, and Cε atoms in each amino acid residue.

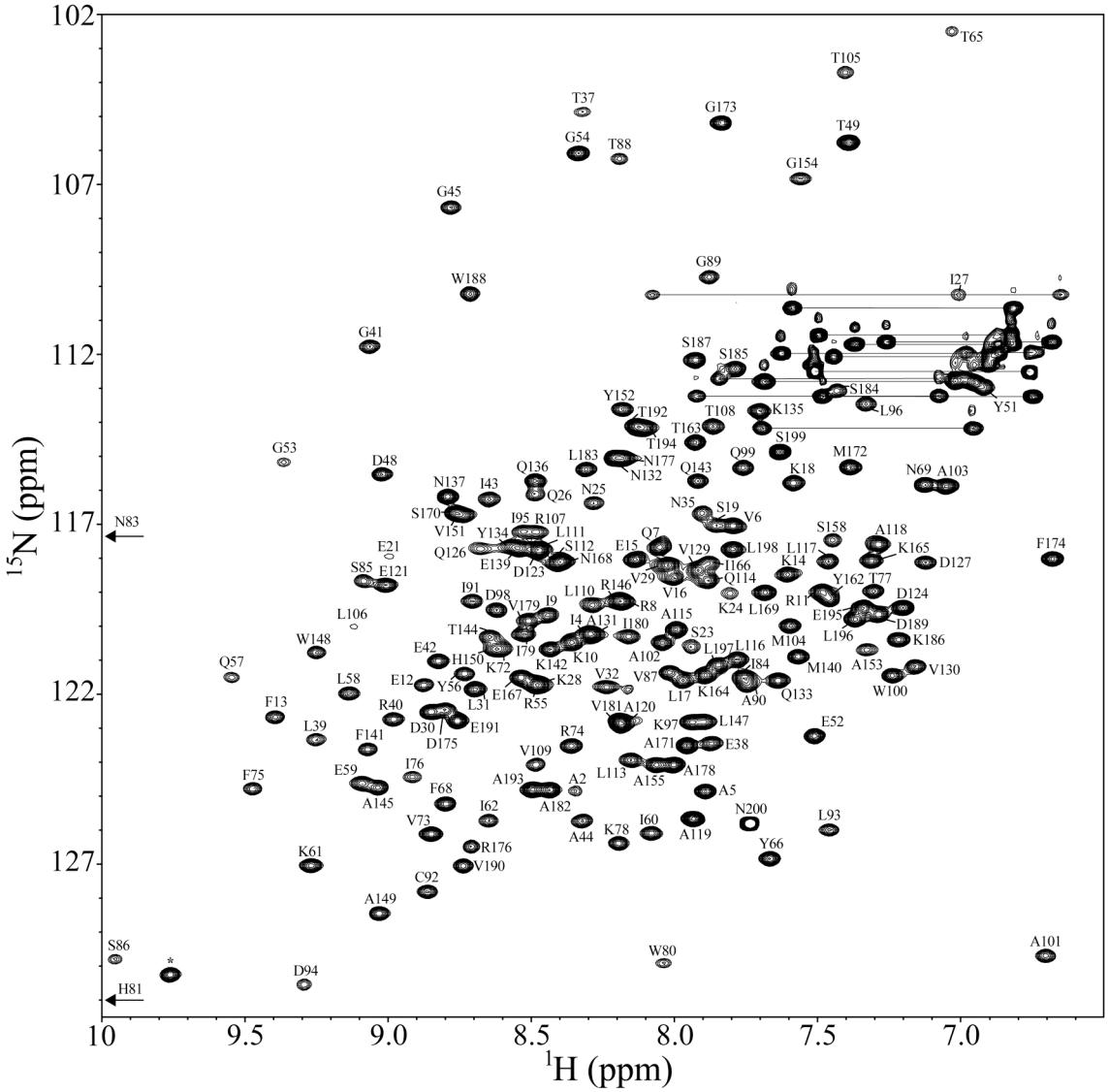

Figure 3.5 Assigned ^{1}H-^{15}N HSQC spectrum of HIP2. Backbone amide signals are labelled by amino acid single letter code and sequence number. Signals connected by lines indicate side chain amide resonances from Asn and Gln residues. The signals marked with (*) represent side chain amides from Trp residues, while arrows indicate signals that are shifted further downfield in ^{1}H than 10ppm. The spectra was collected using a ^{15}N, ^{13}C-labelled HIP2 sample (575 µM) in 10% D_2O, 200 mM NaCl, 5 mM DTT, 1 mM EDTA, 25 mM Tris-HCl pH 7.5 at 30 °C.

Table 3.1 ^{1}H, ^{15}N and ^{13}C backbone resonance assignments for HIP2[a]

Residue	HN	N	C'	Cα	Cβ	Others
M1			176.08	55.83	33.22	
A2	8.344	124.8		52.86	19.28	
N3			176.57	54.60	38.57	
I4	8.288	120.2	177.08	63.47	38.09	Cγ1 28.32, Cγ2 17.33, Cδ1 13.72
A5	7.887	124.8	179.37	55.88	19.33	
V6	7.798	117.0	177.46	66.28	31.87	Cγ1 20.94
Q7	8.055	117.6	179.50	58.98	28.58	Cγ 33.95
R8	8.181	119.4	178.07	58.48	28.80	
I9	8.441	119.6	177.77	62.29	36.19	Cγ1 28.03, Cγ2 18.77
K10	8.361	120.4	179.54	61.07	32.42	Cδ 29.87
R11	7.488	119.0	179.40	59.49	30.15	Cγ 27.26, Cδ 40.40
E12	8.874	121.8	180.11	59.97	30.72	Cγ 33.85
F13	9.393	122.7	176.79	61.57	39.68	
K14	7.606	118.5	178.45	59.56	32.29	Cγ 25.41, Cδ 29.57, Cε 41.58
E15	8.139	118.0	179.69	59.11	29.80	Cγ 36.43
V16	8.007	118.5	178.95	67.01	31.29	Cγ1 22.05
L17	7.974	121.5	178.48	58.02	41.95	
K18	7.587	115.9	176.76	55.90	32.50	Cγ 24.64, Cδ 28.95, Cε 42.16
S19	7.857	117.0		59.64	64.86	
E20			178.65	58.68	29.80	Cγ 36.41
E21	8.992	118.0		61.05	28.69	
T22			175.26	65.17	71.24	
S23	7.944	120.5	175.82	61.23	62.92	
K24	7.812	119.0	176.13	56.55	32.53	Cγ 25.64, Cδ 29.32
N25	8.281	116.5	175.02	54.34	37.81	
Q26	8.486	116.0	175.49	57.45	29.94	
I27	7.009	110.2	174.47	58.99	42.19	Cγ1 26.77, Cγ2 17.91
K28	8.478	121.8	174.29	55.90	36.54	Cγ 24.98, Cδ 29.44
V29	8.024	118.2	172.30	60.48	35.78	Cγ1 22.01
D30	8.854	122.4	175.04	53.07	45.61	
L31	8.695	121.9	177.15	55.23	42.64	Cδ1 24.72
V32	8.236	121.8		63.67	32.73	
E34			175.64	57.30	29.31	Cγ 36.23
N35	7.903	116.6		52.97	39.59	
F36			173.38	60.30		
T37	8.320	104.8	174.85	62.45	69.93	
E38	7.868	123.4	173.39	55.55	32.05	Cγ 36.35
L39	9.254	123.4	175.72	53.54	46.08	Cγ 26.81
R40	8.982	122.8	176.15	53.77	32.26	Cγ 27.43, Cδ 42.58
G41	9.062	111.7	171.76	43.79		
E42	8.828	120.9	174.83	55.65	34.25	Cγ 37.71
I43	8.650	116.3	174.91	58.78	42.31	Cγ2 17.83
A44	8.320	125.8	178.99	51.14	20.16	
G45	8.780	107.7		44.35		
P47			176.18	62.67	32.27	Cγ 27.59
D48	9.025	115.5	175.07	55.83	39.26	
T49	7.391	105.8		59.66	71.28	
P50			173.98	63.68	32.67	Cγ 27.28
Y51	6.922	113.1	176.85	56.40	38.54	
E52	7.513	123.3	175.75	58.27	30.06	Cγ 35.51
G53	9.364	115.1	174.25	45.19		
G54	8.335	106.2	173.34	43.50		
R55	8.486	121.8	174.25	55.40	32.69	Cγ 27.48, Cδ 42.63
Y56	8.736	121.4	174.48	57.79	40.41	
Q57	9.547	121.4	176.14	55.16	30.82	Cγ 34.33
L58	9.143	121.9	175.03	53.64	45.79	Cγ 27.17
E59	9.091	124.6	174.63	55.36	33.10	Cγ 37.10
I60	8.084	126.2	173.85	60.30	40.09	Cγ1 27.50, Cγ2 21.42, Cδ1 17.15
K61	9.272	127.1	175.35	54.61	34.59	Cγ 26.08, Cδ 29.42
I62	8.647	125.8		55.07	36.94	
P63					32.55	
E64	9.053	119.6	176.60	59.02	29.61	Cγ 36.16
T65	7.034	102.4	174.93	60.54	68.74	
Y66	7.670	126.8		58.22	40.61	
P67			174.72	63.35	33.11	
F68	8.799	125.3	175.38	60.48	37.93	
N69	7.128	115.9		50.34	41.00	

Table 3.1 continued ^{1}H, ^{15}N and ^{13}C backbone resonance assignments for HIP2[a]

Residue	HN	N	C'	Cα	Cβ	Others
P71			179.71	61.72	31.80	Cγ 26.25
K72	8.621	120.5	176.05	55.09	32.46	Cγ 24.28, Cδ 28.96, Cε 41.81
V73	8.847	126.2	173.26	60.19	34.47	Cγ1 22.14
R74	8.360	123.4	175.75	54.69	34.84	Cγ 27.54
F75	9.472	124.8	175.97	60.18	38.80	
I76	8.917	124.4	177.47	62.51	39.01	Cγ1 28.22, Cγ2 16.92
T77	7.306	119.0	173.46	63.44	70.89	
K78	8.193	126.3	176.17	56.92	32.84	Cγ 24.78, Cδ 28.54
I79	8.524	120.4	170.26	60.95	41.84	
W80	8.040	129.9		54.52	29.12	
H81	10.570	131.1	174.11	56.01		
P82			176.70	65.44	32.51	Cγ 27.57
N83	11.296	117.4	171.32	55.66	41.05	
I84	7.756	121.4	174.65	59.04	42.93	
S85	9.086	118.5	177.59	58.89	63.14	
S86	9.955	129.7	174.09	61.72	63.52	
V87	8.020	121.4	178.05	64.76	34.18	Cγ1 21.20
T88	8.189	106.2	176.46	61.67	71.74	
G89	7.881	109.7	173.94	46.55		
A90	7.747	121.8	176.48	52.95	19.39	
I91	8.708	119.3	175.81	60.67	42.72	Cγ1 28.54, Cγ2 18.58
C92	8.864	127.8	172.11	57.75	26.42	
L93	7.460	125.9	176.35	54.42	45.60	Cγ 26.70
D94	9.292	130.6	180.28	58.52	38.99	
I95	8.530	117.2	173.36	64.51	38.30	Cγ2 18.73, Cδ1 14.41
L96	7.331	113.6	176.76	53.64	41.38	Cγ 26.30, Cδ1 21.60
K97	7.939	122.9	175.92	56.41	32.84	Cγ 24.59, Cδ 29.51, Cε 41.64
D98	8.621	119.5	176.86	55.80	40.90	
Q99	7.759	115.4	174.66	54.59	28.14	Cγ 33.53
W100	7.241	121.4	175.30	58.90	30.33	
A101	6.706	129.7	175.33	50.10	22.24	
A102	8.044	120.4	176.72	53.91	18.50	
A103	7.049	116.0	178.53	52.39	19.05	
M104	7.597	120.0	172.70	57.21	32.26	
T105	7.405	103.8	176.54	58.94		
L106	9.134	120.0	178.35	58.23	43.00	Cδ1 25.18
R107	8.476	117.2	177.06	60.76	30.03	Cγ 27.69
T108	7.862	114.1	178.43	66.78	68.57	
V109	8.480	123.9	177.30	67.39	31.55	Cγ1 20.68
L110	8.286	119.4	178.73	58.87	41.35	Cγ 27.10, Cδ1 23.65
L111	8.479	117.5	181.18	58.06	41.14	Cγ 25.92
S112	8.409	118.1	176.94	62.73		
L113	8.154	123.9	177.84	57.51	41.90	Cδ1 27.03
Q114	7.884	118.6	177.72	60.76	29.75	Cγ 35.29
A115	7.995	120.0	180.28	54.87	17.85	
L116	7.786	120.9	179.48	56.64	42.29	Cγ 28.30, Cδ1 23.86
L117	7.459	118.0	177.03	58.26	40.58	Cδ1 21.96
A118	7.286	117.5	176.79	52.56	19.61	
A119	7.935	125.8	174.00	51.54	18.95	
A120	8.184	122.9	176.46	52.11	19.45	
E121	9.005	118.9		52.30	30.02	
P122			175.02	64.32	31.94	Cγ 27.35
D123	8.475	117.9	175.36	55.07	40.24	
D124	7.202	119.4		51.75	40.93	
P125			177.09	62.96	33.54	Cγ 30.22
Q126	8.678	117.6	174.59	55.10	30.25	Cγ 33.39
D127	7.124	118.0		52.80	43.82	
A128	8.937	128.7	179.78	55.38	18.75	
V129	7.920	118.4	178.96	66.01	31.62	
V130	7.162	121.2	178.29	65.61	32.03	
A131	8.293	120.3	178.54	55.62	18.80	
N132	8.212	115.1	176.89	56.43	38.34	
Q133	7.641	121.5	176.97	59.94	31.64	Cγ 36.34
Y134	8.572	117.5	176.62	61.55	39.15	
K135	7.705	113.6	178.42	59.00	33.76	Cγ 25.78, Cδ 29.56
Q136	8.488	115.6	177.24	57.62	29.62	Cγ 34.06
N137	8.793	116.1		50.93	39.35	

Table 3.1 continued ^{1}H, ^{15}N and ^{13}C backbone resonance assignments for HIP2[a]

Residue	HN	N	C'	Cα	Cβ	Others
P138			179.19	65.53	31.83	Cγ 27.59, Cδ 50.29
E139	8.543	117.6	178.70	59.62	28.96	Cγ 35.83
M140	7.568	120.9	180.29	58.30	33.82	Cγ 31.22
F141	9.070	123.7	176.58	62.01	38.60	
K142	8.439	120.6	178.68	60.84	32.62	Cδ 26.65, Cε 38.71
Q143	7.921	115.6	179.46	58.46	28.11	Cγ 33.03
T144	8.646	120.4	175.14	68.27	69.24	
A145	9.037	124.8	180.62	55.92	17.85	
R146	8.193	119.2	178.27	58.92	30.77	Cγ 27.59, Cδ 43.42
L147	7.894	122.9	180.13	57.86	40.46	Cγ 25.51, Cδ1 21.45
W148	9.253	120.9	181.17	62.78	28.23	
A149	9.035	128.3	174.70	55.70	18.66	
H150	8.626	120.5	176.74	58.23		
V151	8.737	116.8	178.29	65.86	32.78	Cγ1 19.74
Y152	8.183	113.6	176.33	59.07	39.65	
A153	7.328	120.8	177.85	51.16	22.46	
G154	7.555	106.8	174.61	46.22		
A155	8.067	124.1		51.25	18.15	
V157			174.15	62.07	33.61	Cγ1 20.51
S158	7.450	117.5		56.65	64.70	
E161			179.01	59.23	29.00	Cγ 36.09
Y162	7.461	119.1	178.27	58.13	35.80	
T163	7.931	114.6	176.57	67.05	68.10	Cγ2 22.08
K164	7.893	121.4	178.62	59.52	32.05	Cγ 24.73, Cδ 29.04
K165	7.315	118.0	178.70	60.47	33.81	
I166	7.884	118.0	179.32	64.34	38.80	Cγ1 29.54, Cδ1 16.82
E167	8.539	121.4	179.38	59.32	29.36	Cγ 35.97
N168	8.394	118.0	177.65	56.09	38.30	
L169	7.685	119.0	180.05	57.83	42.76	Cγ 28.86, Cδ1 24.95
S170	8.766	116.6	177.89	62.21	62.99	
A171	7.959	123.4	178.68	54.19	18.11	
M172	7.385	115.4	175.91	56.39	32.79	
G173	7.837	105.3	173.78	44.80		
F174	6.681	118.0	174.64	56.60	41.81	
D175	8.800	122.4	176.59	54.68	43.28	
R176	8.711	126.4	177.91	60.53	30.81	Cγ 27.81, Cδ 43.33
N177	8.183	115.1	177.10	56.86	37.84	
A178	8.000	124.0	180.96	55.12	17.88	
V179	8.509	119.9	176.99	66.90	31.48	Cγ1 25.02
I180	8.160	120.4	179.69	67.10	38.01	Cγ2 16.07, Cδ1 13.94
V181	8.191	122.9	178.20	68.01	32.03	Cγ1 20.84
A182	8.440	124.8	178.71	55.72	18.82	
L183	8.310	115.5	178.50	57.84	40.86	Cγ 27.34, Cδ1 23.13
S184	7.435	113.1	174.88	62.31		
S185	7.789	112.5	174.95	60.79	63.60	
K186	7.217	120.4	176.20	52.85	29.69	
S187	7.927	112.1	172.89	60.10	61.14	
W188	8.714	110.2	172.90	59.47	24.53	
D189	7.288	119.5	175.45	53.39	42.53	
V190	8.736	127.1	178.69	66.92	31.98	Cγ1 22.08
E191	8.760	122.9	179.44	60.65	29.37	Cγ 36.57
T192	8.135	114.1	178.27	65.55	68.44	Cγ2 22.78
A193	8.495	124.8	178.55	55.58	18.35	
T194	8.104	114.1	175.06	68.01		
E195	7.344	119.5	179.08	59.57	29.54	Cγ 36.03
L196	7.372	119.9	179.76	57.90	42.17	Cγ 25.51
L197	7.847	121.0	178.77	57.35	40.83	Cγ 26.85, Cδ1 22.75
L198	7.796	117.6	177.75	55.84	42.82	Cγ 26.30, Cδ1 22.61
S199	7.635	115.0	173.50	59.18	64.10	
N200	7.736	125.8		55.09	40.85	

[a]Referenced to DSS at 0 ppm in ^{1}H. HIP2 NMR data was obtained at 30 °C in 200 mM NaCl, 5 mM DTT, 1 mM EDTA, and 25 mM Tris-HCl pH 7.5. Residues D33, P46, P70, P156, S159 and P160 were not assigned

3.3.6 Determination of HIP2 secondary structure

The backbone chemical shift values of HIP2 (Table 3.1) were used to calculate the secondary structure to ensure that the C170S substitution caused no major structural changes. The assigned chemical shift values for $^{13}C\alpha$, $^{13}C\beta$ and $^{13}C'$ from HIP2 were utilized to predict the secondary structure using the Chemical Shift Index (CSI) protocol (*12, 13*). The CSI compares chemical shift assignments to their deviation from random coil chemical shift values to determine if those particular atoms have a propensity to be α-helical or β-strand in structure. Specifically, $^{13}C\alpha$ and $^{13}C'$ chemical shifts are located more upfield if they are in a β-strand conformation and shifted more downfield in an α-helical conformation, while $^{13}C\beta$ atoms experience opposite field shifts when located in these secondary structures (*12, 13*). The secondary structure calculated for each atom was combined by CSI to give a consensus for each residue. The calculated secondary structure for HIP2 showed residues A5-S19, E20-K24, T105-A120, A128-Y152, P160-M172, R176-W188, and V190-L198 were in an α-helical conformation and residues I27-D30, E38-A44, and R55-K61 were in the β-strand conformation (Fig 3.6). The positions of the CSI calculated α-helices and β-strands are in excellent agreement with secondary structural elements observed in the X-ray crystal structure of HIP2 (PDB: 1YLA) (unpublished). This result indicates that there are no major secondary structural differences of HIP2 in solution compared to that observed in the X-ray crystal, and that the C170S substitution is non-perturbing.

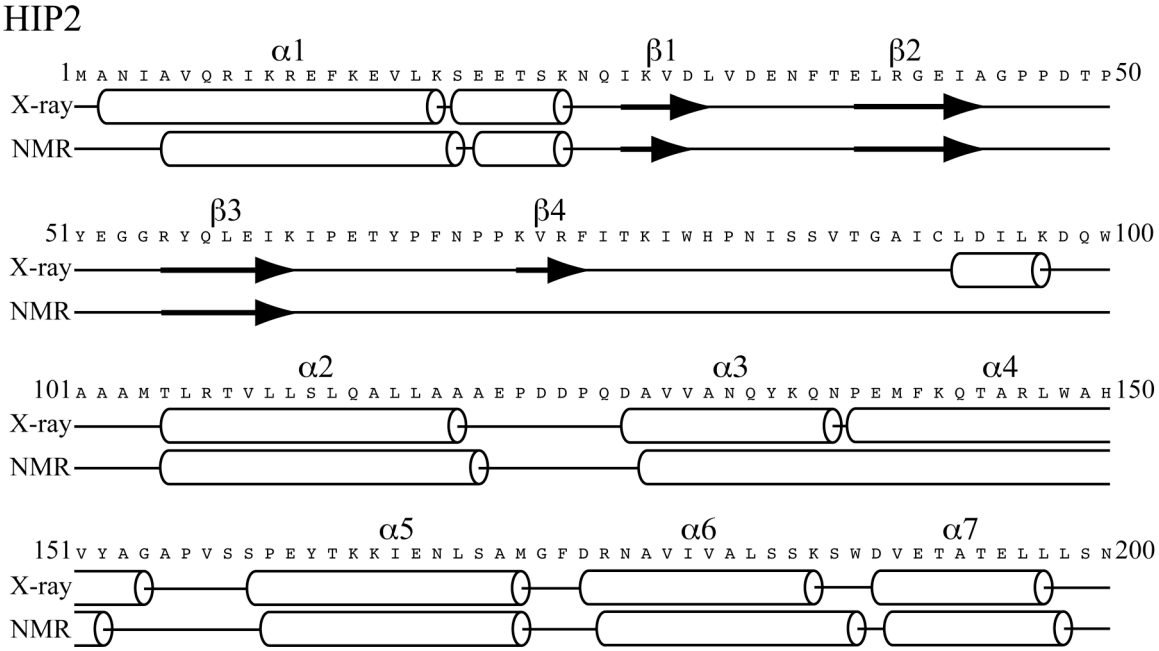

Figure 3.6 Secondary structure calculation of HIP2 by the chemical shift index. Chemical shift values for $^{13}C\alpha$, $^{13}C\beta$ and $^{13}C'$ for each residue are compared to the chemical shift index to determine propensity for α-helical and β-strand secondary structure. The calculated structure is labelled as NMR and is compared to the X-ray crystal structure for HIP2 (PDB: 1YLA) labelled as X-ray. Secondary structural elements are shown pictorially as cylinders for α-helices and arrows for β-strands with the protein sequence listed above. Secondary structure elements are numbered above the protein sequences according to the X-ray structure labelling.

3.4 Discussion

3.4.1 Mutagenesis

The purified His^6-HIP2 fusion protein after thrombin cleavage undergoes degradation at high temperatures (>25 °C). Commercially available thrombin is purified from blood and its purity is measured through specific activity as opposed to finding a single band in SDS-PAGE. Therefore, the thrombin enzyme may contain trace amounts of other proteases. To avoid possible HIP2 degradation from trace proteases, the thrombin cleavage site was replaced with TEV. The use of a His^6-tagged form of the TEV enzyme allows for higher quality purification. The His^6-tag on TEV also allows for efficient removal after His^6-HIP2 cleavage by Ni^{2+}-affinity chromatography. Unfortunately, degradation of HIP2 was still noticed after TEV use and removal, likely due to trace proteases from the *E. coli*.

3.4.2 Optimization of purification protocols and NMR conditions

There were specific changes to the HIP2 purification protocol (outlined in Section 3.2.2) that were required to ensure protein stability for NMR data collection. The first change involved lowering the pH of the buffer from 8.0 to 7.5 to slow the rate of amide exchange. Amide exchange can be acid or base catalyzed and previous studies have shown that amide exchange of an exposed HN in a peptide backbone is minimized at roughly pH 4 depending on surrounding side chain groups (*14*). The pH was reduced from 8.0 to 7.5 to minimize amide exchange and to increase NMR signal intensity.

Importantly, this lower pH was still several pH units away from HIP2's isoelectric point at pH 5.33.

During the purification of HIP2, TCEP was used instead of DTT and EDTA was omitted to ensure the proper functioning of the Ni^{2+}-affinity column. Once Ni^{2+}-affinity chromatography was completed, it was important to substitute DTT for TCEP and to add EDTA to the buffer. EDTA was essential for increased stability of HIP2 at the higher temperatures required to collect quality HSQC data. This indicated that HIP2 degradation was likely due to trace amounts of a metalloprotease from *E. coli*. The addition of various serine and cysteine protease inhibitors (Roche tablets) had little effect on HIP2 stability. The use of DTT in lieu of TCEP was required due to its more stable reducing activity, which was needed to maintain protein stability during NMR data collection. Lastly, NMR data collection was significantly improved upon increasing the temperature to 30 °C. The increase in temperature allows for an increased rate of protein tumbling. Increased protein tumbling leads to increased signal intensity by decreasing the spin-spin ($1/T_2$) relaxation rate. The triple resonance experiments for HIP2 at 25 °C were too low in signal-to-noise to perform backbone assignments. In contrast, the signal-to-noise of triple resonance experiments at 30 °C was significantly increased. The combination of lowering the pH, adding EDTA, using DTT and increasing experimental temperature to 30 °C allowed for the complete unambiguous assignment of HIP2 backbone residues.

3.4.3 Resonance assignments for HIP2

The triple resonance experiments allowed for assignment of the amide H and N, Cα and C' protein backbone atoms, as well as many Cβ, Cγ, Cδ, and Cε atoms in each amino acid residue. The ^{1}H-^{15}N HSQC spectra for HIP2 has every visible signal assigned to yield a 94% assignment (175 / 187) of non-proline residues. NMR protein assignments can be used to study protein-protein interactions in solution. Residue specific protein interaction surfaces can be detected using an assigned ^{1}H-^{15}N HSQC spectrum as specific residues will undergo chemical shift changes upon binding to another protein. The ^{1}H-^{15}N HSQC spectrum of HIP2 will be utilized in this manner to characterize protein interactions in Chapter 4.

3.4.4 Asparagine 83 in HIP2 displays a distinctly deshielded amide proton

An interesting feature of the ^{1}H-^{15}N HSQC spectrum of HIP2 is the distinct downfield amide ^{1}H chemical shift of N83 (^{1}H: 11.296 ppm, ^{15}N: 117.43 ppm). The N83 residue is structurally near the active site cysteine residue (C92) and is part of a highly conserved HPN motif found in many other E2 enzymes (*15, 16*). To perform an in depth structural analysis to explain this unique chemical shift, a comparison of the active sites of other E2 enzymes containing the HPN motif was conducted. Every E2 enzyme that has a high-resolution structure and NMR chemical shift assignment was investigated. Nine human E2 enzymes and the yeast HIP2 homolog Ubc1 have ^{1}H-^{15}N HSQC spectral assignments (Biological Magnetic Resonance Data Bank – BMRB) as well as a high-resolution structures: HIP2 (PDB: 1YLA, 2BEP, 3E46) (unpublished) (*2, 17*), Ubc1 (PDB: 1TTE, BMRB: 6202) (*18*), UbcH5A (PDB: 2C4P, BMRB: 6584) (unpublished),

UbcH5B (PDB: 2ESK, BMRB: 6277) (*19*), Ubc2b (PDB: 1JAS, BMRB: 5038) (*20*), Ubc9 (PDB: 1A3S, BMRB: 4132) (*21*), UbE2G2 (PDB: 2CYX, BMRB: 16404) (*22*), Ubc13 (PDB: 1J7D, BMRB: 15092) (*23*), UbcH7 (PDB: 1FBV, BMRB: 15498) (*24*), and UbcH8 (PDB: 1WZV and 2KJH, BMRB: 16321) (unpublished) (*25*). A segment of the sequence alignment of these 10 proteins is shown in Figure 3.7A. The HPN motif of these proteins can also be structurally aligned showing that the HPN motif adopts a tight turn adjacent to the active site cysteine in all of these proteins. The important catalytic residues include the active site C92, which forms the thiolester linkage with the Ub C-terminus, and the Asn residue in the HPN motif, which has been suggested to stabilize an oxyanion intermediate formed during nucleophilic attack by a substrate lysine (*16, 26, 27*).

Closer inspection of the structure of the HIP2 active site (PDB: 2BEP) (*17*) shows that the amide proton of N83 is involved in a hydrogen bond to the side chain δ nitrogen atom of H81 (Fig 3.7B). Comparison to other HIP2 structures (PDB: 3E46, 1YLA) (*2*) (unpublished) shows that the H81 ring is flipped and a hydrogen bond can form between the H81 protonated ε nitrogen atom and the N83 side chain δ oxygen atom (Fig 3.7C). Although both of these orientations are possible, the purpose of side chain interactions of His and Asn residues in the HPN motif could possibly regulate the oxyanion hole by assuming acidic and basic states (*15*). However, the fact that His is not solvent exposed argues against this acid/base catalysis function, and indicates that the N83 residue alone likely regulates the oxyanion hole (*16*). Hydrogen bonds are known to have a deshielding effect on amide protons (*28*), indicating the highly deshielded N83 amide proton is consistent with the hydrogen bond depicted in Figure 3.7B and cannot

A

```
HIP2    75 F I T K I W H P N I S S V T G A I C ... 124 D P Q D A V ...
Ubc1    71 F D T K V Y H P N I S S V T G A I C ... 120 D P Q D A E ...
Ubc13   71 F M T K I Y H P N V D K L - G R I C ... 119 D P L A N D ...
UbcH5A  69 F T T K I Y H P N I N S N - G S I C ... 117 D P L V P D ...
UbcH5B  69 F T T R I Y H P N I N S N - G S I C ... 117 D P L V P E ...
UbcH7   70 F K T K I Y H P N I D E K - G Q V C ... 119 H P L R A D ...
UbcH8   69 F T T K I Y H P N V D E N - G Q I C ... 118 E P L R M D ...
Ubc2b   72 F L S K M F H P N V Y A D - G S I C ... 120 S P A N S Q ...
Ubc9    77 F E P P L F H P N V Y P S - G T V C ... 127 D P A Q A E ...
UbE2G2  73 F T C E M F H P N I Y P D - G R V C ... 134 S G A N V D ...
```

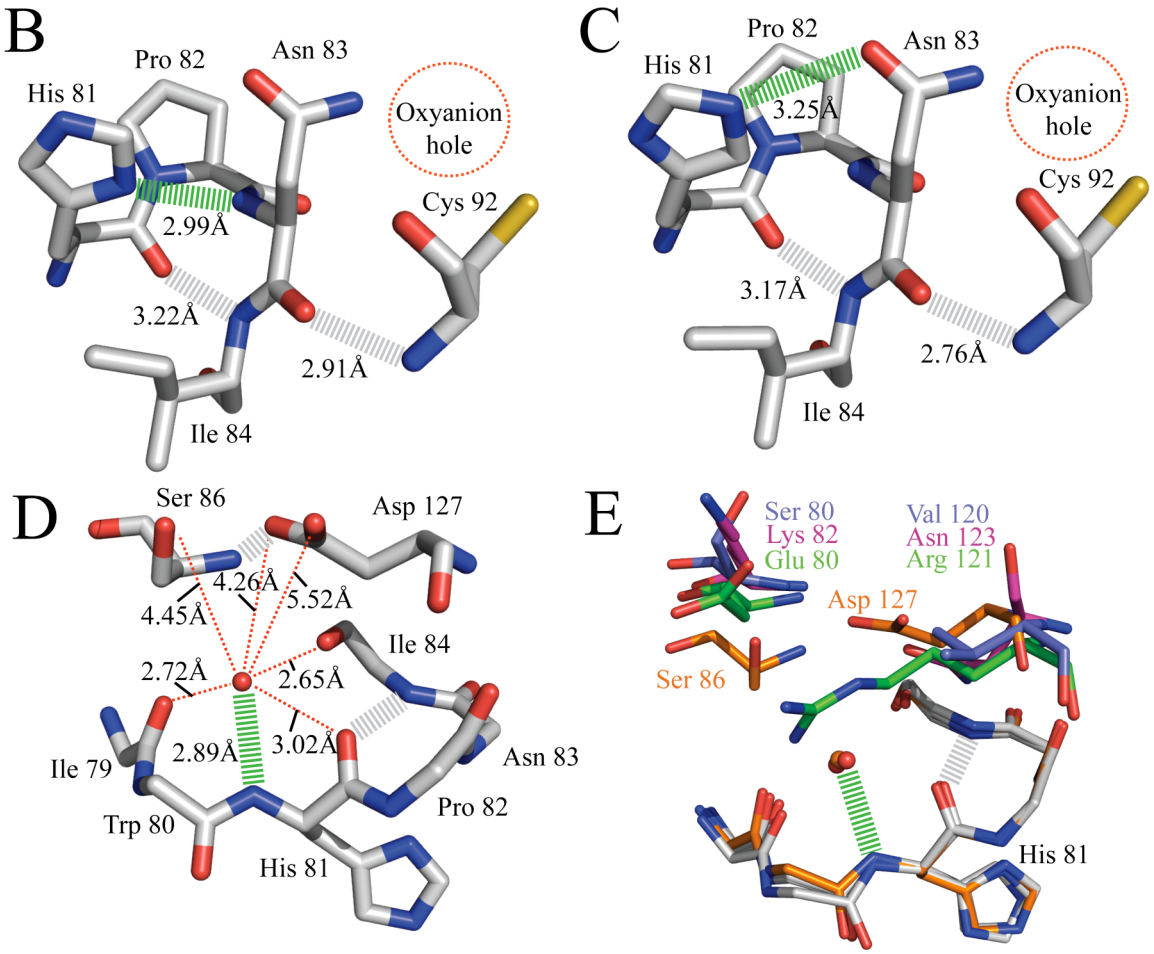

Figure 3.7 Structural analysis of the HPN motif in HIP2. (**A**) Segment of a sequence alignment of 9 human E2 enzymes and Ubc1 (yeast HIP2 homolog) for which NMR chemical shift data and PDB structures exist. Conserved residues are pink, and unique HIP2 residues are blue. (**B**) HIP2 (2BEP) structure and (**C**) HIP2 (3E46) structure showing variations in H81 ring orientation and hydrogen bonding in the HPN motif adjacent to the C92 active site. (**D**) HIP2 (2BEP) structure showing hydrogen bonded water to the H81 amide and surrounding chemical groups (some sidechains hidden for clarity). (**E**) Overlay of HIP2 (2BEP – orange) from (**D**) showing side chains from UbcH5A (2C4P - purple), Ubc13 (1J7D - magenta), and UbcH8 (1WZV - green) with backbone residues in grey. Hydrogen bonds are shown as thick dashed green/grey lines, and distance measurements are shown in thin dashed red lines. Colour scheme for atoms are nitrogen (blue), oxygen (red), carbon (grey) and protons are not shown.

be explained by the absence of the hydrogen bond depicted in Figure 3.7C. In addition to the hydrogen bond, the deshielding of this amide proton is also affected by orientation of the H81 ring such that the deshielding effects of the ring current face the amide bond. This evidence suggests that the HIP2 structure depicted in Figure 3.7B contains the correct H81 orientation and protonation state, while the HIP2 structure depicted in Figure 3.7C incorporates an incorrect orientation for H81 in the HPN motif.

The structures of the other nine E2 enzymes analyzed also display little consensus on the HPN histidine ring orientation. All of these nine proteins however, contain a significantly downfield shifted Asn amide proton in the HPN motif as in HIP2. Therefore, it is likely the His orientation and hydrogen bond depicted in Figure 3.7B is similar for all other E2 enzymes with the HPN motif. Substitutions in the His or Pro residues in the HPN motif for Ubc13 resulted in the production of mostly insoluble protein (*16*). These results indicate that the His side chain is not involved in stabilizing the oxyanion hole in any E2 enzyme's HPN motif. The purpose of the His hydrogen bond to the Asn amide is therefore very important in strengthening the HPN tight turn (Pro trans configuration) to stabilize the catalytic core domain fold. This means the His in the HPN motif structurally stabilizes the active site. The purpose of this important HPN motif structure near catalytic site is likely to properly position the Asn sidechain to stabilize the oxyanion hole. Since all reported E2 enzymes contain this significantly downfield shifted Asn amide proton, the HPN tight turn motif must aid in proper Asn positioning to aid in the function of all E2 enzymes.

3.4.5 Histidine 81 in HIP2 displays a distinctly deshielded amide proton

Another feature of the ^{1}H-^{15}N HSQC spectrum of HIP2 is the distinct downfield amide ^{1}H chemical shift of H81 (^{1}H: 10.570 ppm, ^{15}N: 131.11 ppm) in the HPN motif. Unlike the highly downfield shifted amide proton of N83 that is common in all 10 E2s analyzed, the downfield shift of the H81 amide proton is unique to HIP2 and its yeast homolog Ubc1. There was no observed hydrogen bonding of the H81 amide proton to any other amino acid backbone or side chain atoms. However, the observation of a hydrogen bonded water molecule could account for the deshielded environment experienced by the H81 amide proton (Fig 3.7D). The electronegative atoms from S86 and D127 side chains are outside of hydrogen bonding distance but possibly affect the polar orientation of the water molecule, which would strengthen the hydrogen bond with the H81 amide proton. This is supported by the fact that the D127 residue is unique to HIP2 and the S86 residue, although not unique, is very close to the unique T88 residue insertion in HIP2 that affects the positioning of S86 (Fig 3.7A, D). Comparison to several other E2 enzymes (UbcH5A, Ubc13 and UbcH8) indicated that a hydrogen bonded water molecule was also present in these structures. However, downfield shifted His amide protons were not observed in these other E2 enzymes. To explain the lack of a similar His amide chemical shift, these E2 structures were aligned by the HPN motif and overlayed to display structural differences (Fig 3.7E). There are no additional hydrogen bonds that explain why the HIP2 H81 amide is uniquely downfield shifted. The most obvious difference between HIP2 and UbcH5A, Ubc13 and UbcH8, are the residue identities and geometry equivalent to S86 and D127 in HIP2. In HIP2 S86 and D127 provide electronegative groups that may aid in orientation of the hydrogen bonded water

molecule. This may strengthen the hydrogen bond to H81. The other three E2 enzymes do not retain these proximal electronegative groups. The negative charge on D127 in HIP2 is replaced by positive R121, polar N123 and a hydrophobic V120 in UbcH8, Ubc13 and UbcH5A respectively, which accounts for an obvious change in environment that would not favorably interact with the positive side of a polar water molecule. The insertion of T88 in HIP2 is unique and may cause the S86 sidechain to be moved into closer proximity of this water molecule than S80, K82 or E80 in UbcH5A, Ubc13, and UbcH8 respectively. The proximity and location of electronegative atoms located opposite the hydrogen bonded water appears unique to HIP2 (and Ubc1) and thus hydrogen bond stabilization by these groups is the most reasonable explanation for the H81's unique downfield shifted amide proton. Although the H81 amide unique chemical shift does not seem to adversely affect the active site, these residues may be necessary for the structural stabilization of the active site of the HIP2 enzyme.

Previous experimentation shows that a HIP2 S86Y substitution loses the ability to make poly-Ub chains (*29*). The S86 residue is not adjacent to the active site cysteine or HPN asparagine side chain, but it is close to the HPN histidine backbone amide (Fig 3.7D, E). The S86Y substitution would likely disrupt the hydrogen bonded water depicted in Figure 3.7D, but this substitution will also affect the structure of the HPN motif through steric hindrance by the large hydrophobic Y86 residue with the H81 backbone. Therefore, the S86Y substitution may alter the HPN tight turn structure resulting in a changed orientation of N83 near the active site. This may cause a destabilized oxyanion hole resulting in the loss of poly-Ub chain function.

3.4.6 The predicted secondary structure of HIP2 agrees with the crystal state

Using the NMR chemical shift assignments, the secondary structure of HIP2 was determined and when compared to the secondary structure observed in the crystal state, all of the major α-helices and β-strands are retained in solution. This is an important result supporting the validity of using the crystal structure as an accurate representation of HIP2 in solution. The matching secondary structure also provides evidence that the C170S substitution is non-perturbing, supporting previous enzymatic evidence that this substitution remains fully functional (*30*). The resonance assignments of HIP2 can now be used to perform studies where interacting residues can be identified.

3.4.7 General conclusions

The E2 conjugating enzymes are crucial components involved in both Ub transfer and poly-Ub chain formation in the ubiquitin proteosome pathway. Although all of the enzymes involved in these processes have been identified, the understanding of the structural mechanisms detailing how Ub is built into chains is still poorly explained. The structure of the HIP2 enzyme was solved through X-ray crystallography (unpublished) (*2*), but there were no NMR experiments or data for HIP2 available in the literature. To expand the structural knowledge of HIP2 and its function, the backbone resonances were assigned for the purpose of interaction studies between attached Ub and Ub_2 (Chapter 4). Since NMR provides residue specific details, these interactions can be mapped onto the high-resolution structure of HIP2 that will provide important information on the mechanisms of HIP2 function in Ub transfer and poly-Ub chain formation.

Bibliography

1. Chen, Z., and Pickart, C. M. (1990) A 25-kilodalton ubiquitin carrier protein (E2) catalyzes multi-ubiquitin chain synthesis via lysine 48 of ubiquitin, *J Biol Chem 265*, 21835-21842.

2. Wilson, R. C., Hughes, R. C., Flatt, J. W., Meehan, E. J., Ng, J. D., and Twigg, P. D. (2009) Structure of full-length ubiquitin-conjugating enzyme E2-25K (huntingtin-interacting protein 2), *Acta Crystallogr Sect F Struct Biol Cryst Commun 65*, 440-444.

3. Kay, L. E., Keifer, P., and Saarinen, T. (1992) Pure Absorption Gradient Enhanced Heteronuclear Single Quantum Correlation Spectroscopy with Improved Sensitivity, *Journal of the American Chemical Society 114*, 10663-10665.

4. Grzesiek, S., and Bax, A. (1992) An efficient method for sequential backbone assignment of medium-sized isotopically enriched proteins, *J. Magn. Reson. 99*, 201-207.

5. Bax, A., and Ikura, M. (1991) An efficient 3D NMR technique for correlating the proton and 15N backbone amide resonances with the alpha-carbon of the preceding residue in uniformly 15N/13C enriched proteins, *J Biomol NMR 1*, 99-104.

6. Wittekind, M., and Mueller, L. (1993) Hncacb, a High-Sensitivity 3d Nmr Experiment to Correlate Amide-Proton and Nitrogen Resonances with the Alpha-Carbon and Beta-Carbon Resonances in Proteins, *Journal of Magnetic Resonance Series B 101*, 201-205.

7. Grzesiek, S., and Bax, A. (1992) Correlating Backbone Amide and Side-Chain Resonances in Larger Proteins by Multiple Relayed Triple Resonance Nmr, *Journal of the American Chemical Society 114*, 6291-6293.

8. Grzesiek, S., Anglister, J., and Bax, A. (1993) Correlation of Backbone Amide and Aliphatic Side-Chain Resonances in C-13/N-15-Enriched Proteins by Isotropic Mixing of C-13 Magnetization, *Journal of Magnetic Resonance Series B 101*, 114-119.

9. Kay, L. E., Xu, G. Y., and Yamazaki, T. (1994) Enhanced-Sensitivity Triple-Resonance Spectroscopy with Minimal H2o Saturation, *Journal of Magnetic Resonance Series A 109*, 129-133.

10. Delaglio, F., Grzesiek, S., Vuister, G. W., Zhu, G., Pfeifer, J., and Bax, A. (1995) Nmrpipe - a Multidimensional Spectral Processing System Based on Unix Pipes, *Journal of Biomolecular Nmr 6*, 277-293.

11. Johnson, B. A., and Blevins, R. A. (1994) Nmr View - a Computer-Program for the Visualization and Analysis of Nmr Data, *Journal of Biomolecular Nmr 4*, 603-614.

12. Wishart, D. S., Sykes, B. D., and Richards, F. M. (1992) The Chemical-Shift Index - a Fast and Simple Method for the Assignment of Protein Secondary Structure through Nmr-Spectroscopy, *Biochemistry 31*, 1647-1651.

13. Wishart, D. S., and Sykes, B. D. (1994) The C-13 Chemical-Shift Index - a Simple Method for the Identification of Protein Secondary Structure Using C-13 Chemical-Shift Data, *Journal of Biomolecular Nmr 4*, 171-180.

14. Connelly, G. P., Bai, Y. W., Jeng, M. F., and Englander, S. W. (1993) Isotope Effects in Peptide Group Hydrogen-Exchange, *Proteins-Structure Function and Genetics 17*, 87-92.

15. Burroughs, A. M., Jaffee, M., Iyer, L. M., and Aravind, L. (2008) Anatomy of the E2 ligase fold: implications for enzymology and evolution of ubiquitin/Ub-like protein conjugation, *J Struct Biol 162*, 205-218.

16. Wu, P. Y., Hanlon, M., Eddins, M., Tsui, C., Rogers, R. S., Jensen, J. P., Matunis, M. J., Weissman, A. M., Wolberger, C., and Pickart, C. M. (2003) A conserved catalytic residue in the ubiquitin-conjugating enzyme family, *EMBO J 22*, 5241-5250.

17. Pichler, A., Knipscheer, P., Oberhofer, E., van Dijk, W. J., Korner, R., Olsen, J. V., Jentsch, S., Melchior, F., and Sixma, T. K. (2005) SUMO modification of the ubiquitin-conjugating enzyme E2-25K, *Nat Struct Mol Biol 12*, 264-269.

18. Merkley, N., and Shaw, G. S. (2004) Solution structure of the flexible class II ubiquitin-conjugating enzyme Ubc1 provides insights for polyubiquitin chain assembly, *J Biol Chem 279*, 47139-47147.

19. Ozkan, E., Yu, H., and Deisenhofer, J. (2005) Mechanistic insight into the allosteric activation of a ubiquitin-conjugating enzyme by RING-type ubiquitin ligases, *Proc Natl Acad Sci U S A 102*, 18890-18895.

20. Miura, T., Klaus, W., Ross, A., Guntert, P., and Senn, H. (2002) Letter to the Editor: The NMR structure of the class I human ubiquitin-conjugating enzyme 2b, *J. Biolmol. NMR 22*, 89-92.

21. Giraud, M. F., Desterro, J. M., and Naismith, J. H. (1998) Structure of ubiquitin-conjugating enzyme 9 displays significant differences with other ubiquitin-conjugating enzymes which may reflect its specificity for sumo rather than ubiquitin, *Acta Crystallogr D Biol Crystallogr 54*, 891-898.

22. Arai, R., Yoshikawa, S., Murayama, K., Imai, Y., Takahashi, R., Shirouzu, M., and Yokoyama, S. (2006) Structure of human ubiquitin-conjugating enzyme E2

G2 (UBE2G2/UBC7), *Acta Crystallograph Sect F Struct Biol Cryst Commun 62*, 330-334.

23. Moraes, T. F., Edwards, R. A., McKenna, S., Pastushok, L., Xiao, W., Glover, J. N., and Ellison, M. J. (2001) Crystal structure of the human ubiquitin conjugating enzyme complex, hMms2-hUbc13, *Nat Struct Biol 8*, 669-673.

24. Zheng, N., Wang, P., Jeffrey, P. D., and Pavletich, N. P. (2000) Structure of a c-Cbl-UbcH7 complex: RING domain function in ubiquitin-protein ligases, *Cell 102*, 533-539.

25. Serniwka, S. A., and Shaw, G. S. (2009) The structure of the UbcH8-ubiquitin complex shows a unique ubiquitin interaction site, *Biochemistry 48*, 12169-12179.

26. Reverter, D., and Lima, C. D. (2005) Insights into E3 ligase activity revealed by a SUMO-RanGAP1-Ubc9-Nup358 complex, *Nature 435*, 687-692.

27. Yunus, A. A., and Lima, C. D. (2006) Lysine activation and functional analysis of E2-mediated conjugation in the SUMO pathway, *Nat Struct Mol Biol 13*, 491-499.

28. Pardi, A., Wagner, G., and Wuthrich, K. (1983) Protein conformation and proton nuclear-magnetic-resonance chemical shifts, *Eur J Biochem 137*, 445-454.

29. Mastrandrea, L. D., Kasperek, E. M., Niles, E. G., and Pickart, C. M. (1998) Core domain mutation (S86Y) selectively inactivates polyubiquitin chain synthesis catalyzed by E2-25K, *Biochemistry 37*, 9784-9792.

30. Haldeman, M. T., Xia, G., Kasperek, E. M., and Pickart, C. M. (1997) Structure and function of ubiquitin conjugating enzyme E2-25K: the tail is a core-dependent activity element, *Biochemistry 36*, 10526-10537.

Chapter 4

Novel Intramolecular Contacts Observed Between the HIP2 UBA Domain and Ubiquitin within a HIP2-Ub_2 Thiolester Mimic

4.1 Introduction

The enzyme HIP2 (E2-25K) is known to produce unanchored K48-linked poly-Ub chains in solution using only the E1 activating enzyme and ubiquitin (Ub) molecules as substrates (*1*). The biological significance of unanchored chain building by HIP2 remains debatable, but a better understanding of how HIP2 accomplishes this activity should shed light on how K48-linked poly-Ub chains are constructed. Experiments in Chapter 2 demonstrate that HIP2 and its thiolester mimic do not significantly dimerize. It was also demonstrated that the HIP2~Ub thiolester is the sole reactive species needed to form poly-Ub chains. Therefore, further studies with HIP2 thiolesters should help clarify the mechanisms for HIP2 function. Multiple mechanisms have been proposed for the assembly of poly-Ub chains in various ubiquitination pathways. These mechanisms include the formation of poly-Ub chains on the E2 enzyme, formation of free poly-Ub chains in solution that could then be loaded onto E2 enzymes for transfer to the substrate in a single transfer reaction, and a sequential addition mechanism where a poly-Ub chain bound to a substrate is sequentially extended through a series of transfer reactions. HIP2 may function biologically by any of these mechanisms. Results from Chapter 2 demonstrated that free Ub and HIP2-Ub disulphide could act as Ub acceptors in poly-Ub

chain formation. This indicates that mechanisms of preassembly of poly-Ub chains built on HIP2 or freely in solution and followed by loading these chains onto HIP2 could result in the creation of HIP2~Ub_n thiolester intermediates.

In order to study these possible intermediates, HIP2~Ub and HIP2~Ub_2 thiolester mimics were produced for structural investigation. The backbone assignment of HIP2 from Chapter 3 was essential to determine residue specific chemical shift values for the HIP2 enzyme. NMR studies can provide residue specific information that allows determination of interaction surfaces within HIP2-Ub and HIP2-Ub_2. These studies will help clarify possible mechanisms of HIP2 function.

4.2 Materials and Methods

4.2.1 Protein expression and purification

Ubiquitin variants Ub^{K48R} and Ub^{G76C} were overexpressed as either unlabelled or ^{15}N, ^{13}C-labelled proteins and purified as described previously (*2*). $HIP2^{C170S}$ (simply referred to as HIP2) was overexpressed as either unlabelled, uniform ^{15}N, or ^{15}N, ^{13}C-labelled and purified as described previously (Section 3.2.2). The identity of purified HIP2 was confirmed by mass spectrometry (HIP2 – MW_{obs} 22534.8 ± 0.3 Da, MW_{calc} 22534.7; ^{15}N, ^{13}C-labelled HIP2 (*HIP2) – MW_{obs} 23778.9 ± 1.4 Da, MW_{calc} 23812.8 Da).

4.2.2 Diubiquitin synthesis

A K48-linked diubiquitin chain was constructed using purified Ub^{G76C} (Ub^{P}) and Ub^{K48R} (Ub^{D}) proteins. HIP2 was utilized in a free poly-Ub chain reaction with the reactants Ub^{P} and Ub^{D} to yield predominantly a blocked diubiquitin species (Ub^{P}-Ub^{D}). The formation of Ub^{P}-Ub^{D} was catalyzed by human E1 activating enzyme (UBE1) (BostonBiochem) and HIP2 as previously described (*3*). Purified ^{15}N, ^{13}C-labelled Ub^{P} and Ub^{D} ($*Ub^{P}$ and $*Ub^{D}$) were utilized to alternatively label diubiquitin products ($*Ub^{P}$-Ub^{D} and Ub^{P}-$*Ub^{D}$). The purity of Ub^{P}-Ub^{D}, and thus the purity of each individual ubiquitin variant, was confirmed with electrospray ionization mass spectrometry (unlabelled Ub^{P}-Ub^{D}: MW_{obs} 17169.2 ± 0.7, MW_{calc} 17169.7). The correct mass of $*Ub^{P}$-Ub^{D} and Ub^{P}-$*Ub^{D}$ was confirmed with mass spectrometry on their disulphide complexes with HIP2 (Section 4.2.3).

4.2.3 HIP2-diubiquitin disulphide complex formation

Stock solutions of Ub^{P}, Ub^{P}-Ub^{D} and HIP2 (0.1 mM each) were reduced using freshly made 5 mM TCEP. HIP2 was combined with a 2-fold excess of Ub^{P} or Ub^{P}-Ub^{D} and dialyzed against several changes of 100 mM Na_2HPO_4/NaH_2PO_4, 200 mM NaCl, 10 μM $CuCl_2$ at pH 7.4 and 4 °C. This mild oxidation buffer drives the creation of disulphide bonds between the active site C92 of HIP2 and C76 of Ub^{P} mimicking a thiolester bond. The progress of the disulphide complex formation was monitored by non-reducing SDS-PAGE and was considered complete when the reduced HIP2 was exhausted. The protein solution was concentrated and purified by size exclusion chromatography on a Sephadex G-75 column with 100 mM Na_2HPO_4/NaH_2PO_4, 200 mM

NaCl, 3 mM EDTA at pH 7.4. Fractions containing pure HIP2-Ub^P or HIP2-Ub^P-Ub^D were pooled and extensively dialyzed against 100 mM Na_2HPO_4/NaH_2PO_4, 400 mM NaCl and 3 mM EDTA buffer at pH 7.4 for NMR experiments. Complex formations were confirmed by mass spectrometry for [^{15}N]HIP2-Ub^P (MW_{obs} 31402.9 ± 2.3 Da, MW_{calc} 31402.6 Da), HIP2-Ub^P-*Ub^D (MW_{obs} 40165.56 ± 4.6 Da, MW_{calc} 40184.4), HIP2-*Ub^P (MW_{obs} 31602.5 ± 0.8 Da, MW_{calc} 31616.6 Da) and HIP2-*Ub^P-Ub^D (MW_{obs} 40169.1 ± 2.3 Da, MW_{calc} 40183.4 Da).

4.2.4 NMR sample preparation

In order to properly compare NMR spectra for variably labelled HIP2, Ub^P, Ub^D, Ub^P-Ub^D, HIP2-Ub^P and HIP2-Ub^P-Ub^D complexes, all proteins were extensively dialyzed into identical buffer conditions of 100 mM Na_2HPO_4/NaH_2PO_4, 400 mM NaCl and 3 mM EDTA buffer at pH 7.4. The proteins HIP2, Ub^P and Ub^P-Ub^D include the addition of freshly made 1 mM DTT to ensure cysteine residues remain reduced. The 400 mM NaCl was optimized to maximize solubility of the HIP2-Ub^P complex. All proteins were concentrated using a 10000 MWCO Amicon spin concentrator (Millipore). NMR samples were prepared using concentrated stock solutions of each protein by adding 10% D_2O (v/v), 1% 10 mM DSS (v/v), 0.05% NaN_3 (v/v), and 0.8% Complete MINI EDTA-free protease inhibitor tablet (Roche) solubilized with 1 mL H_2O (v/v). The final concentrations in each NMR sample were 525 μM *HIP2, 357 μM *HIP2-Ub^P, 550 μM *HIP2-Ub^P-Ub^D, 600 μM *Ub^D, 350 μM Ub^P-*Ub^D, 340 μM HIP2-Ub^P-*Ub^D, 600 μM *Ub^P, 600 μM *Ub^P-Ub^D, 433 μM HIP2-*Ub^P, and 325 μM HIP2-*Ub^P-Ub^D. Protein concentrations of Ub were determined by weight of lyophilized proteins and Ub^P-

Ub^D concentrations were estimated by comparison to lyophilized weights and estimating 30% loss of material in reactions. HIP2, HIP2-Ub^P and HIP2-Ub^P-Ub^D protein concentrations were determined with Bradford (BioRad) reactions performed in triplicate.

4.2.5 NMR spectroscopy

The uncomplexed proteins HIP2, Ub^P, Ub^D and Ub^P-Ub^D as well as the HIP2-Ub^P and HIP2-Ub^P-Ub^D disulphide complexes were characterized by NMR spectroscopy by isotopic labelling of only one protein component at a time. In this way *Ub^P, *Ub^D and *HIP2 components allowed for residue specific interaction surfaces to be determined in the larger protein complexes. All NMR data was acquired using a Varian INOVA 600 MHz spectrometer equipped with a triple resonance cold probe with z gradients (Biomolecular NMR Facility, University of Western Ontario). Sequential assignments for the backbone residues of *Ub^D, *Ub^P, *Ub^P-Ub^D and Ub^P-*Ub^D were performed utilizing ^1H-^{15}N HSQC (*4*) and HNCA (*5*) experiments at 30 °C. Disulphide protein complexes with labelled Ub (HIP2-*Ub^P, HIP2-*Ub^P-Ub^D and HIP2–Ub^P-*Ub^D) were used to collect ^1H-^{15}N HSQC spectra at 30 °C and assigned by comparison to the uncomplexed proximal or distal labeled Ub and Ub_2. Protein complexes with labelled HIP2 (*HIP2, *HIP2–Ub^P, and *HIP2–Ub^P-Ub^D) were used to collect ^1H-^{15}N TROSY-HSQC (*6*) spectra at 35 °C, and assigned by comparison to HIP2 assignments from Chapter 3. Chemical shift perturbations were calculated according to $\sum\Delta\delta = [\Delta\delta(^1H)^2 + ((0.2)\Delta\delta(^{15}N))^2]^{0.5}$, where $\Delta\delta(^1H)$ and $\Delta\delta(^{15}N)$ represent the change in chemical shift in ^1H (proton) and ^{15}N (nitrogen) atoms within a protein backbone amide bond (*7*).

4.2.6 Sedimentation equilibrium

Sedimentation equilibrium experiments were performed in a Beckman Optima XL-A analytical ultracentrifuge with UV/VIS optics. An An-60 Ti analytical rotor was used with a 12 mm thick six-channel equilibrium double sector Epon-charcoal centerpiece with quartz windows. Protein samples were loaded in triplicate (100 µL protein) with matching reference samples containing dialysis buffer (110 µL). Absorbance measurements were collected at 280 nm in 0.002 cm radial steps and averaged over 10 readings. Experiments were performed at 5 °C and at rotor speeds of 12, 15, 18 and 21000 rpm. A delay of 20 hours at the first speed was used to allow the sample to reach equilibrium, and further increases in speed were allowed 8 hours to reach equilibrium before readings were measured. At each speed two scans were performed two hours apart and superimposed to confirm that equilibrium had been properly achieved. Prior to centrifugation HIP2-Ub^{P}-*Ub^{D} was dialyzed into 100 mM Na_2HPO_4/NaH_2PO_4, 400 mM NaCl and 3 mM EDTA at pH 7.33 for 24 hours. Sample concentrations (10.9 µM, 8.7 µM and 5.7 µM) were determined by dilution of a higher concentration stock solution using dialysis buffer. The protein integrity was confirmed after the experiments using electrospray mass spectrometry (MW_{obs} 40162.2 ± 2.6 Da; MW_{calc} 40184.4 Da)

4.3 Results

4.3.1 Protein expression and purification

Ubiquitin variants Ub^{K48R}, Ub^{G76C} and $HIP2^{C170S}$ (henceforth referred to as HIP2) were overexpressed as either unlabelled, or uniform ^{15}N, or ^{15}N, ^{13}C-labelled proteins and purified as described previously (Section 2.2.1, 3.2.2). The molecular weight of unlabelled HIP2 was confirmed using electrospray ionization mass spectrometry whereby a major peak was observed (MW_{obs} 22534.8 ± 0.3 Da) at the expected molecular weight (MW_{calc} 22534.7). The molecular weight of ^{15}N, ^{13}C-labelled HIP2 (*HIP2) was also confirmed with mass spectrometry to have 97.3% isotopic label incorporation with a single major peak observed (MW_{obs} 23778.9 ± 1.4 Da) at the expected molecular weight (MW_{calc} 23812.8 Da). The correct molecular weight of ubiquitin variants was confirmed in Ub_2 complexes (Section 4.3.2).

4.3.2 Creation of lysine-48 linked diubiquitin using ubiquitin variants

The enzyme HIP2 is known to produce unanchored K48-linked poly-ubiquitin (poly-Ub) chains in solution using only the E1 activating enzyme and free ubiquitin (Ub) molecules as substrates (*1*). Utilization of the ubiquitin variants Ub^{G76C} (Ub^P) and Ub^{K48R} (Ub^D) allows K48-linked poly-Ub chain extension to be blocked on both sides such that a Ub_2 (Ub^P-Ub^D) product accumulates in solution. The predominant product from this poly-Ub chain reaction is Ub^P-Ub^D since Ub^P is blocked from C-terminal chain extension by the G76C substitution, and Ub^D is blocked from K48 extension by the K48R substitution. The abbreviation Ub^P is used to denote the proximal Ub that can be directly attached to

the E2 enzyme through a disulphide bond. The abbreviation Ub^D is used to denote the distal Ub in Ub_2 that forms a peptide bond to K48 of Ub^P. The formation of the diubiquitin (Ub^P-Ub^D) species was catalyzed by the E1 activating enzyme and HIP2 and purified using anion exchange followed by cation exchange to yield purified diubiquitin as described previously (Fig 4.1) (*3*). The larger Ub_n by-products are likely the result of very low amounts of non K48-linked chains that form after all Ub K48 residues are exhausted. Purified ^{15}N, ^{13}C-labelled Ub^P ($*Ub^P$) and ^{15}N, ^{13}C-labelled Ub^D ($*Ub^D$) proteins were utilized in conjunction with unlabelled Ub^P and unlabelled Ub^D to produce $*Ub^P$-Ub^D and Ub^P-$*Ub^D$. The molecular weight of Ub^P-Ub^D was confirmed using electrospray ionization mass spectrometry as a single major peak was observed (MW_{obs} 17169.2 ± 0.7 Da) at the expected molecular weight (MW_{calc} 17169.7 Da) (Fig 4.1). The correct molecular weight of $*Ub^P$-Ub^D and Ub^P-$*Ub^D$ was confirmed with mass spectrometry on their disulphide complexes with HIP2 (Section 4.3.3).

4.3.3 HIP2-Ub and HIP2-Ub_2 disulphide complex formation

In order to examine the mechanisms of assembly of a poly-Ub chain at the active site cysteine and/or the transfer of preassembled chains thiolester linked to the active site, HIP2 complexes were synthesized carrying either one or two Ub molecules at the active site. To mimic the HIP2~Ub thiolester a disulphide complex was formed between the catalytic cysteine (C92) and ubiquitin carrying a C-terminal cysteine substitution Ub^{G76C} (Ub^P). A C170S substitution in HIP2, shown to retain all activity in comparison to the wild type protein (*8*), was used to provide specificity for the disulphide formation. A single ubiquitin (Ub^P) or diubiquitin (Ub^P-Ub^D) was linked to the catalytic cysteine

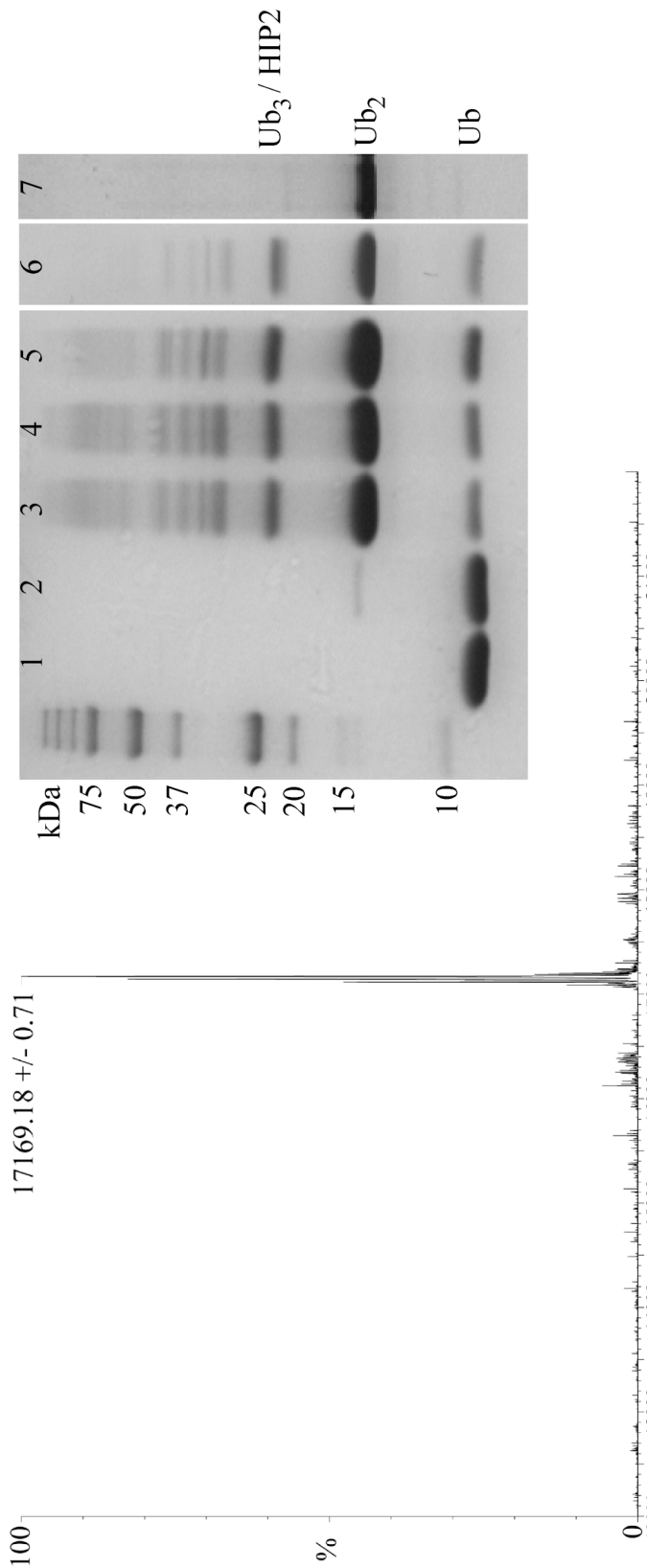

Figure 4.1 Formation and purification of K48-linked diubiquitin (Ub^P-Ub^D). Purified Ub^D (lane 1) and purified Ub^P (lane 2) are reacted at final concentrations of 13.6 mg / mL for each substituted Ub species, with 0.1 µM E1, 20 µM HIP2, 2.5 mM Mg/ATP solution, 0.5mM DTT and 50 mM HEPES pH 8.0 buffer containing ATP regeneration enzymes. The resulting products are predominantly Ub_2 (Ub^P-Ub^D) after 16.5 hrs (lane 3) and 21 hrs (lane 4). The Ub_2 is stable to reducing agent (lane 5) as 5mM DTT was added to confirm peptide bond formation. The Ub_2 product is then purified on an anion exchange column to remove E1, HIP2 and trace high molecular weight ubiquitinated species (lane 6). Finally Ub, Ub_2, and Ub_3 can be separated when the products are acidified to pH 4.5 and cation exchange column (S-column) was used with a very gradual salt elution leaving pure Ub_2 (lane 7). Electrospray ionization mass spectrometry indicates Ub^P-Ub^D is the correct mass.

of HIP2 using mild oxidation, and the HIP2-Ub^P and HIP2-Ub^P-Ub^D products were purified from other disulphide by-products using size exclusion chromatography (Fig 4.2A). This approach allowed for selective isotopic labeling (^{15}N and/or ^{13}C) of each individual protein component in HIP2-Ub^P (*HIP2-Ub^P, HIP2-*Ub^P) or HIP2-Ub^P-Ub^D (*HIP2-Ub^P-Ub^D, HIP2-*Ub^P-Ub^D, HIP2-Ub^P-*Ub^D) complexes for NMR characterization. The creation of HIP2-*Ub^P and HIP2-*Ub^P-Ub^D and purification was monitored with SDS-PAGE in Figure 4.2B. Electrospray ionization mass spectrometry was used to confirm labelled molecular masses of protein complexes. The molecular weight of N^{15}, C^{13} labelled HIP2 (*HIP2) complexes was confirmed with mass spectrometry to have 100% isotopic label incorporation for *HIP2-Ub^P (MW_{obs} 31402.9 ± 2.3 Da, MW_{calc} 31402.6 Da), while the correct molecular weight of *HIP2-Ub^P-Ub^D was confirmed by mass spectrometry on the reactants *HIP2 and Ub^P-Ub^D (Section 4.3.1, 4.3.2). The molecular weight of N^{15}, C^{13} labelled Ub^P (*Ub^P) complexes was confirmed with mass spectrometry to have an isotopic incorporation of 97% for both HIP2-*Ub^P (MW_{obs} 31602.5 ± 0.8 Da, MW_{calc} 31616.6 Da) and HIP2-*Ub^P-Ub^D (MW_{obs} 40169.1 ± 2.3 Da, MW_{calc} 40183.4 Da). The molecular weight of HIP2-Ub^P-*Ub^D was confirmed with mass spectrometry to have an isotopic incorporation of 96% (MW_{obs} 40165.56 ± 4.6 Da, MW_{calc} 40184.4).

4.3.4 Backbone resonance assignment of HIP2 and diubiquitin

In order to identify residues in HIP2 that interact with Ub or Ub_2 in the disulphide linked HIP2-Ub or HIP2-Ub_2 species, the backbone resonance assignments for HIP2 were completed using standard triple resonance experiments (Chapter 3). To maximize

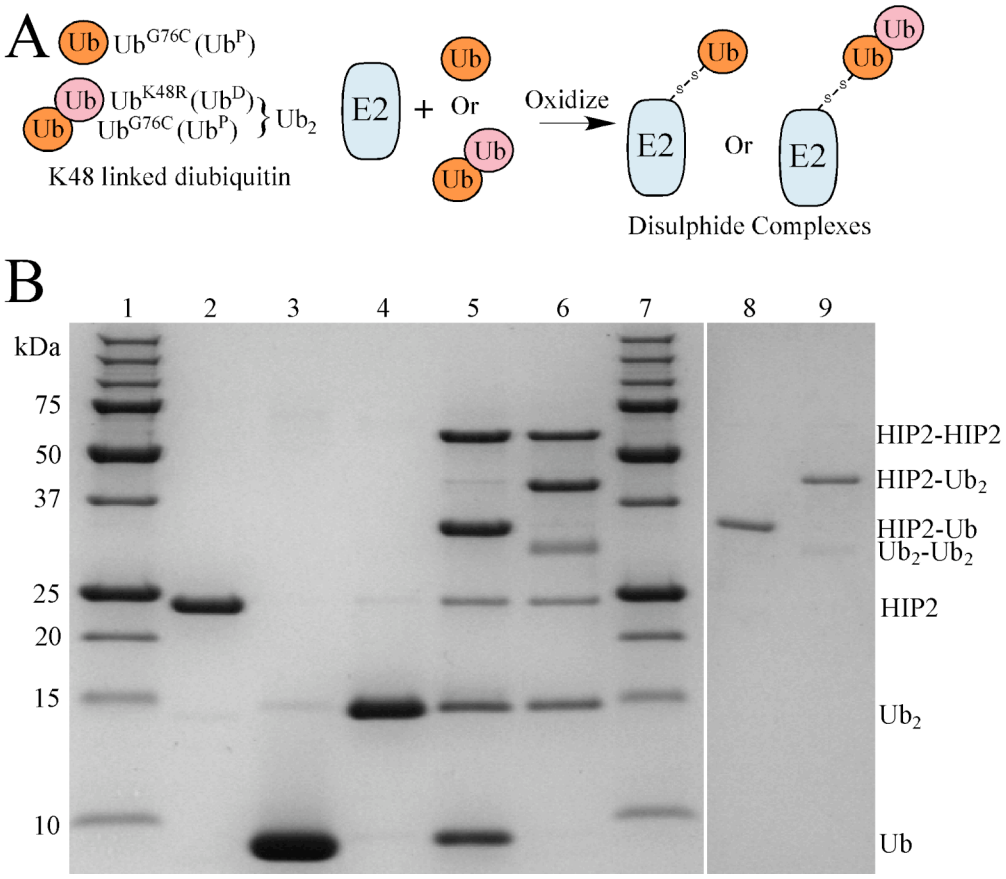

Figure 4.2 Schematic representation of disulphide complex creation. (**A**) The diagram shows the reaction mechanism used to create a disulphide bond (-S-S-) between the E2 conjugating enzyme HIP2 and either a single Ub^{G76C} (Ub^{P}) or diubiquitin Ub^{G76C}-Ub^{K48R} (Ub^{P}-Ub^{D}). (**B**) An SDS-PAGE gel was used to monitor the specific disulphide complex formation with dual labelled proximal Ub ($*Ub^{P}$). Displayed in the gel are molecular weight ladders (lane 1, 7), purified HIP2 (lane 2), purified $*Ub^{P}$ (lane 3), purified K48-linked diubiquitin ($*Ub^{P}$-Ub^{D}) (lane 4), complexation reaction for HIP2-$*Ub^{P}$ (lane 5), complexation reaction for HIP2-$*Ub^{P}$-Ub^{D} (lane 6). Disulphide by-products were removed from disulphide complexes by extensive size exclusion chromatography yielding purified HIP2-$*Ub^{P}$ (lane 8), and purified HIP2-$*Ub^{P}$-Ub^{D} (lane 9). Molecular weights of standards are listed to the left of the gel, and protein species are listed to the right of the gel.

the NMR signal-to-noise of HIP2 in these large protein complexes, collection of a high quality ^{1}H-^{15}N TROSY-HSQC and HNCA spectra of HIP2 was performed at 35 °C. This higher temperature allowed for the assignment of one additional residue, V157 (not seen in Chapter 3), to yield assignment of 176 out of 187 (94%) non-proline ^{1}H and ^{15}N amide resonances (Fig 4.3). Many of the remaining unassigned residues are located in the N-terminus (M1, N3), the loop between α1 and β1 (E20, T22), the loop between β1 and β2 (D33, E34, F36) as well as the proposed flexible linker between the catalytic core α4 and the UBA domain α5 (S159, E161). These residues are likely in highly flexible and solvent exposed regions, resulting in their ^{1}H and ^{15}N amide resonances being unobservable due to fast amide exchange with water.

In order to identify the residues in the proximal and distal Ub moieties that interact within HIP2-Ub and HIP2-Ub_2 complexes the backbone chemical shift assignments were also completed for *Ub^{P}, *Ub^{D}, *Ub^{P}-Ub^{D} and Ub^{P}-*Ub^{D} using HSQC and HNCA experiments to compare to a previous Ub HSQC spectrum (*9*). The remaining spectra of larger HIP2 complexes (*HIP2-Ub^{P}, *HIP2-Ub^{P}-Ub^{D}, HIP2-*Ub^{P}, HIP2-*Ub^{P}-Ub^{D}, HIP2-Ub^{P}-*Ub^{D}) were assigned by HSQC or TROSY-HSQC comparison to the assigned smaller precursor species (*Ub^{P}, *Ub^{D}, *Ub^{P}-Ub^{D}, Ub^{P}-*Ub^{D}, *HIP2).

4.3.5 HIP2 interactions with Ub^{P} within HIP2-Ub^{P}

In the HIP2-Ub^{P} disulphide, Ub^{P} is covalently linked to the active site cysteine (C92) of HIP2. Using ^{1}H-^{15}N TROSY-HSQC spectra and the assigned backbone resonances for HIP2, the position of each residue in HIP2 was assigned upon formation of HIP2-Ub^{P} to

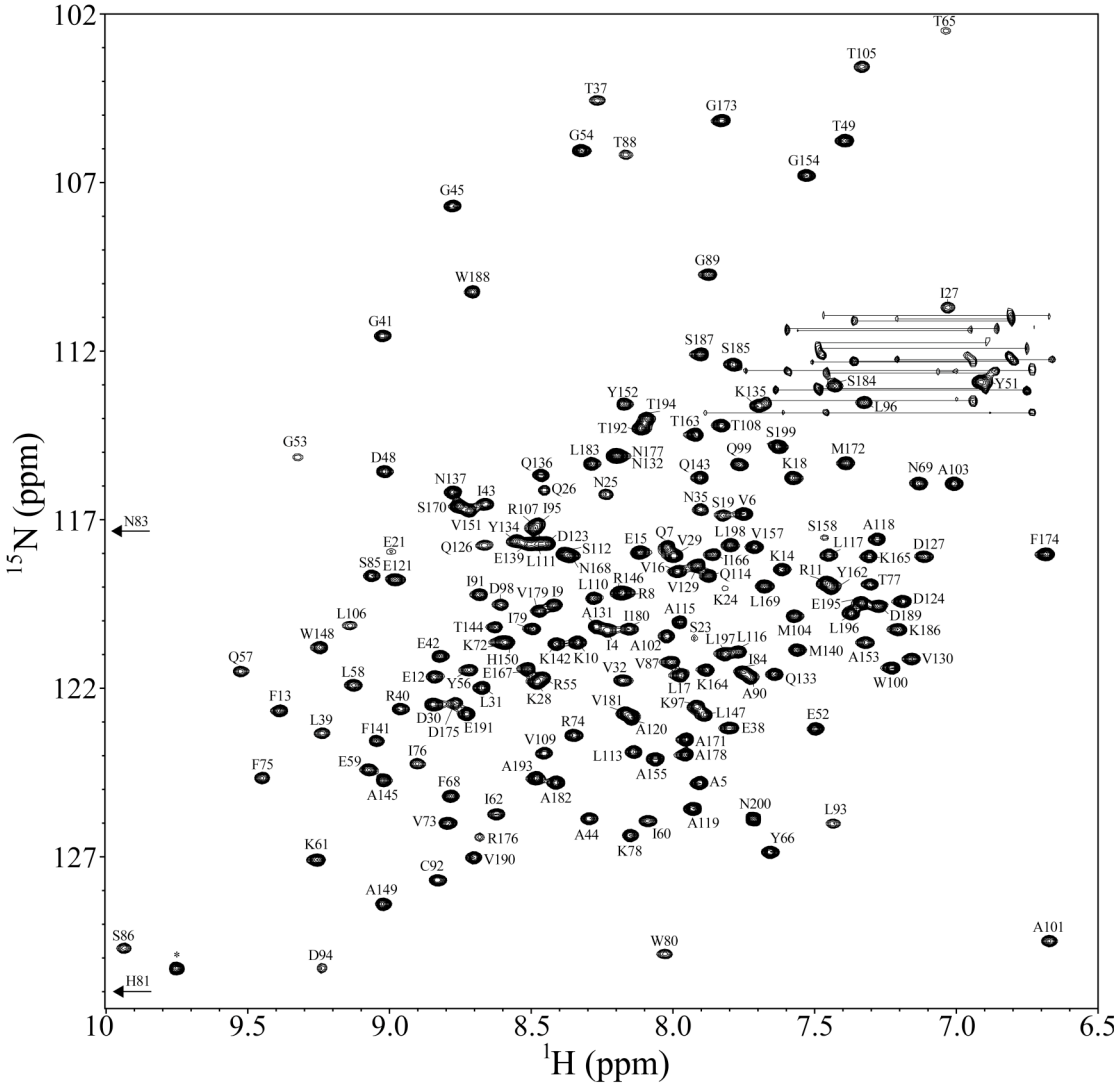

Figure 4.3 ^{1}H-^{15}N TROSY-HSQC spectrum of HIP2. Backbone amide signals are labelled with amino acid single letter codes and sequence numbers. Signals connected by lines indicate side chain amide resonances from Asn and Gln residues. The signals marked with (*) represent side chain amides from Trp residues, while arrows indicate signals that are shifted further downfield in ^{1}H than 10ppm. The spectra was collected on a ^{15}N, ^{13}C-labelled HIP2 sample (525 µM) in 10% D_2O, 400 mM NaCl, 1 mM DTT, 3 mM EDTA, 100 mM Na_2HPO_4/NaH_2PO_4 pH 7.4 at 35 °C.

determine how the Ub moiety interacts with HIP2 (Fig 4.4A). These experiments showed that the largest changes in chemical shift upon formation of HIP2-Ub^P occur in residues found in α1 (R8, I9, R11, F13, K18), β1 (K28, V29, D30), β2 (G41, I43), β3 (K61), the loop containing the active site between β4 and α2 (F75, K78, I79, I84, S85, S86, T88, G89, M104), α2 (L110), the loop between α2 and α3 (E121, D124) and α3 (V129) (Fig 4.4B). Other regions experiencing significant line broadening include the loop between α1 and β1 (K24, I27), β4 (V73), the loop containing the active site between β4 and α2 (H81, V87, I91-D98 (surrounding the active site cysteine C92), A101), α2 (T105, L106, V109), the loop between α2 and α3 (Q126, D127), and α3 (V130) (Fig 4.4B). This significant line broadening is likely due to a decrease in mobility of these residues at the HIP2-Ub^P interface or due to intermediate exchange between structures where the Ub^P might occupy several different locations on HIP2. The residues with the largest changes in chemical shift and line broadening upon formation of HIP2-Ub^P were mapped onto the surface of HIP2 (Fig 4.4C). The most highly affected residues straddle the active site C92 between β4 and α2. Residues I84-G89 undergo the largest chemical shift changes and residues I91-D98 containing a very short 3_{10} helix structure (I95-D98 – hence forward the 'active site' helix) undergo severe line broadening. Another highly affected region near the active site includes residues in the loop between α2 and α3 and the N-terminus of α3. Together all of these residues combine to account for the major surface of HIP2 that is likely in direct contact with the covalently bound Ub^P (Fig 4.4C). It is also evident that there are minimal chemical shift changes in the UBA domain of HIP2 upon formation of HIP2-Ub^P. Although the HIP2 UBA domain has been

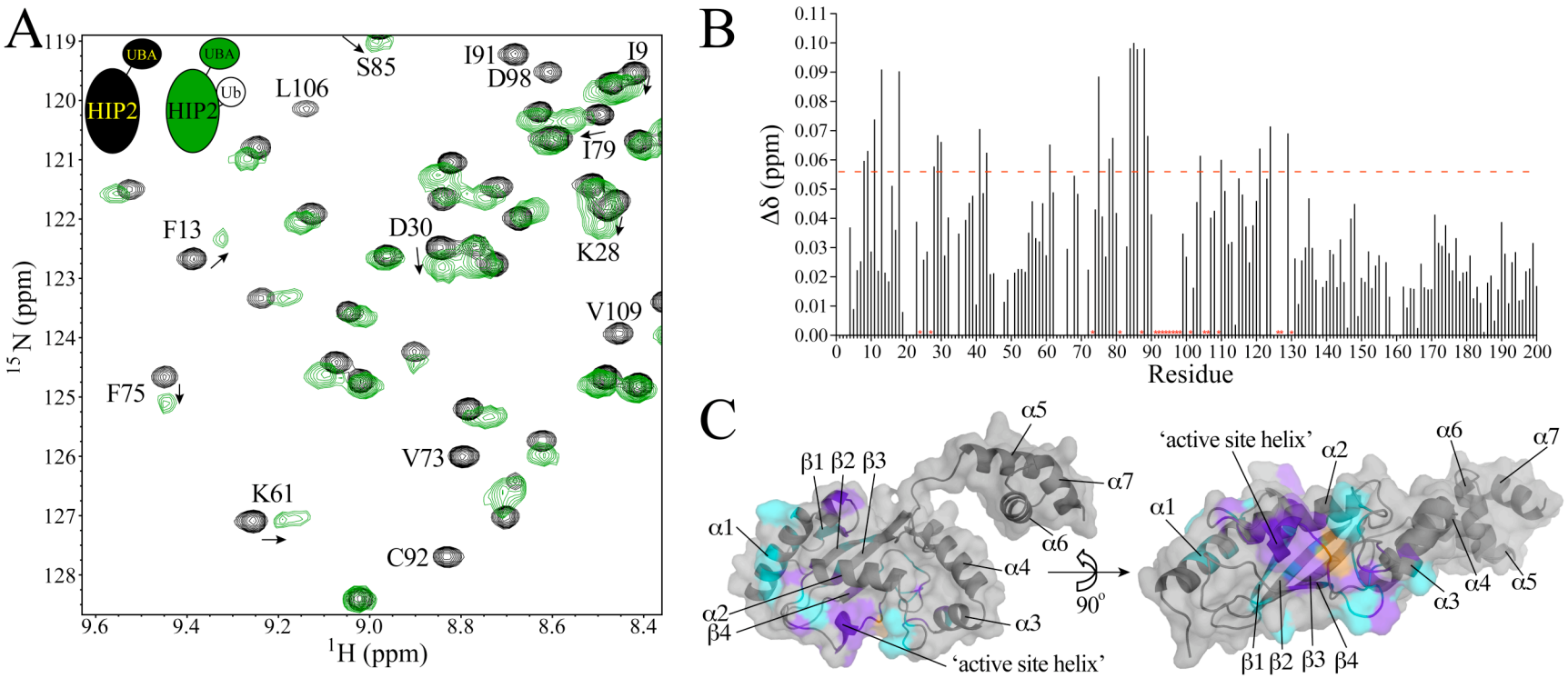

Figure 4.4 Identification of chemical shift changes in HIP2 upon formation of HIP2-Ub^{P}. (**A**) Expanded region of 600 MHz ^{1}H-^{15}N TROSY-HSQC spectra collected for *HIP2 (black) and *HIP2-Ub^{P} (green). Signals that undergo significant chemical shift changes (>1 S.D. above the mean) are labelled by residue and shifts are indicated with arrows, while signals that experience significant line broadening (disappear) are labelled without arrows. (**B**) Bar graph of chemical shift changes observed between *HIP2 and *HIP2-Ub^{P} spectra. The dotted line (red) indicates the threshold for significant chemical shift changes (mean + one standard deviation). Chemical shift changes are calculated using the equation in 4.2.5. Red asterisks indicate signals that undergo significant line broadening. (**C**) Ribbon and surface representation of HIP2 with 'relaxed' tail (Chapter 2) showing interaction with Ub^{P} and labelled according to secondary structure. Residues are coloured to indicate the active site cysteine (orange), residues undergoing significant chemical shift changes (cyan), and residues experiencing significant line broadening (purple).

shown to interact non-covalently with Ub (*10, 11*), the results shown here indicate a UBA interaction with the disulphide bound Ub in HIP2-Ub^P does not occur.

4.3.6 Intramolecular interactions within HIP2-Ub^P-Ub^D

In order to understand the effects of placing a second ubiquitin molecule on the growing poly-Ub chain linked to the catalytic cysteine, the ^1H-^{15}N TROSY-HSQC spectra of *HIP2-Ub^P-Ub^D was compared with that of *HIP2-Ub^P. A structural analysis of HIP2-Ub^P-Ub^D could provide important insights into both the assembly and the mechanism of transfer of prebuilt ubiquitin chains onto substrate molecules. Comparison of *HIP2-Ub^P-Ub^D and *HIP2-Ub^P demonstrate large differences in chemical shift involving residues in α1 (F13), the active site loop between β4 and α2 (I76, N83, I84, G89, A90, A102), the loop between α2 and α3 (A119, D124, Q126), the loop between α5 and α6 (M172, G173, F174), the N-terminus of α6 (N177), and the C-terminus of α7 (V190) (Fig 4.5A). Most of the large chemical shift changes upon diubiquitin attachment occur on the UBA domain of HIP2 (Fig 4.5B), something that was not observed with a single Ub thiolester mimic. Residues M172, G173, F174 and V190 form an exposed hydrophobic interaction surface on the UBA domain in the loop connecting α5 and α6 (Fig 4.5C). Since this hydrophobic MGF patch was not affected upon attachment of Ub^P, these residues must interact with the Ub^D molecule. This hydrophobic patch on the UBA domain has been previously shown to bind free Ub in both HIP2 and Ubc1 (*11, 12*). The same hydrophobic patch on the UBA domain is therefore used to contact both free Ub, and Ub^D in HIP2-Ub_2.

Several residues from the catalytic core of HIP2 are also undergoing

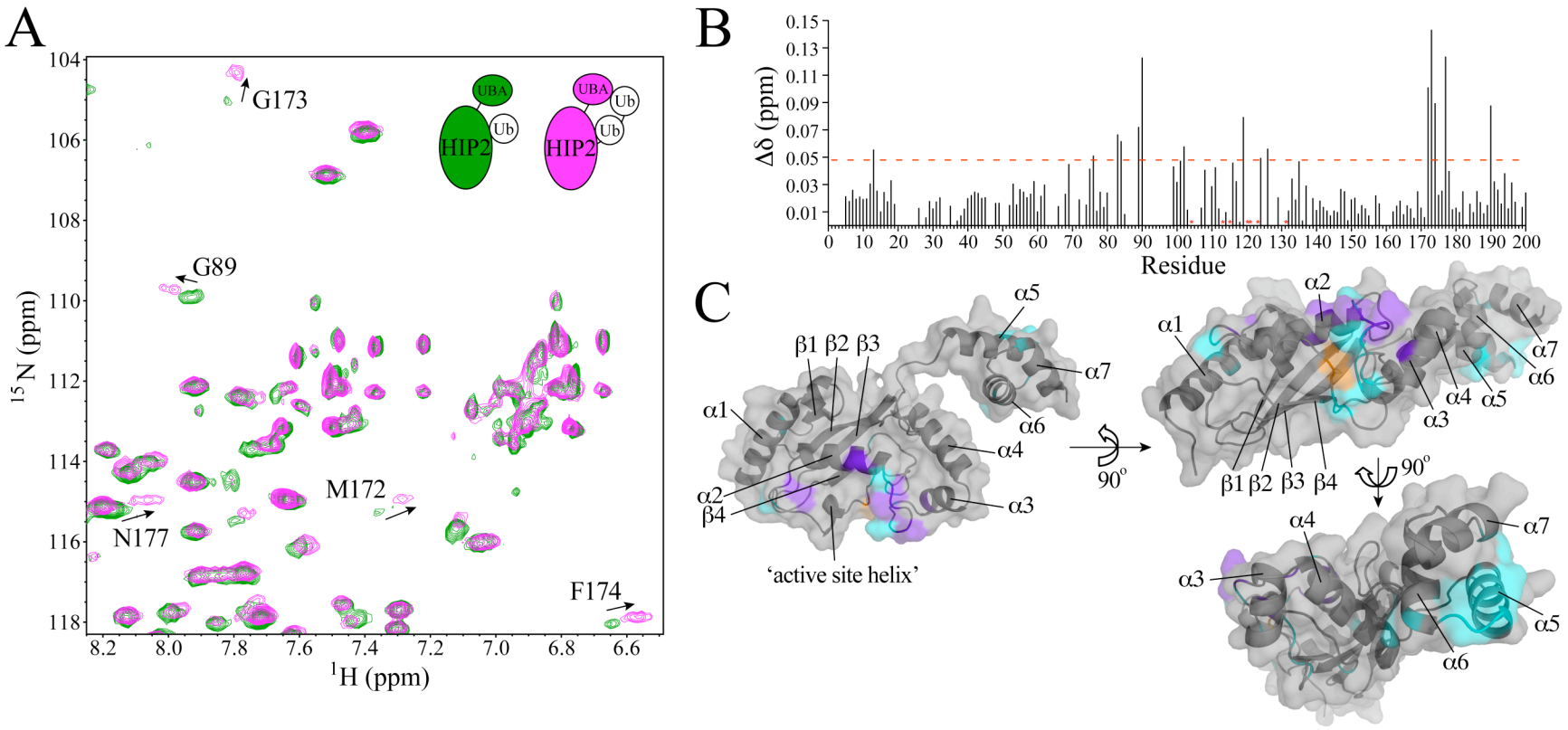

Figure 4.5 Identification of chemical shift changes in HIP2 caused by the addition of Ub^D to HIP2-Ub^P. (**A**) Expanded region of 600 MHz ^{1}H-^{15}N TROSY-HSQC spectra collected for *HIP2-Ub^P (green) and *HIP2-Ub^P-Ub^D (magenta). Signals that undergo significant chemical shift changes (>1 S.D. above the mean) are labelled by residue and shifts are indicated with arrows, while signals that experience significant line broadening (disappear) are labelled without arrows. (**B**) Bar graph of chemical shift changes observed between *HIP2-Ub^P and *HIP2-Ub^P-Ub^D spectra. The dotted line (red) indicates the threshold for significant chemical shift changes (mean + one standard deviation). Chemical shift changes are calculated using the equation in 4.2.5. Red asterisks indicate signals that undergo significant line broadening. (**C**) Ribbon and surface representation of HIP2 with 'relaxed' tail (Chapter 2) showing interaction with Ub^D and labelled according to secondary structure. Residues are coloured to indicate the active site cysteine (orange), residues undergoing significant chemical shift changes (cyan), and residues experiencing significant line broadening (purple).

significant line broadening following attachment of the Ub^D. This includes residues in the loop between the 'active site helix' and α2 (M104), in α2 (L113, A115), and in the loop between α2 and α3 (A120, E121, D123) and α3 (A131). Chemical shift changes on the loop between α2 and α3 (A119, D124, Q126) comprise a small but distinct surface that is interacting with Ub_2 in HIP2-Ub^P-Ub^D but not in HIP2-Ub^P. These chemical shift changes measured around the active site may indicate a slight change in the position of Ub^P upon addition of the second Ub^D. Residues I91-D98 that were significantly line broadened in HIP2-Ub^P remain significantly line broadened in HIP2-Ub^P-Ub^D. This indicates that the surface of interaction previously seen in HIP2-Ub^P is primarily maintained. The loop between α2 and α3 could therefore be in contact with either a slightly repositioned Ub^P that maintains most of the previous interactions or be in contact with a small portion of Ub^D. In either case, the UBA domain is predominantly interacting with the Ub^D and minimal changes are noticed in the vicinity of the active site in HIP2-Ub_2.

4.3.7 HIP2-Ub_2 does not significantly dimerize

The HIP2 UBA domain has been shown to preferentially bind poly-Ub chains over mono Ub in solution (*10*). The structure of another UBA domain that binds K48-linked Ub_2 indicated that this specific UBA domain could contact the hydrophobic face of both Ub moieties at once (*13*). If the HIP2 UBA domain could interact freely with an attached Ub or Ub_2 molecule on neighbouring HIP2 molecules, it is conceivable that UBA binding could result in dimerization and/or oligomerization of HIP2-Ub_2. To test this possibility, sedimentation equilibrium studies were performed with HIP2-Ub_2 (HIP2-

Ub^P-*Ub^D) in solution at 10.9, 8.7 and 5.7 μM giving masses of 41998 ± 798, 43420 ± 387 and 42810 ± 464 Da respectively. These values range from 4.5% to 8% larger than the expected mass of 40184.37 Da. These molecular weights are very close to the approximate error (5%) for this technique, indicating that HIP2-Ub_2 is predominantly monomeric at these three concentrations. These results are consistent with previous dimerization studies on HIP2 and HIP2-Ub (Chapter 2). Previous experimentation on the UbcH5c-Ub construct has shown that oligomerization produces a completely line broadened HSQC spectrum (*14, 15*). HIP2-Ub_2 does not produce a similar NMR spectrum, therefore oligomerization at higher concentrations used in NMR studies was not observed. The UBA interactions observed here are therefore the result of intramolecular interactions and not intermolecular interactions involving oligomeric species.

4.3.8 Combined interactions of both Ub^P and Ub^D within HIP2-Ub_2

As a control for the comparison of HIP2 to HIP2-Ub and HIP2-Ub to HIP2-Ub_2, the chemical position of each residue in HIP2 was evaluated in comparison to HIP2-Ub_2 to determine if the combined addition of Ub_2 is consistent with the individual additions of Ub^P and Ub^D. Comparison of ^1H-^{15}N TROSY-HSQC spectra of *HIP2 with that of the *HIP2-Ub^P-Ub^D identified residues affected by addition of Ub^P-Ub^D (Fig 4.6A). Significant chemical changes were observed for residues in α1 (R11, F13, V16), β1 (V29), the loop between β3 and β4 (N69), the loop containing the active site between β4 and α2 (I79, N83, S85, G89, A90, A102), α2 (T108), the loop between α5 and α6 (M172, G173, F174), the N-terminus of α6 (N177), and the C-terminus of

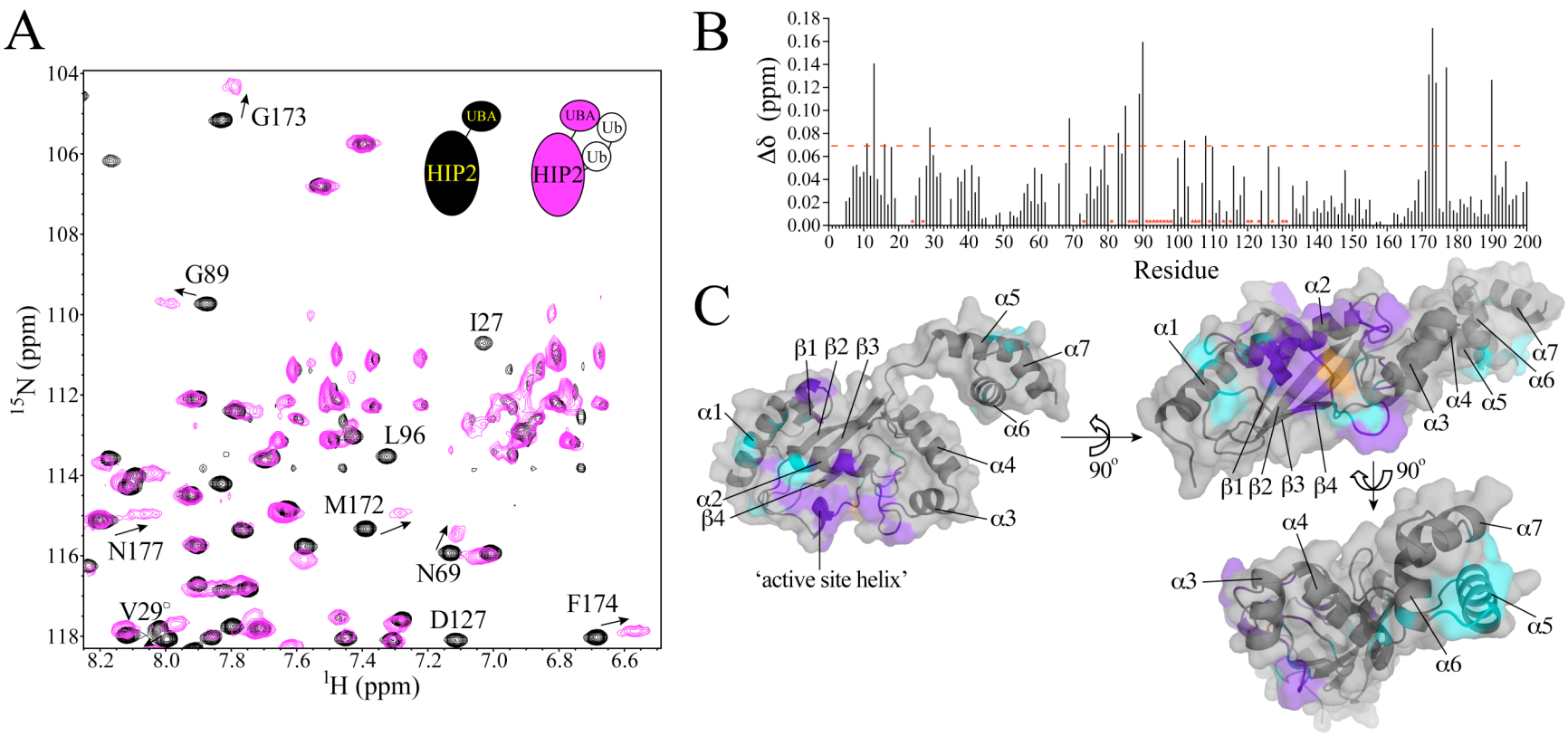

Figure 4.6 Identification of chemical shift changes in HIP2 caused by the addition of Ub^{P}-Ub^{D} to HIP2. (**A**) Expanded region of 600 MHz ^{1}H-^{15}N TROSY-HSQC spectra collected for *HIP2 (black) and *HIP2-Ub^{P}-Ub^{D} (magenta). Signals that undergo significant chemical shift changes (>1 S.D. above the mean) are labelled by residue and shifts are indicated with arrows, while signals that experience significant line broadening (disappear) are labelled without arrows. (**B**) Bar graph of chemical shift changes observed between *HIP2 and *HIP2-Ub^{P}-Ub^{D} spectra. The dotted line (red) indicates the threshold for significant chemical shift changes (mean + one standard deviation). Chemical shift changes are calculated using the equation in 4.2.5. Red asterisks indicate signals that undergo significant line broadening. (**C**) Ribbon and surface representation of HIP2 with 'relaxed' tail (Chapter 2) showing interaction with Ub^{P}-Ub^{D} and labelled according to secondary structure. Residues are coloured to indicate the active site cysteine (orange), residues undergoing significant chemical shift changes (cyan), and residues experiencing significant line broadening (purple).

α7 (V190) (Fig 4.6B). Residues that undergo significant line broadening were identified in the loop between α1 and β1 (K24, I27), β4 (V73), the loop containing the active site between β4 and α2 (H81, V87, I91-D98, M104), α2 (T105, L106, V109, L113, A115), the loop between α2 and α3 (A120, E121, D123, D127), and α3 (V130, A131) (Fig 4.6B). The chemical shift changes observed upon Ub_2 attachment to HIP2 occur at the catalytic core of HIP2 and in the UBA domain of HIP2 that contacts Ub^D (Fig 4.6C). Highly affected residues are consistent with individual residue changes noticed between *HIP2 and *HIP2-Ub^P combined with changes observed between *HIP2-Ub^P and *HIP2-Ub^P-Ub^D.

4.3.9 Ub^D and Ub^P interactions within Ub_2

In order to identify residues in Ub^P or Ub^D that interact with the covalently-linked HIP2 species, the backbone resonance assignments for *Ub^P, *Ub^D, *Ub^P-Ub^D, and Ub^P-*Ub^D were completed using ^{1}H-^{15}N HSQC and HNCA NMR spectra at 30 °C. The assignment of Ub^P was 95% complete (72 / 76) for ^{1}H and ^{15}N amide resonances, while the assignment of Ub^D was 93% complete (71 / 76) for ^{1}H and ^{15}N amide resonances. All assigned residues in Ub^P and Ub^D were reassigned in *Ub^P-Ub^D and Ub^P-*Ub^D except for G76 and R74 which broadened in Ub^D upon the formation of Ub^P-*Ub^D.

Comparison of *Ub^D and Ub^P-*Ub^D spectra indicated that large chemical shift changes occurred in Ub^D for residues in β1 (T7), β2 (G10, I13), the loop between β3 and β4 (G47), β4 (R48, L50), the loop between β4 and α2 (G53), β5 (H68, V70), and the unstructured C-terminus (L73) (Fig 4.7A). Comparison of *Ub^P and *Ub^P-Ub^D spectra demonstrated that large chemical shift changes occur in Ub^P for residues in β1 (T7),

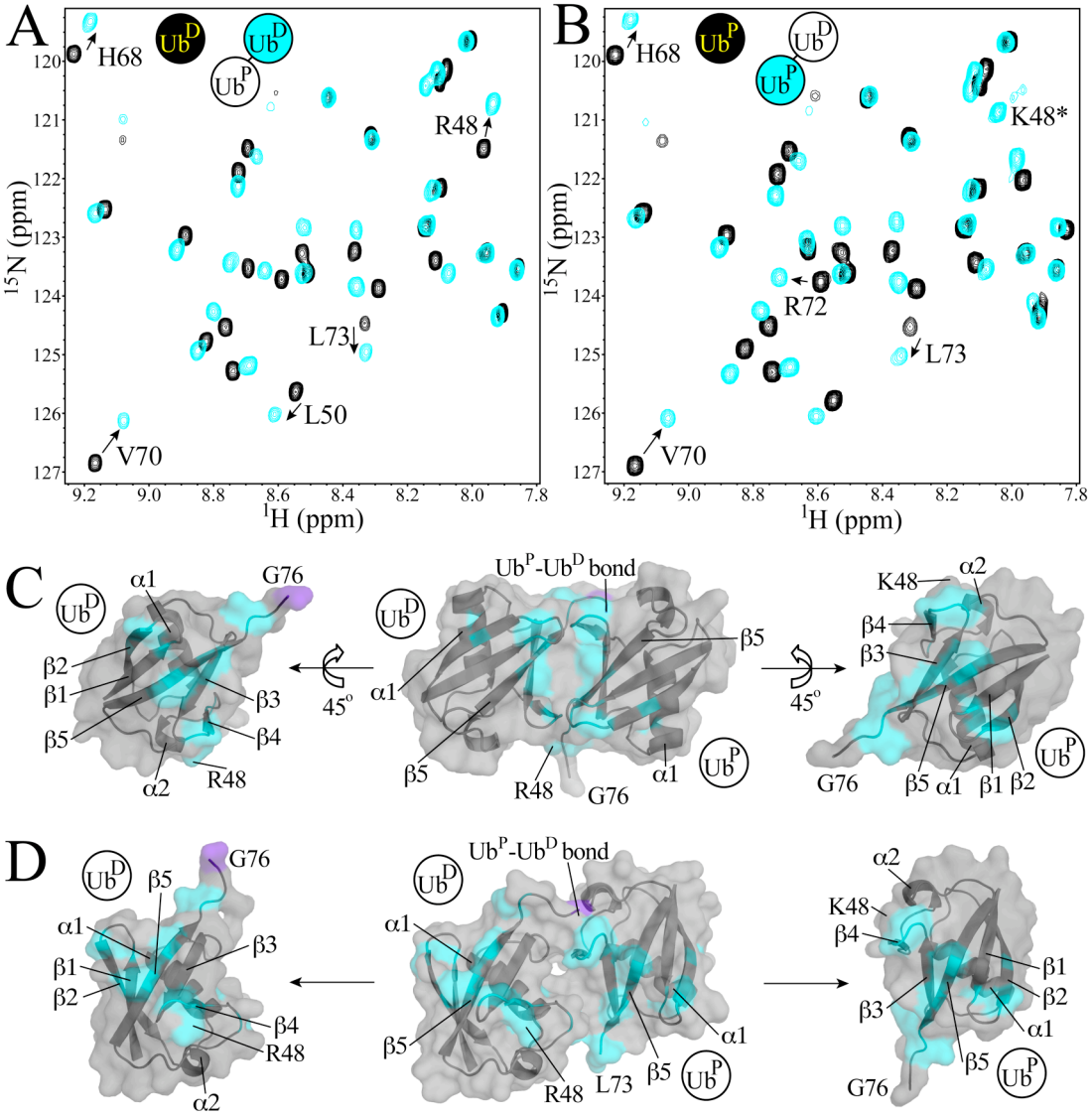

Figure 4.7 Identification of chemical shift changes between Ub^D and Ub^P within Ub_2. (**A**) Expanded region of 600 MHz ^{1}H-^{15}N HSQC spectra displayed for *Ub^D (black) and Ub^P-*Ub^D (cyan). (**B**) Expanded region of 600 MHz ^{1}H-^{15}N HSQC spectra displayed for *Ub^P (black) and *Ub^P-Ub^D (cyan). Signals that undergo significant chemical shift changes (mean + one standard deviation) are labelled by residue and shifts are indicated with arrows. Chemical shift changes are calculated using the equation in 4.2.5, and sample conditions are listed in Section 4.2.4. Ribbon and surface representation for (**C**) a structure for 'closed' Ub^P-Ub^D (PDB: 1AAR) and (**D**) a structure for 'open' Ub^P-Ub^D (PDB: 3AUL). The Ub structure 1UBQ was used to map the interacting residues onto Ub^P and Ub^D. Residues are coloured to indicate residues undergoing significant chemical shift changes (cyan) and residues experiencing significant line broadening (purple). The secondary structure of individual Ub components are fully labelled, while 'open' and 'closed' Ub_2 are only partially labelled. The 'open' Ub_2 is missing residues 74-76 on Ub^P so L73 represents the C-terminus. K48* represents the new isopeptide bond that resembles a backbone amide resonance.

β2 (G10, I13), the loop between β3 and β4 (A46, G47), β4 (R48, L50), the loop between β4 and α2 (G53), β5 (H68, V70, R72), and the unstructured C-terminus (L73) (Fig 4.7B). For both Ub^P and Ub^D, these residues are predominantly located on the same β-sheet of Ub that makes up the classic hydrophobic patch centered on residues L8, I44, and V70. This hydrophobic patch is the main surface utilized by most Ub-binding domains to interact with Ub (*16*). Nearly identical residues in the hydrophobic patch of Ub^P and Ub^D are utilized to interact with each other within the Ub_2 complex. These chemical shift changes are consistent with results obtained by a previous NMR analysis of Ub and Ub_2 (*13*) as well as with the 'closed' Ub_2 conformation observed in the Ub_2 crystal structure (Fig 4.7C) (*17*). This 'closed' conformation was shown to be in equilibrium with an 'open' conformation in solution since relaxation agents can interact with the residues at the buried interface showing they are solvent accessible (*13*). Very recent experimentation has shown the 'open' conformation to be populated approximately 85% of the time (Dr. Kato personal communication). These results indicate that although there are chemical shift changes supporting the presence of a 'closed' Ub_2 structure, this structure is likely populated to a lesser extent than the preferred 'open' state. A structure for this 'open' conformation has been solved in the Kato lab (PDB: 3AUL – personal communication) where the hydrophobic faces of both Ub^P and Ub^D are exposed to solution and point in the same direction (Fig 4.7D). Assuming there is an equilibrium between the 'open' and 'closed' conformation of Ub_2, when the 'open' structure is adopted, the hydrophobic faces of Ub^P and Ub^D would be exposed and accessible for interaction with HIP2 within HIP2-Ub_2.

4.3.10 Distal Ub^D interactions within HIP2-Ub_2

In order to study the distal Ub^D in HIP2-Ub_2, the NMR spectra of Ub^P-*Ub^D was compared to that of the HIP2-Ub^P-*Ub^D complex (Fig 4.8A). Since the size of the compared molecules increases from 17651.7 Da (Ub^P-*Ub^D) to 40184.4 Da (HIP2-Ub^P-*Ub^D), line broadening of signals in the spectra was expected and observed. Comparison of Ub^P-*Ub^D with HIP2-Ub^P-*Ub^D indicates the distal Ub experiences significant chemical shift changes in β1 (T7), the loop between β1 and β2 (L8), β2 (I13, T14), the loop between β4 and α2 (R54), α2 (D58), the loop between α2 and β5 (Q62), β5 (L67, V70), and the unstructured C-terminus (L73) (Fig 4.8B). Significant line broadening was also observed for residues in β3 (I44), β4 (R48, Q49, L50), the loop between β4 and α2 (E51), and β5 (L69, L71) (Fig 4.8B). A significant chemical shift and line broadening of residues on the classic hydrophobic patch of Ub^D indicates that this surface is interacting with HIP2 (Fig 4.8C). Previous analysis of *HIP2-Ub_2 indicated that the hydrophobic MGF patch on the UBA domain of HIP2 was responsible for this interaction. This indicates that the MGF patch of the UBA domain binds to the classic hydrophobic patch of Ub^D in HIP2-Ub_2. The significant line broadening of residues around R48 also indicates that UBA interaction with Ub^D likely blocks accessibility of R48 (naturally K48) to additional protein interactions.

A second observable effect on the distal Ub is the apparent doubling of certain signals. This means that two signals can be observed in relatively close proximity where there used to be a single signal. Two signals were observable for residues in β2 (T14), β3 (L43), the loop between β4 and α2 (R54, T55), α2 (D58, Y59), the loop between α2

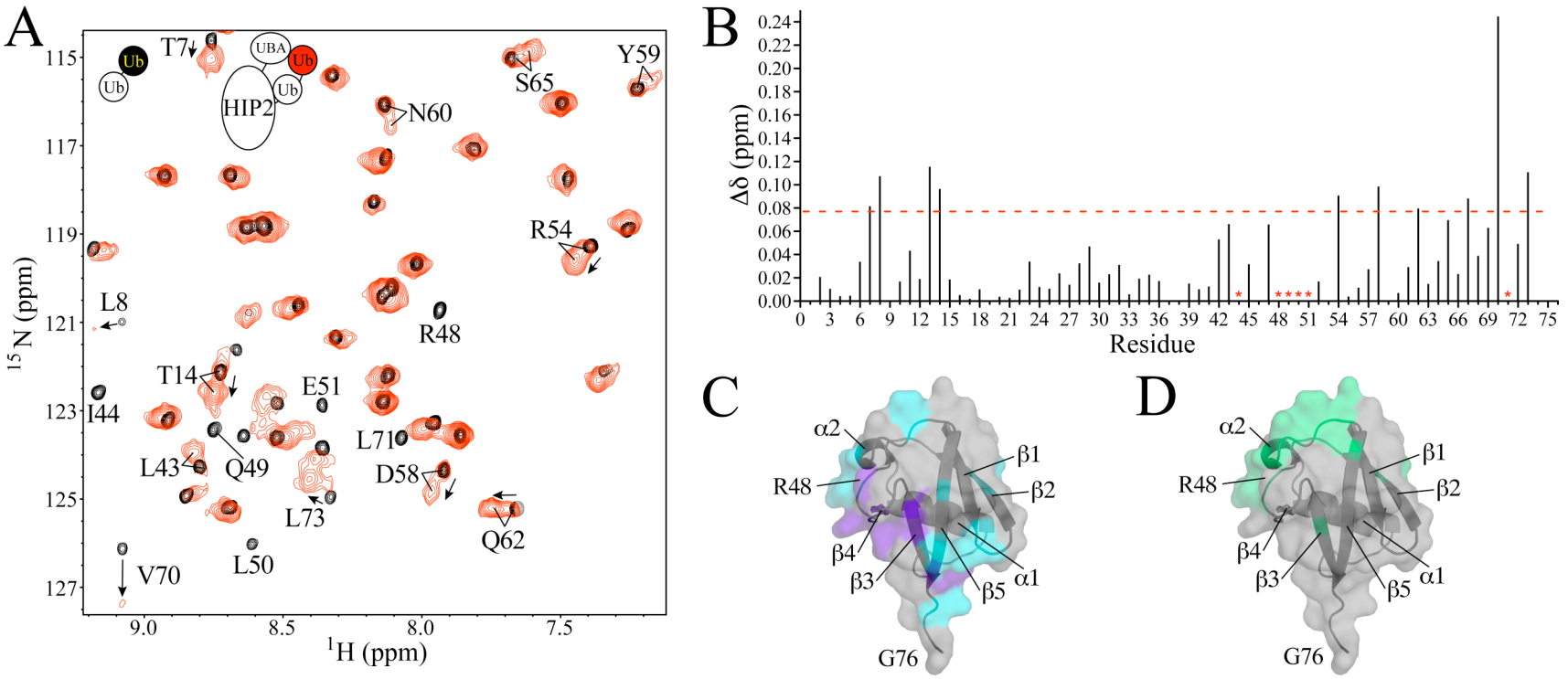

Figure 4.8 Identification of chemical shift changes in Ub^D caused by the formation of HIP2-Ub^P-Ub^D. (**A**) Expanded region of 600 MHz ^{1}H-^{15}N HSQC spectra collected for Ub^P-*Ub^D (black) and HIP2-Ub^P-*Ub^D (red). Signals that undergo significant chemical shift changes (>1 S.D. above the mean) are labelled by residue and shifts are indicated with arrows, signals that experience significant line broadening (disappear) are labelled without arrows, and residues showing signal doubling are indicated with 2 lines. (**B**) Bar graph of chemical shift changes observed between Ub^P-*Ub^D and HIP2-Ub^P-*Ub^D spectra. The dotted line (red) indicates the threshold for significant chemical shift changes (mean + one standard deviation). Chemical shifts are calculated using the equation in 4.2.5. Red asterisks indicate signals that undergo significant line broadening. Ribbon and surface representation of Ub^D coloured for (**C**) residues undergoing significant chemical shift changes (cyan) and residues experiencing significant line broadening (purple) or (**D**) coloured for the presence of signal doubling (green).

and β5 (N60, Q62, K63) and β5 (S65). Most of these 'dual' signals occur with the first signal having no change in chemical shift, and the second signal with a moderate change in chemical shift. These 'dual' signals therefore likely represent an interaction in slow exchange between the Ub^D moiety and a region of HIP2 in HIP2-Ub_2. When mapped onto the surface of Ub^D, the residues associated with the 'dual' signal are all located on the N-terminal side, above the hydrophobic patch centered around α2 (Figure 4.8D). Chemical shift changes between the each set of 'dual' signals were often measured to be insignificant. Therefore, these 'dual' signal surfaces were considered to be a fairly weak interaction. These 'dual' signals were also observed on only a small region (R54-S65) of Ub^D. This region is relatively exposed to solution in both free Ub and in either the 'open' or 'closed' Ub_2 structure and does not overlap with the hydrophobic face of Ub. The lack of observable equivalent signal doubling on HIP2 means the exact complementary interaction surface cannot be confirmed.

When analyzing the data for significant chemical shift changes, the main interaction is clearly on the hydrophobic patch of Ub^D. Therefore, Ub^D likely contacts the MGF hydrophobic region of the UBA domain of HIP2 in HIP2-Ub^P-Ub^D.

4.3.11 Proximal Ub^P Interactions within HIP2-Ub and HIP2-Ub_2

The hydrophobic face of Ub^P was previously identified to interact with Ub^D in the Ub_2 (*Ub^P-Ub^D) complex. In order to study the interactions of Ub^P within HIP2 complexes, the spectra of *Ub^P and *Ub^P-Ub^D were compared to that of HIP2-*Ub^P and HIP2-*Ub^P-Ub^D. Analysis of the labelled Ub^P demonstrated how HIP2 interacts with the surface of Ub^P. This was first accomplished by comparing the *Ub^P spectrum to the HIP2-*Ub^P

spectrum. In this comparison, significant chemical shift changes (>1SD) were observed for residues in β2 (I13), β3 (L43), β4 (K48), and β5 (L67, H68) as well as significant line broadening in the loop between β1 and β2 (L8), β3 (I44), β4 (Q49, L50), β5 (L69-R72), and the unstructured C-terminal residues L73 and G76 (Fig 4.9A). The main conclusion from these results is that the hydrophobic face of Ub clearly rests against the HIP2 core domain upon attachment to the active site of HIP2 (Fig 4.9A – surface diagram). It is interesting that residue K48 is the most highly shifted residue upon single Ub^P attachment to HIP2, as this residue is the key reactive residue in acceptor Ub molecules during poly-Ub chain formation, only this Ub^P represents the donor Ub in poly-Ub chain formation.

Comparison of $*Ub^P$-Ub^D and HIP2-$*Ub^P$-Ub^D was utilized to show how Ub^P in $*Ub^P$-Ub^D was affected through its direct attachment to HIP2. Chemical shift changes were observed for residues in β1 (T7), β3 (R42, I44), the loop between β3 and β4 (G47), β5 (R72), and the unstructured C-terminal L73 (Fig 4.9B). Residues experiencing significant line broadening were observed in β5 (V70, L71) and the unstructured C-terminal G75, G76 (Fig 4.9B). The major changes seen at the C-terminal residues were expected as this is the main attachment point for Ub_2 to the HIP2 core. It is interesting that there are less residues affected at the hydrophobic interface upon Ub_2 attachment to HIP2 (Fig 4.9B) than following attachment of a single ubiquitin to HIP2 (Fig 4.9A). This result indicates that the addition of Ub^D alters the interface between Ub^P and HIP2.

Comparison of HIP2-$*Ub^P$ and HIP2-$*Ub^P$-Ub^D was utilized to show how the attachment of Ub^D affects binding of the proximal Ub^P to the HIP2 catalytic core. Comparison of these spectra resulted in the observation that significant chemical shift

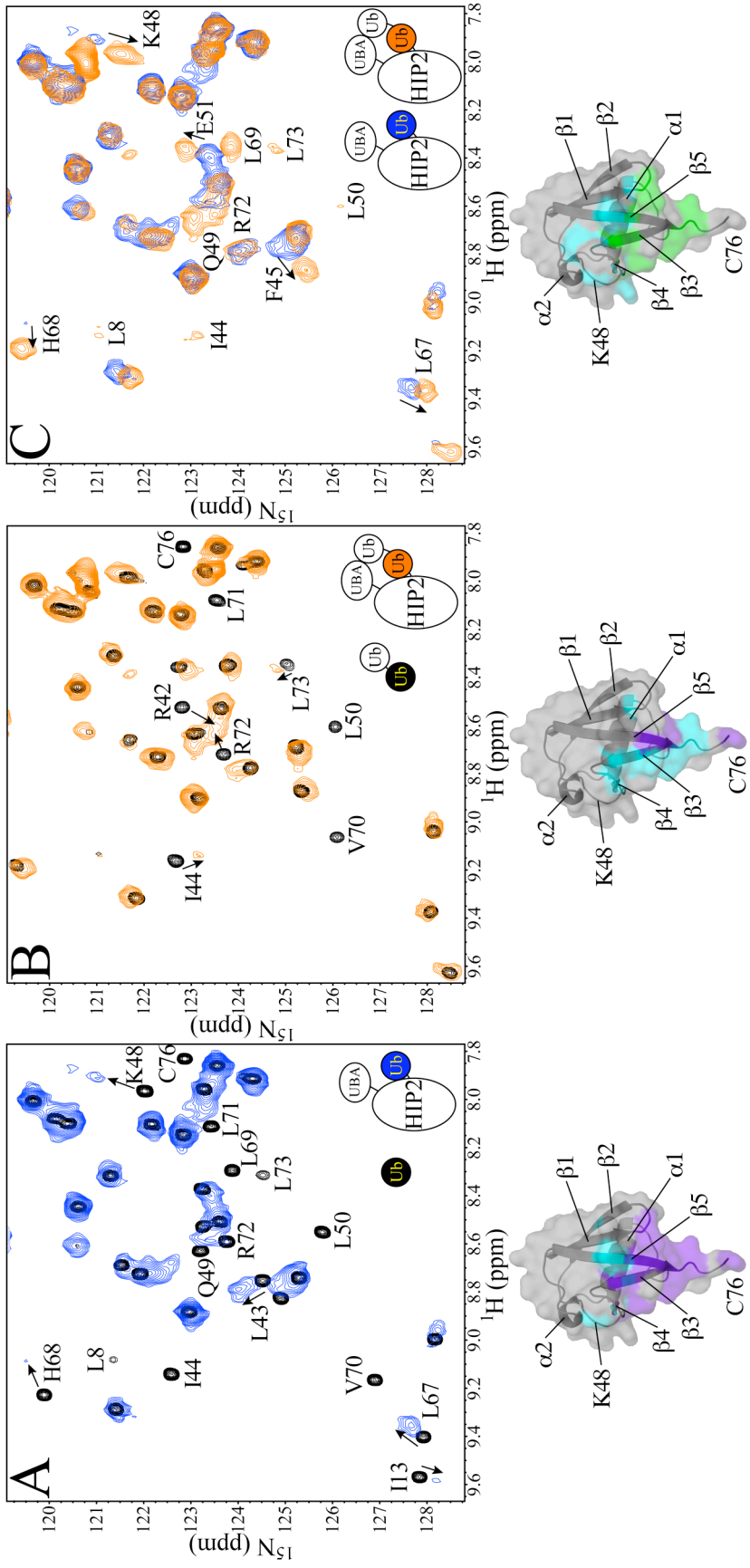

Figure 4.9 Identification of chemical shift changes in Ub^P caused by interaction with HIP2 and Ub^D. (**A**) Expanded region of 600 MHz ^{1}H-^{15}N HSQC spectra collected for $*Ub^P$ (black) and HIP2-$*Ub^P$ (blue). (**B**) Expanded region of 600 MHz ^{1}H-^{15}N HSQC spectra collected for $*Ub^P$-Ub^D (black) and HIP2-$*Ub^P$-Ub^D (orange). (**C**) Expanded region of 600 MHz ^{1}H-^{15}N HSQC spectra collected for HIP2-$*Ub^P$ (blue) and HIP2-$*Ub^P$-Ub^D (orange). Signals that undergo significant chemical shift changes (>1 S.D. above the mean) are labelled by residue and shifts are indicated with arrows, signals that experience significant line broadening (disappear) are labelled without arrows in (**A**) and (**B**), and residues showing signal reappearance are indicated without arrows in (**C**). Ribbon and surface representations of Ub^P are labelled according to secondary structure. Residues are coloured to indicate significant chemical shift changes (cyan), significant line broadening (purple) and signal reappearance (green).

changes are occurring for residues in β1 (T7), β3 (F45), β4 (K48), the loop connecting β4 and α2 (E51), and β5 (L67, H68). The large chemical shift change for K48 is expected on Ub^P as this residue is the attachment site for Ub^D. Significant chemical shift changes are also seen on the N-terminal region of the Ub^P hydrophobic face due to direct contact with Ub^D (Fig 4.9C). Many signals previously line broadened when a single Ub was attached to the HIP2 core were also observed to 'reappear'. These 'reappearing' signals were observed for residues in the loop between β1 and β2 (L8), β3 (I44), β4 (Q49, L50), β5 (L69, R72), and the unstructured C-terminal L73 (Fig 4.9C). These residues are located in the C-terminal region of the Ub^P hydrophobic face showing that this interaction surface that was previously line broadened in HIP2-Ub^P spectra is now visible in the HIP2-Ub^P-Ub^D spectra (Fig 4.9A, C). The cause for the reappearance of signals is likely due to the disruption of protein interactions between HIP2 and Ub^P upon the addition of Ub^D. The resulting Ub^P is therefore less closely associated with the HIP2 core domain.

4.4 Discussion

4.4.1 HIP2 surface involved in interaction with Ub^P

The surface of HIP2 utilized to contact Ub^P was determined by comparing the ^1H-^{15}N TROSY-HSQC spectra of *HIP2 and *HIP2-Ub^P. The residues highly affected in HIP2 upon attachment of Ub^P are located predominantly near the active site cysteine on the catalytic core of HIP2. It is also clear that there are minimal chemical shift changes in the UBA domain of HIP2 upon formation of HIP2-Ub^P. Previous studies support this

observation, as the Ubc1-Ub^P disulphide also shows no contacts between Ub^P and the UBA domain (*2*). Although free Ub has been shown to interact with the UBA domain of HIP2 in solution (*10, 11, 18*), an interaction between the UBA domain and covalently bound Ub in HIP2-Ub^P does not occur (Fig 4.10A).

Models of E2-Ub have been developed for Ubc1-Ub (*20*), and UbcH8-Ub (*19*), and structures have been presented for hUbc13-Ub (*21*), and UbcH5b-Ub (*22, 23*). The positioning of Ub is different for each E2 enzyme. Recent experiments with Ubc13-Ub and UbcH5b-Ub have shown the covalently attached Ub to be highly mobile, indicating the Ub molecule likely does not adopt a single conformation on the surface of these E2 enzymes (*24*). Therefore, the high-resolution models and structures of all E2-Ub complexes may represent 'snap shots' showing a preferential position of an otherwise highly mobile attached Ub that can adopt several orientations when bound to an E2. The interaction surface for Ub on the HIP2 catalytic core seems to include residues radiating out in all directions from the attachment point of C92. No single Ub position can account for all of these chemical shift changes and line broadening signals. This indicates that Ub^P may be sampling various bound positions on the HIP2 core (Fig 4.10A). The missing signals from significantly line broadened residues (I91-D98) may actually represent the strongest interaction surface between HIP2 and Ub^P. Signal broadening may be the result of intermediate exchange between the bound and the unbound position of Ub on HIP2, which could indicate that these residues at the active site and in the 'active site helix' represent the main contact surface between HIP2 and Ub^P in HIP2-Ub^P.

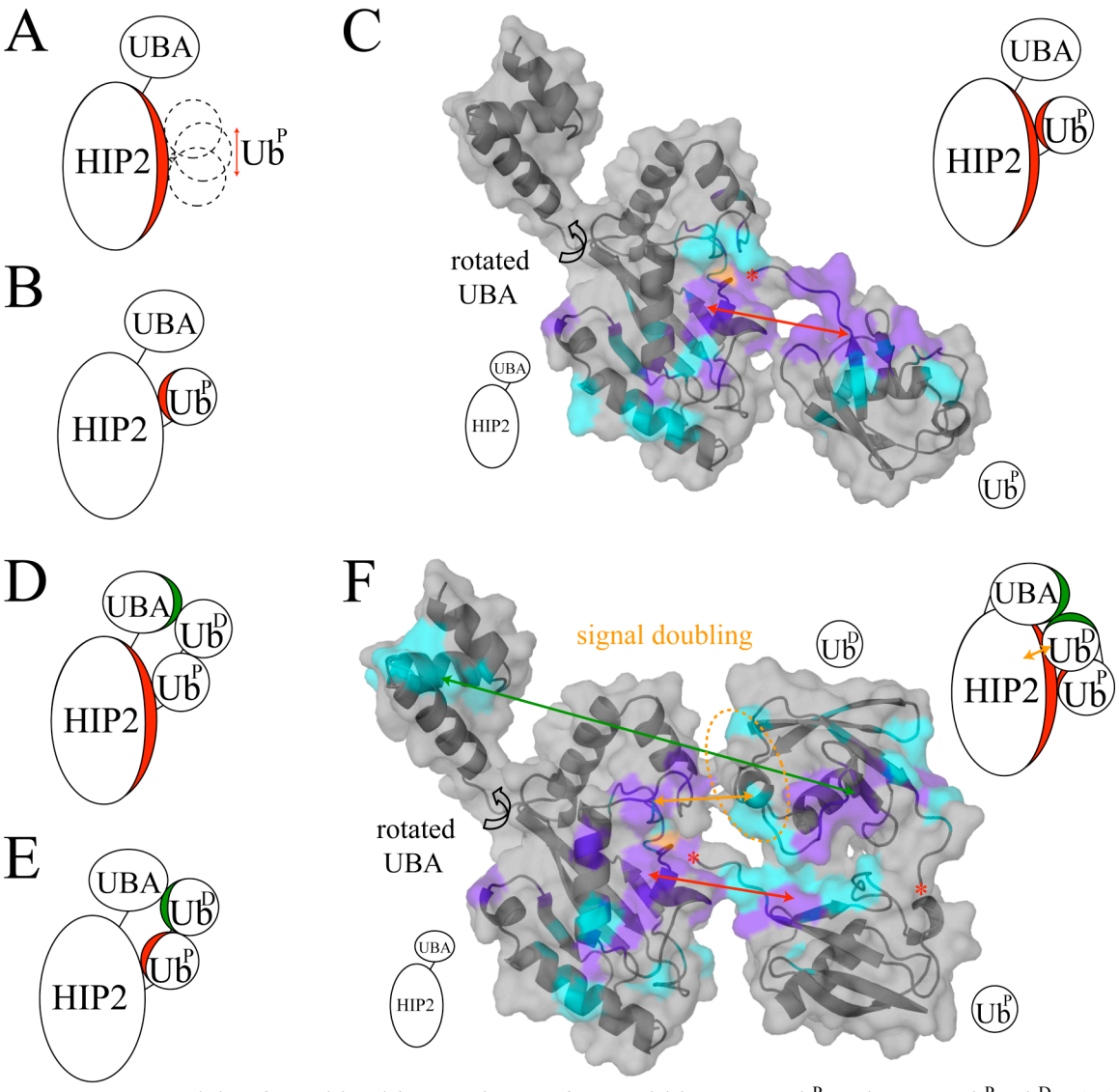

Figure 4.10 Models of combined interaction surfaces within HIP2-Ub^P and HIP2-Ub^P-Ub^D. (**A**) Model of *HIP2-Ub^P indicating interactions on HIP2. (**B**) Model of HIP2-*Ub^P indicating interactions on Ub^P. (**C**) Combined model of HIP2-Ub^P indicating interactions between HIP2 and Ub^P derived from interactions shown in (**A**) and (**B**). (**D**) Model of *HIP2-Ub^P-Ub^D indicating interactions on HIP2 upon addition of Ub_2. (**E**) Model of HIP2-Ub^P-Ub^D indicating surfaces on Ub^P and Ub^D that are affected by interaction with HIP2 derived from *Ub^P-Ub^D versus HIP2-*Ub^P-Ub^D and Ub^P-*Ub^D versus HIP2-Ub^P-*Ub^D. (**F**) Combined model of HIP2-Ub^P-Ub^D derived from interactions observed in (**D**) and (**E**). Models in (**D**) and (**E**) are depicted simplistically, while the slightly altered model in (**F**) is depicted to better represent protein positioning. The UBA domain was rotated to visualize the hydrophobic patch. Ribbon and surface representations are based on previous structures of HIP2-Ub^P (HIP2 PDB:1YLA with altered UBA positioning and PDB:2GMI for Ub^P positioning to match Ubc13~Ub) and HIP2-Ub^P-Ub^D (PDB:3AUL bound manually to HIP2). Residues are coloured for the active site cysteine (orange), significant chemical shift changes (cyan), and significant line broadening (purple). Shaded area of simplistic models indicates interaction surfaces and two sided arrows in ribbon models are coloured identically to indicate these interaction surfaces. The orange arrow and circled region in (**F**) indicates the region of Ub^D that undergoes signal doubling and the probable region of the HIP2 catalytic core that interacts with Ub^D.

Previous experiments with the Ubc1Δ~Ub thiolester (no UBA) indicates Ub interacts with Ubc1Δ α2 helix and is the basis of the 'compact' E2-Ub model (*20*). The results on HIP2 show α2 to be less affected upon Ub^P attachment, indicating a HIP2-Ub^P structure likely would not be identical to the previously reported structure for Ubc1-Ub^P.

Recent studies on Ubc1 found that residues T84 and Q122 were instrumental in poly-Ub chain formation (*25*). The equivalent residues in HIP2, T88 and Q126, undergo either a significant chemical shift (T88) or significant line broadening (Q126) upon Ub^P attachment. This demonstrates that these residues are affected by the attachment of a disulphide bound Ub at the active site. This may indicate these residues are important for the correct positioning of the thiolester bound Ub to aid in poly-ubiquitination activity.

4.4.2 Ub^P surface involved in interaction with HIP2

Comparison of the ^1H-^{15}N HSQC spectra of *Ub^P and HIP2-*Ub^P indicates that the hydrophobic patch on Ub^P binds to the HIP2 catalytic core domain. This interaction was observed through the extreme line broadening of signals from residues on the hydrophobic patch of Ub^P, and confirms the corresponding interaction surface observed around the HIP2 active site (Fig 4.10B). The combined interaction surfaces between HIP2 and Ub^P are depicted in Figure 4.10C whereby the HIP2-Ub^P structure was built by alignment to the Ubc13-Ub structure. This structure is consistent with SAXS data (Chapter 2) indicating that it best represents the average position of Ub within HIP2-Ub^P. It is clear that the Ub^P depicted in Figure 4.10C must undergo a rotation to bury its exposed yet interacting hydrophobic patch, while retaining the same general Ub position to agree with the average SAXS structure. Although Figure 4.10C represents a 'snap

shot' of the average HIP2-Ub^P structure, Ub^P may be mobile allowing for a mixture of elongated and compact structures. A highly mobile Ub^P may transiently bind to several locations on HIP2, which may explain why the interaction surface on HIP2 is located both above and below the Ub^P attachment point (Fig 4.4C). The severe line broadening in select residues is likely due to intermediate exchange between the association and dissociation of Ub^P with the catalytic core of HIP2. Intermediate exchange is consistent with a highly mobile Ub in HIP2-Ub^P that could oscillate between an unbound and at least one bound position for Ub^P.

The hydrophobic patch on Ub^P has been shown to be affected by attachment to other E2 enzyme catalytic cores from Ubc1 (*20*), Ubc13 (*24*), Ubc2b (*26*), and Ube2S (*27*). However, the hydrophobic surface of Ub is not always utilized in E2-Ub contacts. For example, UbcH8 utilizes a different contact surface on Ub^P (*19*), and UbcH5c does not seem to bind Ub^P (*14, 15*). Thus, HIP2 associates with the hydrophobic face of Ub^P while some other E2 enzymes do not. Regardless of high mobility, differences in preferred Ub orientations in E2~Ub thiolester structures may play a role in E3 ligase and substrate specificity by presenting alternate available interaction surfaces on various E2~Ub structures.

4.4.3 HIP2 UBA binds Ub^D

The surface of HIP2 utilized to contact Ub_2 was determined by comparing the ^1H-^{15}N TROSY-HSQC spectra of *HIP2 and *HIP2-Ub^P-Ub^D. Additional changes in HIP2 were observed with the addition of Ub^D. Some chemical shift changes were observed around the active site, but the most significant changes occurred in residues that form a

hydrophobic patch (M172, G173, F174 and V190) on the UBA domain of HIP2. The importance of this MGF hydrophobic patch is demonstrated by the high conservation of this sequence across many UBA domain alignments (*28*). Recent studies on HIP2 show this hydrophobic patch (M172-F174, V190, T194, L198) on the UBA domain binds free Ub (*11, 18*). This result indicates the UBA hydrophobic patch used to bind free Ub in solution is also used to contact Ub^D in a covalently attached HIP2-Ub_2 complex (Fig 4.10D). Ubc1 was also observed to bind free Ub through the UBA domain utilizing the similar QGF residues in the loop between α5 and α6 as well as many residues in α7 (*12*). HIP2 binding to free Ub also involved some α7 residues (T194, L198) (*11*). These residues in α7 that interact with free Ub were not seen to interact with Ub^D of the HIP2-Ub^P-Ub^D construct. The lack of full interaction of the UBA α7 residues with Ub^D may be due to intramolecular steric constraints within the HIP2-Ub_2 complex that allows only a limited surface of the UBA to contact the Ub^D.

Previous experiments with a similar UBA2 domain from hHR23A demonstrated UBA binding to free K48-linked Ub_2 chains (*13*). This UBA2 binding to Ub_2 utilized the end of α2 (α6 in HIP2) and most of α3 (α7 in HIP2) to simultaneously contact both the proximal and distal Ub (*13*). The HIP2 UBA domain has also been shown to bind Ub_2 chains more strongly than a single Ub moiety and thus may bind Ub_2 through the same residues used with UBA2 (*10*). In HIP2-Ub_2, however, very few chemical shift changes in the UBA domain were observed to match the pattern of Ub_2 binding identified in the hHR23A UBA2 domain (*13*). These results indicate that the UBA domain does not position itself in a similar fashion to bind both Ub^P and Ub^D in HIP2-Ub^P-Ub^D as it likely

could with free Ub_2. This is likely the result of intramolecular steric constraints that do not allow Ub^P to contact the UBA domain.

Residue N177 at the beginning of α6 was also affected upon Ub^D attachment, but faces the opposite direction of the hydrophobic patch. This residue was not observed in binding to free Ub or Ub_2 in the UBA2 domain of hHR23A (*13*), to free Ub in Ubc1 (*12*), or to free Ub in the HIP2 UBA domain (*11*). N177 therefore represents a novel interaction point in the HIP2-Ub_2 complex, and its shifting cannot be explained by comparison to other UBA-Ub interactions. It is not immediately apparent what region of the HIP2-Ub_2 complex contacts UBA domain residue N177.

4.4.4 HIP2-Ub_2 does not dimerize

The HIP2 UBA domain has been shown to bind Ub (*11, 18*), and poly-Ub chains with even higher affinity (*10*). These interactions clearly allow for the possibility that two HIP2-Ub_2 thiolesters could homodimerize. However, sedimentation equilibrium results indicated HIP2-Ub_2 had very little tendency to oligomerize in solution. Oligomerization has previously been seen with the UbcH5c-Ub complex that resulted in a completely line broadened NMR spectrum (*14, 15*). The NMR spectrum of HIP2-Ub_2 did not show similar line broadening of all signals indicating that oligomerization does not occur. The mechanism of a UBA driven dimerization is not favoured by the observation that intramolecular contacts occlude the Ub hydrophobic patch within the HIP2-Ub and HIP2-Ub_2 complexes. In HIP2-Ub^P, the hydrophobic surface of Ub^P interacts with the catalytic core of HIP2 and is not easily accessible to the UBA domain of another HIP2 enzyme. Upon formation of HIP2-Ub^P-Ub^D, the UBA domain involves

itself in an intramolecular interaction with the Ub^D. These uni-molecular interactions are likely to be much stronger than a bi-molecular interaction and thus association between different HIP2 molecules (dimerization) is not preferred. Extrapolating from these results, it is expected that the UBA domain will also bind longer chains attached to the E2 enzyme and thus UBA driven dimerization of HIP2 should not be favoured regardless of covalently attached poly-Ub chain length. This knowledge further supports the conclusion that HIP2 poly-Ub chain activity functions in a monomeric fashion as was suggested in Chapter 2. Since no E3 ligase was used in these studies, E3 assisted dimerization of HIP2 cannot be ruled out as a possible function of this enzyme *in vivo*.

4.4.5 The hydrophobic face of Ub^D binds the HIP2 UBA domain

Analysis of the *HIP2-Ub_2 complex indicated that the hydrophobic MGF patch on the HIP2 UBA domain was significantly affected upon addition of Ub^D (Fig 4.10D). Investigation of *Ub^D in the same HIP2-Ub_2 complex identified chemical shift changes involving residues on the classic hydrophobic patch of *Ub^D indicating that this surface was reciprocally affected within this complex (Fig 4.10E). These results indicate that the MGF patch on the HIP2 UBA domain directly interacts with the hydrophobic patch on Ub^D within the HIP2-Ub_2 complex (Fig 4.10F – green shaded areas and arrow). These same interaction surfaces used between Ub^D and the UBA were previously identified upon interaction of free Ub with the HIP2 UBA domain (*11, 18*). This indicates that Ub^D is bound by the UBA in the same manner to which it would interact with free Ub.

In order to allow the UBA domain to contact Ub^D within the HIP2-Ub_2 complex, the hydrophobic face of Ub^D must be exposed. This would only be possible when Ub_2

adopts the 'open' structure allowing for the hydrophobic patch of both Ub^P and Ub^D to be available for interactions with HIP2 (Fig 4.10F). Due to the complex nature of the interactions involving numerous protein species, computational modelling of HIP2-Ub_2 was not performed. However, visual depiction of the protein interaction surfaces are detailed in Figure 4.10F by manual alignments of Figure 4.10C and the 'open' Ub_2 structure. Figure 4.10F should be treated as a visual aid only, and rotation of these proteins to bury the interaction surfaces indicated by double-sided arrows to form a more globular structure likely represents the true form of the HIP2-Ub_2 complex. Visual interpretation of interaction surfaces and use of the 'open' Ub_2 structure appears to place Ub^D above the loop between α2 and α3 on the HIP2 catalytic core (Fig 4.10F). This leaves the N-terminal 'dual' signal surface of Ub^D pointing towards the loop between α2 and α3 on HIP2 (Fig 4.10F – orange arrow), while the UBA domain would interact with the hydrophobic face of Ub^D (Fig 4.10F – green arrow). The N-terminal 'dual' signal region of Ub^D was observed to experience a slow exchange between Ub^D and an unknown region of HIP2 in HIP2-Ub_2. Since many residues in the loop between α2 and α3 on HIP2 were affected upon addition of Ub^D, it is likely that this region contacts the N-terminal 'dual' signal region of Ub^D, although this is only an assumption since equivalent signal doubling was not observed in the HIP2 spectrum (Fig 4.10F – orange arrow and circled region).

The structure of the Ub_2 moiety has been shown to be in equilibrium between the 'open' and 'closed' structures. The incorporation of the 'closed' structure of Ub_2, cannot be fully discounted but appears unlikely. If the HIP2-Ub_2 complex utilized the 'closed' structure of Ub_2, this would leave the UBA domain to interact weakly through an on and

off binding equilibrium to the exposed N-terminal region of Ub^D presumably causing signal doubling in Ub^D. The chemical shift changes and line broadening observed for residues on the buried hydrophobic patch on Ub^D upon attachment of Ub_2 to HIP2 would then be due to a slight rearrangement of Ub^D on the face of Ub^P. This binding mode is unlikely as the highly affected MGF residues in the UBA domain appear significantly shifted and contain no trace of equivalent signal doubling, as would be expected if this region were oscillating between Ub^D bound and unbound states. It is therefore more likely that the weak signal doubling involves a weak interaction between Ub^D and HIP2 within HIP2-Ub_2. This interaction on Ub^D aligns quite nicely with the additional line broadened signals observed on HIP2 within HIP2-Ub_2 (Fig 4.5C, orange arrow in 4.10F).

4.4.6 Ub^P interaction with HIP2 is altered within HIP2-Ub_2

Analysis of Ub^P within HIP2-Ub_2 is complicated in that there are several sub-complexes to be compared to fully understand the interacting proteins. These complexes include both Ub^P-Ub^D and HIP2-Ub^P compared to HIP2-Ub^P-Ub^D allowing for the identification of individual contacts from HIP2 and Ub^D on Ub^P. The spectral comparison of *Ub^P-Ub^D and HIP2-*Ub^P-Ub^D indicates that only the C-terminal residues of Ub^P are affected following attachment of Ub_2 to HIP2. The presence of Ub^D has significantly altered the interaction between HIP2 and Ub^P such that the full hydrophobic patch of Ub^P no longer interacts with HIP2 to yield highly line broadened signals (Fig 4.10B, C versus Fig 4.10E, F – focus on Ub^P surface changes). The weakening of the HIP2 interaction with Ub^P must be caused by either the steric strain of the UBA

interaction with Ub^D, or the simple steric strain caused by the presence of Ub^D that interferes with the HIP2-Ub^P interacting surfaces.

The spectral comparison of HIP2-*Ub^P and HIP2-*Ub^P-Ub^D indicates the effects that addition of Ub^D will have on HIP2-Ub^P. The N-terminal region of the Ub^P hydrophobic face undergoes chemical shift changes due to direct contact with Ub^D. Residues in the C-terminal region of the Ub^P hydrophobic face that were previously line broadened in HIP2-Ub^P were observed to reappear in the spectrum upon addition of Ub^D (Fig 4.10C versus Fig 4.10F – purple signals change to cyan). This reappearance is significant as the size of the molecule is larger and thus increased signal decay would be expected to cause weaker signals, not stronger signals. Increased signal intensities also cannot be explained by differences in protein concentration, as the larger complex is less concentrated than the smaller complex (433 μM HIP2-*Ub^P, 325 μM HIP2-*Ub^P-Ub^D). These results may show that the Ub^P residues are no longer strongly associated with the HIP2 catalytic core domain upon the addition of Ub^D, or it may show that Ub^P no longer samples various bound positions against the HIP2 catalytic core within HIP2-Ub^P-Ub^D.

4.4.7 HIP2-Ub^P and HIP2-Ub_2 model analysis

The ribbon/surface structures depicted for HIP2-Ub^P and HIP2-Ub_2 were developed to aid in visualizing the interaction surfaces (Figure 4.10C, F). SAXS analysis has indicated the structure in Figure 4.10C accurately represents the general shape of HIP2-Ub^P in solution (Chapter 2). This structure shows Ub^P to be fully exposed to solution, but line broadening for the residues on the hydrophobic face of Ub^P and HIP2 indicate these residues are at least transiently interacting (Fig 4.10C). The association of

the HIP2 catalytic core and the hydrophobic surface of Ub^P indicates that Ub^P is at least intermittently blocked from other protein interactions.

The HIP2-Ub_2 structure was constructed through manual alignment of HIP2 (PDB: 1YLA with 'relaxed' UBA position) and the 'open' structure of Ub_2 (PDB: 3AUL). The position of Ub^P within Ub_2 was aligned to that of HIP2-Ub^P depicted in Figure 4.10C. This HIP2-Ub_2 structure is shown only for illustrative purposes (Fig 4.10F), and the true structure likely adopts a much more compact form whereby the HIP2 UBA domain is in contact with Ub^D altering the position of the Ub_2 to create a more globular structure.

4.4.8 Occlusion of K48 within HIP2-Ub^P and HIP2-Ub_2

Upon analysis of HIP2-*Ub^P, it is interesting that residue K48 on Ub^P experiences the most significant chemical shift following attachment to HIP2. Residue R48 was correspondingly seen to shift significantly in the E2-Ub complex of Ubc1, the yeast homolog of HIP2 (*20*). This result likely indicates that the K48 residue on a thiolester bound Ub would be buried on the surface of HIP2 and not be available to serve as an acceptor Ub in chain elongation. Alternatively, this large chemical shift change occurs on the edge of the interaction interface, which could indicate an increased acceptor reactivity of residue K48. The use of HIP2~Ub as a Ub acceptor would require another HIP2~Ub as the Ub donor. A poly-ubiquitination reaction using HIP2-Ub^P as an acceptor was observed to proceed forming HIP2-Ub_2 when no other acceptors were supplied (Chapter 2). This reaction would require a dimeric HIP2 mechanism. The HIP2-Ub/HIP2-Ub association was measured to have a dimerization K_d >1000 μM, while

HIP2 UBA association with Ub and Ub_4 was reported to have a K_d of 400 μM and 155 μM respectively (Chapter 2) (*10*). These results indicate that the HIP2~Ub thiolester (Ub donor) preferably binds free Ub or poly-Ub chains as acceptors as opposed to the HIP2-Ub complex. The reason the HIP2-Ub complex makes a poor Ub acceptor may be related to the hydrophobic surface of Ub interacting with the HIP2 catalytic core. This interaction would make the surface on Ub within HIP2-Ub less accessible to interact with the UBA domain of a second HIP2~Ub thiolester (Ub donor). HIP2-Ub likely still reacts as a Ub acceptor (Chapter 2) due to a mobile Ub^P that can expose its hydrophobic surface and K48 residue. When HIP2-Ub is in its extended (exposed Ub) form the Ub can act as a Ub acceptor by interacting with the UBA domain of another HIP2~Ub thiolester driving poly-Ub chain extension. These results indicate that the large chemical shift in K48 of Ub^P within HIP2-Ub^P is likely based on occlusion of the K48 residue due to it being predominantly buried as opposed to increasing its reactivity as a Ub acceptor.

Upon analysis of HIP2-Ub^P-*Ub^D, significant line broadening of residues I44, R48, Q49, L50 and E51 indicates that the UBA interaction with Ub^D involves direct contacts of R48 (normally K48). Recent experiments examining the UBA domain of HIP2 binding to free Ub showed residues I44, K48 and Q49 to be highly affected (*11, 18*), but residues L50 and E51 were minimally affected. In contrast, L50 and E51 were completely line broadened in UBA binding to Ub^D within HIP2-Ub^P-Ub^D. These results indicate that while residue K48 is on the edge of the interaction surface between free Ub and the UBA domain, it is likely more buried on the interaction between the UBA and Ub^D. The occlusion of K48 on Ub^D within HIP2-Ub_2 would block Ub^D as an acceptor Ub in chain elongation. The blockage of K48 in both HIP2~Ub and HIP2~Ub_2 thiolesters

would make these intermediates act poorly as Ub acceptors for poly-Ub chain extension. The predominantly buried K48 residues should make HIP2~Ub and HIP2~Ub_2 thiolesters act only as Ub donors in poly-Ub chain extension. Previous experiments with the E2 enzyme Ube2g2 have shown that E3 ligase dimerization leads to proposed dimerization of Ube2g2 responsible for active site linked poly-Ub chain formation (*29*). A similar E3 induced dimerization of HIP2-Ub and/or HIP2-Ub_2 complexes is unlikely to aid poly-Ub chain formation as long as the Ub K48 residues remain occluded. These results indicate E3 assisted dimerization is unlikely for HIP2, although this possibility cannot be completely excluded.

4.4.9 HIP2-Ub_2 models can rationalize previous activity assays on Ubc1

The HIP2 UBA domain blockage of K48 residues in Ub^D within HIP2-Ub_2 can be used to explain previous studies investigating auto-ubiquitination of Ubc1 where UBA removal resulted in increased poly-Ub chain length (*30*). In this study, poly-Ub chain activity of wild type Ubc1 was measured through auto-ubiquitination on residue K93 that likely forms through the direct transfer of Ub from the active site C88 to the nearby K93 residue. This auto-ubiquitinated Ubc1 likely undergoes chain extension with Ubc1-K93-Ub acting as a Ub acceptor through a reactive Ub K48 residue. Experiments on full length Ubc1 resulted in K93 attached poly-Ub chains of roughly four Ub's in length, while Ubc1Δ (Ubc1 with no UBA domain) produced much longer poly-Ub chains up to 12 Ub's in length (*30*). On the assumption that the UBA domain in Ubc1 behaves similarly to the UBA domain in HIP2, once Ubc1 has a chain of Ub_2 or longer, the UBA domain should interact with Ub^D and at least temporarily occlude K48 resulting in the

blocking of chain extension. Removal of the UBA domain would increase the exposure of K48 residues making the attached poly-Ub chains better Ub acceptors and therefore increasing the resultant chain length of auto-ubiquitination of Ubc1. The purpose of auto-ubiquitination of Ubc1 remains unknown, and the long reaction time (16 hours) may indicate this activity is not biologically significant, but the model for HIP2-Ub_2 indicating the K48 residue in Ub is occluded can be used to rationalize the experimental results for Ubc1. These results show that the Ubc1 UBA domain inhibits poly-Ub chain extension by blocking the terminal Ub. It is therefore reasonable to assume that the Ubc1 UBA domain likely behaves in a similar manner to the HIP2 UBA domain, as both enzymes likely block Ub K48 residues in thiolester attached poly-Ub chains.

4.4.10 Conclusions

HIP2 can produce unanchored K48-linked poly-Ub chains in solution using only the E1 activating enzyme and ubiquitin (Ub) (*1*). The biological significance of unanchored chain building by HIP2 remains unknown, but the observation that Ub_2 can be loaded onto HIP2 just as easily as Ub indicates these chains can be used to create HIP2~Ub and HIP2~Ub_2 thiolesters and probably HIP2~Ub_n thiolesters (*1*). These intermediates can form *in vitro* but their presence *in vivo* is unconfirmed. These observations are consistent with a poly-Ub chain preassembly mechanism for the labelling of protein substrates. The NMR investigation of HIP2~Ub and HIP2~Ub_2 thiolester mimics has led to a better understanding of the structure of these intermediates. It has been observed that there is a significant interaction between HIP2 and Ub within the HIP2-Ub^P complex. It was also observed that the UBA domain contacts Ub^D within

the HIP2-Ub^P-Ub^D complex. These interactions have resulted in the Ub K48 residues being occluded in these structures. This indicates that HIP2~Ub and HIP2~Ub_2 intermediates should act preferably as Ub donors for poly-Ub chain extension.

The intramolecular interaction of UBA/Ub^D within HIP2-Ub_2 would make the UBA domain less available for interaction with Ub acceptors. If the UBA domain drives poly-Ub chain assembly by affinity to Ub acceptors, then the HIP2-Ub_2 would be resistant to continued poly-Ub chain extension since the UBA is blocked. The intramolecular UBA/Ub^D interaction also explains why HIP2-Ub_2 was observed to be predominantly monomeric, as the HIP2~Ub_2 molecule would have neither the UBA hydrophobic surface nor the Ub^D hydrophobic surface available for interactions with another HIP2-Ub_2. The HIP2 N-terminal region in HIP2-Ub_2 is still available for interaction with both E1 and E3 enzymes in these structures. The available E1 and E3 interaction could allow a HIP2~Ub_n intermediate to connect Ub_n to a substrate through the standard E1-E2-E3 enzyme cascade. The biological presence of E2~Ub_n thiolesters is unknown, although the ability of the HIP2 UBA domain to interact with thiolester attached poly-Ub chains will aid in the clarification of HIP2 functional mechanisms.

Bibliography

1. Chen, Z., and Pickart, C. M. (1990) A 25-kilodalton ubiquitin carrier protein (E2) catalyzes multi-ubiquitin chain synthesis via lysine 48 of ubiquitin, *J Biol Chem 265*, 21835-21842.

2. Merkley, N., Barber, K. R., and Shaw, G. S. (2005) Ubiquitin manipulation by an E2 conjugating enzyme using a novel covalent intermediate, *J Biol Chem 280*, 31732-31738.

3. Pickart, C. M., and Raasi, S. (2005) Controlled synthesis of polyubiquitin chains, *Methods Enzymol 399*, 21-36.

4. Kay, L. E., Keifer, P., and Saarinen, T. (1992) Pure Absorption Gradient Enhanced Heteronuclear Single Quantum Correlation Spectroscopy with Improved Sensitivity, *Journal of the American Chemical Society 114*, 10663-10665.

5. Grzesiek, S., and Bax, A. (1992) An efficient method for sequential backbone assignment of medium-sized isotopically enriched proteins, *J. Magn. Reson. 99*, 201-207.

6. Pervushin, K., Riek, R., Wider, G., and Wuthrich, K. (1997) Attenuated T2 relaxation by mutual cancellation of dipole-dipole coupling and chemical shift anisotropy indicates an avenue to NMR structures of very large biological macromolecules in solution, *Proc Natl Acad Sci U S A 94*, 12366-12371.

7. Shuker, S. B., Hajduk, P. J., Meadows, R. P., and Fesik, S. W. (1996) Discovering high-affinity ligands for proteins: SAR by NMR, *Science 274*, 1531-1534.

8. Haldeman, M. T., Xia, G., Kasperek, E. M., and Pickart, C. M. (1997) Structure and function of ubiquitin conjugating enzyme E2-25K: the tail is a core-dependent activity element, *Biochemistry 36*, 10526-10537.

9. Hamilton, K. S., Ellison, M. J., and Shaw, G. S. (2000) Identification of the ubiquitin interfacial residues in a ubiquitin-E2 covalent complex., *J. Biomol. NMR 18*, 319-327.

10. Raasi, S., Varadan, R., Fushman, D., and Pickart, C. M. (2005) Diverse polyubiquitin interaction properties of ubiquitin-associated domains, *Nat Struct Mol Biol 12*, 708-714.

11. Ko, S., Kang, G. B., Song, S. M., Lee, J. G., Shin, D. Y., Yun, J. H., Sheng, Y., Cheong, C., Jeon, Y. H., Jung, Y. K., Arrowsmith, C. H., Avvakumov, G. V., Dhe-Paganon, S., Yoo, Y. J., Eom, S. H., and Lee, W. (2010) Structural basis of E2-25K/UBB+1 interaction leading to proteasome inhibition and neurotoxicity, *J Biol Chem 285*, 36070-36080.

12. Merkley, N., and Shaw, G. S. (2004) Solution structure of the flexible class II ubiquitin-conjugating enzyme Ubc1 provides insights for polyubiquitin chain assembly, *J Biol Chem 279*, 47139-47147.

13. Varadan, R., Assfalg, M., Raasi, S., Pickart, C., and Fushman, D. (2005) Structural determinants for selective recognition of a Lys48-linked polyubiquitin chain by a UBA domain, *Mol Cell 18*, 687-698.

14. Brzovic, P. S., Lissounov, A., Christensen, D. E., Hoyt, D. W., and Klevit, R. E. (2006) A UbcH5/ubiquitin noncovalent complex is required for processive BRCA1-directed ubiquitination, *Mol Cell 21*, 873-880.

15. Brzovic, P. S., and Klevit, R. E. (2006) Ubiquitin transfer from the E2 perspective: why is UbcH5 so promiscuous?, *Cell Cycle 5*, 2867-2873.

16. Dikic, I., Wakatsuki, S., and Walters, K. J. (2009) Ubiquitin-binding domains - from structures to functions, *Nat Rev Mol Cell Biol 10*, 659-671.

17. Cook, W. J., Jeffrey, L. C., Carson, M., Chen, Z., and Pickart, C. M. (1992) Structure of a diubiquitin conjugate and a model for interaction with ubiquitin conjugating enzyme (E2), *J Biol Chem 267*, 16467-16471.

18. Wilson, R. C., Edmondson, S. P., Flatt, J. W., Helms, K., and Twigg, P. D. (2011) The E2-25K ubiquitin-associated (UBA) domain aids in polyubiquitin chain synthesis and linkage specificity, *Biochem Biophys Res Commun 405*, 662-666.

19. Serniwka, S. A., and Shaw, G. S. (2009) The structure of the UbcH8-ubiquitin complex shows a unique ubiquitin interaction site, *Biochemistry 48*, 12169-12179.

20. Hamilton, K. S., Ellison, M. J., Barber, K. R., Williams, R. S., Huzil, J. T., McKenna, S., Ptak, C., Glover, M., and Shaw, G. S. (2001) Structure of a conjugating enzyme-ubiquitin thiolester intermediate reveals a novel role for the ubiquitin tail, *Structure 9*, 897-904.

21. Eddins, M. J., Carlile, C. M., Gomez, K. M., Pickart, C. M., and Wolberger, C. (2006) Mms2-Ubc13 covalently bound to ubiquitin reveals the structural basis of linkage-specific polyubiquitin chain formation, *Nat Struct Mol Biol 13*, 915-920.

22. Sakata, E., Satoh, T., Yamamoto, S., Yamaguchi, Y., Yagi-Utsumi, M., Kurimoto, E., Tanaka, K., Wakatsuki, S., and Kato, K. (2010) Crystal structure of UbcH5b~ubiquitin intermediate: insight into the formation of the self-assembled E2~Ub conjugates, *Structure 18*, 138-147.

23. Kamadurai, H. B., Souphron, J., Scott, D. C., Duda, D. M., Miller, D. J., Stringer, D., Piper, R. C., and Schulman, B. A. (2009) Insights into ubiquitin transfer cascades from a structure of a UbcH5B approximately ubiquitin-HECT(NEDD4L) complex, *Mol Cell 36*, 1095-1102.

24. Pruneda, J. N., Stoll, K. E., Bolton, L. J., Brzovic, P. S., and Klevit, R. E. (2011) Ubiquitin in motion: structural studies of the ubiquitin-conjugating enzyme approximately ubiquitin conjugate, *Biochemistry 50*, 1624-1633.

25. Rodrigo-Brenni, M. C., Foster, S. A., and Morgan, D. O. (2010) Catalysis of lysine 48-specific ubiquitin chain assembly by residues in E2 and ubiquitin, *Mol Cell 39*, 548-559.

26. Miura, T., Klaus, W., Gsell, B., Miyamoto, C., and Senn, H. (1999) Characterization of the binding interface between ubiquitin and class I human ubiquitin-conjugating enzyme 2b by multidimensional heteronuclear NMR spectroscopy in solution, *J Mol Biol 290*, 213-228.

27. Wickliffe, K. E., Lorenz, S., Wemmer, D. E., Kuriyan, J., and Rape, M. (2011) The mechanism of linkage-specific ubiquitin chain elongation by a single-subunit E2, *Cell 144*, 769-781.

28. Mueller, T. D., and Feigon, J. (2002) Solution structures of UBA domains reveal a conserved hydrophobic surface for protein-protein interactions, *J Mol Biol 319*, 1243-1255.

29. Li, W., Tu, D., Li, L., Wollert, T., Ghirlando, R., Brunger, A. T., and Ye, Y. (2009) Mechanistic insights into active site-associated polyubiquitination by the ubiquitin-conjugating enzyme Ube2g2, *Proc Natl Acad Sci U S A 106*, 3722-3727.

30. Hodgins, R., Gwozd, C., Arnason, T., Cummings, M., and Ellison, M. J. (1996) The tail of a ubiquitin-conjugating enzyme redirects multi-ubiquitin chain synthesis from the lysine 48-linked configuration to a novel nonlysine-linked form, *J Biol Chem 271*, 28766-28771.

Chapter 5

Summary and Discussion

5.1 Introduction

The ubiquitin proteolysis pathway is an essential regulatory mechanism used for the degradation of short-lived, damaged, misfolded or denatured proteins within the cell (*1*). Ubiquitination utilizes three enzymes, E1, E2 and E3 to respectively activate, transfer and ligate ubiquitin (Ub) onto a substrate protein. The creation of K48-linked poly-Ub chains on a substrate will target this protein to be degraded by the 26S proteosome (*1*). Ubiquitination is crucial for maintaining cell homeostasis. Specific mutations in ubiquitination enzymes and interactors can cause disruption of cell homeostasis, leading to several diseases including cancer and neurodegenerative disorders (*2*). The E2 conjugating enzyme is the central enzyme in the ubiquitin proteolysis pathway. Previous studies examining the structural details of E1/E2 and E2/E3 interactions has characterized the general mechanism for Ub transfer through the E1-E2-E3 enzyme cascade. However, how poly-Ub chains are created is much less well understood. Several poly-Ub chain assembly mechanisms have been proposed in various ubiquitination pathways (*3*). The main competing mechanisms include the sequential addition model where poly-Ub chains are built on the substrate one at a time, and the preassembly model where poly-Ub chains are formed prior to attachment to substrate (*3*).

In this thesis, HIP2 and its yeast homolog Ubc1 were investigated to determine their mechanism of poly-Ub chain formation. These enzymes have been observed to have poly-Ub chain activity in the absence of E3 enzymes and substrates (*4, 5*). These

E2 enzymes are also unique in that they contain a C-terminal UBA domain known to bind Ub non-covalently (*6, 7*). The ability of these enzymes to produce poly-Ub chains unattached to substrates suggests poly-Ub chains may be preassembled *in vivo*. The Ubc1 enzyme has recently been shown to preferably extend chains on mono-ubiquitinated substrates indicating it may function through a sequential addition model (*8*). The HIP2 enzyme has very few identified E3 enzyme partners and substrates and therefore has a very poorly understood biological role, although its function has been implicated in the progression of both Huntingtin's and Alzheimer's disease (*9-12*). Experimental investigations on both Ubc1 and HIP2 were performed to help clarify their mechanism of poly-Ub chain formation.

5.2 Previous studies on poly-Ub chain mechanisms

The only structural evidence for the formation of poly-Ub chains comes from the Ubc13/Mms2 E2 heterodimer that is responsible for K63-linked poly-Ub chain assembly (*13*). The main discovery from this structure was that two E2 enzymes could position two Ub molecules to be directly reacted to create a Ub-Ub connection. Many other E2 enzymes have also been implied to either homodimerize or be brought into close proximity through E3 dimerization. Strong evidence for E2 dimerization has been acquired through differentially tagged Ube2g2~Ub thiolesters that can directly react with each other to create a thiolester linked Ube2g2~Ub_2 (*14*). This activity required its cognate E3 enzyme that has been found to dimerize indicating poly-Ub chain assembly in Ube2g2 may occur through E3 assisted dimerization (*15*). These previous experiments

have provided strong evidence that dimerization of E2 or E3 enzymes may be very important in the formation of poly-Ub chains within many ubiquitination pathways.

The non-covalent binding of Ub has also provided another mechanism for poly-Ub chain formation. This was observed on the HECT E3 KIAA10 that was found to bind one Ub through a thiolester, and a second Ub non-covalently. The mechanism of poly-Ub chain assembly is presumably accomplished through the positioning of these 2 Ub molecules in close proximity to allow the C-terminal thiolester of one Ub to react with the lysine side chain of the other Ub (*16*). The ability of KIAA10 to bind two Ub molecules indicates it may function through a monomeric mechanism.

The homologous enzymes Ubc1 and HIP2 have both been shown to have poly-Ub chain activity without E3 enzymes, and have both been shown to bind Ub non-covalently (*4-6, 17*). These results allow for the possibility that Ubc1 and HIP2 may function by either the proposed monomeric or dimeric mechanisms used by KIAA10 and Ube2g2 respectively. This thesis has focused on using physical and structural studies as well as activity assays to clarify the mechanism of poly-Ub chain assembly utilized by HIP2 and Ubc1.

5.3 Dimerization of HIP2 and Ubc1 is not a major determinant for poly-Ub chain activity

HIP2 and Ubc1 both have K48-linked poly-Ub chain activity that is independent of an E3 ligase or substrate (*4, 5*). Since E2 dimerization has been suggested to drive poly-Ub chain formation, the Ubc1 and HIP2 enzymes were investigated for their ability

to dimerize. The Ubc1-Ub, HIP2-Ub and HIP2-Ub_2 thiolester mimic complexes were also studied since previous work on the E2 enzyme Cdc34 indicated that formation of thiolesters may assist dimerization (*18*). Sedimentation equilibrium was performed on low concentrations of Ubc1, Ubc1-Ub, HIP2, HIP2-Ub and HIP2-Ub_2 to determine accurate molecular weights (MW). HIP2 and Ubc1 were found to be very close to their expected monomeric molecular weight. The addition of Ub to these enzymes can result in the reported MW to be as much as 7-11% larger than expected, while the addition of Ub_2 to HIP2 can result in the reported MW to be as much as 8% larger than expected. These values are close to the 5% error range of this technique indicating that the proteins are predominantly monomeric. If dimerization is occurring, a self-association model can be used to estimate the K_d of dimerization, but since dimerization is very weak, a reliable K_d cannot be acquired for these enzymes at low concentrations. Therefore, higher concentrations of Ubc1, Ubc1-Ub, HIP2, and HIP2-Ub proteins were studied with SAXS to determine their dimerization capacity. The SAXS analysis also found these proteins to be predominantly monomeric at concentrations up to 200 μM. Since minimal dimerization was observed even at these higher concentrations, only an estimation of K_d limitations is possible through comparison to theoretical K_d curves. These calculations indicate the K_d values for Ubc1-Ub and HIP2-Ub self-association must be >1000 μM. K_d values of >1000 μM confirm very weak self-association of the Ubc1-Ub and HIP2-Ub indicating thiolester formation did not greatly assist dimerization.

The HIP2 enzyme was further studied with NMR spectroscopy. NMR ^{1}H-^{15}N TROSY-HSQC spectra collected on HIP2, HIP2-Ub and HIP2-Ub_2 did not experience severe line broadening of all amide protons, as was observed for UbcH5c-Ub complex

known to oligomerize (*19*), indicating HIP2 and its thiolester mimics are likely monomeric even at higher NMR concentrations of ~350-550 μM. NMR chemical shift perturbation experiments were used to determine and characterize any protein interactions within HIP2, HIP2-Ub and HIP2-Ub_2. These results indicate that intramolecular interactions occur within both HIP2-Ub and HIP2-Ub_2. These intramolecular interactions occur between the HIP2 catalytic core and Ub^P within HIP2-Ub^P, and between the HIP2 UBA domain and Ub^D within HIP2-Ub^P-Ub^D. These interactions block the hydrophobic surface of Ub^P and Ub^D in HIP2-Ub and HIP2-Ub_2 respectively. The presence of a UBA domain in HIP2 that binds Ub non-covalently could theoretically bind the thiolester bound Ub of another HIP2-Ub complex to cause dimerization. The observed intramolecular interaction within HIP2-Ub and HIP2-Ub_2 limits the availability of these attached Ub and Ub_2 moieties to interact with a second HIP2 UBA domain. As a result, the intramolecular interactions within HIP2-Ub and HIP2-Ub_2 are preferred over any intermolecular interactions between HIP2-Ub and HIP2-Ub_2. These structural observations explain why possible UBA/Ub binding does not result in dimerization of HIP2-Ub or HIP2-Ub_2. Additionally, a dimeric mechanism would also require reactive K48 residues on Ub in either HIP2-Ub or HIP2-Ub_2, and these residues appear buried against HIP2 making them unlikely to act as Ub acceptors (Fig 5.1A). These combined results indicate that Ubc1 and HIP2 very likely do not function using a dimeric mechanism for unanchored poly-Ub chain formation.

Previous experiments on Ubc1Δ resulted in the novel finding that E1 was required for poly-Ub chain extension, suggesting it directly extends chains or may function as an

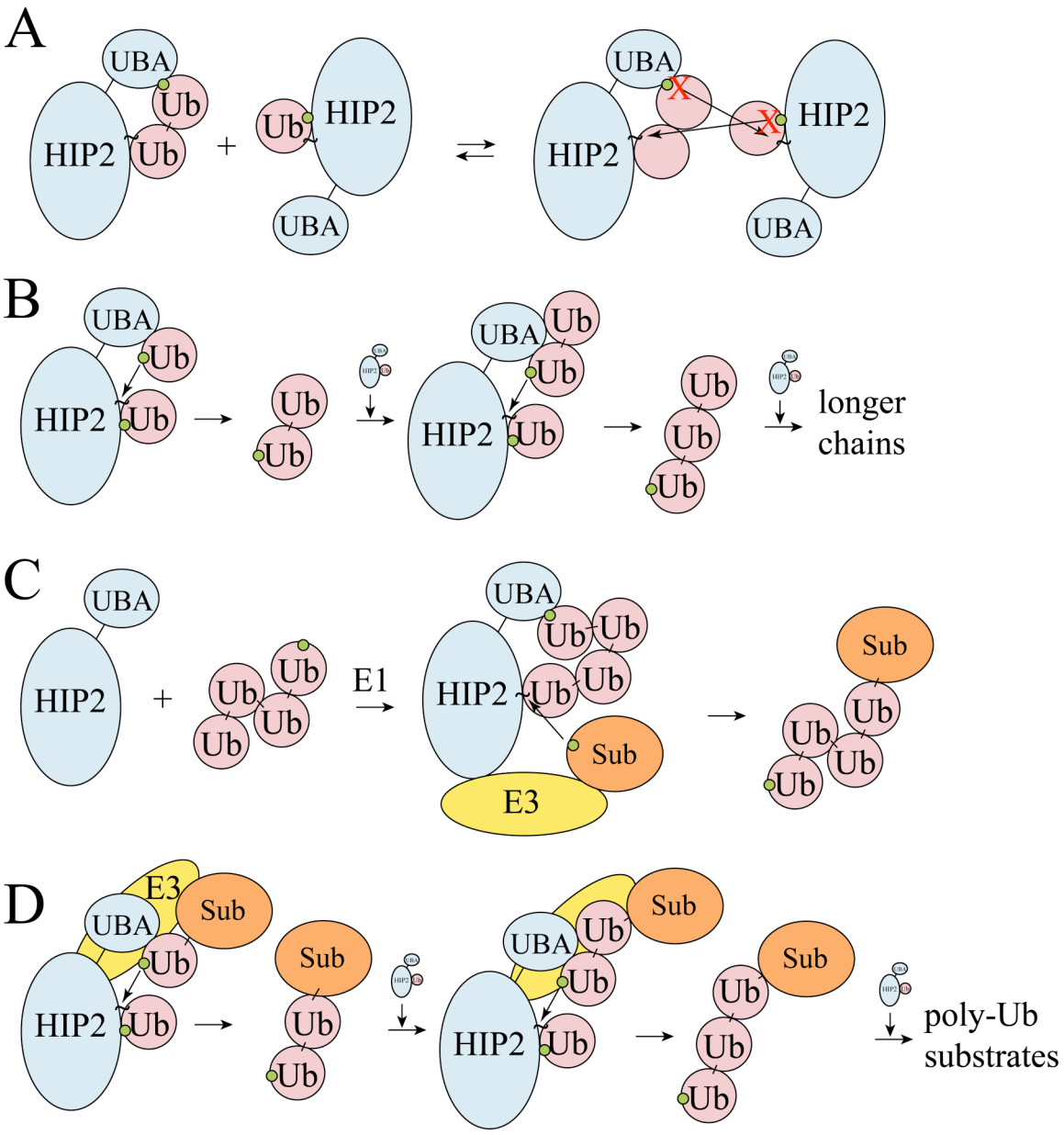

Figure 5.1 Proposed models of HIP2 Function. Ubiquitination pathway components include the HIP2 E2 conjugating enzyme (blue), Ub (pink), an E3 ligating enzyme (yellow), a substrate (orange) to be ubiquitinated, and small green balls represent the reactive K48 on Ub or reactive K residue in the substrate. (**A**) Model of HIP2~Ub and HIP2~Ub_2 indicating blocked K48 residues that do not preferably react with another HIP2~Ub thiolester. (**B**) Model of unanchored poly-Ub chain formation driven by UBA affinity for free Ub and poly-Ub chains. Movement of the UBA domain would bring the Ub K48 lysine into reactive distance with the thiolester bound Ub. (**C**) Model demonstrating how a preassembled poly-Ub chain can be loaded onto the E1 enzyme, transferred to HIP2 and then finally transferred to a substrate protein. (**D**) The sequential addition model for HIP2 using an already mono-ubiquitinated substrate would function nearly identically to (**B**) only substrate-Ub would be bound to both the E3 and the UBA domain. The E3 enzyme contacts the HIP2 catalytic core and the substrate only.

E2 dimerization scaffold (*20*). In contrast, activity assays performed in this work on HIP2 and Ubc1 indicate that E1 enzyme removal after E2 thiolester charging did not affect poly-Ub chain extension. This result shows the E1 enzyme does not directly assist poly-Ub chain extension. The removal of the E1 enzyme also shows that it is not required as an E2 dimerization scaffold. Since E3 enzymes were not studied in this work, we cannot discount the possibility of E3 assisted E2 dimerization, although there is currently no evidence to support E3 assisted HIP2 dimerization.

5.4 The monomeric mechanism employed by HIP2

Since HIP2 has been observed to be more active in unanchored poly-Ub chain activity than Ubc1, and was more thoroughly investigated in this work, only its proposed mechanism will be discussed in detail. The observation that dimerization of HIP2 is very weak indicates these enzymes likely function in a monomeric fashion to build poly-Ub chains without E3 enzymes. A monomeric HIP2 enzyme most likely functions by utilizing its ability to interact with at least two Ub molecules at once, one Ub covalently through a thiolester linkage at the active site, and a second Ub non-covalently using the UBA domain (*17, 21*). These interactions may allow HIP2 to place two Ub molecules in close proximity to assist the formation of Ub_2. This possible mechanism is supported by SAXS data that indicates the HIP2 UBA domain is linked to the catalytic core by a flexible linker, just like Ubc1 (*6*). This flexible linker may give the UBA domain the ability to be repositioned to place the acceptor Ub's K48 residue within range for nucleophilic attack with the thiolester bound Ub donor (Fig 5.1B). In this reaction, the resulting Ub_2 would be unanchored and free in solution. Therefore, this is the likely

mechanism utilized for the observed unanchored poly-Ub chains produced with only E1 enzyme, HIP2 and Ub.

The proposed monomeric HIP2 mechanism depicted in Figure 5.1B would be driven by the UBA affinity for acceptor Ub molecules. The HIP2 UBA domain is known to bind Ub_4 with a K_d of 155 μM while a single Ub moiety binds with a weaker K_d of 400 μM (*7*). These results indicate that the HIP2 UBA domain binds poly-Ub chains preferentially, an observation that has been reported previously on other isolated UBA domains (*7*). The UBA domain's preference for binding longer poly-Ub chains may explain previous studies on HIP2 that have shown that Ub_2 acts as a better acceptor than a single Ub (*4*). The UBA domain's preference for free Ub_2 chains over a single Ub indicates that the rate of unanchored poly-Ub chain formation should increase as these poly-Ub chains grow longer. Activity assays have demonstrated that a HIP2-Ub complex can react with a HIP2~Ub thiolester to make a HIP2-Ub_2 complex. Initially, it was thought that this supported a dimeric mechanism for HIP2. However, the association between HIP2-Ub/HIP2-Ub was determined to have a K_d of >1000 μM. This binding is weaker than that for free Ub_4 (155 μM) and free Ub (400 μM) indicating that HIP2-Ub is a less preferred acceptor. Structural analysis of the HIP2-Ub complex may explain how HIP2-Ub can react with another HIP2~Ub thiolester. SAXS experiments have shown HIP2-Ub to be on average a rather 'elongated' structure, while NMR experiments have found that there are significant contacts between HIP2 and Ub within HIP2-Ub. The interactions between HIP2 and Ub^P in the HIP2-Ub^P complex show few large chemical shift changes and a high number of highly broadened residues on both HIP2 and Ub^P. This indicates that there may be intermediate exchange occurring between HIP2 and Ub^P

as a result of at least 1 tightly bound form and 1 loosely bound form of HIP2-Ub^P. Previous experimentation has shown E2~Ub structures to be highly mobile (*22*), which is consistent with both the observed average 'elongated' structure in SAXS and the proposed intermediate exchange between at least 2 Ub positions within HIP2-Ub in NMR experiments. A mobile HIP2~Ub thiolester structure would result in an equilibrium between blocked and exposed Ub. When Ub is exposed within HIP2~Ub, the Ub would be able to interact with another HIP2~Ub thiolester's UBA domain accounting for its ability to act as an acceptor in activity assays. However, the HIP2-Ub complex was not observed to be a preferred acceptor because the surface of Ub is transiently blocked when HIP2-Ub is in its more tightly associated form. Since HIP2-Ub binds with lower affinity than free Ub, it is likely the HIP2-Ub_2 product is an artifactual by-product of not having any available free Ub acceptor. These results are consistent with the proposed UBA driven monomeric mechanism where longer chains bind more strongly to the UBA domain (Fig 5.1B).

5.5 Preassembled poly-Ub chains may be used *in vivo*

Previous experiments have shown that Ub and Ub_2 can form thiolesters on the HIP2 enzyme with identical kinetics (*4*). These results indicate that preassembled unanchored Ub_2 can then be loaded onto the E1 enzyme and then transferred to HIP2 just as easily as a single Ub molecule. Previous experiments have also shown that unanchored poly-Ub chains are found *in vivo*, and that these chains were able to be connected to substrates with kinetics indistinguishable from mono-ubiquitin using Ubc4 (*23*). The Ube2g2 E2 enzyme was also shown to be able to connect a synthesized poly-

Ub chain directly onto a substrate (*14*). These combined results show that loading E2 enzymes with poly-Ub chains appears kinetically equivalent to using a single Ub moiety, and that poly-Ub chains can be directly transferred to substrates. Therefore, preassembly of poly-Ub chains in solution by HIP2 could be followed by the loading of these chains onto HIP2 creating HIP2~Ub_n thiolester intermediates. The study of HIP2-Ub and HIP2-Ub_2 complexes has shown that the Ub K48 residues are occluded indicating these thiolester linked Ub and Ub_2 moieties are likely to act predominantly as Ub donors in poly-Ub chain extension. In this way, the UBA domain would act as an inhibitor of poly-Ub chain extension on HIP2-Ub_n. HIP2-Ub_n intermediates could then act as Ub donors and interact with both an E3 ligase and a substrate resulting in the transfer of the Ub_n directly to a substrate in a single step (Fig 5.1C). This mechanism describes how preassembled poly-Ub chains could be transferred onto substrates by the HIP2 enzyme.

5.6 HIP2 poly-Ub chain preassembly in Alzheimer's disease

HIP2 has been linked to Alzheimer's disease through involvement with the protein UBB^{+1}. UBB^{+1} is a frameshift mutant of Ub that contains a 19 residue C-terminal extension that cannot form a thiolester with ubiquitination enzymes (*11*). Previous experiments indicate HIP2 can poly-ubiquitinate the UBB^{+1} protein on its K48 residue *in vitro*, and this UBB^{+1}-Ub_n resists disassembly by deubiquitinating enzymes and causes potent proteosome inhibition (*11*). HIP2 activity has also been found to increase neurotoxicity and proteosome inhibition *in vivo* (*12*). The UBA domain of HIP2 has recently been shown to interact with both UBB^{+1} and Ub in a similar manner, and in the same study, *in vivo* experiments showed that HIP2 UBA domain mutations reduced

proteosomal inhibition (*17*). These results indicate that HIP2 poly-ubiquitination of UBB^{+1} is likely involved in the proteosomal inhibition experienced in Alzheimer's disease. UBB^{+1} is simply a normal Ub molecule with a 19-residue extension at the C-terminus meaning it can be recognized as a Ub acceptor by the UBA domain of HIP2, but cannot form a thiolester with ubiquitination enzymes. Therefore, HIP2 likely causes poly-ubiquitination of UBB^{+1} by mistakenly using this molecule as a normal Ub acceptor in unanchored poly-Ub chain assembly (Fig 5.1B). By this mechanism, HIP2 would bind UBB^{+1} with the UBA domain and react it with a thiolester connected Ub to yield UBB^{+1}-Ub. Proceeding reactions would use UBB^{+1}-Ub as the acceptor eventually creating a UBB^{+1}-Ub_n product. This molecule resists disassembly and accumulates to inhibit proteosomes. UBB^{+1} poly-ubiquitination and related proteosomal inhibition has also been shown to increase aggregate formation and cell death in polyglutamine diseases such as Huntington's disease (*9, 24, 25*). The preassembly mechanism for poly-Ub chains by the HIP2 enzyme can therefore be utilized with UBB^{+1} to inhibit the ubiquitination proteolysis pathway resulting in severe pathological consequences.

5.7 The sequential addition model for Ubc1 and HIP2

Although HIP2 can preassemble poly-Ub chains *in vitro*, its major physiological role may be to utilize the sequential addition mechanism where poly-Ub chains are sequentially built on a substrate protein. This mechanism is supported by recent experimentation on the ubiquitination of Cyclin B by the large multisubunit anaphase promoting complex (APC – a RING E3) and the E2 enzymes Ubc4 and Ubc1 (*8*). In this study, Ubc4 and Ubc1 appear to have different functions as Ubc4 was more active in

initial Ub attachment to substrates and Ubc1 was more active in extending chains on substrates that already have a single attached Ub (*8*). HIP2 was also observed to extend chains on substrates in combination with UbcH10, although these results showed very low activity on the substrate Cyclin indicating this substrate may not be a preferred substrate of HIP2 (*8*). Ubc1Δ (no UBA domain) was also investigated, and was found to yield substrate attached poly-Ub chains of shorter length (*8*). The UBA domain of Ubc1 is therefore required for full activity in substrate poly-Ub chain extension (*8*). These results are consistent with a sequential addition model whereby Ubc4 mono ubiquitinates a substrate and Ubc1 adds Ub molecules to the growing chain. It is reasonable to assume HIP2 may function similarly with a proper E3 enzyme and substrate. The sequential addition mechanism may function in a similar manner to unanchored poly-Ub chain formation (Fig 5.1B), whereby the Ub acceptor of free Ub is replaced with a substrate bound Ub (substrate-Ub) (Fig 5.1D). If the true biological function of Ubc1 and HIP2 is to extend poly-Ub chains on substrates, then the UBA domain may aid this activity by directly binding to the Ub attached to a substrate (Fig 5.1D). The E2~Ub/E3/substrate-Ub complex depicted in Figure 5.1D would provide affinity for substrate-Ub through both E3 binding and E2 UBA binding. The UBA domain may therefore increase the reaction rate of this E2 enzyme by providing additional interactions for substrate-Ub extension by directly binding the growing chain. This mechanism would suggest that the formation of poly-Ub chains prior to attachment to substrate observed for HIP2 and Ubc1 is simply an artifactual activity caused by lack of E3 ligases and substrates, and therefore not the major biological function of these enzymes.

The sequential model for HIP2 and Ubc1 poly-Ub chain extension is also supported by analysis of required reaction times. Significant unanchored poly-Ub chain activity requires reaction times on the order of hours without an E3 ligase and substrates (*4, 5*), while poly-ubiquitination of mono-ubiquitinated substrates had reaction times on the order of minutes for Ubc1, and 90 minutes for a non-specific substrate for HIP2 (*8*). These experiments indicate ubiquitination reactions occur more quickly in the presence of E3 enzymes that place E2~Ub thiolesters in close proximity to ubiquitinated substrates. These faster reaction rates are more biologically significant than those for unanchored chain assembly.

Ubiquitination of mono-ubiquitinated substrates was also demonstrated for the E2 enzymes UbcH5 and Cdc34 whereby UbcH5 preferably mono-ubiquitinates substrates and Cdc34 efficiently performs poly-Ub chain extension on these mono-ubiquitinated substrate (*26*). Sequential poly-Ub chain assembly has also been strongly supported for Cdc34 where substrates were seen to have Ub's added one at a time through a millisecond timescale reaction system (*27*). Although little is known of HIP2's E3 enzymes and substrates, support for the sequential addition model with its yeast homolog Ubc1 indicates that HIP2 may function in a similar manner. The biological function of HIP2 may then be to extend chains on already mono-ubiquitinated substrate molecules (Fig 5.1D).

5.8 Conclusions

Structural investigation of HIP2-Ub and HIP2-Ub_2 has characterized the intramolecular interactions observed within these intermediates. HIP2-Ub and HIP2-Ub_2

both have occluded Ub hydrophobic faces including the K48 residue indicating these species are preferred Ub donors and not Ub acceptors in poly-Ub chain extension (Fig 5.1A). These results in addition to thorough dimerization studies indicate HIP2 functions through a monomeric mechanism to build poly-Ub chains (Fig 5.1B). The purpose of preassembling poly-Ub chains remains unknown, although previous kinetic assays indicate these preassembled chains could be loaded onto E2 enzymes and then transferred onto substrates (Fig 5.1C) (*4, 14, 23*). This model would involve the use of the UBA domain to first aid in the construction of poly-Ub chains, followed by inhibiting chain extension during transfer to a substrate. HIP2 may also utilize a sequential addition mechanism where a growing poly-Ub chain is bound to a substrate. This mechanism is supported by the observation that Ubc1 (yeast homolog of HIP2) can preferentially extend chains on mono-ubiquitinated substrates (*8*). HIP2 is suspected to behave in a similar fashion to extend poly-Ub chains on substrates, although there is currently little evidence for such activity. This sequential addition model would utilize both the E3 interaction with substrate, and the UBA interaction with a substrate attached poly-Ub chain (Fig 5.1D).

The monomeric UBA driven mechanism of HIP2 can explain both the preassembly model and sequential addition model (Fig 5.1B, D). The general mechanism of HIP2 function is identical between these two models, but the reaction rates may be faster with the sequential addition model due to additional interaction surfaces provided by the E3 enzyme and monoubiquitinated substrate. Although both mechanisms are possible, the sequential addition model appears to be preferred due to the observation that poly-Ub chain activity of Ubc1 without E3 enzymes required hours, while poly-Ub chain

activity with E3 enzymes and substrates required only minutes (*8*). The mechanisms depicted in Figure 5.1B and 5.1D would utilize the UBA domain's interaction with Ub to position two Ub molecules in close proximity. The affinity of UBA binding to Ub and Ub_4 has a K_d of 400 and 155 μM respectively (*7*). The cellular concentration of Ub is around 10 μM (*28, 29*) and the cellular concentrations of E2 enzymes are likely in the low μM (<10 μM) to nM range. With these cellular concentrations and UBA/Ub K_d values, it is expected that unanchored poly-Ub chain activity would not proceed with significant reaction rates in the absence of an E3 enzyme and substrate. The addition of the E3 enzyme is likely required to greatly increase the effective concentrations of HIP2 and ubiquitinated substrate to increase the reaction rate. Additionally, the mere binding of E3 enzymes to the E2 enzyme also has been shown to increase catalytic activity of the E2 enzyme (*30, 31*). The sequential addition model is preferred over the preassembly model since there are currently no known mechanisms *in vivo* that would increase the kinetic rate of unanchored poly-Ub chain formation observed in HIP2. However, the mechanism of unanchored chain formation appears to function *in vivo* with UBB^{+1}, which can be involved in proteosome inhibition in Alzheimer's and Huntington's disease (*9, 12*).

5.9 Future Work

In this work, low-resolution structural details were acquired for HIP2 and HIP2-Ub using SAXS. Chemical shift perturbation studies were also performed to determine protein interaction surfaces within HIP2-Ub and HIP2-Ub_2 complexes. However, a high-resolution structural model of 'compact' HIP2-Ub and HIP2-Ub_2 was not completed due

to ambiguous constraints for computer-aided protein docking. Additional NMR experiments may be required to provide sufficient protein-protein interaction data to properly dock these structures. These experiments could include hydrogen-deuterium exchange and cross-saturation experiments both of which can provide residue specific information of a protein-protein interface. This additional data may allow for a high quality structural model of HIP2-Ub or HIP2-Ub_2. These structures could then be used to investigate the preferred orientation of Ub and Ub_2 in HIP2-Ub and HIP2-Ub_2. The position of thiolester attached Ub and Ub_2 would determine the available surfaces of these proteins that could interact within larger protein complexes including E3 enzymes and substrates.

Currently HIP2 has only been well studied for its unanchored chain formation activity and very little is known of its biological function with E3 enzymes and substrates. The best identified E3 and substrate for HIP2 may be the E3 enzyme NARF (Nemo-like Kinase (NLK) – associated RING finger) and the transcription factors TCF (T Cell Factor) and LEF (Lymphoid Enhancer Factor). NARF and TCF/LEF were identified by *in vivo* coimmunoprecipitation experiments and ubiquitination assays. A recent study developed an approach that allows for in depth kinetic assays on ubiquitination in the millisecond to second timescale (*27*). If this approach was utilized on HIP2 with a known E3 (NARF) and substrate (TCF/LEF), then the formation of poly-Ub chains can be quantitated as they form. This experiment would provide strong results to show whether HIP2 utilizes a sequential addition model to build poly-Ub chains on the substrate, or whether poly-Ub chains are preassembled by HIP2 and then connected to a substrate.

The monomeric mechanisms for HIP2 proposed in this work suggest that UBA/Ub binding allows HIP2 the ability to place two Ub molecules in close proximity to aid poly-Ub chain formation. It may be possible to capture these two Ub molecules in close proximity using X-ray crystallography. The HIP2 protein has been previously crystallized both alone and in complex with free Ub (*17, 32*). These previous crystallizations should provide details to aid in future crystallizations of HIP2. To determine how HIP2 can position two Ub molecules for poly-Ub chain assembly, it should be possible to crystallize the HIP2-Ub disulphide in complex with free Ub. This crystal structure would be expected to have a significantly altered UBA position to allow a Ub-Ub linkage. If the UBA positions the non-covalently bound Ub in close proximity to the thiolester, then it would be expected that this structure should be fairly compact making it a good candidate for protein crystallization. This structure would be the first E2 structure to mechanistically detail how K48-linked poly-Ub chains can be formed. This structure would be immensely valuable to determining the structural and enzymatic details for how HIP2 performs K48-linked poly-Ub chain formation.

X-ray crystallography could also be utilized to support the proposed sequential addition model depicted in Figure 5.1D. Upon identification of an E3 enzyme and substrate for HIP2, these proteins could be mixed with a HIP2-Ub thiolester mimic to possibly create a tightly interacting complex. The use of a mono-ubiquitinated substrate may increase the affinity of this complex by allowing UBA/Ub-Substrate interactions. Structural details of such a complex would greatly aid in determining HIP2's possible biological role of extending poly-Ub chains on substrates through a sequential addition model.

Bibliography

1. Hershko, A., and Ciechanover, A. (1998) The ubiquitin system, *Annu Rev Biochem 67*, 425-479.

2. Schwartz, A. L., and Ciechanover, A. (2009) Targeting proteins for destruction by the ubiquitin system: implications for human pathobiology, *Annu Rev Pharmacol Toxicol 49*, 73-96.

3. Hochstrasser, M. (2006) Lingering mysteries of ubiquitin-chain assembly, *Cell 124*, 27-34.

4. Chen, Z., and Pickart, C. M. (1990) A 25-kilodalton ubiquitin carrier protein (E2) catalyzes multi-ubiquitin chain synthesis via lysine 48 of ubiquitin, *J Biol Chem 265*, 21835-21842.

5. Hodgins, R., Gwozd, C., Arnason, T., Cummings, M., and Ellison, M. J. (1996) The tail of a ubiquitin-conjugating enzyme redirects multi-ubiquitin chain synthesis from the lysine 48-linked configuration to a novel nonlysine-linked form, *J Biol Chem 271*, 28766-28771.

6. Merkley, N., and Shaw, G. S. (2004) Solution structure of the flexible class II ubiquitin-conjugating enzyme Ubc1 provides insights for polyubiquitin chain assembly, *J Biol Chem 279*, 47139-47147.

7. Raasi, S., Varadan, R., Fushman, D., and Pickart, C. M. (2005) Diverse polyubiquitin interaction properties of ubiquitin-associated domains, *Nat Struct Mol Biol 12*, 708-714.

8. Rodrigo-Brenni, M. C., and Morgan, D. O. (2007) Sequential E2s drive polyubiquitin chain assembly on APC targets, *Cell 130*, 127-139.

9. de Pril, R., Fischer, D. F., Roos, R. A., and van Leeuwen, F. W. (2007) Ubiquitin-conjugating enzyme E2-25K increases aggregate formation and cell death in polyglutamine diseases, *Mol Cell Neurosci 34*, 10-19.

10. Kalchman, M. A., Graham, R. K., Xia, G., Koide, H. B., Hodgson, J. G., Graham, K. C., Goldberg, Y. P., Gietz, R. D., Pickart, C. M., and Hayden, M. R. (1996) Huntingtin is ubiquitinated and interacts with a specific ubiquitin-conjugating enzyme, *J Biol Chem 271*, 19385-19394.

11. Lam, Y. A., Pickart, C. M., Alban, A., Landon, M., Jamieson, C., Ramage, R., Mayer, R. J., and Layfield, R. (2000) Inhibition of the ubiquitin-proteasome system in Alzheimer's disease, *Proc Natl Acad Sci U S A 97*, 9902-9906.

12. Song, S., Kim, S. Y., Hong, Y. M., Jo, D. G., Lee, J. Y., Shim, S. M., Chung, C. W., Seo, S. J., Yoo, Y. J., Koh, J. Y., Lee, M. C., Yates, A. J., Ichijo, H., and

Jung, Y. K. (2003) Essential role of E2-25K/Hip-2 in mediating amyloid-beta neurotoxicity, *Mol Cell 12*, 553-563.

13. McKenna, S., Moraes, T., Pastushok, L., Ptak, C., Xiao, W., Spyracopoulos, L., and Ellison, M. J. (2003) An NMR-based model of the ubiquitin-bound human ubiquitin conjugation complex Mms2.Ubc13. The structural basis for lysine 63 chain catalysis, *J Biol Chem 278*, 13151-13158.

14. Li, W., Tu, D., Brunger, A. T., and Ye, Y. (2007) A ubiquitin ligase transfers preformed polyubiquitin chains from a conjugating enzyme to a substrate, *Nature 446*, 333-337.

15. Li, W., Tu, D., Li, L., Wollert, T., Ghirlando, R., Brunger, A. T., and Ye, Y. (2009) Mechanistic insights into active site-associated polyubiquitination by the ubiquitin-conjugating enzyme Ube2g2, *Proc Natl Acad Sci U S A 106*, 3722-3727.

16. Wang, M., and Pickart, C. M. (2005) Different HECT domain ubiquitin ligases employ distinct mechanisms of polyubiquitin chain synthesis, *EMBO J 24*, 4324-4333.

17. Ko, S., Kang, G. B., Song, S. M., Lee, J. G., Shin, D. Y., Yun, J. H., Sheng, Y., Cheong, C., Jeon, Y. H., Jung, Y. K., Arrowsmith, C. H., Avvakumov, G. V., Dhe-Paganon, S., Yoo, Y. J., Eom, S. H., and Lee, W. (2010) Structural basis of E2-25K/UBB+1 interaction leading to proteasome inhibition and neurotoxicity, *J Biol Chem 285*, 36070-36080.

18. Varelas, X., Ptak, C., and Ellison, M. J. (2003) Cdc34 self-association is facilitated by ubiquitin thiolester formation and is required for its catalytic activity, *Mol Cell Biol 23*, 5388-5400.

19. Brzovic, P. S., Lissounov, A., Christensen, D. E., Hoyt, D. W., and Klevit, R. E. (2006) A UbcH5/ubiquitin noncovalent complex is required for processive BRCA1-directed ubiquitination, *Mol Cell 21*, 873-880.

20. Huzil, J. T., Pannu, R., Ptak, C., Garen, G., and Ellison, M. J. (2007) Direct catalysis of lysine 48-linked polyubiquitin chains by the ubiquitin-activating enzyme, *J Biol Chem 282*, 37454-37460.

21. Wilson, R. C., Edmondson, S. P., Flatt, J. W., Helms, K., and Twigg, P. D. (2011) The E2-25K ubiquitin-associated (UBA) domain aids in polyubiquitin chain synthesis and linkage specificity, *Biochem Biophys Res Commun 405*, 662-666.

22. Pruneda, J. N., Stoll, K. E., Bolton, L. J., Brzovic, P. S., and Klevit, R. E. (2011) Ubiquitin in motion: structural studies of the ubiquitin-conjugating enzyme approximately ubiquitin conjugate, *Biochemistry 50*, 1624-1633.

23. van Nocker, S., and Vierstra, R. D. (1993) Multiubiquitin chains linked through lysine 48 are abundant in vivo and are competent intermediates in the ubiquitin proteolytic pathway, *J Biol Chem 268*, 24766-24773.

24. de Pril, R., Hobo, B., van Tijn, P., Roos, R. A., van Leeuwen, F. W., and Fischer, D. F. (2010) Modest proteasomal inhibition by aberrant ubiquitin exacerbates aggregate formation in a Huntington disease mouse model, *Mol Cell Neurosci 43*, 281-286.

25. Howard, R. A., Sharma, P., Hajjar, C., Caldwell, K. A., Caldwell, G. A., du Breuil, R., Moore, R., and Boyd, L. (2007) Ubiquitin conjugating enzymes participate in polyglutamine protein aggregation, *BMC Cell Biol 8*, 32.

26. Wu, K., Kovacev, J., and Pan, Z. Q. (2010) Priming and extending: a UbcH5/Cdc34 E2 handoff mechanism for polyubiquitination on a SCF substrate, *Mol Cell 37*, 784-796.

27. Pierce, N. W., Kleiger, G., Shan, S. O., and Deshaies, R. J. (2009) Detection of sequential polyubiquitylation on a millisecond timescale, *Nature 462*, 615-619.

28. Mastrandrea, L. D., You, J., Niles, E. G., and Pickart, C. M. (1999) E2/E3-mediated assembly of lysine 29-linked polyubiquitin chains, *J Biol Chem 274*, 27299-27306.

29. Rodrigo-Brenni, M. C., Foster, S. A., and Morgan, D. O. (2010) Catalysis of lysine 48-specific ubiquitin chain assembly by residues in E2 and ubiquitin, *Mol Cell 39*, 548-559.

30. Ozkan, E., Yu, H., and Deisenhofer, J. (2005) Mechanistic insight into the allosteric activation of a ubiquitin-conjugating enzyme by RING-type ubiquitin ligases, *Proc Natl Acad Sci U S A 102*, 18890-18895.

31. Petroski, M. D., and Deshaies, R. J. (2005) Mechanism of lysine 48-linked ubiquitin-chain synthesis by the cullin-RING ubiquitin-ligase complex SCF-Cdc34, *Cell 123*, 1107-1120.

32. Wilson, R. C., Hughes, R. C., Flatt, J. W., Meehan, E. J., Ng, J. D., and Twigg, P. D. (2009) Structure of full-length ubiquitin-conjugating enzyme E2-25K (huntingtin-interacting protein 2), *Acta Crystallogr Sect F Struct Biol Cryst Commun 65*, 440-444.

Curriculum Vitae

Benjamin W. Cook

Department of Biochemistry
The University of Western Ontario, London, ON, N6A 5C1

EDUCATION

Ph.D. candidate in Biochemistry
2004 – Present
Department of Biochemistry, University of Western Ontario • London, ON

Bachelor of Science in Honours Biochemistry and Chemistry
1999 – 2004
University of Western Ontario • London, ON

SCHOLARSHIPS, AND ACADEMIC AWARDS

2005 – 2009 Western Graduate Research Scholarship ($24000)
2005 – 2006 Ontario Graduate Scholarship ($15000)
2004 – 2005 Special University Scholarship ($5000)
2002 – 2004 Dean's Honor List
2000 Dean's Honor List
1999 – 2000 Entrance Scholarship – Western Ontario ($2000)

ACADEMIC AND RESEARCH EXPERIENCE

Sept. 2004 – Sept. 2011
University of Western Ontario • London, ON
Graduate Student / Research Assistant
Supervisor: Dr. G.S. Shaw

January 2006 – April 2009
University of Western Ontario • London, ON
Teaching Assistant
Supervisor: Dr. D.T. McLachlin
Course: Biochemistry 380G - Biochemistry Laboratory

September 2004 – December 2008
University of Western Ontario • London, ON
Teaching Assistant
Supervisor: Dr. S.D. Dunn
Course: Biochemistry 381 - Biological Macromolecules

EXPERIENCE (continued)

May 2004 – August 2004
University of Western Ontario • London, ON
Summer Research Student
Supervisor: Dr. E.H. Ball

Sept. 2003 – April 2004
University of Western Ontario • London, ON
Undergraduate lab technician
Supervisor: Dr. E.H. Ball

PUBLICATIONS

Manuscripts in Preparation:
Cook, B.W. and Shaw, G.S. HIP2 makes novel contacts between its C-terminal UBA domain and a covalently attached lysine 48-linked diubiquitin thiolester mimic.

Cook, B.W., Barber, K.B., Shilton, B.H., and Shaw, G.S. Determination of the dimerization capacity of the E2 conjugating enzymes HIP2 and Ubc1 provides evidence for the mechanism of poly-ubiquitination.

Conference Presentations:
Cook, B.W., Barber, K.B., Shilton, B.H., and Shaw, G.S. Role of dimerization in poly-Ub chain formation. Biophysical Society 54th Annual Meeting, San Francisco, CA USA, Poster presentation. Feb 20-24, 2010.

Abstracts:
Spratt, D.E., **Cook, B.W.**, Barber, K.R., and Shaw, G.S. Protein Interactions of Ubiquitin within E2 and E3 Enzyme Complexes. 94th Canadian Chemistry Conference and Exhibition, Montreal, QC, presentation (June 5 2011).

Cook, B.W., Barber, K.R., Shilton, B.H., and Shaw, G.S. Investigation of the self-association of the E2 enzymes HIP2 and Ubc1. Margaret P. Moffat Research Day, University of Western Ontario, London, ON, Poster presentation (March 20 2008).

Cook, B.W., Barber, K.R., Shilton, B.H., and Shaw, G.S. Investigation of the self-association of the E2 enzymes HIP2 and Ubc1. Margaret P. Moffat Research Day, University of Western Ontario, London, ON, Poster presentation (March 22 2007).

Conference:
Symposium on Structural Genomics. Structural Genomics Consortium. Toronto, Ontario (May 2, 2007).

EXTRACURRICULAR LEADERSHIP ACTIVITIES

2005 – 2010 Team captain in campus recreation co-ed soccer league, UWO
2007 – 2009 Chair of the Society of Graduate Students Finance Committee, UWO
2007 – 2009 Department of Biochemistry Social Committee, UWO
2006 – 2009 Department of Biochemistry Proctoring Committee, UWO
2006 – 2009 Member of the SOGS and Grad Club Finance Committees, UWO
2007 – 2010 Private Tutor for students in 2nd and 3rd year biochemistry courses
2003 – 2004 Elected President of Delta Upsilon Fraternity, UWO.
2002 + 2004 University of Western Ontario orientation week sophomore.